frontiers | Research Topics

Quasi-normal modes, non-selfadjoint operators and pseudospectrum: an interdisciplinary approach

Edited by
Jose Luis Jaramillo and Piotr Bizon

Coordinated by
Edgar Gasperin

Published in
Frontiers in Physics
Frontiers in Applied Mathematics and Statistics
Frontiers in Astronomy and Space Sciences

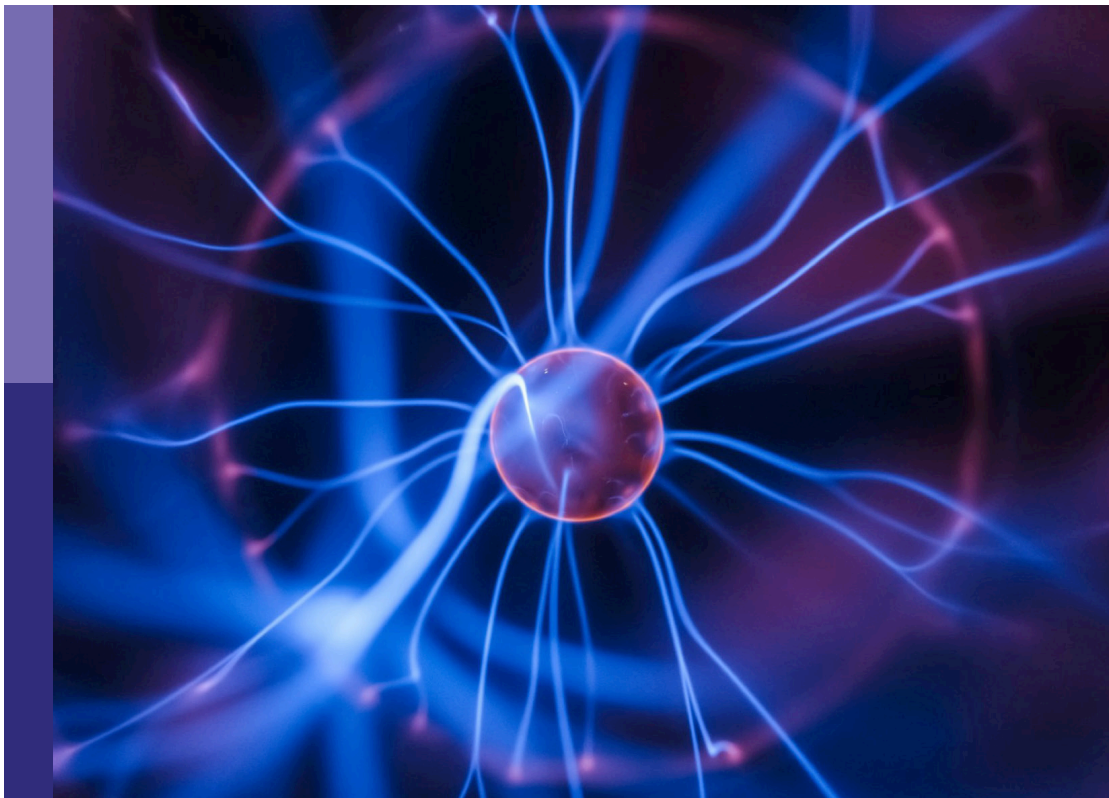

FRONTIERS EBOOK COPYRIGHT STATEMENT

The copyright in the text of individual articles in this ebook is the property of their respective authors or their respective institutions or funders. The copyright in graphics and images within each article may be subject to copyright of other parties. In both cases this is subject to a license granted to Frontiers.

The compilation of articles constituting this ebook is the property of Frontiers.

Each article within this ebook, and the ebook itself, are published under the most recent version of the Creative Commons CC-BY licence. The version current at the date of publication of this ebook is CC-BY 4.0. If the CC-BY licence is updated, the licence granted by Frontiers is automatically updated to the new version.

When exercising any right under the CC-BY licence, Frontiers must be attributed as the original publisher of the article or ebook, as applicable.

Authors have the responsibility of ensuring that any graphics or other materials which are the property of others may be included in the CC-BY licence, but this should be checked before relying on the CC-BY licence to reproduce those materials. Any copyright notices relating to those materials must be complied with.

Copyright and source acknowledgement notices may not be removed and must be displayed in any copy, derivative work or partial copy which includes the elements in question.

All copyright, and all rights therein, are protected by national and international copyright laws. The above represents a summary only. For further information please read Frontiers' Conditions for Website Use and Copyright Statement, and the applicable CC-BY licence.

ISSN 1664-8714
ISBN 978-2-8325-7491-1
DOI 10.3389/978-2-8325-7491-1

Generative AI statement
Any alternative text (Alt text) provided alongside figures in the articles in this ebook has been generated by Frontiers with the support of artificial intelligence and reasonable efforts have been made to ensure accuracy, including review by the authors wherever possible. If you identify any issues, please contact us.

About Frontiers

Frontiers is more than just an open access publisher of scholarly articles: it is a pioneering approach to the world of academia, radically improving the way scholarly research is managed. The grand vision of Frontiers is a world where all people have an equal opportunity to seek, share and generate knowledge. Frontiers provides immediate and permanent online open access to all its publications, but this alone is not enough to realize our grand goals.

Frontiers journal series

The Frontiers journal series is a multi-tier and interdisciplinary set of open-access, online journals, promising a paradigm shift from the current review, selection and dissemination processes in academic publishing. All Frontiers journals are driven by researchers for researchers; therefore, they constitute a service to the scholarly community. At the same time, the *Frontiers journal series* operates on a revolutionary invention, the tiered publishing system, initially addressing specific communities of scholars, and gradually climbing up to broader public understanding, thus serving the interests of the lay society, too.

Dedication to quality

Each Frontiers article is a landmark of the highest quality, thanks to genuinely collaborative interactions between authors and review editors, who include some of the world's best academicians. Research must be certified by peers before entering a stream of knowledge that may eventually reach the public - and shape society; therefore, Frontiers only applies the most rigorous and unbiased reviews. Frontiers revolutionizes research publishing by freely delivering the most outstanding research, evaluated with no bias from both the academic and social point of view. By applying the most advanced information technologies, Frontiers is catapulting scholarly publishing into a new generation.

What are Frontiers Research Topics?

Frontiers Research Topics are very popular trademarks of the *Frontiers journals series*: they are collections of at least ten articles, all centered on a particular subject. With their unique mix of varied contributions from Original Research to Review Articles, Frontiers Research Topics unify the most influential researchers, the latest key findings and historical advances in a hot research area.

Find out more on how to host your own Frontiers Research Topic or contribute to one as an author by contacting the Frontiers editorial office: frontiersin.org/about/contact

Quasi-normal modes, non-selfadjoint operators and pseudospectrum: an interdisciplinary approach

Topic editors
Jose Luis Jaramillo — Université de Bourgogne, France
Piotr Bizon — Jagiellonian University, Poland

Topic coordinator
Edgar Gasperin — University of Lisbon, Portugal

Citation
Jaramillo, J. L., Bizon, P., Gasperin, E., eds. (2026). *Quasi-normal modes, non-selfadjoint operators and pseudospectrum: an interdisciplinary approach*. Lausanne: Frontiers Media SA. doi: 10.3389/978-2-8325-7491-1

Table of contents

frontiers | Frontiers in Physics

TYPE Editorial
PUBLISHED 28 January 2026
DOI 10.3389/fphy.2025.1753507

Check for updates

OPEN ACCESS

EDITED AND REVIEWED BY
Alex Hansen,
NTNU, Norway

*CORRESPONDENCE
José Luis Jaramillo,
jose-luis.jaramillo-martin@ube.fr

RECEIVED 24 November 2025
REVISED 01 December 2025
ACCEPTED 02 December 2025
PUBLISHED 28 January 2026

CITATION
Bizoń P, Gasperín E and Jaramillo JL (2026) Editorial: Quasi-normal modes, non-selfadjoint operators and pseudospectrum: an interdisciplinary approach.
Front. Phys. 13:1753507.
doi: 10.3389/fphy.2025.1753507

COPYRIGHT
© 2026 Bizoń, Gasperín and Jaramillo. This is an open-access article distributed under the terms of the Creative Commons Attribution License (CC BY). The use, distribution or reproduction in other forums is permitted, provided the original author(s) and the copyright owner(s) are credited and that the original publication in this journal is cited, in accordance with accepted academic practice. No use, distribution or reproduction is permitted which does not comply with these terms.

Editorial: Quasi-normal modes, non-selfadjoint operators and pseudospectrum: an interdisciplinary approach

Piotr Bizoń[1], Edgar Gasperín[2] and José Luis Jaramillo[3]*

[1]Institute of Theoretical Physics, Jagiellonian University, Kraków, Poland, [2]CENTRA, Departamento de Física, Instituto Superior Técnico IST, Universidade de Lisboa UL, Lisboa, Portugal, [3]Institut de Mathématiques de Bourgogne UMR 5584, Université Bourgogne Europe, CNRS, Dijon, France

KEYWORDS

quasi-normal modes, non-selfadjoint operators, non-normal dynamics, non-modal analysis, pseudospectrum, non-modal growth transients, black holes, optics and plasmonics

Editorial on the Research Topic
Quasi-normal modes, non-selfadjoint operators and pseudospectrum: an interdisciplinary approach

In recent years, quasi-normal mode frequencies, namely, the complex numbers encoding the linear response of "damped" resonators to external perturbations have acquired major importance in different settings of physics, ranging from astrophysical and theoretical problems in gravitational physics to the study of the scattering properties of optical nanoresonators. Beyond physics, this subject is directly related to the study of the spectral and dynamical properties of non-selfadjoint operators, a very active area of research in applied and fundamental mathematics with direct applications in physics, ranging from hydrodynamics and turbulence to non-Hermitian quantum mechanics. Despite these complementary interests and converging "working knowledge", research interactions among the involved subcommunities appear to be quite scarce. This Research Topic represents an effort to bring attention to the interdisciplinary nature of the research around the notion of quasi-normal modes and non-Hermitian -or non-selfadjoint- dynamics. As mentioned, this interdisciplinarity operates at multiple levels, extending from the dialogue between physics and mathematics to the interchanges among the different subcommunities within these two disciplines.

The notion of normal mode pervades physics, providing a common conceptual and technical thread among different subfields of research and offering a basis for the study of (conservative) linear dynamics. The key mathematical property underlying normal modes is the diagonalizability of self-adjoint operators in terms of an orthonormal basis, which is guaranteed by the "spectral theorem". Its validity extends to operators that commute with their adjoints, namely, "normal operators". Normal modes and their associated spectrum ("normal frequencies") stand as a cornerstone of the dynamics driven by such normal operators.

A fundamental change occurs in non-conservative systems driven by non-selfadjoint operators or, more generally, non-normal operators. Familiar normal modes are then substituted by "quasi-normal modes" (QNMs), which encode in an invariant manner the characteristic linear response of a system to external perturbations and indeed share some of the features of normal modes. However, the loss of the spectral theorem

critically impacts QNMs: their completeness is not guaranteed, their orthogonality is lost, and the corresponding eigenvalues in the spectrum are potentially unstable under small perturbations. "Non-normal dynamics" (Trefethen and Embree [1]) driven by these operators are then subject to characteristic non-normal effects that are absent in the normal case, such as spectral instabilities in QNM frequencies, growth transients, or pseudo-resonances [2]. These differences ultimately respond to a key contrast between the normal and non-normal operator theories: the respective structural status of the spectrum. Whereas the spectrum of normal (time-generator) operators provides a tight control of the full dynamics, in the non-normal case such control is not guaranteed by the spectrum alone—except for late dynamics—and specific tools from non-selfadjoint spectral theory are required.

Non-modal analysis (e.g., Schmid [3]) provides a framework for the study of non-normal dynamics by crucially incorporating concepts and tools from the (spectral) theory of non-self-adjoint operators. This Research Topic highlights the notion of pseudospectra and their relation to QNMs and their properties. Pseudospectra sets in the complex frequency plane contain, notably, the (QNM) spectrum set, but also encode more information crucial to seize all of the dynamics, in particular, the above-mentioned non-normal effects. However, whereas the spectrum concept is built only on the operator itself, the pseudospectra depend on the choice of scalar product and associated norm. The same applies to other key non-modal analysis tools, in particular the "growth function", which is crucial in the study of non-modal growth transients and the assessment of optimal disturbances (see below). The question of the choice of the scalar product becomes a central theme in the non-modal analysis of non-normal dynamics, and in particular in this Research Topic.

We will now present the articles in this Research Topic. Given the interrelation among the contributions, the arrangement by category is somewhat "*ad hoc*", but we hope it illustrates the interdisciplinarity of the subject, both within the physics community and in its connection with ongoing mathematical developments.

1. Quasi-normal modes as an eigenvalue problem.

A key prerequisite for the application of non-normal dynamical concepts to scattering and QNMs is casting the dynamics in terms of a non-selfadjoint (non-normal) time generator. Building on the spacetime geometric insights developed in general relativity, Panosso Macedo and Zenginoğlu review the so-called hyperboloidal approach to scattering on black hole (BH) spacetimes. This geometric scheme provides the required non-selfadjoint operator, with non-normality being associated with losses through spacetime boundaries. BH QNMs are then cast as the eigenvalues of a non-selfadjoint spectral problem. Applications to QNM excitation coefficients, spectral QNM instability, and quadratic QNMs are presented. An interesting extension of such a hyperboloidal scheme to problems with dispersion (e.g., some quantum gravity-motivated problems) is presented in Burgess and König.

Another approach to casting resonances (QNMs) as an eigenvalue problem is the so-called complex scaling method (see, for example, Simon [4] and references therein). Although such a method is referred to in Warnick and Vogel, it is not really discussed in this Research Topic. However, Richarte et al. discuss a spectral problem reminiscent of such complex scaling.They review the approach to QNMs as analytical continuations of bound states of an appropriate self-adjoint operator and, in particular, highlight a non-selfadjoint spectral issue: the failure of the method to recover QNMs whose analytic continuation is not in the domain where the operator defining the bound states is selfadjoint.

2. Non-normal spectral and dynamical aspects in gravitational (black hole) physics.

The first indications of non-normal behavior of QNMs in gravity were implicit in the seminal results on BH QNM instabilities presented in Aguirregabiria and Vishveshwara [5]; Vishveshwara [6] and in Nollert [7]; Nollert and Price [8]. However, it was precisely the hyperboloidal approach, reviewed in Panosso Macedo and Zenginoğlu that allowed to establish transparently in Jaramillo et al. [9] the essential role of non-normal mechanisms. That was the starting point of the rapid development of non-normal dynamics in the gravitational context, one of the main subjects of this Research Topic.

2.i. Black hole QNM spectral (in)stabilities.

Warnick presents the first mathematically rigorous account in the literature of the BH QNM instability phenomenon. Characterized as a "perturbative" spectral instability, an analytical discussion in terms of QNM "modes" and "co-modes" is presented. Sensitivity to perturbations is enhanced as damping increases, a feature that is explained in terms of the need to control higher derivatives to properly define increasing QNM overtones. This feature can be (dually) interpreted as a *spectral stability in high-order Sobolev norms*or, equivalently, as a *spectral instability in the "energy norm"*, the consequence of distributing energy over small scales. A generalization of pseudospectra is introduced, tailored to the non-normality of the operators appearing in the BH scattering problem.

In a complementary work, Boyanov disentangles the confusion between the instability discussed in Warnick from another important BH QNM instability, referred to as the "flea on the elephant" (reminiscent of Simon [10]). These two spectral instabilities respond to distinct instability mechanisms; the first one corresponds to the "perturbation instability" of (already) existing QNMs, whereas the second one involves a "branch instability" with the appearance of a new family of QNMs.

Other aspects of pseudospectra and spectral instability are presented in the articles by Areán et al., Besson et al., Burgess and König, Drysdale and Johnson, Krejčiřík and Siegl, and Vogel.

2.ii. Non-modal growth transients in black holes.

Besson et al. review the first studies on non-modal growth transients in the gravitational setting, namely, for fields scattered on BHs. The discussion covers both frequency (pseudospectrum) and time-domain approaches, crucially presenting the first studies of the time-domain growth function $G(t)$ for BHs. The role of the norm choice for non-modal growth transients is highlighted, something that is further emphasized in Díaz Palencia, where the control of the dynamics of perturbations on BHs is discussed. These articles on growth transients pave the way for the systematic application of non-modal analysis to study non-normal dynamical effects in gravity. Forced systems—that in general relativity arise from second-order perturbation theory–leading to pseudo-resonances, would be a natural next step. Non-modal growth transients are also discussed in the article by Drysdale and Johnson.

3. QNMs and non-normality in high-energy physics.

Areán et al. review holographic duality, also referred to as the AdS/CFT correspondence or gauge/gravity duality, namely, a strong/weak coupling duality between a boundary gauge field theory and a bulk gravitational one. Focus is placed on holographic QNMs controlling the return to thermal equilibrium in the boundary gauge theory, providing a link to "linear response theory" and the Schwinger-Keldysh formalism. The spectral instability and pseudospectra of holographic QNMs are discussed. Non-modal transients in the holographic setting are also reviewed in Besson et al.

4. Quasi-normal modes in optics and plasmonics.

Wu and Lalanne review the remarkable development that QNM theory has recently experienced in optics and plasmonics. Focus is placed on the role of QNM theory in designing and understanding micro- and nano-resonators, which play a key role in current photonics, with an emphasis on the notions of "mode hybridization" and "mode perturbation". As an instance of optics-gravity interdisciplinarity, and motivated by the study of the fiber optical soliton, Burgess and König present an adaptation of the spacetime hyperboloidal approach to scattering and QNMs (see also Al Sheikh [11]) to settings with dispersion. This development is crucial in optics and in some dispersive modified gravity theories.

5. Mathematical aspects of non-normality.

We collect here articles from the Research Topic that cover mathematical subjects and range from pseudospectra, spectral instability and random perturbations, oriented graphs and networks, and partial differential equation (PDE) hyperbolicity. They harmoniously complement the physical contributions:

5.i. Krejčiřík and Siegl discuss the pseudospectrum from the perspective of "pseudomodes", a notion of approximate eigenvector that is not to be confused with QNMs, although it is relevant to the study of the spectral instability of the latter. In particular, a construction of pseudomodes for large "pseudoeigenvalues" is discussed using tools that do not rely on semi-classical analysis. This construction may be relevant in the context of the spectral instability of highly damped BH QNMs, as discussed above.

5.ii. Vogel presents a mathematical account of the pseudospectrum, focusing on three important topics: pseudospectra of semi-classical pseudodifferential operators; pseudospectra of random matrices; and eigenvalue asymptotics of non-selfadjoint random operators; (cf. also Sjöstrand [12]). Particularly important for the BH QNM spectral (perturbative) instability presented above is the discussion of eigenvalue asymptotics and "regularity improvement" for non-selfadjoint random operators.

5.iii. Drysdale and Johnson discuss the directionality of a directed graph, from the non-normality of the associated adjacency matrix. Then, the relation to the "trophic coherence" of a network is studied, and following the analysis, it is suggested to extend the notion of trophic coherence to matrices beyond the network setting, in particular in the context of (non-normal) dynamics and non-modal transients.

5.iv. Abalos et al. discuss the characterization of "strong hyperbolicity" in evolution PDE systems with constraints, in particular through "extensions" of the PDE system with additional variables. Strong hyperbolicity is then controlled by a condition involving the singular value decomposition of the (square matrix) principal symbol of the resulting PDE system. Studying the (non-)normality of the principal symbol may then be a good starting point for assessing the interplay of non-modal effects and hyperbolicity.

In summary, the study of scattering and QNMs from a non-normal dynamics perspective, by adopting a non-modal analysis approach, offers a rich arena for interdisciplinary research at the interface between physics and mathematics, and, within the physics realm, among gravity, optics, and hydrodynamics.

Author contributions

PB: Writing – review and editing. EG: Writing – review and editing. JJ: Writing – review and editing, Writing – original draft.

Funding

The author(s) declared that financial support was received for this work and/or its publication. This work was supported by the European Commission Marie Skłodowska-Curie Grant No. 843152 (Horizon 2020 programme), the ANR "Quantum Fields interacting with Geometry" (QFG) project (ANR-20-CE40-0018-02), the EIPHI Graduate School (contract ANR-17-EURE-0002) and Bourgogne-Franche-Comté Region, and the Narodowe Centrum Nauki, grant no. 2017/26/A/ST2/00530.

Acknowledgements

We would like to thank all the contributors in this Research Topic for their committed work. We would like to thank specially Mauro Pirarba, whose extraordinary editorial engagement and professionalism has rendered this Research Topic possible.

Conflict of interest

The author(s) declared that this work was conducted in the absence of any commercial or financial relationships that could be construed as a potential conflict of interest.

Generative AI statement

The author(s) declared that generative AI was not used in the creation of this manuscript.

Any alternative text (alt text) provided alongside figures in this article has been generated by Frontiers with the support of artificial intelligence and reasonable efforts have been made to ensure accuracy, including review by the authors wherever possible. If you identify any issues, please contact us.

Publisher's note

All claims expressed in this article are solely those of the authors and do not necessarily represent those of their affiliated organizations, or those of the publisher, the editors and the reviewers. Any product that may be evaluated in this article, or claim that may be made by its manufacturer, is not guaranteed or endorsed by the publisher.

References

1. Trefethen L, Embree M. *Spectra and pseudospectra: the behavior of nonnormal matrices and operators*. Princeton, NJ: Princeton University Press (2005).

2. Trefethen LN, Trefethen AE, Reddy SC, Driscoll TA. Hydrodynamic stability without eigenvalues. *Science* (1993) 261:578–84. doi:10.1126/science.261.5121.578

3. Schmid PJ. Nonmodal stability theory. *Annu Rev Fluid Mech* (2007) 39:129–62. doi:10.1146/annurev.fluid.38.050304.092139

4. Simon B. Resonances and complex scaling: a rigorous overview. *Int J Quan Chem* (1978) 14:529–42. doi:10.1002/qua.560140415

5. Aguirregabiria JM, Vishveshwara CV. Scattering by black holes: a simulated potential approach. *Phys Lett A* (1996) 210:251–4. doi:10.1016/0375-9601(95)00937-X

6. Vishveshwara CV. On the black hole trail. In: *18th Conference of the Indian Association for General Relativity and Gravitation Madras*. Madras, India: Institute of Mathematical Science Report, by Madras Univ. Inst. Math. Sci. (1996). p. 11–22.

7. Nollert H-P. About the significance of quasinormal modes of black holes. *Phys Rev D* (1996) 53:4397–402. doi:10.1103/PhysRevD.53.4397

8. Nollert H-P, Price RH. Quantifying excitations of quasinormal mode systems. *J Math Phys* (1999) 40:980–1010. doi:10.1063/1.532698

9. Jaramillo JL, Panosso Macedo R, Al Sheikh L. Pseudospectrum and black hole quasinormal mode instability. *Phys Rev X* (2021) 11:031003. doi:10.1103/PhysRevX.11.031003

10. Simon B. Semiclassical analysis of low lying eigenvalues. iv. the flea on the elephant. *J Functional Analysis* (1985) 63:123–36. doi:10.1016/0022-1236(85)90101-6

11. Al Sheikh L. Scattering resonances and pseudospectrum: stability and completeness aspects in optical and gravitational systems. Theses. Université Bourgogne Franche-Comté (2022). . Available online from: https://theses.hal.science/tel-04116011

12. Sjöstrand J. *Non-self-adjoint differential operators, spectral asymptotics and random perturbations Pseudo-Differential Operators*. New York: Springer International Publishing (2019). Available online from: https://www.springer.com/gp/book/9783030108182

frontiers | Frontiers in Astronomy and Space Sciences

TYPE Brief Research Report
PUBLISHED 20 August 2024
DOI 10.3389/fspas.2024.1426406

Check for updates

OPEN ACCESS

EDITED BY
Jose Luis Jaramillo,
Université de Bourgogne, France

REVIEWED BY
Izzet Sakalli,
Eastern Mediterranean University, Türkiye
Carlos Frajuca,
Federal University of Rio Grande, Brazil
Juan A. Valiente Kroon,
Queen Mary University of London,
United Kingdom

*CORRESPONDENCE
José Luis Díaz Palencia,
joseluis.diaz.p@udima.es

RECEIVED 01 May 2024
ACCEPTED 24 July 2024
PUBLISHED 20 August 2024

CITATION
Díaz Palencia JL (2024) Scalar field solutions and energy bounds for modeling spatial oscillations in Schwarzschild black holes based on the Regge–Wheeler equation. *Front. Astron. Space Sci.* 11:1426406. doi: 10.3389/fspas.2024.1426406

COPYRIGHT
© 2024 Díaz Palencia. This is an open-access article distributed under the terms of the Creative Commons Attribution License (CC BY). The use, distribution or reproduction in other forums is permitted, provided the original author(s) and the copyright owner(s) are credited and that the original publication in this journal is cited, in accordance with accepted academic practice. No use, distribution or reproduction is permitted which does not comply with these terms.

Scalar field solutions and energy bounds for modeling spatial oscillations in Schwarzschild black holes based on the Regge–Wheeler equation

José Luis Díaz Palencia*

Department of Mathematics and Education, Universidad a Distancia de Madrid, Madrid, Spain

This text discusses the behavior of solutions and the energy stability within Schwarzschild spacetimes, with a particular emphasis on the behavior of massless scalar fields under the influence of a non-rotating and spherically symmetric black hole. The stability of solutions in the proximity of the event horizon of black holes in general relativity remains an open question, especially given the difficulties introduced by minor perturbations that may resemble Kerr solutions. To address this, this work explores a simplified model, including massless scalar fields, to better understand perturbation behaviors around black holes under the Schwarzschild approach. We depart from Richard Price's work in connection with how scalar, electromagnetic, and gravitational fields behave. The tortoise coordinate transformation is considered to set the stage for numerical solutions to the wave equations. Afterward, we explore energy estimates, which are used to gauge stability and wave behavior over time. Our analysis reveals that the time evolution of the energy does not exceed twice its initial value. Further and under the assumption of initial conditions in L^2–spaces, we obtain an exponential decreasing behavior in the energy time evolution. A question to continue exploring is how perturbations in L^2 in the initial conditions that introduce Kerr solutions as a second-order effect in the linearized equations perturb this obtained exponential decay.

KEYWORDS

Schwarzschild spacetimes, Quasinormal modes, scalar fields, energy estimates, waves solutions

1 Introduction and problem formulation

The study of the formation and evolution of black holes and the physical processes occurring in their vicinity is an important area of contemporary research. As an example, we can cite the importance of understanding the behavior of primordial black holes (PBHs), which constitute a research area of notable impact for describing dark matter interactions (De Luca et al., 2020). A major unresolved challenge in general relativity is the nonlinear stability of Schwarzschild solutions, which is complicated by the fact that small perturbations in the initial data can inadvertently include Kerr solution characteristics. The presence of an ergosphere further complicates deriving meaningful energy estimates for perturbed Schwarzschild solutions, particularly for rotating black holes or those that are slightly rotating due to perturbations, for example. One relevant option to characterize

black holes is based on the study of their quasinormal modes (QNMs) (see (Kokkotas and Schmidt (1999) and Nollert (1999) for detailed definitions), the damped oscillations of black hole spacetimes, which can provide descriptions when spacetimes are slightly deformed from the Kerr solution (Zimmerman et al., 2015). For Schwarzschild black holes immersed in electromagnetic fields, the perturbation equations can be transformed into confluent Heun's equations, enabling both analytical and numerical analyses of QNMs (Övgün et al., 2018). Greybody factors (GFs) and QNMs are also relevant in the understanding of the radiation spectra emitted by black holes, particularly under the forms of gravitational waves (Sakallı and Kanzi, 2022). Additionally, the relationship between black hole entropy, spin, and QNMs, particularly when considering non-extensive entropies, provides microstates and thermodynamic properties of black holes, with significant modifications for micro black holes (Martínez-Merino and Sabido, 2022).

It is prudent to consider a simplified problem, given the complexities involved in proving the full stability of Schwarzschild solutions. One approach is to investigate the linearized problem, focusing on the stability of the zero solutions. Another simplification can be achieved by considering a simpler linear field theory, such as the linear scalar field. An additional simplification involves restricting the analysis to spherically symmetric cases (Rendall, 2008). In the study of linear massless scalar fields within the context of Schwarzschild spacetime, the Regge–Wheeler equation provides a framework for analyzing perturbations around a Schwarzschild black hole (Regge and Wheeler, 1957). Price (1972) used this framework to derive the long-term behavior of these perturbations. Price's work is particularly relevant for understanding how scalar fields, such as electromagnetic and gravitational fields, behave in the vicinity of a black hole, which may lead to phenomena such as wave scattering and the late-time tail behavior of these fields.

In a Schwarzschild spacetime describing the gravitational field outside a spherically symmetric, non-rotating, uncharged mass, a massless scalar field μ is well known to obey the Klein–Gordon equation for a massless particle:

$$\Box\mu = 0$$

Here, $\Box$ denotes the d'Alembertian operator in generally curved spacetime.

Price's investigations revealed that outside a black hole, perturbations from a massless field decay over time, but interestingly, they do so in a manner that leaves a "tail" of radiation (Price, 1972; Rendall, 2008). This tail is not an immediate cutoff but a slow, power-law decay of the field's amplitude over time. Specifically, Price showed that after the initial wavefront passes, the field decays as $t^{-(2l_0+3)}$, where t is time, and l_0 is the multipole moment (or angular quantum number) of the perturbation. This result implies that the gravitational influence of a black hole extends beyond its immediate vicinity, affecting the propagation of scalar fields over long periods.

In this work, we will make use of the transformation to the tortoise coordinate r^* and the introduction of a scaled wave function $\psi = r\phi$, where ϕ, the original wave function, describes the scalar field. This framework simplifies the analysis of wave equations in Schwarzschild spacetime by flattening the potential barrier experienced by waves as they approach the event horizon (Rendall, 2008).

Let us introduce some basic concepts to derive the main equation to be discussed in this work, typically referred to as the Regge–Wheeler Equation 3. Consider the scalar field ϕ in spherical coordinates (t, r, θ, ϕ) and the spherical harmonics with indices l and m, $Y_{lm}(\theta, \phi)$. Using the tortoise coordinate (as it will be introduced later) along with a radial symmetry condition leads to considering the problem's rotational invariance (Rendall, 2008; Zhao et al., 2022). Then, it holds that

$$\mu(t, r, \theta, \phi) = \sum_{l=0}^{\infty} \sum_{m=-l}^{l} \psi_{lm}(t, r)\, Y_{lm}(\theta, \phi).$$

Here, $\psi_{lm}(t, r)$ are the radial and time-dependent components of the field. For the Schwarzschild metric, the determinant g is $-r^2 \sin\theta$, and the inverse metric components $g^{\mu\nu}$ are

$$g^{tt} = -\left(1 - \frac{2M}{r}\right)^{-1}, \quad g^{rr} = 1 - \frac{2M}{r}, \quad g^{\theta\theta} = \frac{1}{r^2},$$
$$g^{\phi\phi} = \frac{1}{r^2 \sin^2\theta}.$$

The massless Klein–Gordon equation, $\Box\mu = 0$, in this metric becomes

$$-\left(1 - \frac{2M}{r}\right)^{-1} \partial_t^2 \mu + \frac{1}{r^2} \partial_r \left(r^2 \left(1 - \frac{2M}{r}\right) \partial_r \mu\right) + \frac{1}{r^2} \Delta_\Omega \mu = 0,$$

where Δ_Ω is the angular part of the Laplacian in spherical coordinates:

$$\Delta_\Omega \mu = \frac{1}{\sin\theta} \partial_\theta (\sin\theta \partial_\theta \mu) + \frac{1}{\sin^2\theta} \partial_\phi^2 \mu.$$

Substituting the expansion of μ,

$$\mu(t, r, \theta, \phi) = \sum_{l=0}^{\infty} \sum_{m=-l}^{l} \psi_{lm}(t, r)\, Y_{lm}(\theta, \phi),$$

we obtain

$$-\left(1 - \frac{2M}{r}\right)^{-1} \sum_{l,m} \ddot{\psi}_{lm}(t, r)\, Y_{lm} + \frac{1}{r^2} \partial_r \left(r^2 \left(1 - \frac{2M}{r}\right) \partial_r \sum_{l,m} \psi_{lm} Y_{lm}\right) + \frac{1}{r^2} \sum_{l,m} \psi_{lm} \Delta_\Omega Y_{lm} = 0.$$

Using the property of spherical harmonics,

$$\Delta_\Omega Y_{lm} = -l(l+1)\, Y_{lm},$$

we separate the angular and radial parts:

$$-\left(1 - \frac{2M}{r}\right)^{-1} \ddot{\psi}_{lm} + \frac{1}{r^2} \partial_r \left(r^2 \left(1 - \frac{2M}{r}\right) \partial_r \psi_{lm}\right) - \frac{l(l+1)}{r^2} \psi_{lm} = 0.$$

Introducing the tortoise coordinate r_* as

$$\frac{dr^*}{dr} = \left(1 - \frac{2M}{r}\right)^{-1}, \tag{1}$$

the radial part of the Klein–Gordon equation can be written as

$$\left(\frac{\partial^2}{\partial t^2} - \frac{\partial^2}{\partial (r^*)^2} - F_l(r^*)\right) \psi_{lm}(t, r^*) = 0, \tag{2}$$

This decomposition leads to a radial wave equation where $F_l(r^*)$ appears as the effective potential (this can be further observed in our results given in Figure 2) and adopts the following expression:

$$F_l(r^*) = \left(1 - \frac{2M}{r}\right)\left(\frac{l(l+1)}{r^2} + \frac{2M}{r^3}\right),$$

and the spherical harmonics $Y_{lm}(\theta,\phi)$ are given by

$$Y_{lm}(\theta,\phi) = (-1)^m \sqrt{\frac{(2l+1)}{4\pi}\frac{(l-m)!}{(l+m)!}} P_{lm}(\cos\theta)\, e^{im\phi},$$

where $P_{lm}(\cos\theta)$ are the associated Legendre polynomials. The indices l and m are integers with $l \geq 0$ and $-l \leq m \leq l$. The index l determines the total angular momentum, while m determines the projection of the angular momentum on the z-axis.

Upon integration in the Equation (1), the tortoise coordinate r^* can be rewritten as

$$r^* = r + 2M \log\left(\frac{r-2M}{2M}\right)$$

This coordinate stretches the region near the event horizon at $r = 2M$ for a Schwarzschild black hole of mass M. The tortoise coordinate is well known to facilitate the analysis of fields near and at the event horizon. Here, r is the usual radial coordinate in Schwarzschild spacetime.

We now introduce some relevant objectives of our work. We aim to study the QNMs based on Equation 2 with the potential $F_l(r^*)$, in line with Zhao et al. (2022) and Balart et al. (2023) and, more particularly, the behavior of such QNMs with respect to the tortoise coordinate. The QNMs represent solutions to the wave equation that behave like damped oscillations that decay over time, emitting gravitational waves in the process. Hence, and to start our analysis with more familiar assessments, we assume that the QNMs are given based on an expression of the form: $\psi(r^*,t) = e^{-i\omega t}\Psi(r^*)$ and this expression can be written for all m,l so we omit the sub-index for simplification in notation. In addition, we consider a description of the field subjected to the potential $F_l(r^*)$. Then, substituting into the wave Equation 2 and dividing by $e^{-i\omega t}$ yields

$$-\omega^2\Psi(r^*) - \frac{\partial^2\Psi}{\partial(r^*)^2} = F_l(r^*)\,\Psi(r^*).$$

Rearranging terms,

$$\frac{\partial^2\Psi}{\partial(r^*)^2} + \left[\omega^2 - F_l(r^*)\right]\Psi(r^*) = 0. \tag{3}$$

This equation can be seen as analogous to the time-independent Schrödinger equation,

$$-\frac{\hbar^2}{2m_p}\frac{\partial^2\Psi}{\partial x^2} + V(x)\Psi = E\Psi,$$

where the term $[\omega^2 - F_l(r^*)]$ is analogous to the energy E (minus the potential energy $V(x)$) in the Schrödinger equation. Hence, we may consider the theory of potentials available to resolve the Schrödinger-type equations. In the first step, we will provide some numerical solutions for this last equation to describe the behavior of waves with regard to the tortoise coordinate, and afterward, we provide energy estimates to describe the time evolution.

2 Methodology

In the first step, we introduce a numerical implementation to describe the behavior of the wave function described by the radial wave in (Equation 3) along with the effective potential $F_l(r^*)$. The transformation from the Schwarzschild radial coordinate r to the tortoise coordinate r^* is given by expression (5) and provides the non-invertibility of this transformation. Analytically, numerical methods are required to back-calculate r from r^*.

We note that the numerical solutions were obtained using well-established numerical methods, specifically Python's texttttscipy.integrate.solve_ivp function with the solvers "BDF" (Implicit multi-step method) and "LSODA" (that switches between the Adams and BDF methods). The initial range for r^* is selected to ensure that the execution of the routines provides plausible solutions within the requested global error tolerance fixed at 10^{-3}. The numerical process includes continuously validating the numerical solution against expected behaviors and refining the integration parameters to achieve convergence and accuracy.

In the second step, we combine analytical and numerical methods to derive energy estimates for scalar field perturbations in the context of a Schwarzschild non-rotating black hole. Such energy estimates are formulated using the integral of the energy density over the tortoise coordinate, and we employ Poincaré's inequality to control the energy estimates. In addition, we introduce numerical simulations to confirm the theoretical predictions and to show that the energy decays over time following an exponential law provided that the initial conditions belong to L^2 space.

3 Numerical solutions

The numerical solutions illustrated in the graphs in Figure 1 represent the solutions to Equation 2 in the vicinity of the horizon $r \sim 2M$. These solutions were assumed to have the form $\psi(r^*,t) = e^{-i\omega t}\Psi(r^*)$ and to be far from the horizon for increased values of r^*. For our purposes, we consider a fixed time $t = t_0 = 1.0$. Near the horizon ($r \sim 2M$), the potential $V(r^*)$ becomes very small, and the wave equation simplifies to a free wave equation. In addition and in this particular region (given for the coordinate r^* going to negative values), Figure 1 allows us to observe the diverging behavior for a black hole mass of 10 times the solar mass and for different values of angular momentum number l. Indeed, the behavior of $\psi(r^*)$ in this region is dominated by oscillatory modes (refer to Mamani et al. (2022) for additional discussions). Notably, the oscillatory nature is consistent with the expected QNMs behavior, where the modes oscillate but in the time domain (refer again to Keir (2020)). Note that the number l has a significant impact on the transmission and reflection coefficients for wave scattering by the black hole (refer to Futterman et al. (1988) for additional insights), and this may lead to potential avenues for extracting physical information from observational data (Sathyaprakash and Schutz, 2009), a relevant issue in observational astronomy (see Virtanen et al. (2020)).

Based on the provided Figure 1, we can observe an exponentially diverging asymptotic behavior of the wave functions near the horizon for different values of the angular momentum quantum number l. As r^* approaches large negative values, the wave functions $\Psi(r^*)$ in all three panels show an exponential divergence. This

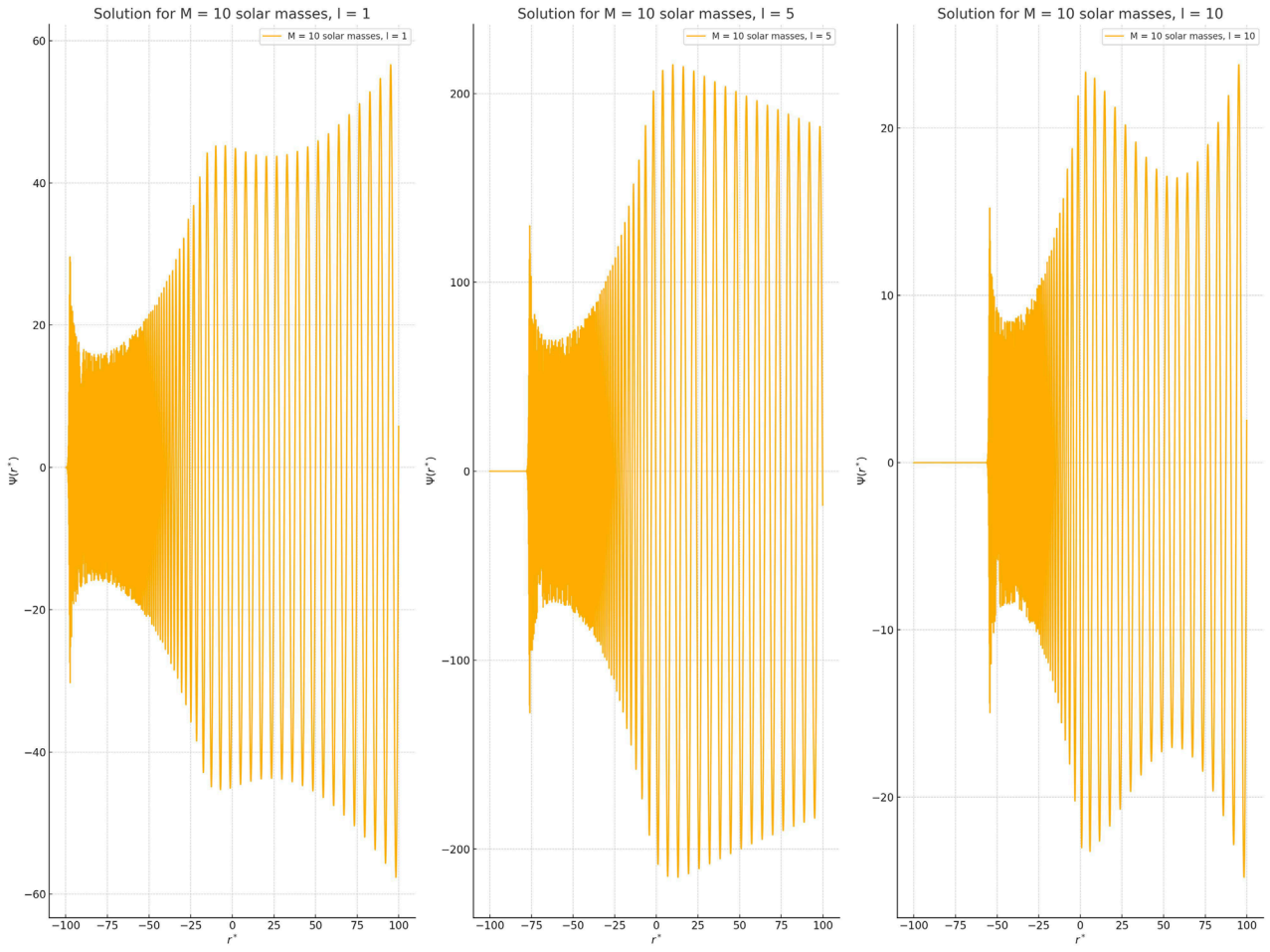

FIGURE 1
Real part of the wave functions $\psi(r^*)$ as a function of the tortoise coordinate r^* for a Schwarzschild black hole with mass $M = 10$ solar masses, for different angular momentum quantum numbers l. The left panel shows $l = 1$, the middle panel shows $l = 5$, and the right panel shows $l = 10$. The exponential divergence near the horizon (left negative values in r^*) increases oscillation complexity for higher l values.

behavior is more pronounced with oscillations superimposed on the exponential growth. This exponential divergence is a characteristic feature near the event horizon and aligns with previous studies (see Zhao et al. (2022)). For small l values (left panel), the exponential divergence starts relatively smoothly, with clear oscillations. As l increases (middle and right panels), the oscillations become more rapid, and the exponential growth becomes more abrupt. Additionally, we observe a form of amplitude modulation in the wave functions, which is considered to be a result of the interference between different modes. As Berti et al. (2009) explain, the QNMs of black holes are not single-frequency oscillations but rather a spectrum of modes with different complex frequencies. When these modes interfere, they can produce beat-like patterns in the wave functions. This interference leads to the observed amplitude modulation, where the envelope of the wave function oscillations varies in a regular pattern. However, there is a key point: throughout the numerical resolution, the value of the frequency ω was fixed to a constant value in the term $e^{-i\omega t}$. Therefore, it is important to mention that the modulations in Figure 1 are due to the spatial modulation effect, not the temporal modulation attributed to temporal propagation. In this regard, we highlight that in conducting numerical analyses to understand the effect of oscillations with respect to the tortoise coordinate, it has been necessary to consider certain values for the frequencies of the QNMs that appear in the temporal phase of the solution $\psi(r^*, t) = e^{-i\omega t}\Psi(r^*)$. For this purpose, different values compatible with the conditions given in [Fig. 5 ref (Berti et al., 2009)] have been considered. Furthermore, the observed behavior shown in Figure 1 has been tested for a wide range of ω values, exhibiting behaviors similar to the ones represented in the mentioned figure.

In addition, we should note that Zhao et al. (2022) provided graphical solutions in this direction, but certain other issues (like additional wave behavior for different values of m, l) were not contemplated, thus motivating us to include our analysis and to discuss further the implications. In addition, Keir (2020) concluded the existence of sublogarithmic time decay rates in the quasimodes for two-charge geometries, but there is no direct result to consider for the evolution with a radial coordinate and even further based on the tortoise coordinate.

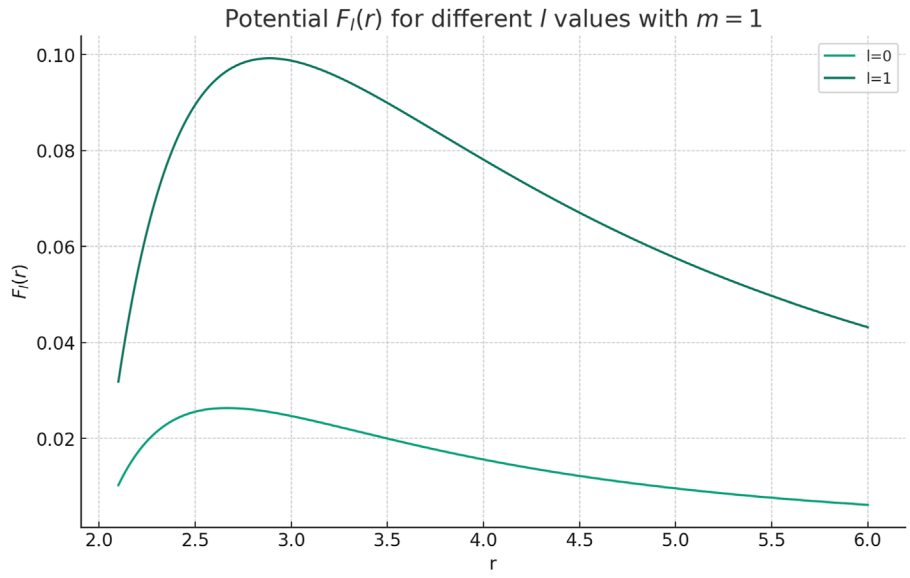

FIGURE 2
Potential $F_l(r)$ as a function of r for $l = 0$ and $l = 1$.

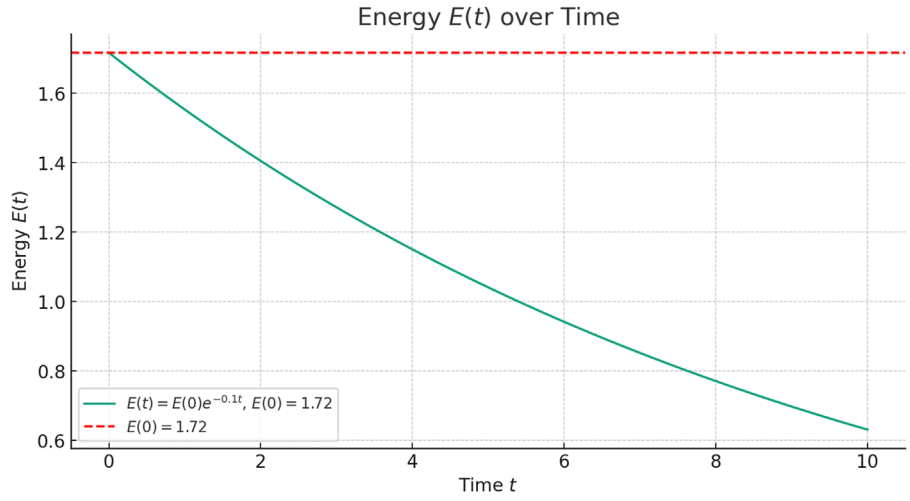

FIGURE 3
The energy $E(t)$ decays over time from its initial value $E(0)$. The horizontal dashed line represents $E(0)$, showing that the initial energy is constant at its initial value, while $E(t)$ decays exponentially from this initial value.

4 Energy estimates

In the context of a Schwarzschild non-rotating black hole (with no ergoregion, or, if experienced, the ergoregion is considered as a second-order negligible term in our linear equations), making energy estimates is feasible both near the event horizon and far from it by utilizing the tortoise coordinate r^*. The Schwarzschild metric admits a static Killing vector field ∂_t that remains time-like everywhere outside the event horizon. The effective potential $F_l(r^*)$ derived from the Schwarzschild metric diminishes at large distances, simplifying the wave equation to a free wave equation, which allows the introduction of energy estimates. In addition, we shall note that the integration of the energy density over a large volume provides estimates of the total energy in the scalar field perturbation, applicable both in the strong regime for $r \sim 2M + \epsilon$ (where ϵ is a positive arbitrary perturbation to avoid convergence issue in the energy integral because of the event horizon) and the weak regime for $r \gg 2M$.

An energy estimate for Equation 2 can be constructed by considering the integral of the energy density over all space in the tortoise coordinate (the reader is referred to Section 8.9 of Rendall (2008) for additional details on energy formulations in wave equations under the frame of general relativity). This energy integral

is given by

$$E = \int \left(\left| \frac{\partial \psi}{\partial t} \right|^2 + \left| \frac{\partial \psi}{\partial r^*} \right|^2 + F_l(r^*) |\psi|^2 \right) dr^*,$$

which includes the kinetic, gradient, and potential energies of the function ψ.

This integral is conserved for time-symmetric perturbations and can be used to study the stability of solutions to the wave equation (refer to Section 6.3 in Wald (1984), where the energy formulation with the static Killing field is a constant of motion in both the strong and weak regimes).

To compute the energy E, one would typically take the initial data of ψ and its derivatives and perform the integration over r^* from $-\infty^+$ (where the super-index+ reflects the strong condition near the horizon given by the radial coordinate $r \sim 2M + \epsilon$) to $+\infty$. In practice, this involves calculating the wave function ψ and its derivatives at all points in space at a given time and then integrating these quantities. Assuming ψ vanishes sufficiently far from the black hole, we can apply the Poincaré inequality to control the norm of ψ by the norm of its derivative:

$$\int_{-\infty^+}^{\infty} |\psi|^2 \, dr^* \leq C_P \int_{-\infty^+}^{\infty} \left| \frac{\partial \psi}{\partial r^*} \right|^2 dr^*,$$

where C_P is a positive constant specific to the domain. This inequality essentially implies that the overall size of ψ is bounded by how much ψ changes, providing a way to estimate the function's magnitude through its gradient. In our case, the use of Poincaré's inequality is of interest, as the effect of the potential given by $|\psi|^2$ is controlled by the term $\left| \frac{\partial \psi}{\partial r^*} \right|^2$ that is the energy contribution of the spatial derivative of the homogeneous wave equation. In other words, we can control the energy of the wave function with potential via the energy of the wave function formulated with a homogeneous equation without potential.

Hence, using the Poincaré inequality, we express the energy functional $E(t)$ bounded as follows:

$$\begin{aligned} E(t) &\leq \int_{-\infty^+}^{\infty} \left(\left| \frac{\partial \psi}{\partial t} \right|^2 \right) dr^* + \int_{-\infty^+}^{\infty} \left| \frac{\partial \psi}{\partial r^*} \right|^2 dr^* \\ &\quad + \max\left(F_l(r^*)\right) \int_{-\infty^+}^{\infty} |\psi|^2 dr^*, \end{aligned}$$

$$\begin{aligned} &\leq \int_{-\infty^+}^{\infty} \left(\left| \frac{\partial \psi}{\partial t} \right|^2 + \left| \frac{\partial \psi}{\partial r^*} \right|^2 \right) dr^* \\ &\quad + C_P \max\left(F_l(r^*)\right) \int_{-\infty^+}^{\infty} \left| \frac{\partial \psi}{\partial r^*} \right|^2 dr^*, \end{aligned}$$

and $F_l(r^*)$ is bounded. Indeed, near the horizon ($r \to 2M$), the term $\left(1 - \frac{2M}{r}\right)$ vanishes as r approaches $2M$, thus $F_l(r^*)$ approaches zero. In addition, as $r \to \infty$, both terms $\frac{2M}{r^3}$ and $\frac{l(l+1)}{r^2}$ in the potential decay to zero. Hence, $F_l(r^*)$ asymptotically approaches zero, indicating that the potential does not contribute significantly at far distances.

Finally, incorporating the control on $F_l(r^*)$ and adjusting constants appropriately, the energy estimate is refined as

$$E(t) \leq C_E \left(\int_{-\infty^+}^{\infty} \left(\left| \frac{\partial \psi}{\partial t} \right|^2 + \left| \frac{\partial \psi}{\partial r^*} \right|^2 \right) dr^* \right),$$

where C_E is a new constant that encapsulates all previous constants and the behavior of $F_l(r^*)$.

Now, consider the initial conditions for a wave function ψ defined in the tortoise coordinate r^* at time $t = 0$:

$$\psi(0, r^*) = \psi_0(r^*), \quad \frac{\partial \psi}{\partial t}(0, r^*) = \psi_1(r^*).$$

Then,

$$E(0) = \int_{-\infty^+}^{\infty} \left(|\psi_1(r^*)|^2 + \left| \frac{d\psi_0}{dr^*} \right|^2 \right) dr^*.$$

To link $E(t)$ to $E(0)$, we can consider a general relation of the form:

$$E(t) \leq f(t) E(0),$$

where $f(t)$ is a function that captures the growth or decay dynamics of the energy depending on wave propagation. To obtain a precise function $f(t)$, we first consider the bound for $E(t)$, and it is standard to check that the associated wave equation is homogeneous. Hence, let us consider the solution of the homogeneous wave equation by d'Alembert's formula:

$$\psi(t, r^*) = \frac{1}{2} \left[\psi_0(r^* + t) + \psi_0(r^* - t) \right] + \frac{1}{2} \int_{r^* - t}^{r^* + t} \psi_1(s) \, ds.$$

Taking derivatives,

$$\begin{aligned} \frac{\partial \psi}{\partial t}(t, r^*) &= \frac{1}{2} \left[\psi_0'(r^* + t) - \psi_0'(r^* - t) \right] \\ &\quad + \frac{1}{2} \left[\psi_1(r^* + t) - \psi_1(r^* - t) \right], \end{aligned}$$

$$\begin{aligned} \frac{\partial \psi}{\partial r^*}(t, r^*) &= \frac{1}{2} \left[\psi_0'(r^* + t) + \psi_0'(r^* - t) \right] \\ &\quad + \frac{1}{2} \left[\psi_1(r^* + t) + \psi_1(r^* - t) \right]. \end{aligned}$$

The energy computation over time leads to

$$\begin{aligned} E(t) \leq \int_{-\infty^+}^{\infty} \Bigg(&\left| \frac{1}{2} \left(\psi_0'(r^* + t) - \psi_0'(r^* - t) \right) + \frac{1}{2} \left(\psi_1(r^* + t) - \psi_1(r^* - t) \right) \right|^2 \\ &+ \left| \frac{1}{2} \left(\psi_0'(r^* + t) + \psi_0'(r^* - t) \right) + \frac{1}{2} \left(\psi_1(r^* + t) + \psi_1(r^* - t) \right) \right|^2 \Bigg) dr^*. \end{aligned}$$

Using the triangle inequality, we can estimate

$$|\psi_0'(r^* \pm t)|^2 + |\psi_1(r^* \pm t)|^2$$

as a sum over $r^* \pm t$.

Thus, $E(t)$ could be bounded by twice the sum of the energy norms of the initial conditions:

$$\begin{aligned} E(t) \leq\ & 2 \left(\int_{-\infty^+}^{\infty} |\psi_0'(r^* + t)|^2 dr^* \right) \\ &+ 2 \left(\int_{-\infty^+}^{\infty} |\psi_0'(r^* - t)|^2 dr^* \right) \\ &+ 2 \left(\int_{-\infty^+}^{\infty} |\psi_1(r^* + t)|^2 dr^* \right) \\ &+ 2 \left(\int_{-\infty^+}^{\infty} |\psi_1(r^* - t)|^2 dr^* \right) \end{aligned}$$

Now, let us assume that the initial data belong to the norm L^2. Mathematically, this is appropriate using the translation-invariance properties of the L^2 norm:

$$E(t) \leq 2 \left(\|\psi_0'\|_{L^2}^2 + \|\psi_1\|_{L^2}^2 \right)$$

where

$$\|\psi_0'\|_{L^2}^2 = \int_{-\infty^+}^{\infty} \left| \frac{d\psi_0}{dr^*} \right|^2 dr^*, \quad \|\psi_1\|_{L^2}^2 = \int_{-\infty^+}^{\infty} |\psi_1(r^*)|^2 dr^*.$$

Therefore, $E(t)$ is bounded by twice the initial energy $E(0)$:

$$E(t) \leq 2E(0)$$

This bound suggests the conservation and controlled growth of energy. Nonetheless, the last expression does not consider any dispersion on the field that may be given as the wave evolves. Specifically, as t increases, the contributions from ψ_0 and ψ_1 spread out over a larger region, effectively diluting the local energy density (refer to Taylor (1996) and Trefethen and Embree (2005) for additional insights).

To determine a new bound, we consider the L^∞ norm instead of the energy formulation and recover some basic aspects of wave propagation. Note that considering a norm connected with the amplitude, such as the L^∞ norm, is relevant because gravitational wave interferometers (unlike traditional electromagnetic observatories) respond to the waves' amplitude to characterize events (refer to Section 9.5 of Berti et al. (2009)). The fundamental solution for the wave equation for a point source located at the origin is given by

$$\Phi(t,x) = \frac{\delta(t-|x|)}{4\pi|x|}.$$

The solution to the wave equation with initial conditions ψ_0 and ψ_1 is represented by

$$\begin{aligned}\psi(t,x) = &\int_{\mathbb{R}^3} \frac{\delta(t-|y|)}{4\pi|y|}\psi_1(y)\,dy \\ &+\int_{\mathbb{R}^3} \frac{\partial}{\partial t}\left(\frac{\delta(t-|y|)}{4\pi|y|}\right)\psi_0(y)\,dy.\end{aligned}$$

This integrates over a spherical shell of radius t:

$$\psi(t,x) = \frac{1}{4\pi t}\int_{|y|=t}\psi_1(y)\,dS_y + \frac{1}{4\pi t}\int_{|y|=t}\partial_t\left(\delta(t-|y|)\right)\psi_0(y)\,dS_y.$$

Considering L^∞ norms, the solution's maximum amplitude at any point decays as

$$\begin{aligned}\|\psi(t,\cdot)\|_{L^\infty} \approx &\frac{1}{t}\left\|\int_{|y|=t}\psi_1(y)\,dS_y\right\|_{L^\infty} \\ &+\frac{1}{t}\left\|\int_{|y|=t}\partial_t\left(\delta(t-|y|)\right)\psi_0(y)\,dS_y\right\|_{L^\infty}.\end{aligned}$$

The surface area of the sphere of radius t is $4\pi t^2$. As the energy spreads over a larger area, the maximum amplitude at any point decreases. Given that the energy is conserved but distributed over an increasing surface area $A = 4\pi t^2$, the amplitude's reduction follows:

$$\|\psi(t,\cdot)\|_{L^\infty} \propto \frac{1}{\sqrt{t}}.$$

This $t^{-\frac{1}{2}}$ decay rate in the L^∞ norm is due to the inverse square root of the increasing area over which the energy is spread and considers the typical dispersion effect in three dimensions.

Now, the Strichartz estimates for the wave equation provide bounds on the solution's spacetime norms in terms of the norms of the initial data and allow us to consider other functional spaces compared with the L^∞ in time. Specifically, the estimates state:

$$\|\psi\|_{L_t^\infty L_x^6(\mathbb{R}\times\mathbb{R}^3)} \leq C\left(\|\psi_0\|_{\dot{H}^1(\mathbb{R}^3)} + \|\psi_1\|_{L^2(\mathbb{R}^3)}\right),$$

where C is a constant dependent on the dimension and the Strichartz pair. This estimate is derived from the fundamental solution's dispersive properties and the conservation of energy (refer to Tao (2006) for additional insights).

Using the Sobolev embedding theorem, which embeds $\dot{H}^1(\mathbb{R}^3)$ into $L^6(\mathbb{R}^3)$, we can relate the Strichartz norms to the L^∞ norm:

$$\|\psi(t,\cdot)\|_{L^\infty(\mathbb{R}^3)} \leq C' t^{-\frac{1}{2}}\left(\|\psi_0\|_{\dot{H}^1(\mathbb{R}^3)} + \|\psi_1\|_{L^2(\mathbb{R}^3)}\right),$$

where C' includes constants from the Sobolev embedding and the dimension-specific Strichartz estimates. The constant C' is determined by considering the spherical dispersion of energy and the associated decrease in amplitude as the wave spreads over a sphere with increasing radius $r = t$. The factor $t^{-\frac{1}{2}}$, introduced *ad hoc*, reflects the decrease in amplitude over the sphere's surface area $4\pi t^2$. Thus, C' can be calculated as

$$C' = \frac{C''}{\sqrt{4\pi}},$$

with C'' being a constant derived from spectral analysis of the wave operator and the embedding constants used in the Sobolev and Strichartz inequalities. Such spectral analysis is normally a difficult task with high mathematical content, but we can introduce some principles to elucidate how to determine the constant. Indeed, in Schwarzschild spacetime, the wave operator $\Box$ for a scalar field ψ, defined in a curved background, is given by $\Box\psi = \frac{1}{\sqrt{-g}}\partial_\mu(\sqrt{-g}g^{\mu\nu}\partial_\nu\psi)$, where $g_{\mu\nu}$ is the metric tensor of Schwarzschild spacetime, and g is the determinant of this metric tensor. The Laplacian in Schwarzschild coordinates is expressed as

$$\begin{aligned}\Delta_{\text{Sch}}\psi = &\frac{1}{r^2}\left(1-\frac{2M}{r}\right)^{-1}\frac{\partial}{\partial r}\left(r^2\left(1-\frac{2M}{r}\right)\frac{\partial\psi}{\partial r}\right) \\ &+\frac{1}{r^2\sin\theta}\frac{\partial}{\partial\theta}\left(\sin\theta\frac{\partial\psi}{\partial\theta}\right)+\frac{1}{r^2\sin^2\theta}\frac{\partial^2\psi}{\partial\phi^2}.\end{aligned}$$

The spectral properties of Δ_{Sch} in Schwarzschild spacetime differ fundamentally from those in $\mathbb{R}^3$. The continuous spectrum is altered by the potential well created by the black hole. If we hypothesize a spectral density function $\rho_{\text{Sch}}(\lambda)$ (here we would need additional physical observations), analogous to the flat space case but adjusted for curvature effects, and integrate this over a bounded domain reflecting the effective potential's influence, we have

$$C''_{\text{Sch}} = \int_{\lambda_0}^{\infty}\rho_{\text{Sch}}(\lambda)\,d\lambda,$$

where λ_0 is a lower bound that accounts for significant gravitational effects near the black hole. A value for such λ_0 can be analytically conceived, given the potential $F_l(r^*)$. Indeed, the potential usually features a peak that influences wave dynamics; this peak can act as a barrier beyond which wave propagation diminishes. The value of λ_0 could be estimated by considering the minimum energy (or corresponding λ) required for a wave to have a significant presence beyond this peak. Mathematically, this is often taken to be the maximum value of the effective potential:

$$\lambda_0 = \max F_l(r).$$

Hence, we compute the derivative to find critical points where the potential may have a maximum:

$$\frac{dF_l}{dr} = \left(1-\frac{2M}{r}\right)\left(-\frac{6M}{r^4}-\frac{2l(l+1)}{r^3}\right)+\left(\frac{2M}{r^3}+\frac{l(l+1)}{r^2}\right)\left(\frac{2M}{r^2}\right).$$

After simplifying and setting to zero, we find $r_{\max}$:

$$\frac{12M^2}{r^6} - \frac{2M(1-2M-2l(l+1))}{r^5} + \frac{2Ml(l+1)}{r^4} = 0.$$

This equation is typically solved numerically given specific values of M and l. Once $r_{\max}$ is determined, $F_l(r_{\max})$ is calculated to estimate λ_0:

$$\lambda_0 = F_l(r_{\max}) = \left(1 - \frac{2M}{r_{\max}}\right)\left(\frac{2M}{r_{\max}^3} + \frac{l(l+1)}{r_{\max}^2}\right).$$

To provide some numerical orders of λ_0, we provide the assessments for the following cases:

A) $M = 1, \quad l = 0.$

B) $M = 1, \quad l = 1.$

For this, we have used Python and its libraries `NumPy` and `SciPy`, which provide efficient numerical routines. The results of λ_0 for the cases A) and B) mentioned are:

- λ_0 for $M = 1, \quad l = 0$: 0.0264
- λ_0 for $M = 1, \quad l = 1$: 0.0993

The plot displayed in Figure 2 shows the potential $F_l(r)$ as a function of r for each value of l. Some relevant observations from the graph indicate:

- The potential has a peak for each l, and these peaks are what we use to estimate λ_0.
- The potential increases as r increases, reaches a maximum, and then decreases again, which is a typical behavior of effective potentials and barriers.
- For $l = 1$, the potential reaches a higher peak than $l = 0$, which aligns with the calculated λ_0 values where λ_0 for $l = 1$ is greater than for $l = 0$.

4.1 Numerical assessments on the energy formulation

The discussion to this point has yielded an energy estimate expressed as

$$E(t) \leq 2E(0).$$

This estimate implies that the energy of the wave function at any time t does not exceed twice its initial value $E(0)$. However, this bound alone does not definitively determine how the energy evolves over time, but it does confirm that the evolution is controlled by the initial energy value. Certainly, this expression leaves open questions regarding potential energy dissipation, conservation, or other complex dynamics that could be exhibited. Hence, we conduct a numerical assessment to gain further details about whether the energy decreases or exhibits other patterns through time. We have carried out a simulation following numerical integration techniques using Python libraries. In the simulation, Gaussian initial data and a decaying sinusoidal initial time derivative were used:

$$\psi_0(r) = e^{-r^2}, \quad \psi_1(r) = \frac{\sin(r)}{1+r^2},$$

both of which belong to L^2 in the domain of integration. The energy at $t = 0$, denoted $E(0)$, was calculated based on these initial conditions. The plot provided in Figure 3 provides the results of the numerical analysis carried out, leading to a graph that depicts the energy $E(t)$ exponential decreasing evolution over time. This result aligns with the classical form of solutions considered to model QNMs and given by the temporal evolution $e^{-i\omega t}$, and we shall recall that our initial data were selected to belong to L^2.

5 Conclusion

This study provided an analysis of the behavior of scalar fields in Schwarzschild spacetime using the tortoise coordinate transformation and spherical harmonics decomposition. From the numerical assessments, we established the behavior of scalar fields considering the tortoise coordinate in Figure 1 for the simplified version of the wave in (Equation 3). In addition, we have obtained estimates for the energy under the L^2 norm and for the evolution of the waves in the L^∞ norm. Interestingly, we showed that a decreasing exponential bound applies for the energy evolution provided that the initial data belong to L^2–space. We postulate that such an evolving bound applies for any other L^2 initial distribution beyond the ones considered in Section 4.1. Another interesting question to explore further is how L^2 perturbations in the initial conditions, which introduce Kerr solutions as a second-order effect in the linearized equations, affect this obtained exponential decay. Certainly, this is a relevant issue that requires additional theoretical and numerical assessments. We will proceed with this in our future work.

Data availability statement

The original contributions presented in the study are included in the article/supplementary material, further inquiries can be directed to the corresponding author.

Author contributions

JD: conceptualization, investigation, data curation, formal analysis, funding acquisition, methodology, project administration, resources, software, supervision, validation, visualization, writing–original draft, writing–review and editing.

Funding

The author(s) declare that no financial support was received for the research, authorship, and/or publication of this article.

Conflict of interest

The author declares that the research was conducted in the absence of any commercial or financial relationships that could be construed as a potential conflict of interest.

Publisher's note

All claims expressed in this article are solely those of the authors and do not necessarily represent those of their affiliated organizations, or those of the publisher, the editors and the reviewers. Any product that may be evaluated in this article, or claim that may be made by its manufacturer, is not guaranteed or endorsed by the publisher.

References

Balart, L., Panotopoulos, G., and Rincón, Á. (2023). Regular charged black holes, energy conditions, and quasinormal modes. *Fortschr. Phys.* 71, 2300075. doi:10.1002/prop.202300075

Berti, E., Cardoso, V., and Starinets, A. O. (2009). Quasinormal modes of black holes and black branes. *Class. Quantum Gravity* 26, 163001. doi:10.1088/0264-9381/26/16/163001

De Luca, V., Franciolini, G., Pani, P., and Riotto, A. (2020). The evolution of primordial black holes and their final observable spins. *J. Cosmol. Astropart. Phys.* 2020 (April), 052. doi:10.1088/1475-7516/2020/04/052

Futterman, J. A. H., Handler, F. A., and Matzner, R. A. (1988). *Scattering from black holes*. Cambridge: Cambridge University Press.

Keir, J. (2020). Wave propagation on microstate geometries. *Ann. Henri Poincaré* 21, 705–760. doi:10.1007/s00023-019-00874-4

Kokkotas, K. D., and Schmidt, B. G. (1999). Quasi-normal modes of stars and black holes. *Living Rev. Relativ.* 2, 2. doi:10.12942/lrr-1999-2

Mamani, L. A. H., Masa, A. D. D., Sanches, L. T., and Zanchin, V. T. (2022). Revisiting the quasinormal modes of the Schwarzschild black hole: numerical analysis. *Eur. Phys. J. C* 82, 897. doi:10.1140/epjc/s10052-022-10865-1

Martínez-Merino, A., and Sabido, M. (2022). On superstatistics and black hole quasinormal modes. *Phys. Lett. B* 829, 137085. doi:10.1016/j.physletb.2022.137085

Nollert, H.-P. (1999). Quasinormal modes: the characteristic 'sound' of black holes and neutron stars. *Class. Quantum Gravity* 16 (R159), R159–R216. doi:10.1088/0264-9381/16/12/201

Övgün, A., Sakallı, İ., and Saavedra, J. (2018). Quasinormal modes of a Schwarzschild black hole immersed in an electromagnetic universe. *Chin. Phys. C* 42 (10), 105102. doi:10.1088/1674-1137/42/10/105102

Price, R. H. (1972). Nonspherical perturbations of relativistic gravitational collapse I scalar and gravitational perturbations. *Phys.Rev. D.* 5, 2419–2438. doi:10.1103/physrevd.5.2419

Regge, T., and Wheeler, J. A. (1957). Stability of a Schwarzschild singularity. *Phys. Rev.* 108 (4), 1063–1069. doi:10.1103/physrev.108.1063

Rendall, A. D. (2008). *Partial differential equations in general relativity*. Oxford, United Kingdom: Oxford Mathematics.

Sakallı, İ., and Kanzi, S. (2022). Topical Review: greybody factors and quasinormal modes for black holes in various theories - fingerprints of invisibles. *Turkish J. Phys.* 46 (2), 51–103. doi:10.55730/1300-0101.2691

Sathyaprakash, B. S., and Schutz, B. F. (2009). Physics, astrophysics and cosmology with gravitational waves. *Living Rev. Relativ.* 12, 2. doi:10.12942/lrr-2009-2

Tao, T. (2006). "Nonlinear dispersive equations: local and global analysis," in *CBMS regional conference series in mathematics, 106*. Providence, RI: American Mathematical Society. Provides a detailed discussion on Strichartz estimates for wave equations.

Taylor, M. E. (1996). *Partial differential equations: basic theory*. New York: Springer.

Trefethen, L. N., and Embree, M. (2005). *Spectra and pseudospectra: the behavior of nonnormal matrices and operators*. Princeton, NJ: Princeton University Press.

Virtanen, P., Gommers, R., Oliphant, T. E., Haberland, M., Reddy, T., Cournapeau, D., et al. (2020). SciPy 1.0: fundamental algorithms for scientific computing in Python. *Nat. Methods* 17, 261–272. doi:10.1038/s41592-019-0686-2

Wald, R. M. (1984). *General relativity*. Chicago: University of Chicago Press.

Zhao, Y., Sun, B., Mai, Z. F., and Cao, Z. (2022). *Quasi normal modes of black holes and detection in ringdown process*. Lausanne, Switzerland: Frontiers.

Zimmerman, A., Yang, H., Mark, Z., Chen, Y., and Lehner, L. (2015). "Quasinormal modes beyond Kerr," in *Gravitational wave astrophysics. Astrophysics and space science proceedings*. Editor C. Sopuerta (Cham: Springer), 40, 217–223. doi:10.1007/978-3-319-10488-1_19

frontiers | Frontiers in Physics

TYPE Brief Research Report
PUBLISHED 30 August 2024
DOI 10.3389/fphy.2024.1461106

Check for updates

OPEN ACCESS

EDITED BY
Jose Luis Jaramillo,
Université de Bourgogne, France

REVIEWED BY
Lamis Al Sheikh,
Gayte.it, France
Theo Torres,
UPR7051 Laboratoire de mécanique et d'acoustique (LMA), France

*CORRESPONDENCE
Tong Wu,
wutong1121@gmail.com
Philippe Lalanne,
philippe.lalanne@institutoptique.fr

RECEIVED 07 July 2024
ACCEPTED 19 August 2024
PUBLISHED 30 August 2024

CITATION
Wu T and Lalanne P (2024) Designing electromagnetic resonators with quasinormal modes.
Front. Phys. 12:1461106.
doi: 10.3389/fphy.2024.1461106

COPYRIGHT
© 2024 Wu and Lalanne. This is an open-access article distributed under the terms of the Creative Commons Attribution License (CC BY). The use, distribution or reproduction in other forums is permitted, provided the original author(s) and the copyright owner(s) are credited and that the original publication in this journal is cited, in accordance with accepted academic practice. No use, distribution or reproduction is permitted which does not comply with these terms.

Designing electromagnetic resonators with quasinormal modes

Tong Wu* and Philippe Lalanne*

Laboratoire Photonique, Numérique et Nanosciences (LP2N), IOGS- Université de Bordeaux-CNRS, Talence, France

Micro- and nanoresonators, which enable light trapping in small volumes for extended durations, play a crucial role in modern photonics. The optical response of these resonators is determined by their fundamental resonances, known as quasinormal modes (QNMs). Over the past decade, the electromagnetic theory of QNMs has undergone significant development and has now reached a level of maturity that allows its reliable application to numerous contemporary electromagnetic problems. In this review, we explore recent applications of QNM theory for designing and understanding micro and nanoresonators. We highlight why QNMs provide deep physical insights and enhance computational efficiency in scenarios involving mode hybridization and perturbation.

KEYWORDS

quasinormal modes 1, microcavities 2, plasmonic nanocavities 3, perturbation theory 4, inverse design 5

1 Introduction

Micro or nanoresonators play a crucial role in advancing modern photonics [1, 2]. The interaction of light with optical resonators is fundamentally governed by the excitation of intrinsic natural resonant modes. When excited by a pulse, these modes initially store energy and subsequently release it through exponential decay. Known as quasinormal modes (QNMs), they are source-free solutions, $[\tilde{\mathbf{E}}_m(\mathbf{r}), \tilde{\mathbf{H}}_m(\mathbf{r})]\exp(-i\tilde{\omega}_m t)$ to Maxwell's equations with complex frequencies $\tilde{\omega}_m$

$$\nabla \times \tilde{\mathbf{E}}_m = i\tilde{\omega}_m \mu_0 \tilde{\mathbf{H}}_m,\ \nabla \times \tilde{\mathbf{H}}_m = -i\tilde{\omega}_m \varepsilon(\mathbf{r}, \tilde{\omega}_m)\tilde{\mathbf{E}}_m, \tag{1}$$

and satisfy the outgoing-wave condition for $|\mathbf{r}| \to \infty$. Hereafter, $\tilde{\mathbf{E}}_m$ and $\tilde{\mathbf{H}}_m$ respectively denote the *normalized* electric and magnetic fields [3, 4], ε denotes the possibly dispersive permittivity tensors. Unlike the normal modes of Hermitian systems, which have real frequencies, the imaginary part $\mathrm{Im}(\tilde{\omega}_m)$ is non-zero, accounting for absorption or radiation losses [3].

The QNMs of electromagnetic resonators are characterized by two main quantities: their mode volume ($\tilde{V}_m$) and quality factor (Q_m) [4, 5]. The former is related to the spatial extent of the electromagnetic field and the latter is proportional to the confinement time in units of the optical period, $Q_m = -(1/2)\mathrm{Re}(\tilde{\omega}_m)/\mathrm{Im}(\tilde{\omega}_m)$ [3, 5, 6].

High-Q resonators trap light for long time, whereas small mode volume resonators confine light in tiny volumes. Resonators with large $Q_m/\tilde{V}_m$ ratios strongly enhance the interaction between the trapped photons and the host materials, giving rise to significant nonlinear, quantum and optomechanical effects [1–4].

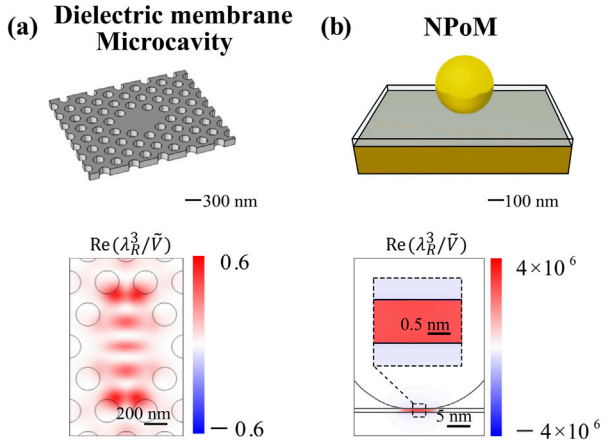

FIGURE 1
Examples of micro and nanocavities. **(A)** A photonic-crystal microcavity with a 330 nm lattice constant in a 320 nm-thick dielectric membrane has typical resonance wavelengths λ_R at 1.5 μm. **(B)** A metal NPoM structure consists of a faceted gold nanoparticle (radius R = 20 nm) separated from a gold substrate by a 1 nm-thick dielectric film. The maps depict the real part of the inverse mode volume, $\mathrm{Re}(1/\tilde{V}_m)$. The microcavity confines light within approximately λ_R^3, whereas the NPoM achieves a minimum mode volume of about $10^{-7}\,\lambda_R^3$. Note that the imaginary part, $\mathrm{Im}(1/\tilde{V}_m)$, of the mode volume is not shown. Adapted from [5].

Photonic applications generally rely on two types of structures which respectively offer high Q_m and small $\tilde{V}_m$. High- Q resonators, typically with $Q_m \sim 10^6$, are usually fabricated using lossless dielectric materials, such as the photonic crystal microcavities (Figure 1A). These structures can confine light for extended periods of time (typically Q_m cycles) within volumes of about the resonant wavelength cube λ_R^3.

Resonators with mode volumes significantly smaller than λ_R^3 are engineered using metallic nanostructures that support localized plasmons [7]. One notable example is the nanoparticle-on-mirror (NPoM) construct (Figure 1B) [2, 8], which represents a current area of research interest. NPoM trap light in nanometer-sized dielectric gaps between two metal surfaces, achieving mode volumes as small as $\sim 10^{-7}\,\lambda_R^3$. However, this exceptional spatial field confinement comes with a drawback: the inherent absorption of the materials restricts the quality factor to small values, $Q \sim 10 - 100$.

QNMs can be used to expand the electromagnetic field $\mathbf{E}^s(\mathbf{r},\omega)\exp(-i\omega t)$ scattered by resonators illuminated by monochromatic waves at frequency ω [3, 9]

$$\mathbf{E}^s(\mathbf{r},\omega) = \sum_m \alpha_m(\omega)\tilde{\mathbf{E}}_m(\mathbf{r}), \tag{2}$$

where the α_m's are modal excitation coefficients. The latter are known analytically and can be calculated as a spatial overlap between the normalized QNM field and the incident wave. They describe the contribution of the resonance modes to the optical response. A time-domain QNM expansion formula can also be derived from Equation 2 by performing a Fourier transformation from the frequency domain to the temporal domain

$$\mathbf{E}^s(\mathbf{r},t) = \mathrm{Re}\left[\sum_m \beta_m(t)\tilde{\mathbf{E}}_m(\mathbf{r})\right]. \tag{3}$$

In the past decade, there have been significant advancements in electromagnetic QNM theory. These include resolving the critical issue of QNM normalization [10–15], testing completeness of the QNM expansion across various systems [10, 16–23], and extending the analysis to the temporal domain [20, 24–27].

Nowadays, QNM theory is extensively utilized in designing optical resonators for various applications [28–30], including second- and higher-harmonic generation [31–33], optical parametric oscillators [34], Bell state generation [35], random lasing [36, 37], cavity QED [38–40], chiral molecule sensing [41, 42], quantum plasmonics [43–45], structural color generation [46], visual appearance generation [47], random medium [48], and ultrafast optics [24, 27]. But why are QNMs essential for nanoresonator design?

One explanation lies in the unique physical insights provided by QNM theory, which are often unattainable from brute-force numerical simulations. While the latter can be used to accurately compute the resonant spectra of resonator responses [2, 49–52], the spectrum interpretation can be indirect and sometimes incomplete. For instance, far-field incident light might not efficiently excite all modes, causing dark modes to be overshadowed by bright ones in the spectra. Additionally, spectrally overlapping resonances are difficult to distinguish, even with semi-analytical tools like the temporal-coupled mode theory [53, 54]. These resonances might merge to form a complex Fano response that appears as a single bell-like response, potentially leading to an incorrect interpretation with a single resonance [11, 55].

In contrast, QNMs are intrinsic to the system and independent of the incident field. By computing QNMs, optical dark modes can be identified unambiguously [56–60], and spectrally overlapping modes can be distinguished [11, 55, 61]. QNM expansion methods allow the reconstruction of optical scattering spectra [3, 9, 14, 20, 62, 63] with a weighted sum of QNMs. They may also provide explicit formula for the local density of electromagnetic states [11, 62, 64–67], a quantity of prime interest to interpret the optical response of resonators coupled with quantum emitters.

Another explanation is that electromagnetic QNM theory may also offer a significant improvement in computational efficiency over classical modeling tools that operate in the real-frequency or temporal domains. In frequency-domain simulations, calculations are repeated for each frequency, while in time-domain simulations, they must be repeated for different excitation fields.

The QNM expansion formula in Equation 2, which includes analytically-known α_m coefficients, allows efficient computation of the optical responses to arbitrary incident waves, once the dominant QNMs are determined [3, 68]. This efficiency is particularly useful for predicting the responses of resonant structures to various incident fields [69]. Applications include calculating the bidirectional reflectance distribution function (BRDF) of disordered metasurfaces [47], and assessing optical forces [70, 71], for instance.

Recent advancements in QNM perturbation [72, 73] and coupled QNM-theory [74–76] enable the prediction of the QNMs of altered geometries based on the QNMs of the initial geometry. They enhance computational efficiency not only for frequency sweeps but also for varying parameters such as shape or permittivity. This is particularly valuable for inverse design problems that require optical responses over plenty of parameter spaces.

This review aims to highlight recent advancements in applying QNMs to nanoresonator design, emphasizing the benefits of using QNM theory. Special focus is placed on how QNMs provide deep physical insights and enhance computational efficiency in mode

hybridization and perturbation scenarios. For readers interested in the detailed physics and mathematical properties of electromagnetic QNMs, references such as [3, 5, 9, 10] are recommended. This article is structured as follows: a brief overview of key concepts on electromagnetic QNMs, followed by a discussion of their applications in resonator design.

2 QNM theory in a nutshell

2.1 Computation of electromagnetic QNMs

The computation of electromagnetic QNMs is now routinely performed using mode solvers for Maxwell's equations [77]. The most common method involves calculating the poles of the resonator response (either a scattering-matrix element or a component of the scattered field at a specific spatial position) by driving the system with a source emitting at complex frequencies until the response diverges. Alternatively, one can directly solve the eigenvalue problem defined by Equation 1.

A few open-source software packages dedicated to QNM computation are available [77–79], including our comprehensive released freeware, MAN [68], which implements the pole-searching method or directly solves the eigenvalue problem.

2.2 The QNM divergence

QNM fields exponentially grow in space far away from the resonators, typically taking the form of a leaky spherical wave, $r^{-1}\exp[i\tilde{\omega}_m(-t+r/c)]$ as $r\to\infty$ in 3D open spaces. The spatial divergence has significantly slowed down the development of the electromagnetic QNM theory, just like in related areas, e.g., gravitational waves [80–84].

First, the spatial divergence raises difficulties in normalizing the QNMs fields [10]. Second, the spatial divergence also raises the question of whether the expansions of Equations 2, 3 are complete or not and when completeness is achieved, for what subspace [3, 85]. Indeed, note that the scattered field at real frequency always vanishes as r^{-1} for $r\to\infty$; it seems unlikely that expansions relying on fields that all divergence for $r\to\infty$ may capture the special decay. In addition to the issue of incompleteness, the divergence appears to contradict our physical intuition, raising doubts about whether it 'truly corresponds to any physical reality,' as was noted long ago [86].

These issues have been addressed through extensive efforts notably over the past three decades.

Various frameworks for QNM normalization have been developed [10–15, 87, 88], and the completeness of QNM expansions (possibly augmented by numerical modes arising from QNM regularization [16, 20]) has been verified analytically and numerically in numerous examples [10, 16–23]. A recent review [10] provides advanced details and traces historical errors.

One widely adopted normalization framework is the PML-regularization method [11]. In this approach, the continuous Maxwell operator from Equation 1 is replaced by a linear operator within a finite physical domain bounded by perfectly matched layers (PMLs). The latter maps infinite open spaces into regularized Hilbert spaces, by converting the exponential growth of QNM fields in open space to an exponential decay within the PMLs. The regularized QNMs become square-integrable and are normalized with a volume integral over the physical domain Ω inside the PML and the PML domain Ω_{PML}

$$\iiint_{\Omega\cup\Omega_{PML}} \tilde{\mathbf{E}}_m\cdot\frac{\partial\omega\varepsilon}{\partial\omega}\tilde{\mathbf{E}}_m-\tilde{\mathbf{H}}_m\cdot\frac{\partial\omega\mu}{\partial\omega}\tilde{\mathbf{H}}_m d^3\mathbf{r}=1. \tag{4}$$

With Equation 4, analytical expressions for the modal expansion coefficients can be derived from first-principle calculations [11, 20]. Moreover, the QNM expansion augmented by numerical modes is complete for all $\mathbf{r}$ within the regularized space, including the PML domain. For non-dispersive resonators, biorthogonality warranties the uniqueness of the expansion coefficients α_m. In the presence of dispersion, formulas of α_m depend on the choosing of the auxiliary field used for linearization and different methods for splitting the source term in Maxwell equation. Once these factors are defined α_m is also uniquely determined [10, 18, 20].

The PML regularization offers a framework to mimic the Hermitian system, by ensuring completeness and eliminating divergence. However, it does not offer a clear physical interpretation of the implications of the impact of QNM spatial divergence when analyzing the interaction of resonance with remote bodies positioned far away from resonators, where QNM fields largely diverge, as demonstrated in a recent study [89]. This study confirms that although QNM divergence leads to spectral instability, it does not cause any inconsistencies. The optical response of resonators disturbed by a distant body remains largely unchanged and can be accurately predicted using first-order QNM perturbation theory. It is also noteworthy that similar conclusions have been drawn in the context of gravitational waves [90–92].

3 Applications of QNMs in the design of optical resonators

The essence of resonance design involves perturbing and hybridizing resonances to achieve specific optical responses. Traditionally, this process involves performing repeated full-wave simulations at real frequencies [2, 28, 49–52]. However, as mentioned in the introduction, this conventional approach encounters significant physical and computational limitations. In this section, we explore several examples to demonstrate how QNM methods overcome these challenges and facilitate the design of modern optical resonators, focusing first on QNM hybridization and then on QNM perturbation.

3.1 QNM hybridization

The motivations for mode hybridization are twofold.

First, hybridization allows us to combine the properties of different resonant modes to create new modes with distinct multifunctional properties [56–61, 93–95], e.g., modes with both magnetic and electric responses [61, 93, 95–97], modes with both high radiative efficiency and small mode volume [2, 56, 58–60, 98]. A well-known example is the hybridization of photonic microcavities and plasmonic resonator modes [99–101]. This

approach utilizes plasmonic components to achieve deep subwavelength confinement (small mode volumes), while preserving a relatively high Q factor, which is inherited from the photonic cavity.

Second, hybridization induces a chemical-like "reaction" between modes, creating new modes with unique properties that go beyond a simple combination of the original modes. This serves as the second motivation for mode hybridization. For instance, when the eigenfrequencies of two QNMs cross each other as a parameter varies, the Q factor of one mode can be significantly boosted reaching exceptionally high values [33, 102, 103]. Additionally, some studies have engineered interactions between modes to achieve exceptional points [104–107], where both the eigenvalues and eigenvectors of the interacting modes coalesce.

3.1.1 Mixing mode properties

A key feature of the QNM framework is its ability to compute the intrinsic properties of resonators and understand how these properties are affected by mode hybridization [56–60]. This capability allows for the design and optimization of nanoresonators, offering both computational efficiency and clear physical insights. This aspect is illustrated in Figure 2, with a structure known as a picocavity [2, 108–110]. The latter consists of a NPoM, but additionally encompasses an individual atomic-scale protuberance on one of the gap surfaces, as shown in Figure 2A. This structure, which has recently garnered significant attention [2, 56, 57, 108–110], demonstrates an impressive capability to confine light.

Picocavities exhibit two types of QNMs [56, 57]. One type features an electric field that is highly localized near the protuberance, while the other exhibits electric field distributions akin to QNMs found in NPoM structures. We classify these as protuberance-like and NPoM-like QNMs, respectively. As depicted in Figure 2C, the protuberance-like QNM (mode II) provides extremely confined field characteristics, achieving a minimum mode volume below one cubic nanometer. However, due to the significant size disparity between the protuberance and the photon wavelength, this mode exhibits very low radiative efficiency. It cannot be efficiently excited by far-field sources (such as plane waves); when excited by a near-field emitter, almost all energy is converted into Ohmic losses in the metal, with minimal photon radiation in the far-field.

The mode volume of the NPoM-like mode (mode I) is much larger than that of the protuberance-like QNM. However, it offers high radiative efficiency and can be excited from the far-field. Its radiative efficiency, characterized by the intrinsic radiative diagram in Figure 2C, is approximately 20 times greater than that of the protuberance-like QNM.

A natural approach to achieve both high radiative efficiency and small mode volume involves coupling these two types of modes. The QNM framework facilitates monitoring the intrinsic properties as the modes hybridize. Figure 2B illustrates the eigenfrequencies of the hybridized QNMs as a function of the protuberance's aspect ratio, depicted by the red and blue solid curves. As the aspect ratio increases, the protuberance-like mode undergoes a redshift, and an anticrossing of resonant frequencies occurs when its eigenfrequency approaches the energy of the NPoM mode. In this region, the QNMs are significantly hybridized. As depicted in Figure 2C, both modes achieve a mode volume of less than 1 nm^3 and demonstrate high radiative efficiency, combining the advantageous characteristics of both NPoM and protuberance modes.

3.1.2 Engineering the mode interaction

Another significant application of QNM theory lies in engineering mode interactions [102, 111–113] to create new modes with properties distinct from a simple mixture of the original modes.

To illustrate our purpose, let us consider a resonator and let us deform it (Figure 3A). If we assume that two dominant QNMs are driving the resonator response, the new eigenfrequencies, $\tilde{\omega}_{hyb}$, of the deformed modes can be determined by solving a 2x2 eigenvalue problem [72]

$$\begin{pmatrix} \tilde{\omega}_1 & 0 \\ 0 & \tilde{\omega}_2 \end{pmatrix}\begin{pmatrix} a_1 \\ a_2 \end{pmatrix} = \tilde{\omega}_{hyb}\begin{pmatrix} 1+V_{11} & V_{12} \\ V_{21} & 1+V_{22} \end{pmatrix}\begin{pmatrix} a_1 \\ a_2 \end{pmatrix} \tag{5}$$

where $\tilde{\omega}_{1(2)}$ are the QNM eigenfrequencies of the undeformed structure, $\tilde{\omega}_{hyb}$ is the unknown eigenfrequency of the deformed structure, and a_1 and a_2 are the modal excitation coefficients of the unperturbed QNMs. The terms V_{ij} (with $i, j = 1, 2$) are evaluated through an integral of the modal fields over the surface S_r of the initial (undeformed) structure: $V_{ij} = \iint_{S_r} h\tilde{\mathbf{E}}_i^+ \cdot \Delta\boldsymbol{\varepsilon}(\tilde{\omega}_j)\tilde{\mathbf{E}}_j^- d^2\mathbf{r}$, where h is the deformation perpendicular to the surface boundary (it varies with the curvilinear coordinate), and $\tilde{\mathbf{E}}_i^+$ and $\tilde{\mathbf{E}}_j^-$ the electric fields of the initial (undeformed) normalized QNMs at the outer (+) or inner (−) surface boundary. Outward deformations ($h > 0$) and inward deformation ($h < 0$) deformations (see Figure 3A) correspond to permittivity changes of $\Delta\boldsymbol{\varepsilon}$ and $-\Delta\boldsymbol{\varepsilon}$, respectively, where $\Delta\boldsymbol{\varepsilon} = \boldsymbol{\varepsilon}_{res} - \boldsymbol{\varepsilon}_b$ is the difference in permittivity between the resonator and background.

The V_{ij} are generally complex numbers, with their imaginary parts arising from the non-Hermitian characteristics of the system. Typically, $V_{12} \neq V_{21}$, however if $\Delta\boldsymbol{\varepsilon}(\tilde{\omega}_2) \approx \Delta\boldsymbol{\varepsilon}(\tilde{\omega}_1)$, they are approximately equal.

The formula is derived using first-order approximations, ignoring contributions proportional to h^2 or higher-order terms for V_{ij}. Higher-order contributions can be included with more complex formulas. Nevertheless, except for specific cases where the first-order contribution vanishes due to symmetry, for instance, Equation 5 is accurate [72].

Using Equation 5, the new QNMs of the deformed structure are directly computed, enabling effective exploration of the parameter space to optimize the resonator shape. Figure 3B demonstrates the application of Equation 5 in designing nanoresonators that support exceptional points. This method significantly reduces the computation time needed to find the optimal design and provides insight into how geometric deformation influences mode hybridization.

3.2 Mode perturbation

QNM perturbation theory of electromagnetic resonators is particularly useful for cavity design and has been used in many applications, including evaluating optical resonator sensitivity for optical biosensing, inverse design of high-Q optical cavities [114], and understanding or engineering the interplay of classical

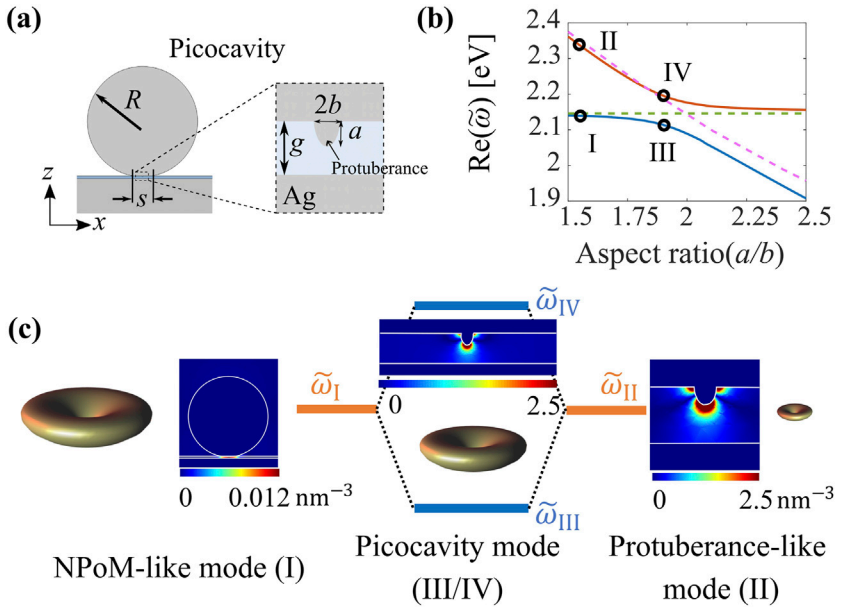

FIGURE 2
Mixing the properties of two QNMs by hybridization. **(A)** Schematic representation of a picocavity comprising an atomic-scale protuberance on a flat metal surface and a NPoM structure, each supporting a QNM. **(B)** Resonance frequencies as a function of the aspect ratio a/b of the protuberance. The mode of the protuberance strongly hybridizes with the mode of the NPoM for $a/b \approx 2$. **(C)** Energy level diagram illustrating the hybridization when the frequencies of the NPoM and protuberance modes are similar for $a/b = 2$. Outside the hybridization region, the structure exhibits an NPoM-like mode (QNM I in (b)) and a protuberance-like mode (QNM II in (b)). The NPoM-like mode has a relatively large mode volume and high radiative efficiency, while the protuberance-like mode features an ultra-small mode volume and a low radiative efficiency. The near-field maps depict the real part of the inverse mode volume $1/\tilde{V}_m$, while the far-field radiation diagrams illustrate how the normalized QNMs radiate in the far field. **(A)** and **(B)** are adapted from [56].

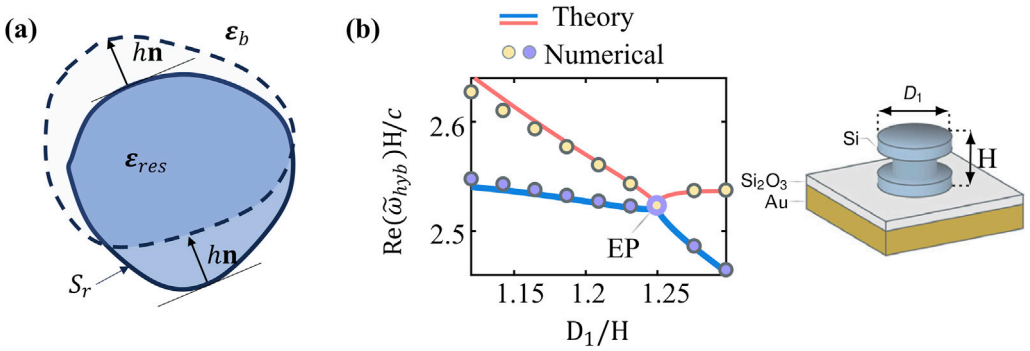

FIGURE 3
QNM interaction by deformation. **(A)** A nanoresonator is deformed with both inward and outward boundary changes. **(B)** Eigenfrequencies can be predicted with the analytical formula Equation 5 as we vary the shape. In **(B)**, an exceptional point (denoted 'EP') is designed by deforming a nanoresonator. Full numerical calculations (circles) are compared to predictions obtained with Equation 5 (solid curves). Adapted from [72].

electromagnetism with other physical phenomena or nonlinear processes, such as thermo-optics [115], Kerr [116, 117], or electron spill-out effects [43].

3.2.1 Perturbation theory for understanding refractive index changes

Traditionally, designing optical sensors involves calculating numerous resonance spectrum variations for various perturbation instances (such as position, shape, and material), which is time-consuming when using a parametric frequency scan approach. Furthermore, for very small perturbations, simulations must achieve extremely high accuracy to ensure that signal changes caused by the perturbation are not obscured by numerical noise.

Small perturbations cause a small change of the complex frequency of all the QNMs, as illustrated in Figure 4A. The

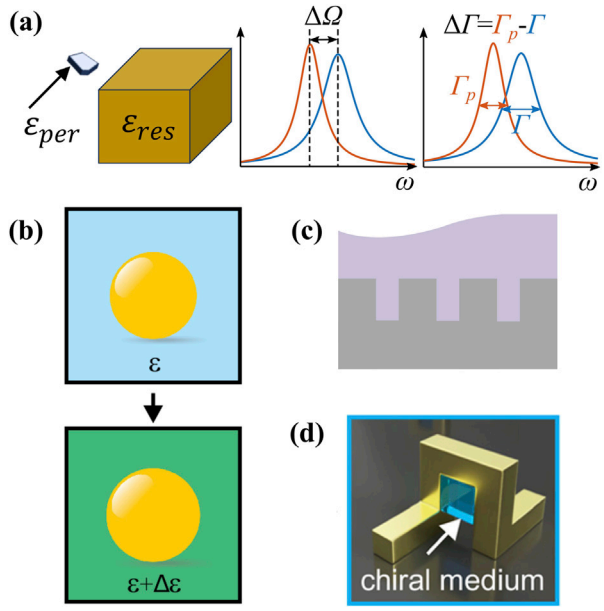

FIGURE 4
QNM perturbation theory for optical biosensors. **(A)** The introduction of a perturbation causes a resonant frequency shift $\Delta\Omega$ and a linewidth change $\Delta\Gamma$ in the spectral response (Equation 6) [118]. **(B)** The perturbation formula of Equation 6 has been extended for refractive-index changes extending over the entire open space surrounding the resonator [119]. **(C)** A perturbation formalism also exists for periodic structures [120]. **(D)** Perturbation formula has been developed for studying the index change caused by chiral mediums [41]. **(B)** is adapted from [119]; **(C)** is adapted from [120]; **(D)** is adapted from [41].

small variation is conveniently predicted using cavity perturbation theory.

The correct QNM normalization allows for deriving an accurate first-order perturbation formula for non-Hermitian systems [118].

$$\Delta\tilde{\omega}_m = -\tilde{\omega}_m \iiint_{\Omega_{per}} \Delta\varepsilon \tilde{\mathbf{E}}_m \cdot \tilde{\mathbf{E}}_m d^3\mathbf{r} + O(|\Delta\varepsilon|^2), \quad (6)$$

where Ω_{per} is the finite volume of the perturber, and $\Delta\varepsilon = \varepsilon_{per} - \varepsilon_u$ is the difference in permittivity between the perturbed and unperturbed systems.

The predictive force of Equation 6 has been successfully validated for high-Q cavities by comparison with experimental data [121] and for low-Q plasmonic nanoresonators by comparison with full-wave computational data for various perturber shapes [118].

We may have noticed a difficulty also encountered in gravitational wave theory [80–84]: as the separation distance between the perturber and the resonator increases, the QNM field experienced by the perturber diverges. According to Equation 6, $\Delta\tilde{\omega}_m$ should also diverge, contradicting our intuitive expectations that remote perturbers should not affect resonator characteristics. This apparent contradiction has been recently studied in detail [89]. The conclusion is clear: Equation 6 remains valid regardless of how far away the perturbations are.

The issue of remote perturbations and divergent coupling requires much care as it leads to spectral instabilities. The complex frequency plane becomes increasingly populated with numerous Fabry-Perot QNMs, and the optical response of the perturbed system is dominated by these Fabry-Perot QNMs instead of the initially perturbed one. Similar QNM instability issues are encountered in the gravitational wave physics of black holes [80–84, 90–92]. The instability, also called 'the flea in the elephant effect', is caused by a small and remotely localized perturbation added to the black hole environment.

Equation 6 allows for the analytical evaluation of a crucial figure-of-merit (FoM) for optical resonators used in sensing applications, given by FoM = $S/\Delta\lambda$. Here S represents the sensitivity, defined as the wavelength shift per unit change of the embedding medium refractive index, and $\Delta\lambda$ is the bandwidth of the resonance. Since $1/\Delta\lambda$ is proportional to the Q factor and S is proportional to $\Delta\tilde{\omega}_m$, from Equation 6, one can readily realize that FoM $\propto Q_m/\tilde{V}_m$, implying that an excellent candidate for an optical sensor should either possess a large Q or a small mode volume.

The QNM perturbation toolbox for nanophotonic biosensor design has significantly expanded in recent years [41, 119, 120, 122, 123]. Equation 6 is valid for finite resonators perturbed by perturbers with finite size. This result has been extended to perturbations that cover the entire open space surrounding finite size resonators or periodic structures [119, 120, 123]. Equation 6 has also been extended to study systems that are perturbed by magnetic objects [122] or chiral molecules [41]. Refer to Figure 4 for more pictural details.

More recently, QNM perturbation theory has been further extended to predict the impact of perturbations on the optical scattering matrix [9, 41]. This extension allows for the prediction of variations in optical responses, such as changes in spectrum intensity and lineshape, beyond just frequency shifts and linewidth changes. The theory has proven crucial in the design of nanophotonic sensors for chiral molecules [124, 125]. It facilitates the rapid computation of the difference in circular dichroism spectra (ΔCD) with and without a chiral molecule. This is particularly important because, according to one of the authors [126], if the Pasteur parameter κ of the chiral molecule is extremely small, obtaining ΔCD can be computationally expensive due to the need for fine meshing to ensure the signal is above numerical noise.

3.2.2 Inverse design of optical resonators

QNM perturbation theory can be especially useful for inverse design. Equation 6 is not accurate for this critical case, as boundary variations cause abrupt field changes inside the perturbation volume Ω_{per}. This issue can be resolved using a technique known as local-field correction [127], which accounts for abrupt field changes by considering boundary conditions or the continuity of the electric field. By using local-field correction and assuming the perturbation does not cause hybridization between different QNMs, the frequency shift caused by shape deformation is given by $\Delta\tilde{\omega}_m = -\tilde{\omega}_m \iint_{S_r} h\tilde{\mathbf{E}}_m^+ \cdot \Delta\boldsymbol{\varepsilon}(\tilde{\omega}_m)\tilde{\mathbf{E}}_m^- d^2\mathbf{r}$ [72, 118], where the variables are the same as those used in Equation 5. In fact, Equation 5 reduces to the present formula in the absence of mode hybridization.

One recent application of the formula can be found in [114], where QNM perturbation theory was used in combination with a gradient-based algorithm to maximize the Q-factor of cavities formed in dielectric slabs with disordered nanoholes.

3.2.3 Quantum effect

QNM perturbation theory has also been successfully applied to understand the role of quantum effects in the response of nanoresonators with ultrasmall volumes, such as NPoM structures or picocavities. In these systems, strong confinement leads to non-classical effects, such as nonlocality and electron spill-out, which cannot be predicted by Maxwell's equations alone [128]. To accurately model these effects, numerical sampling must be significantly smaller than the Fermi wavelength, which is typically well below 1 nm [129]. This poses a significant challenge for incorporating quantum effects into classical Maxwell solvers.

QNM perturbation theory can potentially address this issue by treating non-classical effects as first-order perturbations of classical QNM fields. This approach allows for the analytical prediction of eigenfrequency changes due to non-classical corrections [43]. Recent advancements have further streamlined the computation of optical responses, such as Purcell factors and field enhancement factors [45]. They offer a quick method to evaluate how non-classical effects impact the optical properties of nanoresonators, including field confinement capability and scattering efficiency.

4 Perspectives and conclusion

Over the past decade, substantial advancements have been made in electromagnetic QNM theory, effectively addressing numerous critical challenges. The normalization of QNMs has been resolved [10–14], the completeness of QNM expansions has been confirmed for a variety of systems [10, 20, 21, 74], and the physical implications and causes of QNM divergence are beginning to be understood [89].

These developments have facilitated the creation of various analytical QNM frameworks that significantly improve the design and comprehension of micro and nanoresonators. In this review, we have highlighted recent progress, showcasing their benefits in offering greater numerical efficiency and physical insights compared to traditional design approaches. We hope this will encourage a wider adoption of QNMs and further innovation in electromagnetism and other areas of physics.

Despite these successes, research on QNMs in electromagnetism continues vigorously and several open questions remain.

One of the foremost issues is the convergence of QNM reconstruction, as described in Equations 2, 3. Achieving robust convergence is complex and influenced by numerous factors, including the material properties of the resonators [68], the choice of the formula for α_m [17, 18], and the configuration of perfectly matched layers (PML) used for regularization [19]. Currently, the community lacks a definitive guideline on optimizing these parameters to improve convergence.

Another unresolved issue is understanding the existence of various QNM decomposition formulas. As discussed in Section 2.2, in dispersive systems, the formula for α_m is sensitive to the choice of auxiliary fields and source terms. Although all formulas share a resonant pole term $1/(\tilde{\omega}_m - \omega)$, they differ in a non-resonant term $f(\omega)$, which is a slow-varying function of ω. Recent studies have shown that certain choice of $f(\omega)$ leads to β_m in Equation 3, derived from α_m, exhibiting an instantaneous response term [27, 130]. It would be important to verify that $f(\omega)$ for all the formulas offer a consistent physical interpretation.

From an application standpoint, there are numerous domains where QNM theory has yet to be fully utilized. For instance, QNM theory could potentially be applied to the analysis of spectra in photoemission electron microscopy (PEEM) [24], electron energy-loss spectroscopy (EELS), or high-order nonlinear optics [131], offering new insights and computational methods in these fields.

Finally, the recent interest in time-varying nanoresonators [132, 133], whose optical properties can be modulated on time scales comparable to the oscillation period of electromagnetic fields, has opened up new avenues for QNM research. Extending the QNM framework to model the optical response of these dynamic, non-Hermitian systems could help discover a wide range of novel effects and applications.

Data availability statement

The original contributions presented in the study are included in the article/supplementary material, further inquiries can be directed to the corresponding authors.

Author contributions

TW: Writing–review and editing, Writing–original draft. PL: Writing–review and editing, Writing–original draft.

Funding

The author(s) declare that financial support was received for the research, authorship, and/or publication of this article. Agence Nationale de la Recherche (22CE24-0012-03).

Acknowledgments

PL acknowledges financial support from the WHEEL (ANR-22CE24-0012-03) Project.

Conflict of interest

The authors declare that the research was conducted in the absence of any commercial or financial relationships that could be construed as a potential conflict of interest.

Publisher's note

All claims expressed in this article are solely those of the authors and do not necessarily represent those of their affiliated organizations, or those of the publisher, the editors and the reviewers. Any product that may be evaluated in this article, or claim that may be made by its manufacturer, is not guaranteed or endorsed by the publisher.

References

1. Vahala KJ. Optical microcavities. *Nature* (2003) 424:839–46. doi:10.1038/nature01939

2. Baumberg JJ, Aizpurua J, Mikkelsen MH, Smith DR. Extreme nanophotonics from ultrathin metallic gaps. *Nat Mater* (2019) 18:668–78. doi:10.1038/s41563-019-0290-y

3. Lalanne P, Yan W, Vynck K, Sauvan C, Hugonin JP. Light interaction with photonic and plasmonic resonances. *Laser Photon Rev* (2018) 12:1700113. doi:10.1002/lpor.201700113

4. Benisty H, Greffet JJ, Lalanne P. *Introduction to nanophotonics*. Oxford University Press (2022). doi:10.1093/oso/9780198786139.001.0001

5. Wu T, Gurioli M, Lalanne P. Nanoscale light confinement: the Q's and V's. *ACS Photon* (2021) 8:1522–38. doi:10.1021/acsphotonics.1c00336

6. Christopoulos T, Tsilipakos O, Sinatkas G, Kriezis EE. On the calculation of the quality factor in contemporary photonic resonant structures. *Opt Expr* (2019) 27:14505–22. doi:10.1364/OE.27.014505

7. Giannini V, Fernández-Domínguez AI, Heck SC, Maier SA. Plasmonic nanoantennas: fundamentals and their use in controlling the radiative properties of nanoemitters. *Chem Rev* (2011) 111:3888–912. doi:10.1021/cr1002672

8. Chikkaraddy R, De Nijs B, Benz F, Barrow SJ, Scherman OA, Rosta E, et al. Single-molecule strong coupling at room temperature in plasmonic nanocavities. *Nature* (2016) 535:127–30. doi:10.1038/nature17974

9. Both S, Weiss T. Resonant states and their role in nanophotonics. *Semicond Sci Technol* (2022) 37:013002. doi:10.1088/1361-6641/ac3290

10. Sauvan C, Wu T, Zarouf R, Muljarov EA, Lalanne P. Normalization, orthogonality, and completeness of quasinormal modes of open systems: the case of electromagnetism [Invited]. *Opt Expr* (2022) 30:6846–85. doi:10.1364/OE.443656

11. Sauvan C, Hugonin JP, Maksymov IS, Lalanne P. Theory of the spontaneous optical emission of nanosize photonic and plasmon resonators. *Phys Rev Lett* (2013) 110:237401. doi:10.1103/PhysRevLett.110.237401

12. Muljarov EA, Langbein W, Zimmermann R. Brillouin-Wigner perturbation theory in open electromagnetic systems. *Europhys Lett* (2010) 92:50010. doi:10.1209/0295-5075/92/50010

13. Muljarov EA, Langbein W. Exact mode volume and Purcell factor of open optical systems. *Phys Rev B* (2016) 94:235438. doi:10.1103/PhysRevB.94.235438

14. Bai Q, Perrin M, Sauvan C, Hugonin JP, Lalanne P. Efficient and intuitive method for the analysis of light scattering by a resonant nanostructure. *Opt Expr* (2013) 21:27371. doi:10.1364/OE.21.027371

15. Stout B, Colom R, Bonod N, McPhedran RC. Spectral expansions of open and dispersive optical systems: Gaussian regularization and convergence. *New J Phys* (2021) 23:083004. doi:10.1088/1367-2630/ac10a6

16. Vial B, Nicolet A, Zolla F, Commandré M. Quasimodal expansion of electromagnetic fields in open two-dimensional structures. *Phys Rev A* (2014) 89:023829. doi:10.1103/PhysRevA.89.023829

17. Truong MD, Nicolet A, Demésy G, Zolla F. Continuous family of exact Dispersive Quasi-Normal Modal (DQNM) expansions for dispersive photonic structures. *Opt Expr* (2020) 28:29016–32. doi:10.1364/OE.401742

18. Gras A, Lalanne P, Duruflé M. Non-uniqueness of the quasinormal mode expansion of electromagnetic lorentz dispersive materials. *J Opt Soc Am A* (2020) 37:1219–28. doi:10.1364/JOSAA.394206

19. Demésy G, Wu T, Brûlé Y, Zolla F, Nicolet A, Lalanne P, et al. Dispersive perfectly matched layers and high-order absorbing boundary conditions for electromagnetic quasinormal modes. *J Opt Soc Am A* (2023) 40:1947–58. doi:10.1364/JOSAA.499370

20. Yan W, Faggiani R, Lalanne P. Rigorous modal analysis of plasmonic nanoresonators. *Phys Rev B* (2018) 97:205422. doi:10.1103/PhysRevB.97.205422

21. Zolla F, Nicolet A, Demésy G. Photonics in highly dispersive media: the exact modal expansion. *Opt Lett* (2018) 43:5813–6. doi:10.1364/OL.43.005813

22. Besbes M, Sauvan C. Role of static modes in quasinormal modes expansions: when and how to take them into account? *Mathematics* (2022) 10:3542. doi:10.3390/math10193542

23. Sauvan C. Quasinormal modes expansions for nanoresonators made of absorbing dielectric materials: study of the role of static modes. *Opt Expr* (2021) 29:8268–82. doi:10.1364/OE.417909

24. Faggiani R, Losquin A, Yang J, Marsell E, Mikkelsen A, Lalanne P. Modal analysis of the ultrafast dynamics of optical nanoresonators. *ACS Photon* (2017) 4:897–904. doi:10.1021/acsphotonics.6b00992

25. Baldassari L, Millien P, Vanel AL. Modal approximation for plasmonic resonators in the time domain: the scalar case. *Partial Differ Equations Appl* (2021) 2:46. doi:10.1007/s42985-021-00098-4

26. Ben Soltane I, Colom R, Stout B, Bonod N. Derivation of the transient and steady optical states from the Poles of the S-matrix. *Laser Photon Rev* (2023) 17:2200141. doi:10.1002/lpor.202200141

27. Wu T, Lalanne P. Exact maxwell evolution equation of resonator dynamics: temporal coupled-mode theory revisited. *Opt Expr* (2024) 32:20904–14. doi:10.1364/OE.517237

28. Huang L, Xu L, Powell DA, Padilla WJ, Miroshnichenko AE. Resonant leaky modes in all-dielectric metasystems: fundamentals and applications. *Phys Rep* (2023) 1008:1–66. doi:10.1016/j.physrep.2023.01.001

29. Klimov VV. Optical nanoresonators. *Phys Usp* (2023) 193:263–87. doi:10.3367/UFNe.2022.02.039153

30. Chang RK, Campillo AJ. Optical processes in microcavities. *World Scientific* (1996). doi:10.1142/2828

31. Gigli C, Wu T, Marino G, Borne A, Leo G, Lalanne P. Quasinormal-mode non-hermitian modeling and design in nonlinear nano-optics. *ACS Photon* (2020) 7:1197–205. doi:10.1021/acsphotonics.0c00014

32. Christopoulos T, Kriezis EE, Tsilipakos O. Multimode non-Hermitian framework for third harmonic generation in nonlinear photonic systems comprising two-dimensional materials. *Phys Rev B* (2023) 107:035413. doi:10.1103/PhysRevB.107.035413

33. Koshelev K, Kruk S, Melik-Gaykazyan E, Choi J-H, Bogdanov A, Park H-G, et al. Subwavelength dielectric resonators for nonlinear nanophotonics. *Science* (2020) 367:288–92. doi:10.1126/science.aaz3985

34. Jahani S, Roy A, Marandi A. Wavelength-scale optical parametric oscillators. *Optica* (2021) 8:262–8. doi:10.1364/OPTICA.411708

35. Weissflog MA, Dezert R, Vinel V, Gigli C, Leo G, Pertsch T, et al. Nonlinear nanoresonators for Bell state generation. *Appl Phys Rev* (2024) 11:011403. doi:10.1063/5.0172240

36. Türeci HE, Stone AD, Collier B. Self-consistent multimode lasing theory for complex or random lasing media. *Phys Rev A* (2006) 74:043822. doi:10.1103/PhysRevA.74.043822

37. Andreasen J, Asatryan AA, Botten LC, Byrne MA, Cao H, Ge L, et al. Modes of random lasers. *Adv Opt Photon* (2011) 3:88–127. doi:10.1364/AOP.3.000088

38. Lentrodt D, Evers J. *Ab initio* few-mode theory for quantum potential scattering problems. *Phys Rev X* (2020) 10:011008. doi:10.1103/PhysRevX.10.011008

39. Lentrodt D, Diekmann O, Keitel CH, Rotter S, Evers J. Certifying multimode light-matter interaction in lossy resonators. *Phys Rev Lett* (2023) 130:263602. doi:10.1103/PhysRevLett.130.263602

40. Medina I, García-Vidal FJ, Fernández-Domínguez AI, Feist J. Few-mode field quantization of arbitrary electromagnetic spectral densities. *Phys Rev Lett* (2021) 126:093601. doi:10.1103/PhysRevLett.126.093601

41. Both S, Schäferling M, Sterl F, Muljarov EA, Giessen H, Weiss T. Nanophotonic chiral sensing: how does it actually work? *ACS Nano* (2022) 16:2822–32. doi:10.1021/acsnano.1c09796

42. Almousa SF, Weiss T, Muljarov EA. Employing quasidegenerate optical modes for chiral sensing. *Phys Rev B* (2024) 109:L041410. doi:10.1103/PhysRevB.109.L041410

43. Yang Y, Zhu D, Yan W, Agarwal A, Zheng M, Joannopoulos JD, et al. A general theoretical and experimental framework for nanoscale electromagnetism. *Nature* (2019) 576:248–52. doi:10.1038/s41586-019-1803-1

44. Zhou Q, Zhang P, Chen X-W. General framework of canonical quasinormal mode analysis for extreme nano-optics. *Phys Rev Lett* (2021) 127:267401. doi:10.1103/PhysRevLett.127.267401

45. Tao C, Zhong Y, Liu H. Quasinormal mode expansion theory for mesoscale plasmonic nanoresonators: an analytical treatment of nonclassical electromagnetic boundary condition. *Phys Rev Lett* (2022) 129:197401. doi:10.1103/PhysRevLett.129.197401

46. Li Q, Wu T, van de Groep J, Lalanne P, Brongersma ML. Structural color from a coupled nanowire pair beyond the bonding and antibonding model. *Optica* (2021) 8:464–70. doi:10.1364/OPTICA.418888

47. Agreda A, Wu T, Hereu A, Treguer-Delapierre M, Drisko GL, Vynck K, et al. Tailoring iridescent visual appearance with disordered resonant metasurfaces. *ACS Nano.* (2023) 17:6362–72. doi:10.1021/acsnano.2c10962

48. Genack AZ, Zhang S. *Wave interference and modes in random media in tutorials in complex photonic media in tutorials in complex photonic media*. Bellingham, Washington, United States: SPIE Publications (2009). doi:10.1117/3.832717

49. Kuznetsov AI, Miroshnichenko AE, Brongersma ML, Kivshar YS, Luk'yanchuk B. Optically resonant dielectric nanostructures. *Science* (2016) 354:aag2472. doi:10.1126/science.aag2472

50. Limonov MF, Rybin MV, Poddubny AN, Kivshar YS. Fano resonances in photonics. *Nat Photon* (2017) 11:543–54. doi:10.1038/nphoton.2017.142

51. Luk'Yanchuk B, Zheludev NI, Maier SA, Halas NJ, Nordlander P, Giessen H, et al. The Fano resonance in plasmonic nanostructures and metamaterials. *Nat Mater* (2010) 9:707–15. doi:10.1038/nmat2810

52. Alaee R, Rockstuhl C, Fernandez-Corbaton I. Exact multipolar decompositions with applications in nanophotonics. *Adv Opt Mater* (2019) 7:1800783. doi:10.1002/adom.201800783

53. Fan S, Suh W, Joannopoulos JD. Temporal coupled-mode theory for the Fano resonance in optical resonators. *J Opt Soc Am A* (2003) 20:569–72. doi:10.1364/JOSAA.20.000569

54. Christopoulos T, Tsilipakos O, Kriezis EE. Temporal coupled-mode theory in nonlinear resonant photonics: from basic principles to contemporary systems with 2D materials, dispersion, loss, and gain. *J Appl Phys* (2024) 136:011101. doi:10.1063/5.0190631

55. Pellegrino D, Balestri D, Granchi N, Ciardi M, Intonti F, Pagliano F, et al. Non-Lorentzian local density of states in coupled photonic crystal cavities probed by near- and far-field emission. *Phys Rev Lett* (2020) 124:123902. doi:10.1103/PhysRevLett.124.123902

56. Wu T, Yan W, Lalanne P. Bright plasmons with cubic nanometer mode volumes through mode hybridization. *ACS Photon* (2021) 8:307–14. doi:10.1021/acsphotonics.0c01569

57. Li W, Zhou Q, Zhang P, Chen XW. Bright optical eigenmode of 1 nm^3 mode volume. *Phys Rev Lett* (2021) 126:257401. doi:10.1103/PhysRevLett.126.257401

58. Zhang C, Hugonin JP, Greffet JJ, Sauvan C. Surface plasmon polaritons emission with nanopatch antennas: enhancement by means of mode hybridization. *ACS Photon* (2019) 6:2788–96. doi:10.1021/acsphotonics.9b00797

59. Kongsuwan N, Demetriadou A, Horton M, Chikkaraddy R, Baumberg JJ, Hess O. Plasmonic nanocavity modes: from near-field to far-field radiation. *ACS Photon* (2020) 7:463–71. doi:10.1021/acsphotonics.9b01445

60. Elliott E, Bedingfield K, Huang J, Hu S, De Nijs B, Demetriadou A, et al. Fingerprinting the hidden facets of plasmonic nanocavities. *ACS Photon* (2022) 9:2643–51. doi:10.1021/acsphotonics.2c00116

61. Wu T, Baron A, Lalanne P, Vynck K. Intrinsic multipolar contents of nanoresonators for tailored scattering. *Phys Rev A* (2020) 101:011803. doi:10.1103/PhysRevA.101.011803

62. Zschiedrich L, Binkowski F, Nikolay N, Benson O, Kewes G, Burger S. Riesz-projection-based theory of light-matter interaction in dispersive nanoresonators. *Phys Rev A* (2018) 98:043806. doi:10.1103/PhysRevA.98.043806

63. Ming X. Quasinormal mode expansion method for resonators with partial-fraction material dispersion. *arXiv preprint arXiv:2312.11048* (2023). doi:10.48550/arXiv.2312.11048

64. Tang XT, Ma L, You Y, Du XJ, Qiu H, Guan XH, et al. Relations between near-field enhancements and Purcell factors in hybrid nanostructures of plasmonic antennas and dielectric cavities. *Opt Expr* (2024) 32:16746–60. doi:10.1364/OE.521090

65. Miller OD. Fundamental limits to near-field optical response. In: *Advances in near-field optics*. Springer (2023). doi:10.1007/978-3-031-34742-9_2

66. Netherwood KS, Riley H, Muljarov EA. Exceptional points in optical systems: a resonant-state expansion study. *arXiv preprint arXiv:2309.12536* (2023). doi:10.48550/arXiv.2309.12536

67. Pick A, Zhen B, Miller OD, Hsu CW, Hernandez F, Rodriguez AW, et al. General theory of spontaneous emission near exceptional points. *Opt Expr* (2017) 25:12325–48. doi:10.1364/OE.25.012325

68. Wu T, Arrivault D, Yan W, Lalanne P. Modal analysis of electromagnetic resonators: user guide for the MAN program. *Comput Phys Commun* (2023) 284:108627. doi:10.1016/j.cpc.2022.108627

69. Wu T, Arrivault D, Duruflé M, Gras A, Binkowski F, Burger S, et al. Efficient hybrid method for the modal analysis of optical microcavities and nanoresonators. *J Opt Soc Am A* (2021) 38:1224–31. doi:10.1364/JOSAA.428224

70. Qi Z, Tao C, Rong S, Zhong Y, Liu H. Efficient method for the calculation of the optical force of a single nanoparticle based on the quasinormal mode expansion. *Opt Lett* (2021) 46:2658–61. doi:10.1364/OL.426423

71. Lu X, Tao Q, Zhong Y, Liu H. Efficient method for the electrodynamics Langevin-dynamics simulation of multiple nanoparticles based on the coupling theory of quasinormal mode. *ACS Photon* (2024). doi:10.1021/acsphotonics.3c01904

72. Yan W, Lalanne P, Qiu M. Shape deformation of nanoresonator: a quasinormal-mode perturbation theory. *Phys Rev Lett* (2020) 125:013901. doi:10.1103/PhysRevLett.125.013901

73. Sztranyovszky Z, Langbein W, Muljarov EA. First-order perturbation theory of eigenmodes for systems with interfaces. *Phys Rev Res* (2023) 5:013209. doi:10.1103/PhysRevResearch.5.013209

74. Muljarov EA, Langbein W. Resonant-state expansion of dispersive open optical systems: creating gold from sand. *Phys Rev B* (2016) 93:075417. doi:10.1103/PhysRevB.93.075417

75. Tao C, Zhu J, Zhong Y, Liu H. Coupling theory of quasinormal modes for lossy and dispersive plasmonic nanoresonators. *Phys Rev B* (2020) 102:045430. doi:10.1103/PhysRevB.102.045430

76. Tao Q, Su Y, Tao C, Zhong Y, Liu H. Efficient method for modeling large-scale arrays of optical nanoresonators based on the coupling theory of quasinormal mode. *Opt Expr* (2024) 32:7171–84. doi:10.1364/OE.515087

77. Lalanne P, Yan W, Gras A, Sauvan C, Hugonin JP, Besbes M, et al. Quasinormal mode solvers for resonators with dispersive materials. *J Opt Soc Am A* (2019) 36:686–704. doi:10.1364/JOSAA.36.000686

78. Demésy G, Nicolet A, Gralak B, Geuzaine C, Campos C, Roman JE. Non-linear eigenvalue problems with GetDP and SLEPc: eigenmode computations of frequencydispersive photonic open structures. *Comput Phys Commun* (2020) 257:107509. doi:10.1016/j.cpc.2020.107509

79. Betz F, Binkowski F, Burger S. RPExpand: software for Riesz projection expansion of resonance phenomena. *SoftwareX* (2021) 15:100763. doi:10.1016/j.softx.2021.100763

80. Nollert HP. Quasinormal modes: the characteristic `sound' of black holes and neutron stars. *Class Quan Grav* (1999) 16:R159–216. doi:10.1088/0264-9381/16/12/201

81. Barausse E, Cardoso V, Pani P. Can environmental effects spoil precision gravitational-wave astrophysics? *Phys Rev D* (2014) 89:104059. doi:10.1103/PhysRevD.89.104059

82. Jaramillo JL, Macedo RP, Al Sheikh L. Pseudospectrum and black hole quasinormal mode instability. *Phys Rev X* (2021) 11:031003. doi:10.1103/PhysRevX.11.031003

83. Cheung M, Destounis K, Macedo RP, Berti E, Cardoso V. Destabilizing the fundamental mode of black holes: the elephant and the flea. *Phys Rev Lett* (2022) 128:111103. doi:10.1103/PhysRevLett.128.111103

84. Jaramillo JL, Macedo RP, Al Sheikh L. Gravitational wave signatures of black hole quasinormal mode instability. *Phys Rev Lett* (2022) 128:211102. doi:10.1103/PhysRevLett.128.211102

85. Ching ESC, Leung PT, Van Den Brink AM, Suen WM, Tong SS, Young K. Quasinormal-mode expansion for waves in open systems. *Rev Mod Phys* (1998) 70:1545–54. doi:10.1103/RevModPhys.70.1545

86. Lamb H. On a peculiarity of the wave-system due to the free vibrations of a nucleus in an extended medium. *Proc Lond Math. Soc.* (1900) XXXII:208–13. doi:10.1112/plms/s1-32.1.208

87. Leung PT, Pang KM. Completeness and time-independent perturbation of morphology-dependent resonances in dielectric spheres. *J Opt Soc Am B* (1996) 13:805–17. doi:10.1364/JOSAB.13.000805

88. Lalanne P. Mode volume of electromagnetic resonators: let us try giving credit where it is due. In: *arXiv preprint arXiv:2011.00218* (2020). doi:10.48550/arXiv.2011.00218

89. Wu T, Jaramillo JL, Lalanne P. Understanding the physics related to the spatial exponential growth of electromagnetic quasinormal modes. *arXiv preprint arXiv:2401*(2024):15112. doi:10.48550/arXiv.2401.15112

90. Berti E, Cardoso V, Cheung Y, Di Filippo F, Duque F, Martens P, et al. Stability of the fundamental quasinormal mode in time-domain observations against small perturbations. *Phys Rev D* (2022) 106:084011. doi:10.1103/PhysRevD.106.084011

91. Rosato RF, Destounis K, Pani P. Ringdown stability: greybody factors as stable gravitational-wave observables. arXiv preprint arXiv:2406.01692. (2024)

92. Torres T. From black hole spectral instability to stable observables. *Phys Rev Lett* (2023) 131:111401. doi:10.1103/PhysRevLett.131.111401

93. Chen W, Chen Y, Liu W. Multipolar conversion induced subwavelength high-Q Kerker supermodes with unidirectional radiations. *Laser Photon Rev* (2019) 13:1900067. doi:10.1002/lpor.201900067

94. Halas NJ, Lal S, Chang WS, Link S, Nordlander P. Plasmons in strongly coupled metallic nanostructures. *Chem Rev* (2011) 111:3913–61. doi:10.1021/cr200061k

95. Sheikholeslami SN, García-Etxarri A, Dionne JA. Controlling the interplay of electric and magnetic modes via Fano-like plasmon resonances. *Nano Lett* (2011) 11:3927–34. doi:10.1021/nl202143j

96. Cheng Y, Oyesina KA, Xue B, Lei D, Wong AM, Wang S. Directional dipole dice enabled by anisotropic chirality. *Proc Natl Acad Sci* (2023) 120:e2301620120. doi:10.1073/pnas.2301620120

97. Alaee R, Albooyeh M, Rahimzadegan A, Mirmoosa MS, Kivshar YS, Rockstuhl C. All-dielectric reciprocal bianisotropic nanoparticles. *Phys Rev B* (2015) 92:245130. doi:10.1103/PhysRevB.92.245130

98. Tserkezis C, Esteban R, Sigle DO, Mertens J, Herrmann LO, Baumberg JJ, et al. Hybridization of plasmonic antenna and cavity modes: extreme optics of nanoparticle-on-mirror nanogaps. *Phys Rev A* (2015) 92:053811. doi:10.1103/PhysRevA.92.053811

99. Cognée KG, Doeleman HM, Lalanne P, Koenderink AF. Cooperative interactions between nano-antennas in a high-Q cavity for unidirectional light sources. *Light Sci Appl* (2019) 8:115. doi:10.1038/s41377-019-0227-x

100. Baaske M, Foreman M, Vollmer F. Single-molecule nucleic acid interactions monitored on a label-free microcavity biosensor platform. *Nat Nanotechnol* (2014) 9:933–9. doi:10.1038/nnano.2014.180

101. Fu Y, Qing YM, Li Z, Zayats AV, Lei D. Tale of two resonances: waveguide–plasmon coupling and high Q-factor engineering on the nanoscale. *ACS Photon* (2022) 10:2–12. doi:10.1021/acsphotonics.2c01271

102. Rybin MV, Koshelev KL, Sadrieva ZF, Samusev KB, Bogdanov AA, Limonov MF, et al. High-Q supercavity modes in subwavelength dielectric resonators. *Phys Rev Lett* (2017) 119:243901. doi:10.1103/PhysRevLett.119.243901

103. Mikhailovskii MS, Poleva MA, Solodovchenko NS, Sidorenko MS, Sadrieva ZF, Petrov MI, et al. Engineering of high-Q states via collective mode coupling in chains of Mie resonators. *ACS Photon* (2024) 11:1657–63. doi:10.1021/acsphotonics.3c01874

104. Miri MA, Alu A. Exceptional points in optics and photonics. *Science* (2019) 363: eaar7709. doi:10.1126/science.aar7709

105. Li A, Wei H, Cotrufo M, Chen W, Mann S, Ni X, et al. Exceptional points and non-Hermitian photonics at the nanoscale. *Nat Nanotechnol* (2023) 18:706–20. doi:10.1038/s41565-023-01408-0

106. Özdemir ŞK, Rotter S, Nori F, Yang L. Parity–time symmetry and exceptional points in photonics. *Nat Mater* (2019) 18:783–98. doi:10.1038/s41563-019-0304-9

107. Solodovchenko NS, Samusev KB, Limonov MF. Quadruplets of exceptional points and bound states in the continuum in dielectric rings. *Phys Rev B* (2024) 109: 075131. doi:10.1103/PhysRevB.109.075131

108. Benz F, Schmidt MK, Dreismann A, Chikkaraddy R, Zhang Y, Demetriadou A, et al. Single-molecule optomechanics in picocavities. *Science* (2016) 354:726–9. doi:10.1126/science.aah5243

109. Baumberg JJ. Picocavities: a primer. *Nano Lett* (2022) 22:5859–65. doi:10.1021/acs.nanolett.2c01695

110. Griffiths J, De Nijs B, Chikkaraddy R, Baumberg JJ. Locating single-atom optical picocavities using wavelength-multiplexed Raman scattering. *ACS Photon* (2021) 8: 2868–75. doi:10.1021/acsphotonics.1c01100

111. Canós VA, Bobrovs V, Weiss T, Gao L, Shalin AS, Kivshar Y. Bianisotropic exceptional points in an isolated dielectric nanoparticle. *Phys Rev Res* (2024) 6:013053. doi:10.1103/PhysRevResearch.6.013053

112. Canós Valero A, Shamkhi HK, Kupriianov AS, Weiss T, Pavlov AA, Redka D, et al. Superscattering emerging from the physics of bound states in the continuum. *Nat Commun* (2023) 14:4689. doi:10.1038/s41467-023-40382-y

113. Colom R, Binkowski F, Betz F, Kivshar Y, Burger S. Enhanced Purcell factor for nanoantennas supporting interfering resonances. *Phys Rev Res* (2022) 4:023189. doi:10.1103/PhysRevResearch.4.023189

114. Granchi N, Intonti F, Florescu M, García PD, Gurioli M, Arregui G. Q-factor optimization of modes in ordered and disordered photonic systems using non-Hermitian perturbation theory. *ACS Photon* (2023) 10:2808–15. doi:10.1021/acsphotonics.3c00510

115. Lewi T, Evans HA, Butakov NA, Schuller JA. Ultrawide thermo-optic tuning of PbTe meta-atoms. *Nano Lett* (2017) 17:3940–5. doi:10.1021/acs.nanolett.7b01529

116. Shcherbakov MR, Vabishchevich PP, Shorokhov AS, Chong KE, Choi DY, Staude I, et al. Ultrafast all-optical switching with magnetic resonances in nonlinear dielectric nanostructures. *Nano Lett* (2015) 15:6985–90. doi:10.1021/acs.nanolett.5b02989

117. Christopoulos T, Tsilipakos O, Kriezis EE. Perturbation theory for Kerr nonlinear leaky cavities. *Opt Lett* (2020) 45:6442–5. doi:10.1364/OL.408336

118. Yang J, Giessen H, Lalanne P. Simple analytical expression for the peak-frequency shifts of plasmonic resonances for sensing. *Nano Lett* (2015) 15:3439–44. doi:10.1021/acs.nanolett.5b00771

119. Both S, Weiss T. First-order perturbation theory for changes in the surrounding of open optical resonators. *Opt Lett* (2019) 44:5917–20. doi:10.1364/OL.44.005917

120. Gras A, Yan W, Lalanne P. Quasinormal-mode analysis of grating spectra at fixed incidence angles. *Opt Lett* (2019) 44:3494–7. doi:10.1364/OL.44.003494

121. Cognée KG, Yan W, La China F, Balestri D, Intonti F, Gurioli M, et al. Mapping complex mode volumes with cavity perturbation theory. *Optica* (2019) 6:269–73. doi:10.1364/OPTICA.6.000269

122. Caselli N, Wu T, Arregui G, Granchi N, Intonti F, Lalanne P, et al. Near-field imaging of magnetic complex mode volume. *ACS Photon* (2021) 8(8):1258–63. doi:10.1021/acsphotonics.0c01943

123. Almousa SF, Muljarov EA. Exact theory and approximations for optical resonators in a changing external medium. *Phys Rev B* (2023) 107:L081401. doi:10.1103/PhysRevB.107.L081401

124. Tang Y, Cohen AE. Optical chirality and its interaction with matter. *Phys Rev Lett* (2010) 104:163901. doi:10.1103/PhysRevLett.104.163901

125. Warning LA, Miandashti AR, McCarthy LA, Zhang Q, Landes CF, Link S. Nanophotonic approaches for chirality sensing. *ACS Nano* (2021) 15:15538–66. doi:10.1021/acsnano.1c04992

126. Zhang W, Wu T, Wang R, Zhang X. Surface-enhanced circular dichroism of oriented chiral molecules by plasmonic nanostructures. *J Phys Chem C* (2017) 121: 666–75. doi:10.1021/acs.jpcc.6b09435

127. Harrington RF. *Time harmonic electromagnetic fields*. McGraw-Hill (1961).

128. Zhu W, Esteban R, Borisov AG, Baumberg JJ, Nordlander P, Lezec HJ, et al. Quantum mechanical effects in plasmonic structures with subnanometre gaps. *Nat Commun* (2016) 7:11495. doi:10.1038/ncomms11495

129. Gallinet B, Butet J, Martin OJ. Numerical methods for nanophotonics: standard problems and future challenges. *Laser Photon Rev* (2015) 9(9):577–603. doi:10.1002/lpor.201500122

130. Zarouf R, Wu T, Lalanne P. The Maxwell evolution equation of electromagnetic resonators: a mathematical proof with explicit derivation. *arXiv preprint arXiv: 2405.00455* (2024). doi:10.48550/arXiv.2405.00455

131. Zhu B, Cai Q, Liu Y, Zhang S, Liu W, He Q, et al. Super-resolution 3D tomography of vector near-fields in dielectric resonators. *arXiv preprint arXiv: 2406.13171* (2024). doi:10.48550/arXiv.2406.13171

132. Fomra D, Ball A, Saha S, Wu J, Sojib M, Agrawal A, et al. Nonlinear optics at epsilon near zero: from origins to new materials. *Appl Phys Rev* (2024) 11:011317. doi:10.1063/5.0186961

133. Maiuri M, Schirato A, Cerullo G, Della VG. Ultrafast all-optical metasurfaces: challenges and new frontiers. *ACS Photon* (2024). doi:10.1021/acsphotonics.4c00776

frontiers | Frontiers in Physics

TYPE Perspective
PUBLISHED 04 September 2024
DOI 10.3389/fphy.2024.1457543

Check for updates

OPEN ACCESS

EDITED BY
Jose Luis Jaramillo,
Université de Bourgogne, France

REVIEWED BY
Rodrigo Panosso Macedo,
University of Copenhagen, Denmark
Theo Torres,
UPR7051 Laboratoire de mécanique et d'acoustique (LMA), France

*CORRESPONDENCE
Friedrich König,
fewk@st-andrews.ac.uk

RECEIVED 30 June 2024
ACCEPTED 12 August 2024
PUBLISHED 04 September 2024

CITATION
Burgess C and König F (2024) Hyperboloidal method for quasinormal modes of non-relativistic operators.
Front. Phys. 12:1457543.
doi: 10.3389/fphy.2024.1457543

COPYRIGHT
© 2024 Burgess and König. This is an open-access article distributed under the terms of the Creative Commons Attribution License (CC BY). The use, distribution or reproduction in other forums is permitted, provided the original author(s) and the copyright owner(s) are credited and that the original publication in this journal is cited, in accordance with accepted academic practice. No use, distribution or reproduction is permitted which does not comply with these terms.

Hyperboloidal method for quasinormal modes of non-relativistic operators

Christopher Burgess and Friedrich König*

School of Physics and Astronomy, SUPA, University of St. Andrews, St. Andrews, United Kingdom

The recently reported compactified hyperboloidal method has found wide use in the numerical computation of quasinormal modes, with implications for fields as diverse as gravitational physics and optics. We extend this intrinsically relativistic method into the non-relativistic domain, demonstrating its use to calculate the quasinormal modes of the Schrödinger equation and solve related bound-state problems. We also describe how to further generalize this method, offering a perspective on the importance of non-relativistic quasinormal modes for the programme of black hole spectroscopy.

KEYWORDS

quasinormal modes (QNMs), optical soliton, numerical method, black hole spectroscopy, spectral instability, Schrödinger equation

Introduction

Quasinormal modes (QNMs) are complex frequency modes which characterize the resonant response of a system to linear perturbations. They are prevalent in the physics of waves, with special prominence in optics and gravitational physics. In optics, QNMs are useful for understanding the behaviour of resonant photonic structures, such as plasmonic crystals, nanoparticle traps, metal gratings, and optical sensors [1–5]. In gravitational physics, they are thought relevant to tests of black hole no-hair conjectures [6–8], and central to the emerging project of black hole spectroscopy with gravitational waves [9, 10]. While the QNM literature in optics treats dispersion as a matter of necessity [11, 12], the prevailing methods in gravitational physics are concerned with non-dispersive, relativistic wave propagation [13–15]. We believe there are good reasons to go beyond relativistic wave propagation in the gravitational context. A variety of quantum gravity models predict the dispersive propagation of gravitational waves [16–19], for example, in models with a non-zero graviton mass, violation of Lorentz invariance, and higher dimensions [20–22]. Indeed, it has been proposed that QNMs may be used to probe gravity beyond general relativity, through imprints on radiative emission from black holes [23–27]. More generally, we anticipate that developments of QNM methods for non-relativistic operators will broaden the scope of existing questions in QNM theory.

Numerical methods underpin much of the progress in QNMs over recent years. Indeed, efficient schemes for computing the QNMs of potentials are likely indispensable for future developments in both theory and the modelling of observations. Recently, the so-called compactified hyperboloidal method [28–31] has proven to be a powerful tool, finding wide use in the computation of black hole QNM spectra and bringing within reach the systematic exploration of their connection to pseudospectra [32–39]. Beyond this, it is natural to ask whether the method can also find use in optical systems. We believe it can, but it cannot be widely applied in optics without modification. This is because optical media create non-

relativistic and dispersive dynamics, while the present formulation of the method treats only relativistic and non-dispersive dynamics, as may be seen from its use of hyperbolic spatial slices penetrating the black hole horizon and future null infinity.

A notable optical system that motivates the development of a hyperboloidal method for optics is the fiber optical soliton, which has recently been established as a black hole analogue with an exactly known QNM spectrum [40]. As such, the soliton is the ideal system with which to develop the method, as the resulting numerics can be compared both to known analytical results and to the numerics of the corresponding relativistic system. Moreover, perturbations to the soliton realize the Schrödinger equation with a Pöschl-Teller potential, making the soliton a promising experimental platform with which to address questions in QNM theory, such as the physical status of spectral instabilities observed in QNM numerics, where the Pöschl-Teller potential is paradigmatic [30, 41–44].

In this article, we outline a new method for the numerical computation of QNM spectra for operators with a non-relativistic dispersion relation, by adapting the compactified hyperboloidal method. We begin by showing how to compute the QNMs of the Schrödinger equation for an arbitrary potential, noting that the relativistic and non-relativistic spectra are related by a simple endomorphism. We subsequently demonstrate the method for the Pöschl-Teller potential, explicitly calculating the soliton QNM spectrum numerically. Finally, we sketch how to develop these ideas in order to treat generalized non-relativistic dispersion relations, and discuss potential applications of the more general method, with emphasis on its future use in black hole spectroscopy.

Compactified hyperboloidal method for the Schrödinger equation

We begin by considering a scalar field ϕ which obeys a Schrödinger equation of the form,

$$(i\partial_t - \partial_r^2 + V)\phi = 0, \tag{1}$$

with V a potential that vanishes for $r \to \pm\infty$. The boundary conditions for QNMs describe solutions that transport energy away from the potential, as discussed in more detail in [40]. It can be shown, using the asymptotic dispersion relation of Equation 1, that QNM solutions must diverge for $r \to \pm\infty$. That is, the asymptotic form of the solution must be $\phi \sim \exp(iKr - i\Omega t)$, with the requirement that $\mathrm{Im}(K)$ is positive and negative on the left and right, respectively. These spatial divergences are problematic for numerical methods, but they can be removed by using a hyperboloidal coordinate transformation. Following [30], we adopt coordinates,

$$t = \tau - h(x), \quad r = g(x), \tag{2}$$

where $g(x), h(x)$ are yet to be given, and $\partial_\tau = \partial_t$ by construction. In the relativistic context, these are used to compute QNMs of black holes, with $h(x)$ chosen so that contours of τ tend to null curves that intersect the horizon and future null infinity. There, Equation 2 is intended to respect the asymptotic hyperbolic geometry of the spacetime, giving rise to bounded and well-behaved QNM solutions. However, there is no preferred speed in our non-relativistic system, meaning that no coordinate transformation will consistently give rise to bounded solutions. This requires a different approach.

In order to construct bounded QNM solutions, we first parameterize $h(x)$ by a new variable v_g such that contours of τ tend asymptotically to trajectories directed outwards with $|dr/dt| = v_g$. In particular, we write

$$g(x) = \operatorname{arctanh} x, \quad h(x) = \left(2v_g\right)^{-1} \log(1 - x^2), \tag{3}$$

where $g(x)$ compactifies the space such that the real line of r gives $x \in [-1, 1]$ if we close the set by including the boundaries. In the Supplementary Appendix, we show that QNMs whose asymptotic group velocity is v_g in (r, t) coordinates are finite at the spatial boundaries, $x = \pm 1$. This enforces the boundary conditions for these modes, but does not guarantee that any such modes exist.

In contrast to the relativistic case, dispersion in non-relativistic systems means that group and phase velocities are not the same. As a result, QNMs whose asymptotic phase velocity is $v_p \neq v_g$ in (r, t) coordinates will undergo phase divergences at the boundaries. This can be removed by a phase-rotation of the field,

$$\hat{\phi} = e^{-\Delta \log(1-x^2)/2}\phi, \tag{4}$$

where we introduce $\Delta = i(v_g - v_p)/2$, so that the phase rotation is parameterized by both v_g and v_p. The form of the required phase rotation follows from the asymptotic dispersion relation of Equation 1 and the choice of height function, $h(x)$. Intuitively, it depends on the mismatch of the two velocities. The result is that the field $\hat{\phi}$ is bounded and well-defined on the new space.

The cost of the above construction is that we introduce two unknown real parameters, v_g and v_p, into the problem. In fact, identifying velocity pairs that correspond to actual QNM solutions is as difficult a problem as determining the QNM spectrum itself. This may be seen by the relation,

$$\Omega = -\frac{1}{2}v_g\left(v_p + i\sqrt{v_g\left(v_g - 2v_p\right)}\right), \tag{5}$$

which we derive, in the Supplementary Appendix, from the asymptotic dispersion relation of Equation 1. This holds true for any mode whose asymptotic group and phase velocities are v_g and v_p, respectively. The existence of a relation such as Equation 5 is a direct consequence of dispersion. In a relativistic system, all asymptotic speeds are the speed of light, so Ω cannot be expressed in terms of asymptotic velocities. This difference between the relativistic and non-relativistic methods is crucial. Equations 3, 4 mean we obtain an equation of motion, and an eigenvalue equation for the complex frequency Ω, both of which are parameterized by v_g and v_p. The significance of Equation 5 is that these additional parameters can ultimately be eliminated, leaving Ω as the only unknown in the problem.

We proceed as in [30], by rewriting Equation 1 in the new coordinates and performing a first-order reduction in time, introducing the auxiliary field $\hat{\psi}$. The equation of motion becomes $\partial_\tau\hat{\phi} = \hat{\psi}$ with

$$x^2\partial_\tau\hat{\psi} = J_1\hat{\phi} + J_2\hat{\psi}, \tag{6}$$

where J_1 and J_2, given in the Supplementary Appendix, are spatial operators depending on the potential and the asymptotic velocities. In contrast to the relativistic method, $\partial_\tau\hat{\psi}$ cannot be isolated by

division in Equation 6 because its pre-factor vanishes at $x = 0$. This occurs because the contours of τ have to "turn around" in order to be outgoing in the (r, t) coordinates. Our alternative approach is to construct $\partial_\tau \hat{\psi}$ using a Taylor series around $x = 0$, obtaining the required derivatives by repeated differentiation of Equation 6. In fact, this treatment is necessary only for terms indivisible by x^2, and we obtain a simpler result if we initially separate the terms in this way. This separation is mostly trivial, but for the potential, where we write $V = V_0 + xV_1 + x^2\tilde{V}(x)$, with V_0 and V_1 Taylor series coefficients about $x = 0$ and $\tilde{V}$ accounting for the remaining terms. We obtain

$$\partial_\tau \hat{\psi} = L_1 \hat{\phi} + L_2 \hat{\psi}, \tag{7}$$

where L_1 and L_2 are spatial operators that we derive in the Supplementary Appendix. Equation 7 is formally identical to that obtained in the relativistic method [30], but the operators are quite different, containing arbitrarily high spatial derivatives and depending on the asymptotic velocities.

In matrix form, we write $i\partial_\tau u = Lu$ with

$$u \equiv \begin{pmatrix} \hat{\phi} \\ \hat{\psi} \end{pmatrix}, \quad L \equiv i \begin{pmatrix} 0 & 1 \\ L_1 & L_2 \end{pmatrix},$$

and obtain the mode equation

$$Lu = \Omega u. \tag{8}$$

The operator L is parameterized by v_g and v_p, giving rise to a family of operators. For each operator, Equation 8 defines a unique eigenvalue problem and a corresponding spectrum. However, only a subset of the frequencies from these spectra obey Equation 5, and it is this subset which comprises the QNM spectrum of Equation 1. Using Equation 5 to eliminate v_g and v_p, one obtains a problem in which the frequency Ω is the only unknown and all solutions correspond to QNMs. In this formulation, L is parameterized by Ω, which constitutes an essential difference from the relativistic method, wherein the corresponding operator does not depend on Ω [30]. Importantly, Equation 8 unambiguously determines the QNM spectrum.

Equation 8 is discretized using N-point Chebyshev nodes of the second kind. In this way, fields are approximated by N-dimensional vectors and spatial operators by N-dimensional matrices. It follows that the vector u and the operator L are approximated by $2N$-dimensional vectors and matrices, respectively. The result is

$$L^N u^N = \Omega u^N. \tag{9}$$

The QNM spectrum may then be obtained from Equation 9 in the usual way using $\det(L^N - \Omega\,\mathrm{Id}) = 0$. In the Supplementary Appendix, we show that this determinant may be rewritten as that of a smaller N-dimensional matrix, M. Its elements are quadratic in the square root of the QNM frequency, giving rise to a polynomial of degree $2N$ in $\sqrt{\Omega}$. For a given potential V, the roots may be numerically determined in order to give $2N$ of the QNM frequencies. The fact that the frequency enters via its square root is a result of the Schrödinger equation having a first derivative in time, rather than a second derivative in time like the wave equation. Indeed, the exact QNM spectra of the Schrödinger and wave equations are related to each other by $i\sqrt{\Omega} = \omega$, as was elaborated in [40]. This means we can relate the results of the non-relativistic method to those of the relativistic method, allowing us to better evaluate the accuracy of the new method.

Quasinormal modes of the Pöschl-Teller potential

In this section, we use the above numerical method to calculate the QNMs of the Schrödinger equation with the Pöschl-Teller potential,

$$V = V_0 \,\mathrm{sech}^2(r) = V_0(1 - x^2), \tag{10}$$

which serves as an exemplar for both the relativistic and non-relativistic methods. The QNMs of Equation 10 are finite polynomials in the compactified spatial coordinate, with the result that an N-point discretization reproduces the first $2N$ QNMs to arbitrary precision. The Pöschl-Teller potential is also ideal because the corresponding QNM spectrum of the Schrödinger equation is given analytically by

$$\Omega_n = \left[n + \frac{1}{2} - i\sqrt{V_0 - \frac{1}{4}} \right]^2, \tag{11}$$

allowing us to verify our results [40]. In regards to the non-relativistic method, we note that the Pöschl-Teller potential is especially simple because all its QNMs have the same v_g parameter, which is a result of the fact that $i\sqrt{\Omega}$ is aligned along vertical lines in the complex plane for this potential. While this simplicity does not influence the operation of the method, it does allow us to more easily assess the spectrum. Lastly, we partition the Pöschl-Teller potential with $V_1 = 0$ and $\tilde{V} = -V_0$, which reinforces the simplicity of the potential.

Now, we make some comments on the specifics of our implementation of the method. We find the calculation is significantly more efficient for odd N. This is a consequence of discretization. The Taylor series expansions of L_1 and L_2 involve spatial derivatives at $x = 0$, which are obtained by integration with a Dirac delta function in the continuous case, and by matrix multiplications in the discretized case. For odd N, the relevant matrix is zero everywhere but a central column whose entries are unity. However, for even N, the matrix is everywhere populated, and this increases the computational cost of the calculation. We also find that evaluating the determinant of the large symbolic matrix M is inefficient, so we instead sample the determinant in the complex plane and reconstruct the symbolic determinant using polynomial interpolation. This uses that the method produces a polynomial of degree $2N$ in $\sqrt{\Omega}$. Importantly, this is true no matter what potential we consider.

In Figure 1A, we plot the exact QNM frequencies of the unperturbed Pöschl-Teller potential, given in Equation 11 [40] alongside those calculated by the new numerical method, with a resolution of $N = 201$. We find excellent agreement for all frequencies, with an error which may be made arbitrarily small by increasing the working precision. These results are given in Figure 2. We also calculate the QNM spectrum of a perturbed Pöschl-Teller potential,

$$V = V_0(1 - x^2) + \epsilon \Delta V, \tag{12}$$

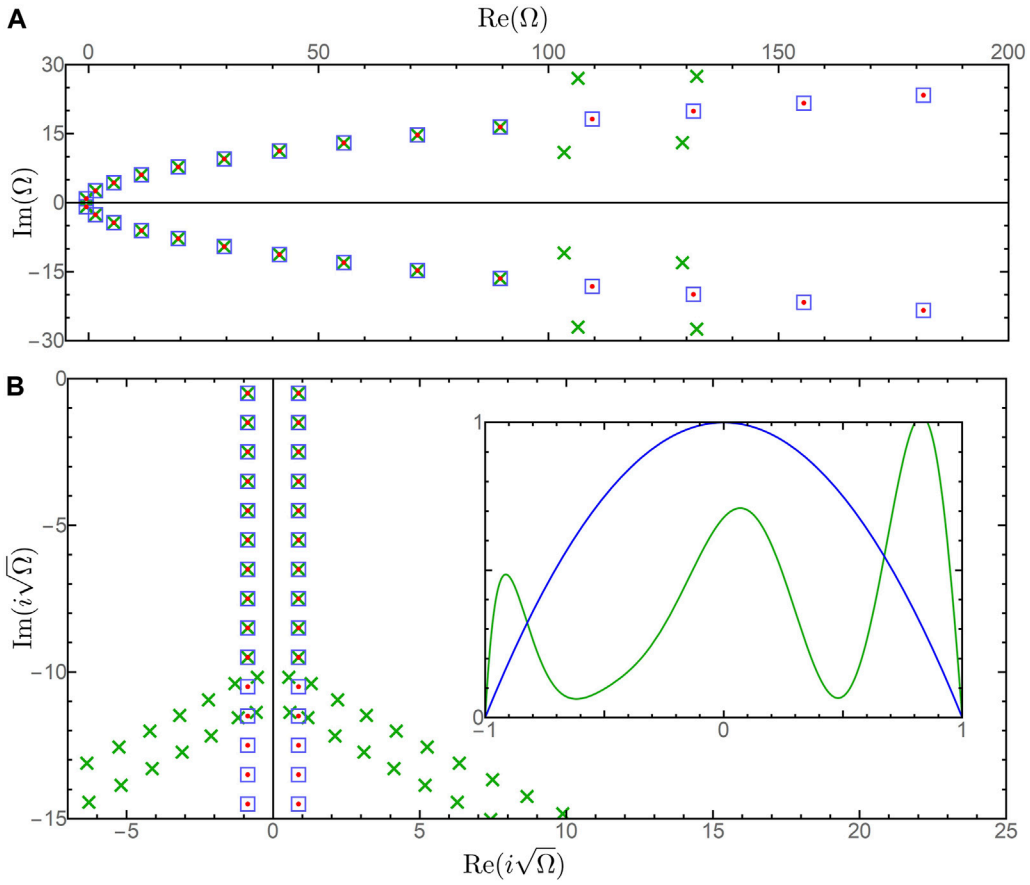

FIGURE 1
QNM spectra for the Schrödinger equation with a potential $V = V_0\,\mathrm{sech}^2(r) + \epsilon\Delta V$, where $V_0 = 1$ and ΔV is the perturbation shown in green in the inset, alongside the unperturbed Pöschl-Teller potential in blue. The red dots and blue boxes correspond to the unperturbed Pöschl-Teller potential ($\epsilon = 0$), with red dots (●) given by the exact formula and blue boxes (□) numerically determined by the new method. The green crosses (⊠) correspond to a perturbed potential ($\epsilon = 10^{-30}$) and are also numerically determined. **(A)** Displays the three QNM spectra, while **(B)** Displays the same spectra under the transformation $\Omega \to i\sqrt{\Omega}$, which relates the spectra to those of a corresponding relativistic operator.

where $\epsilon = 10^{-30}$ and ΔV is a randomly chosen polynomial of degree 9, shown in the inset of Figure 1. We find that the spectrum for Equation 12 closely resembles the unperturbed spectrum up to the 10^{th} overtone index, beyond which the frequencies are significantly displaced from their unperturbed values, as shown in Figure 2. These numerical results are then indicative of spectral instabilities that have been reported by previous authors [30, 45, 46].

The simple relationship between the QNMs of the Schrödinger and wave equations becomes visible under the transformation $\Omega \to i\sqrt{\Omega}$, which maps the spectrum of the former onto that of the latter. In Figure 1B, we plot $i\sqrt{\Omega}$ for the same spectra as above, obtaining the recognizable vertical lines in the complex plane that are characteristic of the wave equation with a Pöschl-Teller potential. In this way, we illustrate how one can cross-verify the results of the relativistic and non-relativistic methods against each other, for arbitrary potentials.

Discussion

In this section, we discuss potential applications of the non-relativistic compactified hyperboloidal method that we developed in the preceding text, suggesting well-motivated directions in which to further develop the method and providing a sketch of how this can be achieved. The main motivations for this method were the modelling of QNMs of optical solitons, and the development of a framework within which one can treat QNMs in quantum gravity models with dispersive gravitational wave propagation. Beyond these, we note that this non-relativistic method may be employed equally well in any system governed by a Schrödinger equation equipped with a general potential. In this paper, we numerically calculated QNM spectra for the Pöschl-Teller potential and perturbations of that potential, finding agreement with earlier works [40, 47, 50]. For potentials with different long-range behaviour than the Pöschl-Teller potential, one typically requires different choices of height function $h(x)$, but this requirement is shared by the relativistic method, and may be addressed by the same techniques [29, 48, 49]. In addition, we note that this method may also be used to numerically solve for the quantum mechanical bound-states of a general potential well, using the well-known connection between the QNMs of a potential barrier and the bound-states of the corresponding well [41, 51–53].

As described above, the non-relativistic method we have presented is closely related to the relativistic method, sharing

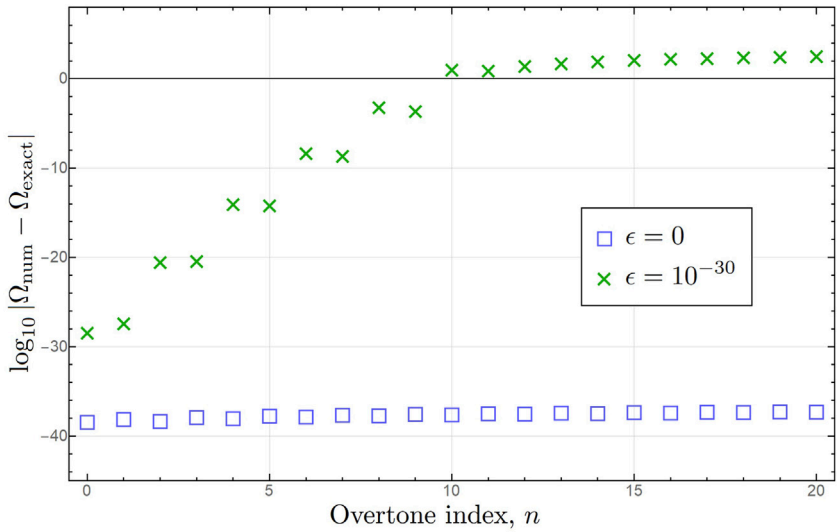

FIGURE 2
Comparisons of exact and numerically determined QNM frequencies for the Schrödinger equation with a potential $V = V_0\,\mathrm{sech}^2(r) + \epsilon\Delta V$, where $V_0 = 1$ and ΔV is the perturbation shown in Figure 1. The first 21 QNM frequencies are displayed. The unperturbed ($\epsilon = 0$) spectrum is recovered well by the new numerical method, with errors smaller than 10^{-37} for the chosen working precision. We also obtain the perturbed ($\epsilon = 10^{-30}$) spectrum and find the deviation from the exact spectrum grows rapidly with overtone index, n, as in previous works on spectral instability.

many essential features with it. For instance, the classes of potentials that can be treated by the two methods are the same, and they have the same maximum achievable accuracy for a given resolution. As a result, the methods are comparable in their scope and power. They also share the same advantages and disadvantages when compared to other popular numerical methods, such as Leaver's continued fraction method [54]. For example, in this case, both the relativistic and non-relativistic methods enjoy the advantage that they recover the entire spectrum simultaneously, and do not require initial seed values close to the QNM frequencies one wishes to compute [30, 54–56].

The non-relativistic method we have presented readily generalizes beyond the Schrödinger equation, allowing us to treat a large class of more general non-relativistic operators. Indeed, the method presented in this paper primarily serves a didactic purpose, as a demonstration of a general approach with which one may calculate QNMs of these more general operators. The primary motivation for this is to facilitate the efficient computation of QNMs of operators that deviate from the wave equation only by the presence of weak dispersion, as are known to arise in models of quantum gravity, where a thoroughgoing understanding of QNMs is of special interest. The modelling of dispersive gravitational wave propagation and its influence on the observable QNM spectrum will be essential if black hole spectroscopy is to be an effective probe into the domain of quantum gravity.

A further motivation for generalizing the non-relativistic method is to shed light on QNM spectral instabilities, and facilitate experimental tests of the recent ultraviolet universality conjecture, which posits that sufficiently high overtones converge to logarithmic Regge branches in the complex plane, in the high-frequency limit of potential perturbations [30, 36]. This effect is easily seen in numerical calculations of the Pöschl-Teller spectrum, on account of its simplicity, but has yet to be experimentally confirmed. Using the optical soliton, whose perturbations realize this potential, experimental tests become possible. The numerical method presented above is essential for the modelling of these experiments, as one cannot realize an exact soliton in practice, and must always work with near-soliton potentials. In addition, higher-order dispersive effects will also be present in any experiment, and these must be understood in order to interpret observations of QNM spectral migration with the soliton. In particular, the influence of weak third-order dispersion acting on the perturbative probe field should be incorporated into the analysis, in order to provide the best test of the above conjecture. This motivates the development of the non-relativistic method beyond the Schrödinger equation, to include higher-order dispersive terms.

In view of the above reasons to generalize the non-relativistic method, we present a sketch of the more general method, which we will elaborate in future work. Suppose we have a non-relativistic equation of the form

$$\big(\alpha(i\partial_t) + \beta(i\partial_r) + V\big)\phi = 0, \tag{13}$$

with $\alpha(z)$ and $\beta(z)$ finite polynomials in z, and d the larger degree among the two polynomials. In principle, we can apply a hyperboloidal coordinate transformation and a phase rotation of the fields, parameterised by the asymptotic velocities, v_g and v_p. Then, we introduce auxiliary fields to effect a dth-order reduction in time, defining

$$\phi_1 = \phi, \quad \phi_{k+1} = \partial_\tau \phi_k, \tag{14}$$

with $1 \le k < d$. Equation 14 closely mirrors the treatment of resonator QNMs in optics [11]. The equations of motion of these fields are trivial for all fields but ϕ_d, whose equation of motion more closely resembles Equation 6. If we use a Taylor series expansion of $\partial_\tau \phi_d$ around zero, we can write it in terms of spatial operators acting

on the fields. The general form of the now d-dimensional operator L is

$$L = \begin{pmatrix} 0 & 1 & 0 & \cdots & 0 \\ 0 & 0 & 1 & \cdots & 0 \\ 0 & 0 & 0 & \cdots & 0 \\ \vdots & \vdots & \vdots & \ddots & 1 \\ L_1 & L_2 & L_3 & \cdots & L_d \end{pmatrix}, \tag{15}$$

which we discretize as before. Then, we use the asymptotic dispersion relation of Equation 13 to eliminate the asymptotic velocities, obtaining a vector equation for the QNM frequencies. From Equation 15, it can be shown that it is always possible to construct an N-dimensional matrix M whose determinant is a finite polynomial for the QNM frequencies. This may then be solved numerically and the frequencies Ω determined. This generalization is largely straight-forward. However, the divergences in space are multi-exponential with higher derivatives, leading to non-polynomial modes in the compactified coordinates. This complicates the imposition of QNM boundary conditions, and further work is required to address this. For example, approaches that augment the function space to include additional non-polynomial functions can be investigated. Future work can investigate how this generalized method compares with other numerical schemes, as the connection to the relativistic method is less concrete in this case.

The method presented is primarily intended for the gravitational context and long-range potentials, but the authors note that extensions to optical cavities or plasmonic resonators may be possible. Beyond QNMs, the non-relativistic method can be applied to spectra of non-selfadjoint operators, connecting with a larger research effort. We believe an explicit formulation in this context is a promising research direction. In addition, future works can develop the method, along the lines of [30], in order to calculate the pseudospectra of non-relativistic operators. It is our view that the relationship between perturbed QNM spectra and the pseudospectrum is best understood from a broader perspective, not limited to relativistic wave operators. We expect that numerical methods will become increasingly important for addressing questions in the theory of QNMs, and anticipate that investigations into the QNMs of non-relativistic fields will provide new avenues to explore these questions.

Data availability statement

The original contributions presented in the study are included in the article/Supplementary Material, further inquiries can be directed to the corresponding author. The supporting data for this article are openly available from [57].

Author contributions

CB: Conceptualization, Formal Analysis, Investigation, Methodology, Software, Visualization, Writing–original draft, Writing–review and editing. FK: Funding acquisition, Project administration, Supervision, Writing–original draft, Writing–review and editing.

Funding

The author(s) declare that financial support was received for the research, authorship, and/or publication of this article. This work was supported in part by the Science and Technology Facilities Council through the UKRI Quantum Technologies for Fundamental Physics Programme (Grant ST/T005866/1). CB was supported by the UK Engineering and Physical Sciences Research Council (Grant EP/T518062/1).

Acknowledgments

We would like to express our thanks to Théo Torres for providing us a useful overview at the outset of this research.

Conflict of interest

The authors declare that the research was conducted in the absence of any commercial or financial relationships that could be construed as a potential conflict of interest.

The reviewer TT declared a past co-authorship with the authors to the handling editor.

Publisher's note

All claims expressed in this article are solely those of the authors and do not necessarily represent those of their affiliated organizations, or those of the publisher, the editors and the reviewers. Any product that may be evaluated in this article, or claim that may be made by its manufacturer, is not guaranteed or endorsed by the publisher.

Supplementary material

The Supplementary Material for this article can be found online at: https://www.frontiersin.org/articles/10.3389/fphy.2024.1457543/full#supplementary-material

References

1. Lalanne P, Yan W, Vynck K, Sauvan C, Hugonin J. Light interaction with photonic and plasmonic resonances. *Laser Photonics Rev* (2018) 12:1700113. doi:10.1002/lpor.201700113

2. Yan W, Faggiani R, Lalanne P. Rigorous modal analysis of plasmonic nanoresonators. *Phys Rev B* (2018) 97:205422. doi:10.1103/physrevb.97.205422

3. Qi Z, Tao C, Rong S, Zhong Y, Liu H. Efficient method for the calculation of the optical force of a single nanoparticle based on the quasinormal mode expansion. *Opt Lett* (2021) 46:2658. doi:10.1364/ol.426423

4. Gras A, Yan W, Lalanne P. Quasinormal-mode analysis of grating spectra at fixed incidence angles. *Opt Lett* (2019) 44:3494. doi:10.1364/ol.44.003494

5. Juanjuan R, Franke S, Hughes S. Quasinormal modes, local density of states, and classical purcell factors for coupled loss-gain resonators. *Phys Rev X* (2021) 11:041020. doi:10.1103/physrevx.11.041020

6. Gossan S, Veitch J, Sathyaprakash BS. Bayesian model selection for testing the no-hair theorem with black hole ringdowns. *Phys Rev D* (2012) 85:124056. doi:10.1103/physrevd.85.124056

7. Shi C, Bao J, Wang HT, Zhang JD, Hu YM, Sesana A, et al. Science with the TianQin observatory: Preliminary results on testing the no-hair theorem with ringdown signals. *Phys Rev D* (2019) 100:044036. doi:10.1103/physrevd.100.044036

8. Ma S, Sun L, Chen Y. Black hole spectroscopy by mode cleaning. *Phys Rev Lett* (2023) 130:141401. doi:10.1103/physrevlett.130.141401

9. Dreyer O, Kelly B, Krishnan B, Finn LS, Garrison D, Lopez-Aleman R. Black-hole spectroscopy: testing general relativity through gravitational-wave observations. *Class Quantum Gravity* (2004) 21:787–803. doi:10.1088/0264-9381/21/4/003

10. Cabero M, Westerweck J, Capano CD, Kumar S, Nielsen AB, Krishnan B. Black hole spectroscopy in the next decade. *Phys Rev D* (2020) 101:064044. doi:10.1103/physrevd.101.064044

11. Lalanne P, Yan W, Gras A, Sauvan C, Hugonin JP, Besbes M, et al. Quasinormal mode solvers for resonators with dispersive materials. *J Opt Soc Am* (2019) 36:686. doi:10.1364/josaa.36.000686

12. Primo AG, Carvalho NC, Kersul CM, Frateschi NC, Wiederhecker GS, Alegre TP. Quasinormal-mode perturbation theory for dissipative and dispersive optomechanics. *Phys Rev Lett* (2020) 125:233601. doi:10.1103/physrevlett.125.233601

13. Kokkotas KD, Schmidt BG. Quasi-normal modes of stars and black holes. *Living Rev Relativ* (1999) 2:2. doi:10.12942/lrr-1999-2

14. Berti E, Cardoso V, Starinets AO. Quasinormal modes of black holes and black branes. *Class Quantum Gravity* (2009) 26:163001. doi:10.1088/0264-9381/26/16/163001

15. Konoplya RA, Zhidenko A. Quasinormal modes of black holes: From astrophysics to string theory. *Rev Mod Phys* (2011) 83:793. doi:10.1103/revmodphys.83.793

16. Nishizawa A. Generalized framework for testing gravity with gravitational-wave propagation. I. Formulation. *Phys Rev D* (2018) 97:104037. doi:10.1103/physrevd.97.104037

17. Mastrogiovanni S, Steer D, Barsuglia M. Probing modified gravity theories and cosmology using gravitational-waves and associated electromagnetic counterparts. *Phys Rev D* (2020) 102:044009. doi:10.1103/physrevd.102.044009

18. Ezquiaga JM, Hu W, Lagos M, Lin MX. Gravitational wave propagation beyond general relativity: waveform distortions and echoes. *JCAP* (2021) 11:048. doi:10.1088/1475-7516/2021/11/048

19. Aydogdu O, Salti M. Gravitational waves in f(R, T)-rainbow gravity: even modes and the Huygens principle. *Phys Scr* (2022) 97:125013. doi:10.1088/1402-4896/aca0cc

20. Kostelecky VA, Mewes M. Testing local Lorentz invariance with gravitational waves. *Phys Lett B* (2016) 757:510–4. doi:10.1016/j.physletb.2016.04.040

21. Will CM. Bounding the mass of the graviton using gravitational-wave observations of inspiralling compact binaries. *Phys Rev D* (1998) 57:2061–8. doi:10.1103/physrevd.57.2061

22. Sefiedgar AS, Nozari K, Sepangi H. Modified dispersion relations in extra dimensions. *Phys Lett B* (2011) 696:119–23. doi:10.1016/j.physletb.2010.11.067

23. Glampedakis K, Silva HO. Eikonal quasinormal modes of black holes beyond general relativity. *Phys Rev D* (2019) 100:044040. doi:10.1103/physrevd.100.044040

24. Agullo I, Cardoso V, del Rio A, Maggiore M, Pullin J. Potential gravitational wave signatures of quantum gravity. *Phys Rev Lett* (2021) 126:041302. doi:10.1103/physrevlett.126.041302

25. Srivastava M, Chen Y, Shankaranarayanan S. Analytical computation of quasinormal modes of slowly rotating black holes in dynamical Chern-Simons gravity. *Phys Rev D* (2021) 104:064034. doi:10.1103/physrevd.104.064034

26. Chen C-Y, Bouhmadi-López M, Chen P. Lessons from black hole quasinormal modes in modified gravity. *Eur Phys J Plus* (2021) 136:253. doi:10.1140/epjp/s13360-021-01227-z

27. Fu G, Zhang D, Liu P, Kuang XM, Wu JP. Peculiar properties in quasinormal spectra from loop quantum gravity effect. *Phys Rev D* (2024) 109:026010. doi:10.1103/physrevd.109.026010

28. Zenginoğlu A. Hyperboloidal foliations and scri-fixing. *Class Quantum Gravity* (2008) 25:145002. doi:10.1088/0264-9381/25/14/145002

29. Zenginoğlu A. A geometric framework for black hole perturbations. *Phys Rev D* (2011) 83:127502. doi:10.1103/physrevd.83.127502

30. Jaramillo JL, Macedo RP, Sheikh LA. Pseudospectrum and black hole quasinormal mode instability. *Phys Rev X* (2021) 11:031003. doi:10.1103/physrevx.11.031003

31. Macedo RP. Hyperboloidal approach for static spherically symmetric spacetimes: a didactical introduction and applications in black-hole physics. *Phil Trans Roy Soc Lond* (2024) A 382:20230046. doi:10.1098/rsta.2023.0046

32. Destounis K, Macedo RP, Berti E, Cardoso V, Jaramillo JL. Pseudospectrum of Reissner-Nordström black holes: quasinormal mode instability and universality. *Phys Rev D* (2021) 104:084091. doi:10.1103/physrevd.104.084091

33. Ripley JL. Computing the quasinormal modes and eigenfunctions for the Teukolsky equation using horizon penetrating, hyperboloidally compactified coordinates. *Class Quantum Gravity* (2022) 39:145009. doi:10.1088/1361-6382/ac776d

34. Gasperín E, Jaramillo JL. Energy scales and black hole pseudospectra: the structural role of the scalar product. *Class Quantum Gravity* (2022) 39:115010. doi:10.1088/1361-6382/ac5054

35. Sarkar S, Rahman M, Chakraborty S. Perturbing the perturbed: stability of quasinormal modes in presence of a positive cosmological constant. *Phys Rev D* (2023) 108:104002. doi:10.1103/physrevd.108.104002

36. Boyanov V, Cardoso V, Destounis K, Jaramillo JL, Macedo RP. Structural aspects of the anti–de Sitter black hole pseudospectrum. *Phys Rev D* (2024) 109:064068. doi:10.1103/physrevd.109.064068

37. Cao L-M, Chen JN, Wu LB, Xie L, Zhou YS. The pseudospectrum and spectrum (in)stability of quantum corrected Schwarzschild black hole. *arXiv preprint* (2024). arXiv:2401.09907. doi:10.48550/arXiv.2401.09907

38. Zhu H, Ripley JL, Cárdenas-Avendaño A, Pretorius F. Challenges in quasinormal mode extraction: Perspectives from numerical solutions to the Teukolsky equation. *Phys Rev D* (2024) 109:044010. doi:10.1103/physrevd.109.044010

39. Destounis K, Boyanov V, Macedo RP. Pseudospectrum of de Sitter black holes. *Phys Rev D* (2024) 109:044023. doi:10.1103/physrevd.109.044023

40. Burgess C, Patrick S, Torres T, Gregory R, König F. Quasinormal modes of optical solitons. *Phys Rev Lett* (2024) 132:053802. doi:10.1103/physrevlett.132.053802

41. Ferrari V, Mashhoon B. New approach to the quasinormal modes of a black hole. *Phys Rev D* (1984) 30:295–304. doi:10.1103/physrevd.30.295

42. Nollert H-P. Quasinormal modes of Schwarzschild black holes: the determination of quasinormal frequencies with very large imaginary parts. *Phys Rev D* (1993) 47:5253–8. doi:10.1103/physrevd.47.5253

43. Cho HT, Cornell AS, Doukas J, Huang TR, Naylor W. A New Approach to Black Hole Quasinormal Modes: A Review of the Asymptotic Iteration Method. *Adv Math Phys* (2012) 2012:281705. doi:10.1155/2012/281705

44. Cardoso V, Kastha S, Macedo RP. Physical significance of the black hole quasinormal mode spectra instability. *Phys Rev D* (2024) 110: 024016. doi:10.1103/physrevd.110.024016

45. Nollert H-P. About the significance of quasinormal modes of black holes. *Phys Rev D* (1996) 53:4397–402. doi:10.1103/physrevd.53.4397

46. Daghigh RG, Green MD, Morey JC. Significance of black hole quasinormal modes: a closer look. *Phys Rev D* (2020) 101:104009. doi:10.1103/physrevd.101.104009

47. Boonserm P, Visser M. Quasi-normal frequencies: key analytic results. *JHEP* (2011) 2011:73. doi:10.1007/jhep03(2011)073

48. Cardona AF, Molina C. Quasinormal modes of generalized Pöschl–Teller potentials. *Class Quantum Gravity* (2017) 34:245002. doi:10.1088/1361-6382/aa9428

49. Jasiulek M. Hyperboloidal slices for the wave equation of Kerr–Schild metrics and numerical applications. *Class Quantum Gravity* (2012) 29:015008. doi:10.1088/0264-9381/29/1/015008

50. Macedo RP, Jaramillo JL, Ansorg M. Hyperboloidal slicing approach to quasinormal mode expansions: the Reissner-Nordström case. *Phys Rev D* (2018) 98:124005. doi:10.1103/physrevd.98.124005

51. Ferrari V, Mashhoon B. Oscillations of a black hole. *Phys Rev Lett* (1984) 52:1361–4. doi:10.1103/physrevlett.52.1361

52. Churilova MS, Konoplya R, Zhidenko A. Analytic formula for quasinormal modes in the near-extreme Kerr-Newman–de Sitter spacetime governed by a non-Pöschl-Teller potential. *Phys Rev D* (2022) 105:084003. doi:10.1103/physrevd.105.084003

53. Völkel SH. Quasinormal modes from bound states: the numerical approach. *Phys Rev D* (2022) 106:124009. doi:10.1103/physrevd.106.124009

54. Leaver EW. Spectral decomposition of the perturbation response of the Schwarzschild geometry. *Phys Rev D* (1986) 34:384–408. doi:10.1103/physrevd.34.384

55. Zenginoğlu A, Núñez D, Husa S. Gravitational perturbations of Schwarzschild spacetime at null infinity and the hyperboloidal initial value problem. *Class Quantum Gravity* (2009) 26:035009. doi:10.1088/0264-9381/26/3/035009

56. Ansorg M, Macedo RP. Spectral decomposition of black-hole perturbations on hyperboloidal slices. *Phys Rev D* (2016) 93:124016. doi:10.1103/physrevd.93.124016

57. Burgess CD, König FEW. Hyperboloidal method for quasinormal modes of non-relativistic operators (dataset). *Dataset, Univ St Andrews Res Portal* (2024). doi:10.17630/61aeab90-f629-41b8-bb36-e4df8ac40150

frontiers | Frontiers in Applied Mathematics and Statistics

TYPE Original Research
PUBLISHED 02 October 2024
DOI 10.3389/fams.2024.1472401

Check for updates

OPEN ACCESS

EDITED BY
Jose Luis Jaramillo,
Université de Bourgogne, France

REVIEWED BY
Piotr Bizon,
Jagiellonian University, Poland
Jonas Lampart,
Laboratoire Interdisciplinaire Carnot de Bourgogne, France

*CORRESPONDENCE
C. M. Warnick
✉ c.m.warnick@maths.cam.ac.uk

RECEIVED 29 July 2024
ACCEPTED 11 September 2024
PUBLISHED 02 October 2024

CITATION
Warnick CM (2024) (In)stability of de Sitter quasinormal mode spectra.
Front. Appl. Math. Stat. 10:1472401.
doi: 10.3389/fams.2024.1472401

COPYRIGHT
© 2024 Warnick. This is an open-access article distributed under the terms of the Creative Commons Attribution License (CC BY). The use, distribution or reproduction in other forums is permitted, provided the original author(s) and the copyright owner(s) are credited and that the original publication in this journal is cited, in accordance with accepted academic practice. No use, distribution or reproduction is permitted which does not comply with these terms.

(In)stability of de Sitter quasinormal mode spectra

C. M. Warnick[1,2]*

[1]Department of Pure Mathematics and Mathematical Statistics, University of Cambridge, Cambridge, United Kingdom, [2]Department of Applied Mathematics and Theoretical Physics, University of Cambridge, Cambridge, United Kingdom

We consider how the quasinormal spectrum for the conformal wave operator on the static patch of de Sitter changes in response to the addition of a small potential. Since the quasinormal modes and co-modes are explicitly known, we are able to give explicit formulae for the instantaneous rate of change of each frequency in terms of the perturbing potential. We verify these exact computations numerically using a novel technique extending the spectral hyperboloidal approach of Jaramillo et al. (2021). We propose a definition for a family of pseudospectra that we show capture the instability properties of the quasinormal frequencies.

KEYWORDS

quasinomal modes of black holes, black holes, spectral instability, non-normal, wave equation

1 Introduction

For asymptotically de Sitter and anti-de Sitter black hole spacetimes, the problem of defining the quasinormal frequencies has been satisfactorily resolved based on making use of a hyperboloidal foliation of the spacetime [1, 2].[1] For asymptotically flat black hole spacetimes, the situation is not as fully developed, but nevertheless in many cases a suitably robust mathematical definition exists either through casting the problem in terms of scattering resonances and making use of the method of complex scaling [3, 5] or through using a hyperboloidal slicing [4, 6, 7]. In all cases, the quasinormal frequencies can ultimately be understood as eigenvalues of some operator which is not self-adjoint.

A feature of operators which are not self-adjoint is that their spectra can be unstable to "small" perturbations. For a simple example in finite dimensions, consider the matrices

$$A = \begin{pmatrix} 0 & \epsilon^{-3} \\ 0 & 0 \end{pmatrix}, \qquad A' = \begin{pmatrix} 0 & \epsilon^{-3} \\ \epsilon & 0 \end{pmatrix}.$$

Clearly for $0 < \epsilon \ll 1$, $A' - A$ is "small" by any reasonable notion of smallness; however, A has a repeated eigenvalue at 0, while A' has eigenvalues $\pm\epsilon^{-1}$, so the spectra diverge as $\epsilon \to 0$.

In the context of black hole quasinormal spectra, it was noticed already by Aguirregabiria–Vishveshwara Nollert–Price in the 90's [8–11] that seemingly innocuous changes to the operators used in defining quasinormal modes could have dramatic effects on the spectrum. Motivated in part by mathematical [2, 4, 6, 12] and numerical [13–15] studies which cast the problem of finding the quasinormal spectrum as an eigenvalue problem for the time evolution operator on a hyperboloidal foliation, there has been a resurgence of interest in the problem of quasinormal spectral stability, see [16, 17] in the

1 see [3, 4] and references therein for a historical overview of this problem

specific context of instability arising from non-self-adjoint operators as well as [18–23] and references therein for many other studies.

In this short article, we shall consider the problem of the conformal wave equation on the static patch of de Sitter space. The high degree of symmetry enjoyed by the de Sitter spacetime means that the problem of determining the quasinormal spectrum is completely solvable, and the various objects involved can be computed explicitly. This makes this a helpful test-bed for understanding the effects on the spectrum of small perturbations. The perturbations we consider consist of stationary modifications to the potential. In a more physically motivated situation, we should consider the linearized gravitational field (rather than a conformal scalar field) and permit perturbations to the geometry of the background rather than just a potential. Our methods can, in principle, be applied in this situation, but for simplicity, we focus on the toy model.[2]

We are able to compute exactly the first order correction to each quasinormal frequency in terms of the perturbing potential. We find that the answer to the question of whether an individual quasinormal frequency is stable to "small" perturbations depends sensitively on what is meant by "small" [cf [25, footnote 18]]. In particular, the relevant notion of smallness varies depending on which modes we are considering, and those representing more rapidly decaying modes require a more stringent notion of smallness. One may alternatively view this by first fixing the notion of smallness considered and then one observes that the more rapidly decaying modes are more unstable to small perturbations, consistent with expectations going back to [9].[3]

To confirm the analytic computations, we also perform some numerics. For this, we make use of a spectral method on a hyperboloidal (or null) slicing, similar to that used in [16], but applied to an enlarged system obtained by differentiating the equation by hand k-times motivated by the analysis of [2]. This has a doubly beneficial effect—First, it stabilizes the numerical computation of quasinormal frequencies; second, it permits us to stably compute a family of pseudospectra that we define, associated with the problem, which allow the stability properties to be directly visualized. In this context, we should also mention the forthcoming study [26] which also provides a numerically stable computation of pseudospectra.

2 Set-up and defining the quasinormal spectrum

We consider the static patch of the de Sitter spacetime, written in coordinates that are regular at the future horizon. This is a metric on $\mathbb{R}^4 = \{(t, \boldsymbol{x}) : t \in \mathbb{R}, \boldsymbol{x} \in \mathbb{R}^3\}$

$$g = -\left(1 - \kappa^2 \delta_{ij} x^i x^j\right) dt^2 - 2\kappa \delta_{ij} x^i dx^j dt + \delta_{ij} dx^i dx^j \tag{1}$$

with δ_{ij} the usual Kronecker delta and $\kappa > 0$ a constant. The static patch is the region $\mathcal{R} = \mathbb{R}_t \times B$ where $B = \{\boldsymbol{x} \in \mathbb{R}^3 : |\boldsymbol{x}| < \kappa^{-1}\}$ is the ball of radius κ^{-1}, and the future cosmological horizon is $\mathcal{H}_+ = \mathbb{R}_t \times \partial B$. This metric is Einstein with cosmological constant $\Lambda = 3\kappa^2$. We will keep track of κ for later discussion, but nothing is lost by setting $\kappa = 1$ throughout.

The wave operator in these coordinates takes the form

$$\Box_g \psi = -\left(\frac{\partial}{\partial t} + \kappa x^i \frac{\partial}{\partial x^i}\right)^2 \psi - 3\kappa \left(\frac{\partial}{\partial t} + \kappa x^i \frac{\partial}{\partial x^i}\right) \psi + \delta^{ij} \frac{\partial^2 \psi}{\partial x^i \partial x^j}.$$

We shall consider the following family of equations on this background

$$L(h)\psi := \Box_g \psi - \kappa^2 V_h \psi = 0. \tag{2}$$

Here, V_h is a time-independent potential depending on some small parameter $|h| < \epsilon$, and we assume that the map $(h, \boldsymbol{x}) \mapsto V_h(\boldsymbol{x})$ is smooth on $(-\epsilon, \epsilon) \times \mathbb{R}^3$. We are interested in particular in the quasinormal ring-down behavior of solutions to this equation. To discuss this, we introduce the Laplace transformed operator which acts on functions $u : B \to \mathbb{C}$

$$\hat{L}(s, h)u := e^{-st} L(h)(e^{st} u). \tag{3}$$

We define the quasinormal frequencies through the solvability properties of this operator. More precisely, for $k = 0, 1, 2, \ldots$ we define an inner product and norm on functions $u, w : B \to \mathbb{C}$ by

$$(u, w)_k := \sum_{l=0}^{k} \int_B \left(\overline{\nabla^{(l)} u} \cdot \nabla^{(l)} w\right) d^3x, \qquad ||u||_k := (u, u)_k^{\frac{1}{2}}. \tag{4}$$

Here, $\nabla^{(l)} u$ is the rank l-tensor $\nabla_{i_1} \cdots \nabla_{i_l} u$, and $\cdot$ means contraction on all indices.[4] Notice that $(u, w)_0$ is the usual L^2-inner product. We define H^k, the Sobolev space of order k, to consist of those functions $u : B \to \mathbb{C}$ with $||u||_k < \infty$. This is a Hilbert space with the corresponding inner product. We define the domain of L_s to be

$$D^k = \{u \in H^k : \hat{L}(1, 0)u \in H^k\}.$$

It can be shown that $H^{k+2} \subset D^k \subset H^{k+1}$, so that $u \in D^k \implies \hat{L}(s, h)u \in H^k$ for all s, h.

With this definition in hand, we can state the basic theorem we shall require, which follows straightforwardly from Vasy, Warnick, and Hintz and Xie [1, 2, 27, 28]:

Theorem 1. Fix $|h| < \epsilon$, $k \in \mathbb{N}$ and let $U_k = \{z \in \mathbb{C} : \Re(z) > -(k + \frac{1}{2})\kappa\}$. Then, the operator $\hat{L}(s, h) : D^k \to H^k$ is invertible for $s \in U_k$, except at a discrete set $\Lambda_k(h) \subset U_k$. Moreover, for each $\sigma \in \Lambda_k(h)$ there is an integer $d > 0$ such that:

1. There exists a d-dimensional space of smooth functions $w : B \to \mathbb{C}$ which extend smoothly to ∂B and satisfy $\hat{L}(\sigma, h)w = 0$.
2. There exists a d-dimensional space of distributions $X \in \mathscr{D}'(\mathbb{R}^3)$ which satisfy

$$X[\hat{L}(\sigma, h)\phi] = 0, \qquad |X[\phi]| \leqslant c\, ||\phi|_B||_k, \tag{5}$$

for some $c > 0$ and all test functions $\phi \in C_c^\infty(\mathbb{R}^3)$.

2 A further complication can arise where the perturbations are presumed to have a time dependence with a typical timescale much shorter than the quasinormal frequencies, in which case one may hope to attempt some averaging procedure (see [24, §3.5 d]).

3 *"...we find that the fundamental mode is, in general, insensitive to small changes in the potential, whereas the higher modes could alter drastically."*

4 Derivatives should be understood in the distributional sense.

3. As s varies, the meromorphic family of operators $\hat{L}(s,h)^{-1}: H^k \to D^k$ has a pole at σ.

It follows from the characterization of points in $\Lambda_k(h)$ that $\Lambda_{k+1}(h) \cap U_k = \Lambda_k(h)$. We call any $\sigma \in \Lambda_k(h)$ for some k a quasinormal frequency of $L(h)$, with geometric multiplicity d. A corresponding smooth solution to $\hat{L}(\sigma,h)w = 0$ is a quasinormal mode, and a distribution X satisfying *ii*) above we call a co-mode. Notice that the condition on X implies that X is supported in $\overline{B}$ and so can be uniquely extended to act on test functions in $C^\infty(\overline{B})$.

The residue of $\hat{L}(s,h)^{-1}$ at $s = \sigma$ is a finite rank operator, and we identify the rank of this residue with the algebraic multiplicity of σ. As in the familiar case of matrices, the algebraic multiplicity is an upper bound for the geometric multiplicity. We say that a quasinormal frequency $\sigma \in \Lambda_k(h)$ is *simple* if it has algebraic multiplicity one.

The result above holds for h fixed. The question we shall consider in this study, that of quasinormal spectral instability, amounts to trying to understand how the set $\Lambda_k(h)$ changes as h varies.

3 Stability of quasinormal frequencies

3.1 Simple quasinormal frequencies

Let us suppose that for the unperturbed operator, that is, at $h = 0$, we can compute the quasinormal frequencies, modes, and co-modes, and we consider some simple $\sigma \in \Lambda_k(0)$ with corresponding quasinormal mode w and co-mode X. It was shown in Joykutty [29] that that as h varies, there is some smooth curve of quasinormal frequencies $\sigma(h) \in \Lambda_k(h)$, with $\sigma(0) = \sigma$, together with an associated curve of quasinormal modes $w(h)$ with $w(0) = w$, depending smoothly on h such that

$$\hat{L}(\sigma(h),h)w(h) = 0$$

holds for all $|h| < \epsilon$. Moreover, in Joykutty [29] an explicit power series expansion for $\sigma(h)$ is given in terms of the trace of certain operator valued contour integrals. We shall take a more elementary approach to find a formula for $\sigma'(0)$.

Since $\hat{L}$ depends smoothly on its arguments, we can differentiate with respect to h at $h = 0$ to find:

$$\sigma'(0)\frac{\partial \hat{L}}{\partial s}(\sigma,0)w + \frac{\partial \hat{L}}{\partial h}(\sigma,0)w + \hat{L}(\sigma,0)w'(0) = 0. \tag{6}$$

By assumption, we know $\frac{\partial \hat{L}}{\partial s}(\sigma,0)$, $\frac{\partial \hat{L}}{\partial h}(\sigma,0)$ and w, but we do not know anything about $w'(0)$. If, however, we act on Equation 6 with the co-mode X, the term involving $w'(0)$ will be annihilated. We find then:

$$\sigma'(0)X\left[\frac{\partial \hat{L}}{\partial s}(\sigma,0)w\right] + X\left[\frac{\partial \hat{L}}{\partial h}(\sigma,0)w\right] = 0$$

or, rearranging

$$\sigma'(0) = -\frac{X\left[\frac{\partial \hat{L}}{\partial h}(\sigma,0)w\right]}{X\left[\frac{\partial \hat{L}}{\partial s}(\sigma,0)w\right]}. \tag{7}$$

This formula gives us an exact expression for the velocity of the curve of quasinormal frequencies $\sigma(h)$ as it passes through σ.

We observe that only the numerator of Equation 7 depends on the perturbation—the denominator can be computed from the unperturbed operator alone. Recalling that the operator norm of a linear map $A: V \to W$ between normed spaces is given by

$$\|A\|_{V\to W} = \sup_{u\in V, \|u\|_V = 1} \|Au\|_W,$$

we can estimate $\sigma'(0)$ in terms of an operator norm of the linearized perturbation as

$$|\sigma'(0)| \leqslant \gamma_\sigma \left\| \frac{\partial \hat{L}}{\partial h}(\sigma,0) \right\|_{H^k \to H^k}. \tag{8}$$

Here, the sensitivity, or condition number, γ_σ depends only on the unperturbed operator and is given by

$$\gamma_\sigma = \frac{\|w\|_k \|X\|_{k*}}{\left|X\left[\frac{\partial \hat{L}}{\partial s}(\sigma,0)w\right]\right|}$$

where $\|X\|_{k*} := \|X\|_{H^k\to\mathbb{C}}$. We can think of the expression for γ as a generalization of the formula for the sensitivity of a matrix eigenvalue.

At this stage, it is worth commenting on the role of k in the discussion. Increasing k increases the region of the complex plane in which we can study the quasinormal frequencies; however, the price we pay for this in Equation 8 is an increase in the control that we require on the perturbation. We can mitigate this by choosing k to be as small as possible, consistent with $\sigma \in \Lambda_k(0)$. Even doing this we see that to bound the rate of change of a quasinormal frequency σ, we (roughly speaking) need control of more than $-\kappa^{-1}(\mathrm{Re}\,\sigma)$ derivatives of the perturbation. We shall see this more explicitly later on. We should note that 'control of higher derivatives' may appear to be an unphysical condition, but one can also view this condition as asking that the perturbations should not have too much of their energy at high wavenumbers.[5]

The arguments above do not rely strongly on the particular form of the metric, or the family of operators we consider. As long as a result broadly analogous to the conclusions of Theorem 1 holds, we can expect to be able to repeat this argument.

3.2 Non-simple quasinormal frequencies

In the discussion above, we made the assumption that the quasinormal frequency σ was simple, which was needed to establish that σ sits on a smooth curve of quasinormal frequencies. If σ is not simple, then this need not be the case in general—see Figure 3 for a situation where this arises in our numerics. It does follow from [29] that the number of QNFs, counted with suitable multiplicity, inside a small circle around σ is independent of h for small h, so that QNFs in particular cannot be locally "created" or "destroyed"

5 Roughly speaking, for a perturbation in H^k, the fraction of the total energy carried by wavenumbers greater than μ is bounded by a constant multiple of μ^{-2k} for large μ.

by small perturbations of the type we consider—QNFs can only appear from infinity or by splitting off from a QNF with algebraic multiplicity greater than one.

In general, it does not appear to be a straightforward question to determine whether a particular non-simple quasinormal frequency lies on a smooth curve. In some cases, however, it may be that evolution under $L(h)$ leaves invariant some subspace (such as an angular momentum eigenspace) so we can consider the problem of finding quasinormal frequencies restricted to this subspace. If σ is a simple quasinormal frequency of the restricted problem, then the results of the previous section will apply.

4 The generalized pseudospectrum

In Jaramillo et al. [16] and subsequently [see Boyanov et al. [23] and references therein], the instability of the quasinormal spectrum has been investigated using the notion of pseudospectrum, comparing the results from this approach to computations with explicit perturbations. Recall that for a matrix A we can define the $\epsilon-$pseudospectrum to be[6]

$$\Lambda^\epsilon = \{s \in \mathbb{C} : \left|\left|(A - s\imath)^{-1}\right|\right|_{\mathbb{R}^n \to \mathbb{R}^n} > \epsilon^{-1}\}.$$

where we define $\left|\left|(A - s\imath)^{-1}\right|\right|_{\mathbb{R}^n \to \mathbb{R}^n} = \infty$ whenever $A - s\imath$ is not invertible. It can be shown [30–32] that Λ^ϵ corresponds to the set of points which can appear in the spectrum of $A + \delta A$, where δA is a perturbation satisfying $||\delta A||_{\mathbb{R}^n \to \mathbb{R}^n} < \epsilon$.

This notion generalizes to operators on infinite dimensional spaces in the obvious way. However, this definition cannot immediately be applied to our problem above because $\hat{L}(s, h)$ is not of the form $A - sI$ for some operator A. There are two possible approaches to resolve this. The approach taken by Jaramillo et al. [16] is to follow [2, 13, 14] and recast the problem of finding the quasinormal frequencies as a genuine eigenvalue problem by writing

$$\hat{L}(s, h) = L_2(h) + sL_1(h) + s^2$$

where $L_j(h)$ is a differential operator of order j. Then, we can verify that $\hat{L}(s, h)w = 0$ has a solution if and only if

$$\begin{pmatrix} -s & 1 \\ -L_2(h) & -L_1(h) - s \end{pmatrix} \begin{pmatrix} w \\ v \end{pmatrix} = 0$$

has a smooth solution. Thus, the set $\Lambda_k(h)$ can be identified with the part of the spectrum of

$$\mathcal{L}(h) = \begin{pmatrix} 0 & 1 \\ -L_2(h) & -L_1(h) \end{pmatrix}$$

in U_k, where $\mathcal{L}(h)$ is thought of as a closed unbounded operator on $\mathcal{H}^k := H^{k+1} \times H^k$. This motivates one definition of the $\epsilon-$pseudospectrum[7] as

$$\tilde{\Lambda}^\epsilon_k = \{s \in \mathbb{C} : \left|\left|(\mathcal{L}(0) - s\imath)^{-1}\right|\right|_{\mathcal{H}^k \to \mathcal{H}^k} > \epsilon^{-1}\}.$$

This has the advantage of being the standard definition applied to $\mathcal{L}$, but the disadvantage that in numerical computations one has to double the dimension of the approximation space to account for the two functions w, v. Moreover, since $\mathcal{L}$ does not have compact resolvent, approximation by matrices can be more challenging.

An alternative approach is to generalize the notion of $\epsilon-$pseudospectrum by declaring

$$\Lambda^\epsilon_k = \{s \in U_k : \left|\left|\hat{L}(s, 0)^{-1}\right|\right|_{H^k \to H^k} > \epsilon^{-1}\}. \tag{9}$$

This has the advantage that $\hat{L}(s, 0)^{-1} : H^k \to H^k$ is compact, but the disadvantage that since it is not the standard definition of pseudospectrum, one cannot readily make use of existing numerical libraries. We note as an aside that we could also consider the $H^k \to D^k$ norm in place of the $H^k \to H^k$ norm in Equation 9, but it will not make a significant difference for the type of perturbations we consider.

We shall take Equation 9 as our definition of the pseudospectrum for the rest of the study [see Besson et al. [26] for an alternative approach]. A modification of the usual arguments for pseudospectra [31, 32] shows that Λ^ϵ_k is precisely the set of points in U_k which can occur as quasinormal frequencies of $L(s, 0) + E$ for some operator $E : H^k \to H^k$ satisfying $||E||_{H^k \to H^k} < \epsilon$. One can verify that the fact that s does not appear linearly in $L(s, 0)$ does not affect this argument. In particular, provided $||V_h||_{C^k} < \epsilon/\kappa^2$ we have $\Lambda_k(h) \subset \Lambda^\epsilon_k$.

We note that this definition agrees with that for the null slicing in Cownden et al. and Boyanov et al. [22, 23]; however, we do not assume that the slicing is everywhere null.

5 Explicit computations for perturbations of the conformal wave operator

To give a concrete demonstration of the ideas above, we will work in a setting where the quasinormal frequencies, modes, and co-modes of the operator are known explicitly at $h = 0$. In particular, from now on we assume that we perturb about the conformal wave operator on de Sitter, in our language:

$$V_0(\boldsymbol{x}) = 2.$$

Under this assumption, we have [27, 28]:

Lemma 2. Suppose $V_0(\boldsymbol{x}) = 2$. Then:

1. $\Lambda_k(0) = \{-\kappa, -2\kappa, -3\kappa, \ldots, -k\kappa\}$.
2. The quasinormal frequency $\sigma_n := -n\kappa \in \Lambda_k(0)$ has geometric and algebraic multiplicity n^2, and a basis for the corresponding

6 The pseudospectrum is usually defined as a closed set, with $\geqslant$ in place of $>$; however, the open condition generalizes more straightforwardly to the infinite dimensional case.

7 The pseudospectrum is a property of the *unperturbed* operator; hence, we set $h = 0$.

TABLE 1A Coefficients $A^i_{n,l}$ for the first six quasinormal frequencies with in each of the angular sectors $l = 0, 1, 2$. (A) $l = 0$.

n \ i	0	1	2	3	4	5
1	1					
2	1	1				
3	0	2	1			
4	0	0	3	1		
5	0	0	0	4	1	
6	0	0	0	0	5	1

TABLE 1B $l = 1$.

n \ i	0	1	2	3	4	5	6
2	2	1					
3	0	3	1				
4	0	0	4	1			
5	0	0	0	5	1		
6	0	0	0	0	6	1	
7	0	0	0	0	0	7	1

space of quasinormal frequencies is given in terms of the standard spherical polar coordinates (r, θ, ϕ) on B_κ by

$$w_{n,l,m} = (\kappa r)^l Y_{l,m}(\theta,\phi)\, {}_2F_1\left[\frac{1+l-n}{2}, \frac{2+l-n}{2}, \frac{3+2l}{2}; \kappa^2 r^2\right].$$

Here, $Y_{l,m}$ are the spherical harmonics, ${}_2F_1$ is the hypergeometric function and the integers m, l satisfy $|m| \leqslant l \leqslant n$.

3. For each $\sigma_n \in \Lambda_k(0)$, the corresponding quasinormal co-modes are supported on ∂B. A basis for the space of co-modes is given in terms of the action on a smooth test function by

$$X_{n,l,m}[\varphi] = \sum_{i=0}^{n-1} A^i_{n,l} \frac{1}{\kappa^i} \left.\frac{d^i \varphi_{l,m}}{dr^i}\right|_{r=\kappa^{-1}} \tag{10}$$

where $|m| \leqslant l \leqslant n$, $A^i_{n,l}$ are constants, and $\varphi_{l,m}(r)$ is the projection of φ onto the $(l, m)-$spherical mode.

While it is possible to specify the constants $A^i_{n,l}$ explicitly, see Hintz and Xie; Joykutty [27, 28, 33], for the purposes of our results below it is more computationally efficient to find $X_{n,l,m}$ for any particular choice of n, l, m by simply using Equation 10 as an ansatz in Equation 5 and solving the resulting linear system for $A^i_{n,l}$. Doing so using Mathematica to perform the computations, we find the results in Table 1.

Since for $\sigma \neq -\kappa$ the quasinormal frequencies are not simple, to make use of Equation 7 to estimate the change in the QNF, we shall make the additional assumption that the potential V_h is spherically symmetric. Under this assumption, the QNFs are simple once we restrict our attention to a single fixed angular mode. If we fix l, m with $|m| \leqslant l$, then for $k \geqslant l$, the

TABLE 1C $l = 2$.

n \ i	0	1	2	3	4	5	6	7
3	3	5	1					
4	−3	3	6	1				
5	6	−6	3	7	1			
6	−18	18	−9	3	8	1		
7	72	−72	36	−12	3	9	1	
8	−360	360	−180	60	−15	3	10	1

unperturbed quasinormal spectrum restricted to the l, m angular mode is $\Lambda_k^{l,m}(0) = \{-l\kappa, \ldots, -k\kappa\}$ and all the QNFs are simple. We can compute the rate of change of the QNF at $-\kappa n$ by

$$\sigma'_{n,l,m}(0) = -\frac{X_{n,l,m}\left[\frac{\partial \hat{L}}{\partial h}(\sigma, 0) w_{n,l,m}\right]}{X_{n,l,m}\left[\frac{\partial \hat{L}}{\partial s}(\sigma, 0) w_{n,l,m}\right]}.$$

To use this formula, we also need $\frac{\partial \hat{L}}{\partial s}$ and $\frac{\partial \hat{L}}{\partial h}$. For the particular case of interest, with $L(h)$ given by Equation 2, we have

$$\hat{L}(s,h)u = -\left(s + \kappa x^i \frac{\partial}{\partial x^i}\right)^2 u - 3\kappa\left(s + \kappa x^i \frac{\partial}{\partial x^i}\right) u + \delta^{ij}\frac{\partial^2 u}{\partial x^i \partial x^j} - \kappa^2 V_h u$$

so that

$$\frac{\partial \hat{L}}{\partial s}(\sigma, 0)u = -2\kappa x^i \frac{\partial u}{\partial x^i} - (2s + 3\kappa)u = -2\kappa r \frac{\partial u}{\partial r} - (2s + 3\kappa)u.$$

and

$$\frac{\partial \hat{L}}{\partial h}(\sigma, 0)u = -\kappa^2 W u,$$

where we introduce $W = \left.\frac{\partial V_h}{\partial h}\right|_{h=0}$, the first order perturbation to the potential.

We now have all that is required to compute $\sigma'_{n,l,m}(0)$. In view of the structure of the operator $X_{n,l,m}$, we can write

$$\sigma'_{n,l,m}(0) = \kappa \sum_{i=0}^{n-1} B^i_{n,l} \frac{1}{\kappa^i} W^{(i)}(\kappa^{-1})$$

for some constants $B^i_{n,l}$. Note that this is independent of m due to the spherical symmetry of the perturbing potential. We can again use Mathematica to compute these constants and present the results for the first few modes in the $l = 0, 1, 2$ angular sectors in Table 2.

Picking two cases as examples, we can read off from the tables that

$$\sigma'_{1,0,0}(0) = -\kappa W(\kappa^{-1})$$
$$\sigma'_{3,1,1}(0) = \kappa W(\kappa^{-1}) + \frac{5}{3} W'(\kappa^{-1}) + \frac{1}{3\kappa} W''(\kappa^{-1}).$$

We see very explicitly here and from Table 8 that the rate of change of the quasinormal frequency depends on higher derivatives of

TABLE 2A Coefficients $B^i_{n,l}$ for the first six quasinormal frequencies within each of the angular sectors $l = 0, 1, 2$. (A) $l = 0$.

n \ i	0	1	2	3	4	5
1	-1					
2	1	1				
3	-1	-2	$-\frac{2}{3}$			
4	1	3	2	$\frac{1}{3}$		
5	-1	-4	-4	$-\frac{4}{3}$	$-\frac{2}{15}$	
6	1	5	$\frac{20}{3}$	$\frac{10}{3}$	$\frac{2}{3}$	$\frac{2}{45}$

TABLE 2B $l = 1$.

n \ i	0	1	2	3	4	5	6
2	-1	$-\frac{1}{3}$					
3	1	$\frac{5}{3}$	$\frac{1}{3}$				
4	-1	$-\frac{41}{15}$	$-\frac{8}{5}$	$-\frac{1}{5}$			
5	1	$\frac{19}{5}$	$\frac{53}{15}$	$\frac{16}{15}$	$\frac{4}{45}$		
6	-1	$-\frac{169}{35}$	$-\frac{216}{35}$	$-\frac{102}{35}$	$-\frac{34}{63}$	$-\frac{2}{63}$	
7	1	$\frac{41}{7}$	$\frac{199}{21}$	$\frac{128}{21}$	$\frac{110}{63}$	$\frac{23}{105}$	$\frac{1}{105}$

TABLE 2C $l = 2$.

n \ i	0	1	2	3	4	5	6	7
3	-1	$-\frac{3}{5}$	$-\frac{1}{15}$					
4	1	$\frac{11}{5}$	$\frac{4}{5}$	$\frac{1}{15}$				
5	-1	$-\frac{117}{35}$	$-\frac{93}{35}$	$-\frac{64}{105}$	$-\frac{4}{105}$			
6	1	$\frac{157}{35}$	$\frac{544}{105}$	$\frac{227}{105}$	$\frac{1}{3}$	$\frac{1}{63}$		
7	-1	$-\frac{583}{105}$	$-\frac{887}{105}$	$-\frac{316}{63}$	$-\frac{82}{63}$	$-\frac{1}{7}$	$-\frac{1}{189}$	
8	1	$\frac{139}{21}$	$\frac{260}{21}$	$\frac{601}{63}$	$\frac{52}{15}$	$\frac{194}{315}$	$\frac{34}{675}$	$\frac{1}{675}$

the perturbing potential, and the larger n, that is, the deeper into the stable plane we go, the more derivatives that are required. Equivalently, the deeper into the stable plane, the more control we require on the high wavenumber component of our perturbation. The increasing order of the operator norm that appears on the right-hand side of Equation 8 as we probe deeper into the plane is not simply an artifact of our framework but is necessary.

To see why it is necessary to use higher order norms to constrain the perturbations, let us consider the case $\kappa = 1$ and consider a family of perturbations $W(r) = \epsilon^3 \exp(-\frac{r^2}{\epsilon^2})$. We clearly have that

$$|W(r)| + |W'(r)| \lesssim \epsilon$$

so in particular as $\epsilon \to 0$, we see that in the 'energy norm', that is, the operator norm associated to the H^1 norm we have that the perturbation tends to zero. However, $W''(1) = (4\epsilon^{-1} - 2\epsilon)\exp(-1/\epsilon^2) \sim \epsilon^{-1}$ as $\epsilon \to 0$, so that using the expression above we see that the $l = m = 1, n = 3$ mode is displaced (to first order) by a term proportional to ϵ^{-1}. Hence, smallness of the perturbation in the energy norm is no guarantee of stability of the quasinormal modes lying sufficiently deep in the stable half-plane.

For the choice of potential $V_h(r) = 2 + h\exp(-r^2)$, with $\kappa = 1$, which we study numerically below, we have computed $\left|\sigma'_{n,l,m}(0)\right|$ for $n \leqslant 20, l \leqslant 2$ and presented the results graphically in Figure 1. Noting the logarithmic scale on the $y-$axis, we see that for this choice of perturbing potential $\left|\sigma'_{n,l,m}(0)\right|$ grows roughly exponentially in n, consistent with our expectation that modes deeper in the stable plane become more and more unstable.

6 Numerical calculation of QNFs and comparison to analytic results

To test numerically the computations above, we have computed the quasinormal frequencies for the choice $V_h(r) = 2 + h\exp(-r^2)$. We first present the results and then comment on the methods used below.

6.1 Results

Since the equation is real, as is the quasinormal spectrum of $\hat{L}(s, 0)$, frequencies can only move off the real axis in complex conjugate pairs. Restricted to each angular sector the QNFs are simple, so each QNF must remain real for a range of h values near 0. Accordingly, in Figure 2 we show the directly computed real part of the quasinormal frequencies as a function of h. Superposed on this, we also plot the linear approximation to the QNFs given by

$$\sigma_{n,l,m}(h) \approx \sigma_{n,l,m}(0) + h\sigma'_{n,l,m}(0),$$

with $\sigma'_{n,l,m}(0)$ computed using the exact methods of §5 and we see very good agreement with the full numerical computation. We have experimented and this result is robust to changes to the potential, provided it remains smooth. We have thus verified the results of §5. We note that this is a non-trivial test of our numerical scheme (described below) as it correctly predicts the values of the QNFs for $h = 0$ and agrees with the analytical computations for the gradient of the blue curves at these points.

Figure 2 shows that pairs of QNFs do eventually meet and move off the real axis. In Figure 3, we show an example of one such interaction in the complex plane, which occurs when the quasinormal frequencies with $l = 0, \sigma(0) = -2, -3$ coalesce and move into the complex plane at $h \approx 0.4645$. We note that (within the accuracy of the numerics) it appears that we cannot identify a smooth curve $\sigma(h)$ of QNFs passing through the point at which the QNFs meet (and hence cease to be simple). Whichever branch we pick, the curve will have to turn through an angle of $\pi/2$ as h passes the critical value. The choices of h to plot were determined by setting $h_i = 0.4645 + \epsilon_i|\epsilon_i|$, and taking ϵ_i to be spaced uniformly in $[-1, 1]$. This figure was computed with a depth $k = 3$ and $N = 25$ gridpoints, see §6.2.

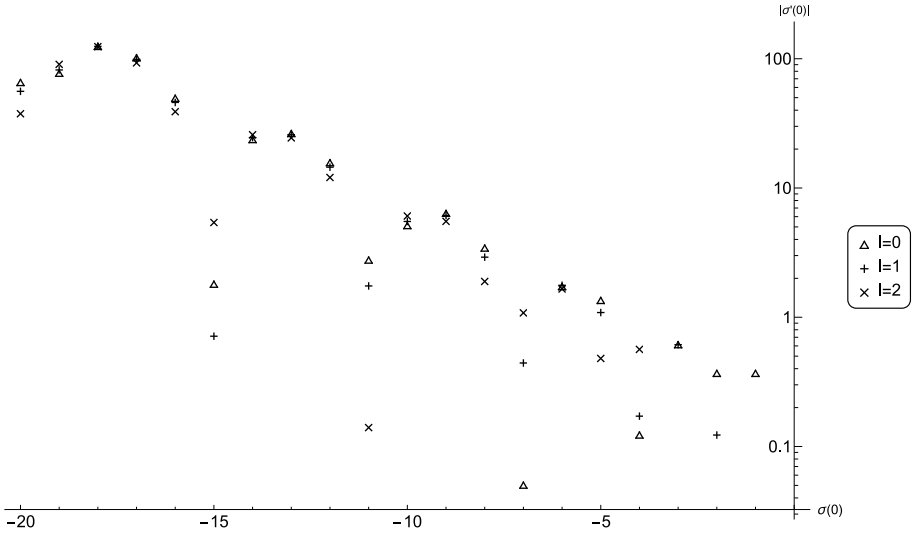

FIGURE 1
Magnitude of $\sigma'_{n,l,m}(0)$ for $n \leqslant 20$, $l \leqslant 2$ for the potential $V_h(r) = 2 + h\exp(-r^2)$, with $\kappa = 1$.

6.2 The numerical scheme

The numerics in this section are performed using a null slicing, rather than the spacelike slicing introduced above, but the scheme can be readily adapted for a spacelike slicing. For convenience, we will take $\kappa = 1$ from now on. Setting

$$\tau = t - \log(1 + r)$$

the metric takes the form

$$g = -\left(1 - r^2\right) d\tau^2 - 2dr d\tau + r^2(d\theta^2 + \sin^2\theta d\phi^2). \tag{11}$$

To find the quasinormal frequencies, we seek solutions to $\hat{L}(s,h)u = 0$ of the form

$$u(r,\theta,\phi) = \frac{R(r)}{r} Y_{l,m}(\theta,\phi)$$

If we define

$$\mathcal{L}R := \frac{d}{dr}\left((1-r^2)\frac{dR}{dr}\right) - \frac{l(l+1)}{r^2}R + V_h R$$

then

$$r\hat{L}(s,h)u = \mathcal{L}R - 2s\frac{dR}{dr}$$

so that to find quasinormal frequencies, we are led to consider the solvability of

$$\mathcal{L}R - 2s\frac{dR}{dr} = f \tag{12}$$

for given f, with $f(0) = R(0) = 0$ and R regular $r = 1$. Rather than directly discretize Equation 12, we first expand to a system of equations by differentiating the equation. We have the commutation relation

$$\left[r\frac{d}{dr}, \mathcal{L}\right] = -2\mathcal{L} - 2\left(r\frac{d}{dr}\right)^2 - 2r\frac{d}{dr} + 2V_h + r\frac{dV_h}{dr}.$$

Let $R^p = \left(r\frac{d}{dr}\right)^p R$, $V_h^p = \left(r\frac{d}{dr}\right)^p V_h$, and $f^i = \left(r\frac{d}{dr}\right)^i f$. Then using the commutation relation, we can show that Equation 12 implies

$$\mathcal{L}R^p + \sum_{i=1}^{p+1}\alpha_i^p R^i + \sum_{i,j=0}^{p}\beta_{i,j}^p V_h^i R^j - s\sum_{i=0}^{p}\gamma_i^p\frac{dR^i}{dr} = \sum_{i=0}^{p}\mu_i^p f^i$$

where $\alpha_i^p, \beta_{i,j}^p, \gamma_i^p$ are numerical (indeed integer) constants determined recursively by

$$\alpha_i^{p+1} = \alpha_{i-1}^p + 2\alpha_i^p \ (1 \leqslant i \leqslant p), \qquad \alpha_{p+1}^{p+1} = \alpha_p^p + 2\alpha_{p+1}^p - 2,$$
$$\alpha_{p+2}^{p+1} = \alpha_p^{p+1} - 2$$

with $\alpha_i^0 = 0$ for all i. Next, we set $\beta_{i,j}^p = 0$ for all i,j and recursively define

$$\beta_{0,p}^{p+1} = \beta_{0,p-1}^p + 2\beta_{0,p}^p + 2, \qquad \beta_{1,p}^{p+1} = \beta_{0,p-1}^p + \beta_{1,p-1}^p + 2\beta_{1,p}^p + 1.$$

with

$$\beta_{i,j}^{p+1} = \beta_{i-1,j}^p + \beta_{i,j-1}^p + 2\beta_{i,j}$$

otherwise. Finally, set $\gamma_0^0 = 1 = \mu_0^0, \gamma_i^0 = 0 = \mu_i^0$ for all $i \neq 0$ and

$$\gamma_i^{p+1} = \gamma_{i+1}^p + \gamma_i^p, \qquad \mu_i^{p+1} = \mu_{i-1}^p + 2\mu_i^p.$$

We can verify that $\alpha_{p+1}^p = -2p$, which we expect as a consequence of the enhanced redshift effect (see Warnick and Dafermos–Rodninski [2, 34]).

To construct our numerical scheme, we fix an integer $k \geqslant 0$, which we call the depth of the scheme. If Equation 12 holds, then the system of equations:

$$\left[\mathcal{L} - 2kr\tfrac{d}{dr}\right]R^p + 2kR^{p+1} + \textstyle\sum_{i=1}^{p+1}\alpha_i^p R^i + \sum_{i,j=0}^{p}\beta_{i,j}^p V_h^i R^j$$
$$-s\textstyle\sum_{i=0}^{p}\gamma_i^p\frac{dR^i}{dr} = \sum_{i=1}^{p}\mu_i^p f^i \quad (0 \leqslant p < k)$$
$$\left[\mathcal{L} - 2kr\tfrac{d}{dr}\right]R^k + \textstyle\sum_{i=1}^{k}\alpha_i^k R^i + \sum_{i,j=0}^{k}\beta_{i,j}^k V_h^i R^j - s\sum_{i=0}^{k}\gamma_i^k\frac{dR^i}{dr}$$
$$= \textstyle\sum_{i=1}^{k}\mu_i^k f^i \tag{13}$$

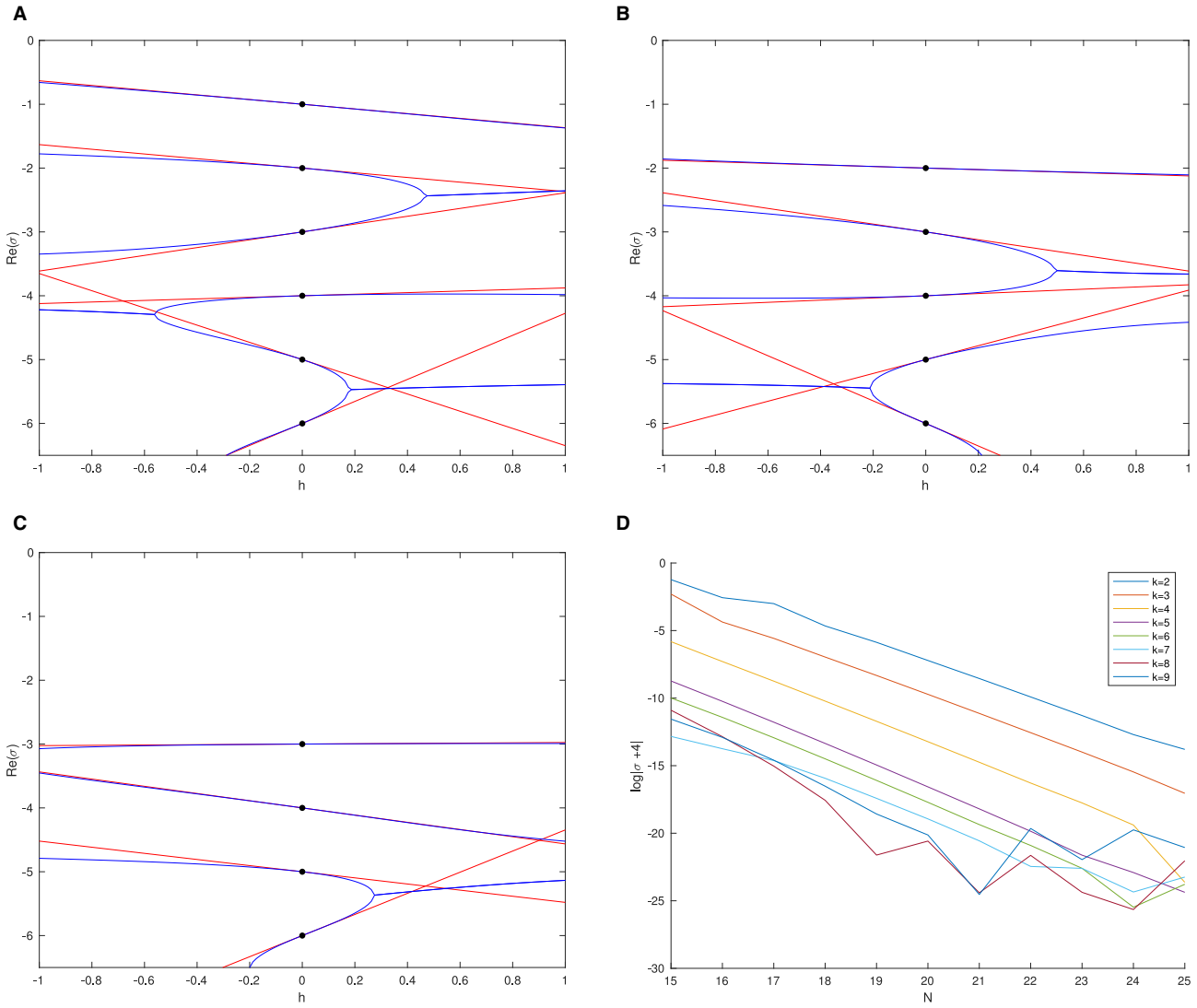

FIGURE 2
Re($\sigma(h)$) plotted against h for numerically computed QNFs for $V_h = h\exp(-r^2)$ (blue lines) together with the linear approximations (red lines) in the $l = 0, 1, 2$ sector. The black dots mark the location of the analytically known QNFs for $h = 0$. **(A)** $l = 0$. **(B)** $l = 1$. **(C)** $l = 2$. **(D)** Logarithmic error against N for $k = 2, \ldots, 9$.

will also hold. Here, we have used the fact that $r\frac{d}{dr}R^p = R^{p+1}$ to arrange that we have the operator $\left[\mathcal{L} - 2kr\frac{d}{dr}\right]$ acting as the principle differential operator on all components. This is the approach taken to increase the working regularity in the analysis of Warnick [2].

We now treat $R^0, \ldots, R^k$ as independent functions, and we discretize on the interval $[0, 1]$ using a pseudospectral method, following Trefethen [35]. The constants α, β, γ are found recursively, and the derivatives V_h^i are computed exactly using Matlab's *Symbolic Math Toolbox* before discretization. We note that $R^p(0) = 0$ which gives a Dirichlet boundary condition at one end of our interval, and we do not need a boundary condition at $r = 1$ as the pseudospectral discretization will impose smoothness there automatically.

After discretizing on N points, Equation 13 becomes

$$(A - sB)V = CF \tag{14}$$

for $(kN) \times (kN)$-matrices A, B, C and column vectors V, F which represent the discretization of $(R^0, \ldots, R^k)$, $(f^0, \ldots, f^k)$, respectively. We work throughout at standard machine precision.

6.2.1 The quasinormal spectrum

If σ is a quasinormal frequency, then we expect the generalized eigenvalue problem

$$(A - sB)V = 0$$

to have an eigenvalue near σ. Thus, we can find the quasinormal frequencies by applying Matlab's generalized eigenvalue finder to Equation 14. However, by enlarging the original problem to

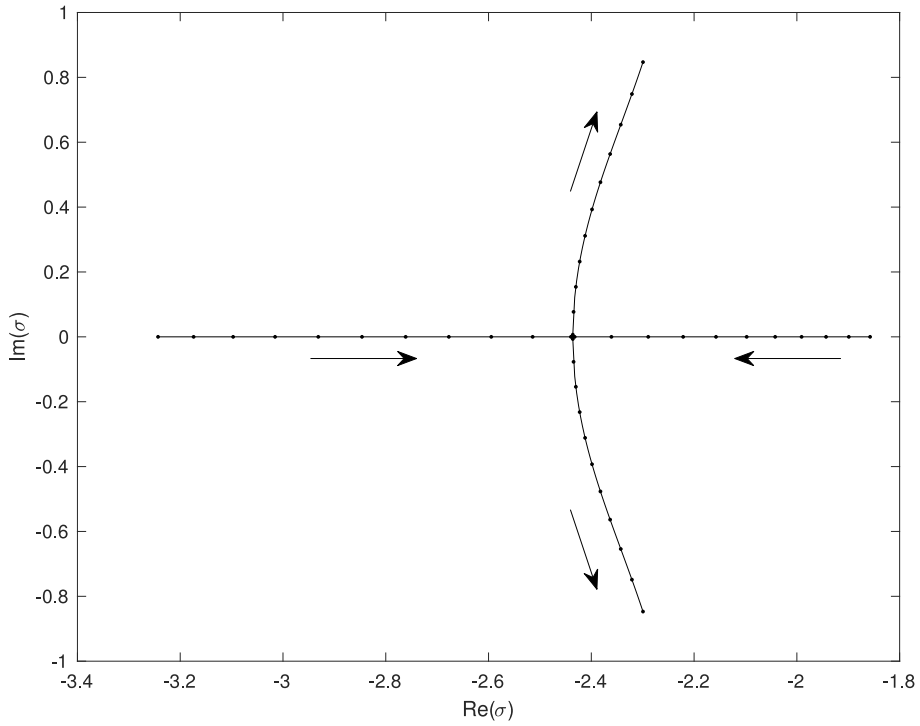

FIGURE 3
Numerically determined QNFs in a neighborhood of the transition point at $h \approx 0.4645$, at which the two real QNFs with $l = 0, \sigma(0) = -2, -3$ meet and branch into a conjugate pair of complex QNFs. Arrows indicate the direction of increasing h.

a system, we may have introduced spurious eigenvalues which correspond to vectors V for which the condition

$$R^{p+1} = r\frac{dR^p}{dr}, \qquad 0 \leqslant p < k \tag{15}$$

does not hold. To enforce this condition, we select only those eigenvalues of 14 for which (the discretized version of)

$$\sum_{p=0}^{k-1} \left|\left| R^{p+1} - r\frac{dR^p}{dr} \right|\right|^2 < e$$

holds, where e is a sufficiently small threshold parameter, which we take to be 10^{-1} for the computations in this study.

Plots 2a–c show the numerically computed quasinormal spectrum in the $l = 0, 1, 2$ sector as h varies, computed using $k = 6, N = 25$. Plot 2d shows the error in the scheme when computing the eigenvalue at $\sigma = -4$ for various values of k. We see (as has been observed in other situations [16]) that for a given value of k, the pseudospectral method in fact can accurately find quasinormal frequencies even outside the domain U_k in which we expect the numerics to converge.

6.2.2 The pseudospectra

To compute pseudospectra for different k, we need to numerically approximate $\left|\left|\hat{L}(s,0)^{-1}\right|\right|_{H^k \to H^k}$. We can approximate this by computing

$$\left|\left|\hat{L}(s,0)^{-1}\right|\right|_{H^k \to H^k} \approx \left|\left|(A - sB)^{-1} C\Pi\right|\right|_{\ell^2 \to \ell^2}$$

where Π is the L^2-orthogonal projector onto the space of vectors F of the form $(f^0, \ldots, f^k)$, where $f^i = \left(r\frac{d}{dr}\right)^i f$. This projection is necessary to account for the enlargement of our space by considering the system of higher derivatives. Since for such an F we have[8] $||F||_{\ell^2} \approx \left|\left|f\right|\right|_{H^k}$ we can approximately compute the H^k operator norm of $\hat{L}(s,0)^{-1}$ by the ℓ^2 operator norm of the approximating matrix.

In Figure 4, we show the numerically computed pseudospectra for $k = 1, \ldots, 6$. We see that in all cases the pseudospectrum is well-behaved in the region U_k, but that the contours open out significantly once we leave this region. We expect that the fact that the contour curves can leave U_k at all is a feature of the finite truncation. We observe the phenomenon noted above that the spectral method finds quasinormal frequencies accurately, even in the region of the plane that we expect significant numerical instability. For example, in Figure 4A we see the first five frequencies accurately computed, even though only the first is actually in U_1.

To verify convergence of the numerical operator norm, in Figure 5 we show the approximated values of $\left|\left|\hat{L}(s,0)^{-1}\right|\right|_{H^k \to H^k}$ at $s = -4 + i$ for $k = 2$ and $k = 4$ as N varies. As expected, in the $k = 2$ case we see divergence, since for this k our choice of s does not belong to U_k. For the case $k = 4$, we are in the region U_k, and we see good

8 In fact this is the discretized version of a *weighted* Sobolev nor; however, since the weights only degenerate near $r = 0$, this is adequate for our purposes.

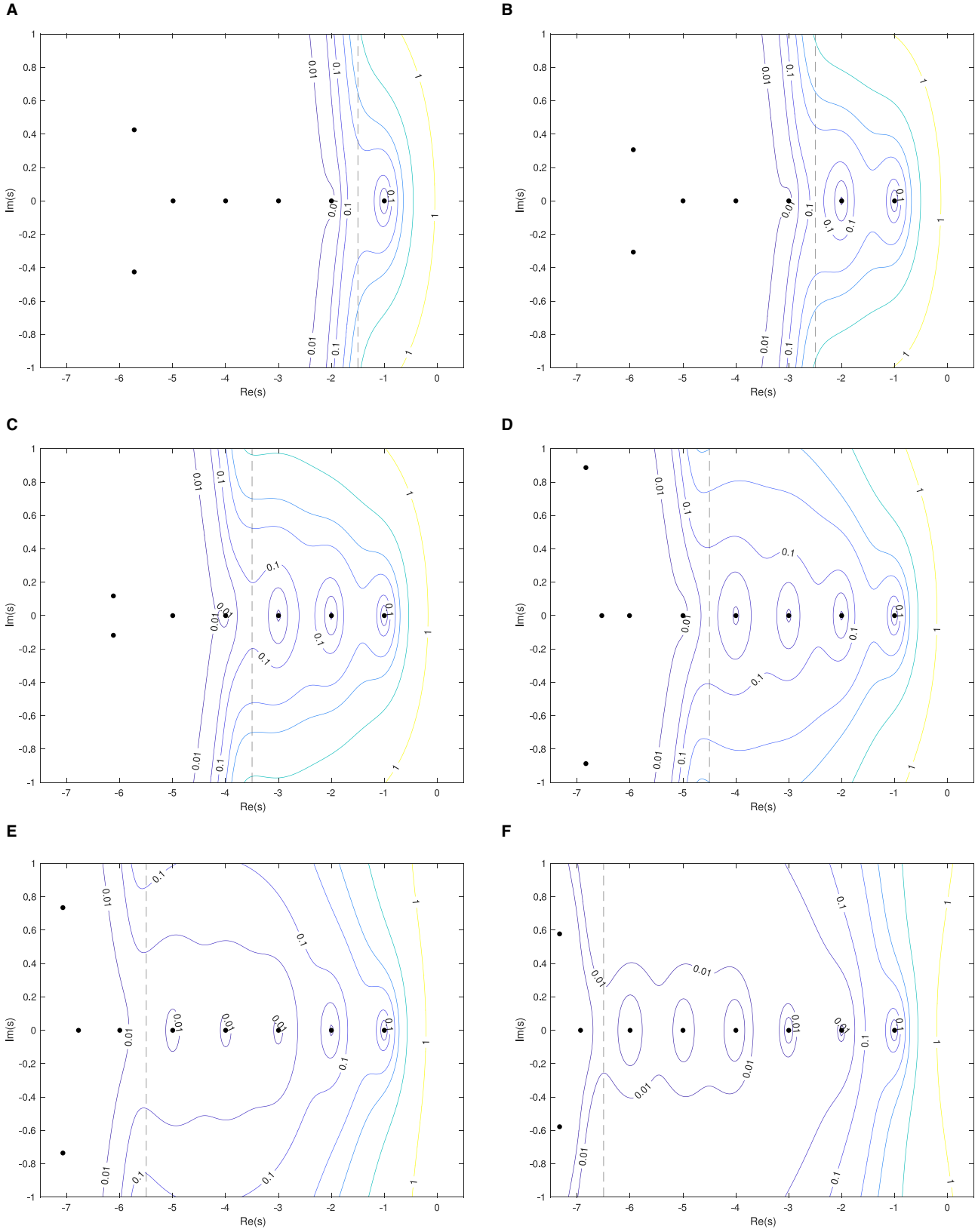

FIGURE 4
Numerically computed contour lines $\left|\left|\hat{L}(s,0)^{-1}\right|\right|_{H^k \to H^k} = \epsilon^{-1}$ for $1 \leqslant k \leqslant 6$. The black dashed line indicates the boundary of U_k. Black dots are the QNFs of $\hat{L}(s,0)^{-1}$ computed by the numerical algorithm with $N = 35$. **(A)** $k = 1$. **(B)** $k = 2$. **(C)** $k = 3$. **(D)** $k = 4$. **(E)** $k = 5$. **(F)** $k = 6$.

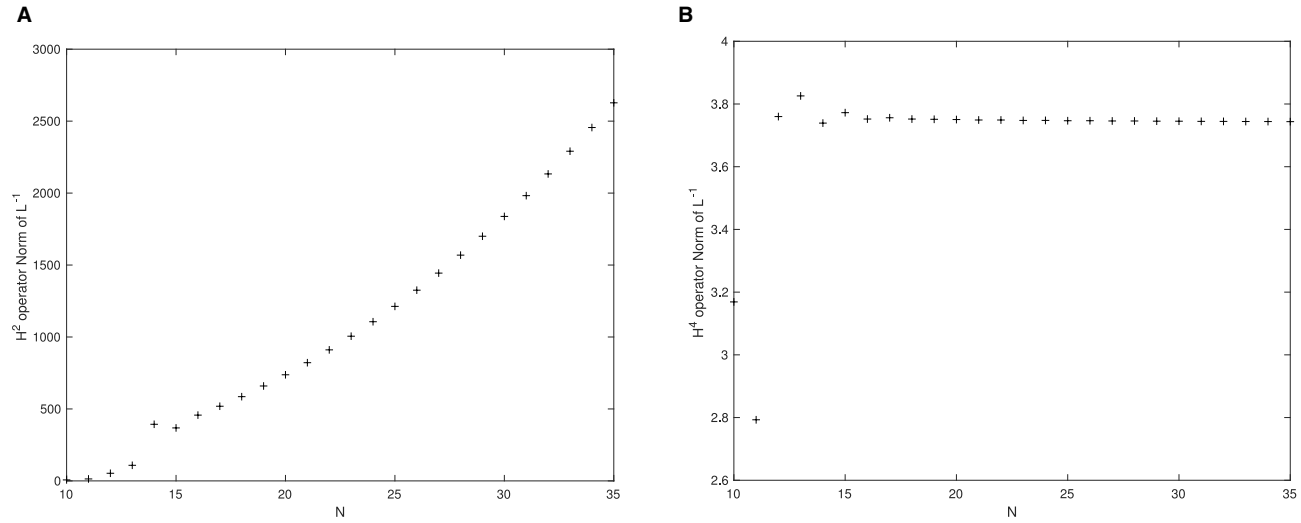

FIGURE 5
Convergence of $\left\|\hat{L}^{-1}(s_0, 0)\right\|_{H^k \to H^k}$ at $s_0 = -4 + i$ for $k = 2$ and $k = 4$. **(A)** $k = 2$. **(B)** $k = 4$.

convergence. This can be compared to Figure 7 of [23]. We should mention that the pseudospectrum for this operator according to the standard definition has been computed for $k = 1$ in [36], which appeared slightly before this study—see their Figure 11.

7 Conclusion

We have investigated the stability of the quasinormal spectrum of the conformal wave equation on the static patch of de Sitter. We find that the quasinormal frequencies are stable, provided the perturbing potential is small in a sufficiently high regularity norm. Conversely, one could instead interpret this as a spectral *instability* for perturbing potentials which are not sufficiently regular at the cosmological horizon. We numerically verify our computations using a spectral method and propose a definition for a family of pseudospectra that demonstrate good convergence properties and capture the (in)stability of the quasinormal frequencies.

Data availability statement

The original contributions presented in the study are included in the article/supplementary material, further inquiries can be directed to the corresponding author.

Author contributions

CW: Writing – original draft, Writing – review & editing.

Funding

The author(s) declare that no financial support was received for the research, authorship, and/or publication of this article.

Acknowledgments

I am grateful to Jason Joykutty and Dejan Gajic for several valuable discussions on the topic of pseudospectral instability of black holes. I am especially grateful to José Luis Jaramillo for discussions and very helpful comments on this manuscript. I am also grateful to the The Erwin Schrödinger International Institute for Mathematics and Physics in Vienna for hosting the programme "Spectral Theory and Mathematical Relativity" in Summer 2023, during which I started thinking about this problem.

Conflict of interest

The author declares that the research was conducted in the absence of any commercial or financial relationships that could be construed as a potential conflict of interest.

Publisher's note

All claims expressed in this article are solely those of the authors and do not necessarily represent those of their affiliated organizations, or those of the publisher, the editors and the reviewers. Any product that may be evaluated in this article, or claim that may be made by its manufacturer, is not guaranteed or endorsed by the publisher.

References

1. Vasy A. Microlocal analysis of asymptotically hyperbolic and Kerr-de Sitter spaces (with an appendix by Semyon Dyatlov). *Inventiones Mathematicae*. (2013) 194:381–513. doi: 10.48550/arXiv.1012.4391

2. Warnick CM. On quasinormal modes of asymptotically Anti-de Sitter black holes. *Commun Math Phys*. (2015) 333:5760. doi: 10.48550/arXiv.1306.5760

3. Dyatlov S, Zworski M. *Mathematical Theory of Scattering Resonances. Graduate Studies in Mathematics*. (2019). Available at: https://api.semanticscholar.org/CorpusID:216573983

4. Gajic D, Warnick C. Quasinormal modes in extremal Reissner—Nordström Spacetimes. *Commun Math Phys*. (2021) 385:8479. doi: 10.48550/arXiv.1910.08479

5. Stucker T. *Quasinormal Modes for the Kerr Black Hole* (2024). p. 7.

6. Gajic D, Warnick C. A model problem for quasinormal ringdown of asymptotically flat or extremal black holes. *J Math Phys*. (2020) 61:8481. doi: 10.48550/arXiv.1910.08481

7. Gajic D, Warnick CM. *Quasinormal Modes on Kerr Spacetimes* (2024). p. 7.

8. Aguirregabiria JM, Vishveshwara CV. Scattering by black holes: a simulated potential approach. *Phys Lett A*. (1996) 210:251–4.

9. Vishveshwara CV. On the black hole trail ...: a personal journey. In: *18th Conference of the Indian Association for General Relativity and Gravitation* (1996). p. 11–22.

10. Nollert HP. About the significance of quasinormal modes of black holes. *Phys Rev D*. (1996) 53:4397–402.

11. Nollert HP, Price RH. Quantifying excitations of quasinormal mode systems. *J Math Phys*. (1999) 40:980–1010.

12. Bizoń P, Chmaj T, Mach P. A toy model of hyperboloidal approach to quasinormal modes. *Acta Phys Polon B*. (2020) 51:1007. doi: 10.48550/arXiv.2002.01770

13. Ansorg M, Macedo RP. Spectral decomposition of black-hole perturbations on hyperboloidal slices. *Phys Rev D*. (2016) 93:124016. doi: 10.48550/arXiv.1604.02261

14. Panosso Macedo R, Jaramillo JL, Ansorg M. Hyperboloidal slicing approach to quasi-normal mode expansions: the Reissner-Nordström case. *Phys Rev D*. (2018) 98:124005. doi: 10.48550/arXiv.1809.02837

15. Panosso Macedo R. Hyperboloidal framework for the Kerr spacetime. *Class Quant Grav*. (2020) 37:65019. doi: 10.48550/arXiv.1910.13452

16. Jaramillo JL, Panosso Macedo R, Al Sheikh L. Pseudospectrum and black hole quasinormal mode instability. *Phys Rev X*. (2021) 11:31003. doi: 10.48550/arXiv.2004.06434

17. Al Sheikh L. *Scattering Resonances and Pseudospectrum: Stability and Completeness Aspects in Optical and Gravitational Systems*. Besançon: Université Bourgogne Franche-Comté (2022).

18. Cheung MHY, Destounis K, Macedo RP, Berti E, Cardoso V. Destabilizing the fundamental mode of black holes: the elephant and the flea. *Phys Rev Lett*. (2022) 128:111103. doi: 10.48550/arXiv.2111.05415

19. Sarkar S, Rahman M, Chakraborty S. Perturbing the perturbed: stability of quasinormal modes in presence of a positive cosmological constant. *Phys Rev D*. (2023) 108:104002. doi: 10.48550/arXiv.2304.06829

20. Areán D, Fariña DG, Landsteiner K. Pseudospectra of holographic quasinormal modes. *J High Energy Phys*. (2023) 2023:187. doi: 10.48550/arXiv.2307.08751

21. Destounis K, Duque F. Black-hole spectroscopy: quasinormal modes, ringdown stability and the pseudospectrum. In: Papantonopoulos E, Mavromatos N, editors. *Compact Objects in the Universe*. Cham: Springer (2024). doi: 10.1007/978-3-031-55098-0_6

22. Cownden B, Pantelidou C, Zilhão M. The pseudospectra of black holes in AdS. *J High Energy Phys*. (2024) 2024:202. doi: 10.48550/arXiv.2312.08352

23. Boyanov V, Cardoso V, Destounis K, Jaramillo JL, Panosso Macedo R. Structural aspects of the anti-de Sitter black hole pseudospectrum. *Phys Rev D*. (2024) 109:64068. doi: 10.48550/arXiv.2312.11998

24. Jaramillo JL. Pseudospectrum and binary black hole merger transients. *Class Quant Grav*. (2022) 39:217002. doi: 10.48550/arXiv.2206.08025

25. Gasperín E, Jaramillo JL. Energy scales and black hole pseudospectra: the structural role of the scalar product. *Class Quant Grav*. (2022) 39:115010. doi: 10.48550/arXiv.2107.12865

26. Besson J, Boyanov V, Jaramillo JL. *Black Hole Quasi-Normal Modes as Eigenvalues: Definition and Stability Problem, in Preparation*.

27. Hintz P, Xie Y. Quasinormal modes and dual resonant states on de Sitter space. *Phys Rev D*. (2021) 104:64037. doi: 10.48550/arXiv.2104.11810

28. Hintz P, Xie Y. Quasinormal modes of small Schwarzschil—de Sitter black holes. *J Math Phys*. (2022) 63:2347. doi: 10.48550/arXiv.2105.02347

29. Joykutty J. Existence of zero-damped quasinormal frequencies for nearly extremal black holes. *Annales Henri Poincaré*. (2022) 23:4343–90. doi: 10.48550/arXiv.2112.05669

30. Trefethen LN. Spectra and pseudospectra. In: Ainsworth M, Levesley J, Marletta M, editors. *The Graduate Student's Guide to Numerical Analysis 98: Lecture Notes from the VIII EPSRC Summer School in Numerical Analysis*. Berlin; Heidelberg: Springer Berlin Heidelberg (1999). p. 217–50.

31. Embree M, Trefethen LN. *Pseudospectra Gateway*. Available at: http://www.comlab.ox.ac.uk/pseudospectra (accessed July 28, 2024).

32. van Dorsselaer JLM, Kraaijevanger JFBM, Spijker MN. Linear stability analysis in the numerical solution of initial value problems. *Acta Numerica*. (1993) 2:199–237.

33. Joykutty J. *Quasinormal Modes of Nearly Extremal Black Holes*. Cambridge: Department of Applied Mathematics And Theoretical Physics, Cambridge University (2024).

34. Dafermos M, Rodnianski I. Lectures on black holes and linear waves. *Clay Math Proc*. (2013) 17:97–205. doi: 10.48550/arXiv.0811.0354

35. Trefethen LN. *Spectral Methods in MATLAB*. Society for Industrial and Applied Mathematics (2000). doi: 10.1137/1.9780898719598

36. Carballo J, Withers B. Transient dynamics of quasinormal mode sums. *arXiv:240606685*. doi: 10.48550/arXiv.2406.06685

frontiers | Frontiers in Physics

TYPE Mini Review
PUBLISHED 11 October 2024
DOI 10.3389/fphy.2024.1490016

Check for updates

OPEN ACCESS

EDITED BY
Jose Luis Jaramillo,
Université de Bourgogne, France

REVIEWED BY
Raimundo Silva,
Federal University of Rio Grande do Norte, Brazil

*CORRESPONDENCE
Alberto Saa,
asaa@ime.unicamp.br

RECEIVED 02 September 2024
ACCEPTED 23 September 2024
PUBLISHED 11 October 2024

CITATION
Richarte MG, Fabris JC and Saa A (2024) Quasinormal modes and the analytical continuation of non-self-adjoint operators. *Front. Phys.* 12:1490016. doi: 10.3389/fphy.2024.1490016

COPYRIGHT
© 2024 Richarte, Fabris and Saa. This is an open-access article distributed under the terms of the Creative Commons Attribution License (CC BY). The use, distribution or reproduction in other forums is permitted, provided the original author(s) and the copyright owner(s) are credited and that the original publication in this journal is cited, in accordance with accepted academic practice. No use, distribution or reproduction is permitted which does not comply with these terms.

Quasinormal modes and the analytical continuation of non-self-adjoint operators

Martín G. Richarte[1,2], Júlio C. Fabris[1,3] and Alberto Saa[4]*

[1]PPGCosmo, CCE - Universidade Federal do Espírito Santo, Vitória, Brazil, [2]Departamento de Física, Facultad de Ciencias Exactas y Naturales, Universidad de Buenos Aires, Ciudad Universitaria, Buenos Aires, Argentina, [3]Núcleo Cosmo-ufes, Departamento de Física - Universidade Federal do Espírito Santo, Vitória, Brazil, [4]Departamento de Matemática Aplicada, Universidade Estadual de Campinas, Campinas, Brazil

We briefly review the analytical continuation method for determining quasinormal modes (QNMs) and the associated frequencies in open systems. We explore two exactly solvable cases based on the Pöschl–Teller potential to show that the analytical continuation method cannot determine the full set of QNMs and frequencies of a given problem starting from the associated bound state problem in quantum mechanics. The root of the problem is that many QNMs are the analytically continued counterparts of solutions that do not belong to the domain where the associated Schrödinger operator is self-adjoint, challenging the application of the method for determining full sets of QNMs. We illustrate these problems through the physically relevant case of BTZ black holes, where the natural domain of the problem is the negative real line.

KEYWORDS

self-adjoint extensions, Schrödinger operator, quasinormal modes, black hole, general relativity (GR)

1 Introduction

Quasinormal mode (QNM) analysis is one of the main strategies used to inspect the stability of many physical open systems, with many applications ranging from optics to general relativity [1–3]. In their simplest formulation, QNMs are separable solutions

$$\Psi(t,x) = e^{-i\omega t}u(x)$$

of an $(1+1)$-dimensional wave equation. After a separation of variables procedure, $u(x)$ is typically expected to obey a Schrödinger-like second-order linear differential equation,

$$\left(-\frac{d^2}{dx^2} + V(x)\right)u = \omega^2 u \tag{1}$$

on a certain domain of $\mathbb{R}$. For situations where the modes u are defined on the entire real line $\mathbb{R}$, and the potential $V(x)$ vanishes sufficiently fast for $x \to \pm\infty$, the QNM frequencies are defined as the (typically complex) values of ω such that the solutions of (2) behave as outgoing waves at $x \to \infty$ and ingoing ones at $x \to -\infty$, corresponding intuitively to solutions that disperse toward infinity. According to our definition for Ψ, these outgoing/ingoing waves correspond, respectively, to solutions of (2) such that

$$u \propto e^{i\omega x}, \quad \text{for} \quad x \to \infty,$$

and

$$u \propto e^{-i\omega x}, \quad \text{for} \quad \to -\infty\,.$$

Because (2) admits as solutions both ω and $-\omega$, we need to assume here $\Re(\omega) \geq 0$; otherwise, the QNMs are not unambiguously defined. According to our definition, the modes will be exponentially suppressed in time if $\Im(\omega) < 0$. Notice that, in contrast with the usual spectral theory of Schrödinger operators in quantum mechanics, the eigenvalues ω^2 in (2) can be, and usually are, complex, and the QNMs are not, in general, a complete set for the problem [1].

In standard situations involving asymptotically flat black holes in general relativity (see, for references, [2, 3]), the equivalent of Equation (1) is obtained by introducing some sort of radial tortoise coordinate x in the exterior region of the black hole. Typically, in these cases, the effective potential $V(x)$ is non-negative and has a barrier shape. Moreover, conditions (3) and (4) have the usual interpretation of wave solutions escaping to infinity and plunging into the event horizon, respectively, implying that QNMs are always associated with dispersive phenomena for these systems because they imply a net transport of energy outside the system.

In the present article, we will review the analytical continuation method for determining QNMs and frequencies for problems of type (2), starting from an associated bound state problem in quantum mechanics. Through two explicit examples based on exactly solvable Pöschl–Teller potentials, we will show that the analytical continuation method cannot determine the complete set of QNMs and that the origin of the problem is that QNMs are typically the analytically continued counterparts of solutions that belong to domains where the associated Schrödinger operator fails to be self-adjoint.

2 Analytical continuation of Schrödinger operators

It is rather common to compute the QNMs and their associate frequencies ω for Equation 1 with a given potential barrier V through a formal analytical continuation performed in the bound state problem of a Schrödinger operator $\mathcal{H}$ associated with the potential well corresponding to the inverted potential $\tilde{V} = -V$. Such an approach, introduced decades ago by Blome, Ferrari, and Mashhoon [4–6], is one of the best options we have at hand to obtain analytical answers and gain some physical insights into the QNM problem. The approach consists basically of a formal map between the QNM solutions of (2) and the bound states of the quantum mechanical problem governed by the Schrödinger operator

$$\mathcal{H}\psi = \left(-\frac{\hbar^2}{2m}\frac{d^2}{dx^2} + \tilde{V}(x)\right)\psi = E\psi. \tag{2}$$

We know that for $\tilde{V}(x)$ vanishing sufficiently fast for $x \to \pm\infty$, the bound states of $\mathcal{H}$ will decay exponentially, that is,

$$\psi \propto e^{-\sqrt{-\frac{2mE}{\hbar^2}}x}, \quad \text{for} \quad x \to \infty,$$

and

$$\psi \propto e^{\sqrt{-\frac{2mE}{\hbar^2}}x}, \quad \text{for} \quad \to -\infty\,.$$

Because the literature on bound states of Schrödinger operators is huge, with many studies exploring a vast range of different potentials, this method is commonly beneficial for identifying exact or approximate QNMs.

The original approach is based on the extension of the solutions of (2) or (5) for the entire complex plane by means of the formal substitution (Wick rotation) $x \to ix$, which reduces the QNM boundary conditions (3) and (4) to the bound state ones (6) and (7). After some parameter redefinitions in the potential $V(x)$, one can effectively map the QNMs on the bound states of (5) and, consequently, relate the QNM frequencies ω of (2) with the energy spectrum E of $\mathcal{H}$. More explicitly, suppose we know a bound state ψ of (5). It should have an associate eigenvalue (energy) $E < 0$ because $\tilde{V}$ is assumed to be a non-positive potential well. Suppose also that the potential $\tilde{V}$ depends on a set of real parameters α_k, $k = 1, 2, \ldots$, $\tilde{V} = \tilde{V}(x, \alpha_k)$. Clearly, both the eigenfunction ψ and the energy E may have a similar dependence on the parameters, that is, $\psi = \psi(x, \alpha_k)$ and $E = E(\alpha_k)$. After the formal substitution $x \to -ix$, the Schrödinger Equation (2) will read

$$\left(-\frac{d^2}{dx^2} - \frac{2m}{\hbar^2}\tilde{V}(-ix, \alpha_k)\right)\psi = -E(\alpha_k)\psi, \tag{3}$$

and the asymptotic conditions (6) and (7) for ψ are formally transformed in (3) and (4) for $\psi(-ix)$. Suppose now we can transform the parameter α_k in such a way that the potential $\tilde{V}$ remains invariant under the Wick rotation; that is, let us introduce a new set of parameters α_k' such that

$$\tilde{V}(x, \alpha_k) = \tilde{V}(-ix, \alpha_k').$$

With this transformation, Equation 3 will read

$$\left(-\frac{d^2}{dx^2} - \tilde{V}(x, \alpha_k)\right)u = -E(\alpha_k')u,$$

with $u(x) = \psi(-ix, \alpha_k')$. For the sake of simplicity, we have set $\frac{\hbar^2}{2m} = 1$, without generality loss. Comparing (10) with (2), we see that $u(x)$ is a QNM of the barrier potential corresponding to the inverted potential well $\tilde{V}$ with QNM frequency ω such that

$$\omega^2 = -E(\alpha_k').$$

This method was sensibly simplified by the prescription introduced recently by Hatsuda [7], which is based on the following observation. Let us consider the Schrödinger operator

$$\mathcal{H}_\epsilon\psi = \left(-\epsilon^2\frac{d^2}{dx^2} + \tilde{V}(x)\right)\psi = E_\epsilon\psi,$$

where $\tilde{V}$ is a well-behaved potential well in the entire real line $\mathbb{R}$, and $\epsilon > 0$ is some typical scale of the problem. Suppose $\psi_\epsilon(x)$ is a bound state of $\mathcal{H}_\epsilon$ with energy E_ϵ. Consider now the analytical continuation of the Schrödinger operator given by $\mathcal{H}_{i\epsilon}$. The function $u_\epsilon = \psi_{i\epsilon}$ is a QNM of the inverted potential $-\tilde{V}$, with frequency given by $\omega_\epsilon^2 = -E_{i\epsilon}$.

Before we consider the physically relevant case of BTZ black holes, let us consider a simple explicit example to illustrate better the analytical continuation method.

2.1 The Pöschl–Teller potential well

The Pöschl–Teller potentials [8] were the first family of non-elementary exactly soluble potentials in quantum mechanics. We will illustrate the analytical continuation method with the Pöschl–Teller potential corresponding to the potential well defined for the entire real line $\mathbb{R}$:

$$\tilde{V}(x) = -\frac{V_0}{\cosh^2 x},$$

The Schrödinger Equation 3 with this potential admits bound states with energy spectrum given by (see, for instance, [9])

$$E_\epsilon^{(n)} = -\left(\sqrt{V_0 + \frac{\epsilon^2}{4}} - \epsilon\left(n + \frac{1}{2}\right)\right)^2,$$

with n integer such that $0 \leq n \leq n_{\max}$, where

$$n_{\max} = \left\lfloor \frac{1}{2}\left(1 + \sqrt{\frac{4V_0}{\epsilon^2} + 1}\right)\right\rfloor. \tag{4}$$

It is important to stress that we have only a finite number of bound states for the Pöschl–Teller potential well. This is a well-known property in quantum mechanics for potential wells vanishing sufficiently fast for $x \to \pm\infty$.

We can now apply the Hatsuda prescription, and we will have the following set of QNM frequencies

$$\omega_\epsilon^{(n)} = \sqrt{V_0 - \frac{\epsilon^2}{4}} - i\epsilon\left(n + \frac{1}{2}\right)$$

for the Pöschl–Teller potential barrier $V = -\tilde{V}$. However, one could exactly solve the QNM problem for the inverted Pöschl–Teller potential well V (see, for instance, [2]), and we would get the QNM frequencies (16) without the restriction $0 \leq n \leq n_{\max}$. In other words, the Pöschl–Teller potential barrier has infinitely many QNM frequencies, and only a small set of them can be obtained from the analytical continuation of the Schrödinger operator. If one reverses the analytical continuation procedure, we will have that the QNMs with $n > n_{\max}$ are mapped in solutions of the Schrödinger equation that do not correspond to bound states and, hence, do not belong the usual domain where $\mathcal{H}_\epsilon$ is self-adjoint. This simple example shows that one cannot get the full set of QNM frequencies starting from the bound states of the associated quantum mechanics problem. Notwithstanding, the Pöschl–Teller potential is effectively used to compute some QNMs in the space-times of black holes as far as they can mimetize the effective potential in the vicinity of the horizon. The results using Pöschl–Teller potential can be compared with a numerical analysis, and the agreement is generally very good. The difference between both computations is less than 1% and decreases as the effective potential becomes more localized; see Ref. [10].

3 BTZ black holes

The BTZ black hole [11] is an appealing solution in three-dimensional gravity with a negative cosmological constant, $\Lambda = -1/\ell^2$. In the case of zero angular momentum ($J = 0$), its event horizon is determined solely by its mass M and the Anti-de Sitter (AdS) space length scale, ℓ. To begin with, we note that the line element for the exterior BTZ black hole with $J = 0$ can be expressed as follows:

$$ds^2 = -\frac{r^2 - r_+^2}{\ell^2}dt^2 + \frac{\ell^2}{r^2 - r_+^2}dr^2 + r^2 d\theta^2,$$

where $t \in \mathbb{R}$, $r > r_+$, and $\theta \in [0, 2\pi)$. In this context, the horizon can be expressed in terms of ℓ and M as follows: $r_+^2 = M\ell^2$ [11], as previously noted.

We consider a massless Klein–Gordon scalar field on this background,

$$\Box\Phi = 0.$$

We express the scalar field by means of the parametrization $\Phi = e^{-i\omega t}e^{i\mu\theta}u(r)/\sqrt{r}$, where $\mu \in \mathbb{Z}$ and $\omega \in \mathbb{C}$, the latter representing the quasinormal mode frequencies according with our definitions. The case of a massive scalar field propagating on the rotating BTZ background can be found in [12].

Considering the definition of the tortoise coordinate, expressed through the familiar relation $dx = dr/f(r)$. We arrive at the following expression:

$$x = -\frac{\ell^2}{r_+}\coth^{-1}\left(\frac{r}{r_+}\right). \tag{5}$$

Equation 5 tells us that the tortoise coordinate effectively maps the interval $(r_+, +\infty)$ onto $(-\infty, 0)$. Combining this result (19) with the equation outlined in (18) leads to a Schrödinger-like second-order linear differential equation:

$$\left(-\frac{d^2}{dx^2} + V[r(x)]\right)u = \omega^2 u, \tag{6}$$

where $f = \frac{r^2 - r_+^2}{\ell^2}$, and the effective potential reads

$$V = \frac{V_0}{\sinh^2(\alpha x)} + \frac{V_1}{\cosh^2(\alpha x)}.$$

Here, we define $\alpha = r_+/\ell^2$, $V_0 = 3\frac{r_+^2}{4\ell^2} > 0$, and $V_1 = \frac{r_+^2}{4\ell^2}\left(1 + \frac{4\mu^2}{r_+^2}\right) > 0$. It is important to note that when $\mu = 0$, we return to the scenario examined in [13]. From this point onward, our goal will be to identify the QNMs associated with the equations given in (20) and (21). In this context, we will analyze the boundary conditions pertinent to the half-real (negative) line. As is widely known, this generalized Pöschl–Teller potential represents an exactly integrable problem, as established in [10, 14]. Yet the physical contexts differ significantly. The investigation of the QNMs for the pure de Sitter spacetime is addressed in [14], whereas the scattering problem associated with the generalized Pöschl–Teller potential is thoroughly explored in [10]. The boundary conditions typically imposed at the horizon must be a purely incoming wave, represented as $e^{i\omega x}$, provided that a BTZ black hole is present. Conversely, at spatial infinity, we require an outgoing wave, $e^{-i\omega x}$, in order to eliminate any incoming radiation. However, the BTZ potential given in (21) approaches 0 at the horizon while diverging as one moves toward infinity. For a solution to

be well defined near infinity, it must decay to 0. The specific cases wherein this decay condition is satisfied are what determine the QNMs frequencies [10, 15].

After applying a new variable $z = \cosh^{-2}(\alpha x) \in [0, 1)$, which compactifies the interval $\mathbb{R}_-$, the original master Equation 6 can be recast as the Gaussian hypergeometric equation [4]:

$$z(1-z)u'' + [c - (a+b+1)z]u' - abu = 0,$$

where the parameters of the Gaussian hypergeometric are given by

$$a = \frac{1}{2} - i\frac{\omega}{2\alpha} + \frac{1}{4}(\nu + \zeta),$$
$$b = \frac{1}{2} - i\frac{\omega}{2\alpha} + \frac{1}{4}(\nu - \zeta),$$
$$c = 1 - i\frac{\omega}{\alpha}.$$

Here, $\nu = \sqrt{1 + 4\frac{V_0}{\alpha^2}}$ and $\zeta = \sqrt{1 - 4\frac{V_1}{\alpha^2}}$.

We can derive various types of solutions depending on the value of c. Specifically, when $c \notin \mathbb{Z}$, we find that the basis of linearly independent solutions is

$$u_I = z^{-i\frac{\omega}{2\alpha}}(1-z)^{\frac{1}{4}(1+\nu)}{}_2F_1(a, b, c, z),$$
$$u_{II} = z^{+i\frac{\omega}{2\alpha}}(1-z)^{\frac{1}{4}(1+\nu)}{}_2F_1(a-c+1, b-c+1, 2-c, z).$$

At this stage, several comments are in order. When we consider the limit as $x \to -\infty$ and the fact that the hypergeometric function is equal to 1 when evaluated at the origin, the boundary condition of having an ingoing-wave at the horizon implies that the second solution u_{II} must be discarded. The other boundary condition corresponds to imposing that at infinity $(z \to 1^-)$, the solution decays to 0, $\lim_{x\to 0} u_I = 0$. To do so, we employ Gursat's transformation to write ${}_2F_1(a, b, c, z)$ in terms of a combination of ${}_2F_1(a, b, c, 1-z)$ [16]. Expanding $z = 1 - (\alpha x)^2 + \mathcal{O}[(\alpha x)^2]$, the local expansion of the solution reads,

$$u_I \simeq A(\alpha x)^{\frac{1}{4}(1+\nu)} + B(\alpha x)^{\frac{1}{4}(1-\nu)},$$

with

$$A = \frac{\Gamma\left(1 - i\frac{\omega}{\alpha}\right)\Gamma\left(-\frac{\nu}{\alpha}\right)}{\Gamma\left(\frac{1}{2} - i\frac{\omega}{2\alpha} - \frac{1}{4}(\nu+\zeta)\right)\Gamma\left(\frac{1}{2} - i\frac{\omega}{2\alpha} - \frac{1}{4}(\nu-\zeta)\right)}$$

and

$$B = \frac{\Gamma\left(1 - i\frac{\omega}{\alpha}\right)\Gamma\left(\frac{\nu}{\alpha}\right)}{\Gamma\left(\frac{1}{2} - i\frac{\omega}{2\alpha} + \frac{1}{4}(\nu+\zeta)\right)\Gamma\left(\frac{1}{2} - i\frac{\omega}{2\alpha} + \frac{1}{4}(\nu-\zeta)\right)}.$$

For $\nu > 1$, we notice that the power-law term $(\alpha x)^{\frac{1}{4}(1-\nu)}$ in (28) diverges as one approaches infinity (which corresponds to $\alpha x \to 0^-$), while the other term decays toward 0. However, the presence of poles in the Gamma function at negative integers may effectively make this problematic term vanish. As a result, we derive a discrete set of countable frequencies that characterize the QNM solutions,

$$\omega_\pm = -i\alpha\left(2n + 1 + \frac{1}{2}(\nu \pm \zeta)\right), \tag{7}$$

with $n \in \mathbb{Z}_{\geq 0}$. These results, as shown in (7), are consistent with those presented in [10, 14], and [15]. In addition, Equation 7 can be derived by analyzing the singular points in the transfer matrix—or transmission coefficient—where $\mathbb{T}(\omega_\pm) = \infty$. This approach was previously demonstrated in the context of the Pöschl–Teller potential [17] and also in the case of a generalized Pöschl–Teller potential [18]. It should be mentioned that other interesting situations were analyzed in [15], such as:

i. QNMs with the usual exponentially suppressed oscillatory behavior for $V_0 > 0$ and $V_1 > \alpha^2/4$,
ii. The so-called algebraically special QNMs for $V_1 \leq \alpha^2/4$, and
iii. Unstable modes for small V_1/α^2.

For more information on these possibilities, the reader may consult Ref. [15].

The QNM solutions have the following effective boundary condition at $x = 0$,

$$\lim_{x\to 0^-}(\alpha x)^{-\kappa}\left[(\alpha x)^{\frac{3}{4}}u'_I(x) - \frac{1}{(\alpha x)^{\frac{1}{4}}}\alpha\left(\frac{1}{4} + \kappa\right)u_I(x)\right] = 0, \tag{8}$$

where $\kappa = \sqrt{\frac{1}{16} + \frac{V_0}{\alpha^2}} > 0$. Equation 8 resembles the condition reported in [15]. Another interesting point is to examine whether or not the functional energy remains bounded spatially for the QNMs solution at infinity [15]. As long as $\kappa > 7/4$, the functional energy converges to 0 as $\alpha x \to 0^-$.

Now, we are in a position to discuss the role played by the analytical continuation of the QNM problem in the case of the BTZ black hole. We will give a proof of concept by analyzing one case based on the ideas presented in Section 2. The outcome of applying the analytical continuation, defined as $x = iy$, to the QNMs of the BTZ black hole [7] is as follows. The solution $u_I(x)$ associated with the potential $V(x)$ will transform into quantum eigenstates $\psi = u_I(V \to -V(iy, \alpha'), \omega \to -i\omega)$ of the inverted potential barrier, $\tilde{V} = -V$. Thus, the Schrödinger equation becomes

$$\left(-\frac{d^2}{dy^2} - \frac{V_0}{\sinh^2(\alpha' y)} - \frac{V_1}{\cosh^2(\alpha' y)}\right)\psi = E\psi.$$

It is important to stress that α parameter must accommodate the modification introduced by the analytic continuation in order to keep the shape of potential unspoiled [6]. As result of that procedure, the energy eigenvalue $(E = -\omega^2)$ now reads

$$E = -\alpha'^2\left(2n + 1 + \frac{1}{2}(\nu \pm \zeta)\right)^2.$$

Including these transformations in the definitions of ν and ζ, the combination appearing in (34) becomes $\nu \pm \zeta = \sqrt{1 - 4\frac{V_0}{\alpha'^2}} \pm \sqrt{1 + 4\frac{V_1}{\alpha'^2}}$. The latter fact pinpoints a potential issue regarding the self-adjoint property of the Schrödinger operator presented in (33), provided the energy can take complex value. The reason for suspecting that something might have gone wrong around $y = 0$ can be easily confirmed by expanding the inverted potential around that point. The leading term is $\tilde{V} = -V_0/(\alpha' y)^2 < 0$. This kind of potential yields a non-self-adjoint operator on a Hilbert space $\mathbb{L}^2[(-\infty, 0), dy]$ [19, 20].

From now on, we will focus on the properties of the Schrödinger operator (33) and the effective boundary condition around $y = 0$. To do so, we follow a well-established protocol based on Von Neumann's theorem [21, 22]. We begin by computing the

subspace of solutions with purely imaginary eigenvalues denoted as $N_\pm = \{\phi \in D(\mathcal{H}^\dagger),\ \ \mathcal{H}\phi = \pm i\phi\}$ [21], where $\mathcal{H}$ stands for the Schrödinger operator presented in (33). In our case, near $y = 0$, these solutions are given by

$$\phi_\pm = (\alpha' y)^{1/4}\left(A_\pm (\alpha' y)^{\bar{\kappa}} + B_\pm (\alpha' y)^{-\bar{\kappa}}\right). \tag{9}$$

Here, $\bar{\kappa} = \kappa(V_0 \to -V_0, \alpha \to \alpha')$. Equation 9 indicates that, locally, in each case ±, only one of the solutions is square-integrable with respect to the measure dy. This fact shows that the dimension of the subspaces $N_\pm$ is at least 1 in both cases. Consequently, the operator admits a self-adjoint extension parametrized by the $U(1)$ group. In other words, there are an infinite number of self-adjoint extensions which can be written as $\phi = \phi_+ + s\phi_-$ with $s \in \mathbb{C}$ such that $|s| = 1$. For any element $\psi \in D(\mathcal{H}^\dagger)$, in order to ensure that the self-adjoint extensions are well defined, they must fulfill the following boundary condition,

$$\langle \phi, \mathcal{H}\psi\rangle - \langle \mathcal{H}\phi, \psi\rangle = \lim_{y\to 0^-}\left[\bar{\phi}(y)\psi'(y) - \bar{\phi}'(y)\psi(y)\right] = 0,$$

where the bracket $\langle , \rangle$ refers to the usual inner product in $\mathbb{L}^2([-\infty, 0), dy)$. For the sake of simplicity, let us corroborate whether the analytically continued eigenstates satisfy the same effective boundary condition of the QNMs (32). We only consider the situation associated with the QNMs, so from the general combination, the $A_\pm$ terms must be omitted, while the identification $u = \psi$ is made explicit. To keep things simple, we consider the case in which $\bar{\kappa} \in \mathbb{R}$; thus, $0 < V_0/\alpha'^2 < 1/4$ [15]. The boundary condition (36) can be recast as

$$\lim_{y\to 0^-} (\alpha' y)^{-\bar{\kappa}}\left[(\alpha' y)^{\frac{3}{4}} u'(y) - \frac{1}{(\alpha y)^{\frac{1}{4}}}\alpha'\left(\frac{1}{4} - \bar{\kappa}\right)u(y)\right] = 0. \tag{10}$$

The physical implications derived from Equation 10 can be summarized as follows. Upon determining the self-adjointness of the generalized (inverted) Pöschl–Teller operator as described in (33) and imposing the necessary conditions for self-adjointness at the boundary $y = 0$, we find that the effective boundary conditions associated with the quasinormal modes differ from the original conditions presented in (32). Specifically, for the range $0 < \frac{V_0}{\alpha'^2} < \frac{1}{4}$, the self-adjoint extensions do not fulfill to the same boundary condition specified in (32). This indicates that the analytically continued QNMs do not belong within the domain of any self-adjoint extension [15]. This observation further supports our conclusions regarding the analytical continuation method and the (inverted) Pöschl–Teller potential, as presented in Section 2.

4 Summary

We discussed the issues that emerge when employing the analytical continuation method to obtain the complete set of quasinormal modes in solvable scenarios, including the Pöschl–Teller potential and the BTZ black hole case. The absence of (essentially) self-adjointness in the Schrödinger operator with the inverted potential significantly restricts the viability of this approach [15]. Nevertheless, it would be interesting to revisit this BTZ case in light of the recent developments for the pseudospectrum of the Pöschl–Teller operator [23, 24] and in the case where the black hole is asymptotically AdS [25–28]. The latter point will be addressed elsewhere.

Author contributions

MR: writing–original draft and writing–review and editing. JF: writing–review and editing. AS: writing–original draft and writing–review and editing.

Funding

The author(s) declare that financial support was received for the research, authorship, and/or publication of this article. JF is supported by Conselho Nacional de Desenvolvimento Científico e Tecnológico (CNPq, Brazil) and Fundação de Amparo à Pesquisa e Inovação Espírito Santo (FAPES, Brazil). AS is partially supported by Conselho Nacional de Desenvolvimento Científico e Tecnológico (CNPq, Brazil).

Conflict of interest

The authors declare that the research was conducted in the absence of any commercial or financial relationships that could be construed as a potential conflict of interest.

Publisher's note

All claims expressed in this article are solely those of the authors and do not necessarily represent those of their affiliated organizations, or those of the publisher, the editors, and the reviewers. Any product that may be evaluated in this article, or claim that may be made by its manufacturer, is not guaranteed or endorsed by the publisher.

References

1. Ching ESC, Leung PT, Maassen van den Brink A, Suen WM, Tong SS, Young K. Waves in open systems: eigenfunction expansions. *Rev. Mod. Phys.* (1998) 70:1545–54. doi:10.1103/revmodphys.70.1545

2. Berti E, Cardoso V, Starinets AO. Class. *Quasinormal modes of black holes and black branes. Quan Grav* (2009) 26:163001. doi:10.1088/0264-9381/26/16/163001

3. Konoplya RA, Zhidenko A. Quasinormal modes of black holes: from astrophysics to string theory. *Rev. Mod. Phys.* (2011) 83:793–836. doi:10.1103/revmodphys.83.793

4. Blome HJ, Mashhoon B. Quasi-normal oscillations of a schwarzschild black hole. *Phys. Lett.* (1984) 110A:231–4. doi:10.1016/0375-9601(84)90769-2

5. Ferrari V, Mashhoon B. Oscillations of a black hole. *Phys. Rev. Lett.* (1984) 52: 1361–4. doi:10.1103/physrevlett.52.1361

6. Ferrari V, Mashhoon B. New approach to the quasinormal modes of a black hole. *Phys. Rev. D* (1984) 30:295–304. doi:10.1103/physrevd.30.295

7. Hatsuda Y. Quasinormal modes of black holes and Borel summation. *Phys. Rev. D* (2020) 101:024008. doi:10.1103/physrevd.101.024008

8. Poschl G, Teller E. Bemerkungen zur Quantenmechanik des anharmonischen Oszillators. *Z. Physik* (1933) 83:143–51. doi:10.1007/bf01331132

9. Flugge S. *Practical quantum Mechanics*. Springer (1998).

10. Cardona AF, Molina C. Quasinormal modes of generalized Pöschl-Teller potentials. *Class. Quan Grav.* (2017) 44:245002. doi:10.1088/1361-6382/aa9428

11. Bañados M, Teitelboim C, Zanelli J. Black hole in three-dimensional spacetime. *Phys. Rev. Lett.* (1992) 69:1849–51. doi:10.1103/physrevlett.69.1849

12. Birmingham D. Choptuik scaling and quasinormal modes in the anti-de Sitter space conformal-field theory correspondence. *Phys. Rev. D* (2001) 64:064024. doi:10.1103/physrevd.64.064024

13. Govindarajan TR, Suneeta V. Quasi-normal modes of AdS black holes: a superpotential approach. *Class. Quant. Grav.* (2001) 18:265–76. doi:10.1088/0264-9381/18/2/306

14. Du DP, Wang B, Su RK. Quasinormal modes in pure de sitter spacetimes. *Phys. Rev. D* (2004) 70:064024. doi:10.1103/physrevd.70.064024

15. Fabris JC, Richarte MG, Saa A. Quasinormal modes and self-adjoint extensions of the Schrödinger operator. *Phys. Rev. D* (2021) 103(4):045001. doi:10.1103/physrevd.103.045001

16. Abramowitz M, Stegun I. *Handbook of mathematical functions: with formulas, graphs, and mathematical tables*. Dover Publications (1965).

17. Cevik D, Gadella M, Kuru S, Negro J. Resonances and antibound states of Pöschl-Teller potential: ladder operators and SUSY partners. *Phys Lett A* (2016) 380:1600–9. [arXiv:1601.05134]. doi:10.1016/j.physleta.2016.03.003

18. da Silva UC, Pereira CFS, Lima AA. Renormalization group and spectra of the generalized Pöschl–Teller potential. *Ann Phys* (2024) 460:169549. doi:10.1016/j.aop.2023.169549

19. Essin AM, Griffiths DJ. Quantum mechanics of the $1/x^2$ potential. *Am. J. Phys.* (2006) 74:109–17. doi:10.1119/1.2165248

20. Fülöp T. Singular potentials in quantum mechanics and ambiguity in the self-adjoint Hamiltonian. *Symmetry, Integrability Geometry: Methods Appl* (2007) 3(0):107–12. doi:10.3842/sigma.2007.107

21. Gitman DM, Tyutin IV, Voronov BL. *Self-adjoint extensions in quantum Mechanics: general theory and applications to Schrödinger and Dirac equations with singular potentials* (2012).

22. Bonneau G, Faraut J, Valent G. Self-adjoint extensions of operators and the teaching of quantum mechanics. *Am. J. Phys.* (2001) 69:322–31. doi:10.1119/1.1328351

23. Sheikh LA. Scattering resonances and Pseudospectrum: stability and completeness aspects in optical and gravitational systems. Available from: https://theses.hal.science/tel-04116011 (Accessed April 27, 2012). doi:10.1007/978-0-8176-4662-2

24. Jaramillo JL, Macedo RP, Sheikh L. Pseudospectrum and black hole quasi-normal mode (in)stability. *Phys. Rev. X* (2021) 11:031003. doi:10.1103/physrevx.11.031003

25. Boyanov V, Cardoso V, Destounis K, Jaramillo JL, Macedo RP. Structural aspects of the anti-de Sitter black hole pseudospectrum. *Phys. Rev. D* (2024) 109:064068. doi:10.1103/physrevd.109.064068

26. Cownden B, Pantelidou C, Zilhão M. The pseudospectra of black holes in AdS. *JHEP* (2024) 05:202. doi:10.1007/jhep05(2024)202

27. Areán D, Fariña DG, Landsteiner K. Pseudospectra of holographic quasi-normal modes. *JHEP* (2023) 12:187. doi:10.1007/jhep12(2023)187

28. Areán D, Fariña DG, Landsteiner K, Romeu PG, Saura-Bastida P. *Pseudospectra of complex momentum modes*.

frontiers | Frontiers in Physics

TYPE Brief Research Report
PUBLISHED 22 October 2024
DOI 10.3389/fphy.2024.1479658

Check for updates

OPEN ACCESS

EDITED BY
Jose Luis Jaramillo,
Université de Bourgogne, France

REVIEWED BY
Catherine Drysdale,
University of Birmingham, United Kingdom
Michael Hitrik,
University of California, Los Angeles,
United States

*CORRESPONDENCE
David Krejčiřík,
david.krejcirik@fjfi.cvut.cz

RECEIVED 12 August 2024
ACCEPTED 30 September 2024
PUBLISHED 22 October 2024

CITATION
Krejčiřík D and Siegl P (2024) Pseudomodes of Schrödinger operators.
Front. Phys. 12:1479658.
doi: 10.3389/fphy.2024.1479658

COPYRIGHT
© 2024 Krejčiřík and Siegl. This is an open-access article distributed under the terms of the Creative Commons Attribution License (CC BY). The use, distribution or reproduction in other forums is permitted, provided the original author(s) and the copyright owner(s) are credited and that the original publication in this journal is cited, in accordance with accepted academic practice. No use, distribution or reproduction is permitted which does not comply with these terms.

Pseudomodes of Schrödinger operators

David Krejčiřík[1]* and Petr Siegl[2]

[1]Department of Mathematics, Faculty of Nuclear Sciences and Physical Engineering, Czech Technical University in Prague, Prague, Czechia, [2]Institute of Applied Mathematics, Graz University of Technology, Graz, Austria

Pseudomodes of non-self-adjoint Schrödinger operators corresponding to large pseudoeigenvalues are constructed. The approach is non-semiclassical and extendable to other types of models including the damped wave equation and Dirac operators.

KEYWORDS

pseudospectrum, non-self-adjointness, Schrödinger operators, complex potentials, WKB method

1 Introduction

The (ε-)pseudospectrum $\sigma_\varepsilon(H)$ (with positive ε) of an operator H in a Hilbert space is the union of the spectrum $\sigma(H)$ of H and all those complex numbers λ from the resolvent set $\rho(H)$ of H for which

$$\|(H-\lambda)^{-1}\| > \frac{1}{\varepsilon}.$$

Equivalently, $\sigma_\varepsilon(H)$ comprises the spectrum of H and $\lambda \in \mathbb{C}$ (pseudoeigenvalues) for which there exists a vector ψ (pseudomode) in the domain of H such that

$$\|(H-\lambda)\psi\| < \varepsilon \|\psi\|.$$

If H is self-adjoint (or, more generally, normal), the ε-pseudospectrum is trivial in the sense that it is just the ε-tubular neighbourhood of the spectrum of H. In general, however, the pseudoeigenvalues can lie outside the ε-tubular neighbourhood and their location is important to correctly seize various properties of H, see [1–3].

The goal of this brief research report is to explain in a succinct way the approach in Krejčiřík and Siegl [4] to locate pseudoeigenvalues of (non-semiclassical) Schrödinger operators

$$-\frac{\mathrm{d}^2}{\mathrm{d}x^2} + V(x) \qquad \text{in} \qquad L^2(\mathbb{R}), \tag{1}$$

where $V\colon \mathbb{R} \to \mathbb{C}$ is at least locally square-integrable and $\Re V \geq 0$. In such a case, there exists a unique m-accretive extension H_V of Equation 1 initially defined on $C_0^\infty(\mathbb{R})$, see ([5], Thm. VII.2.6). Since our constructed pseudomodes are compactly supported and at least twice weakly differentiable, they belong to the domain of H_V.

The operator H_V is self-adjoint (respectively, normal) if, and only if, V is real-valued (respectively, $\Im V$ is constant). To ensure non-trivial pseudospectra, we shall therefore adopt the standing hypothesis

$$\limsup_{x\to-\infty} \Im V(x) < 0 < \liminf_{x\to+\infty} \Im V(x), \tag{2}$$

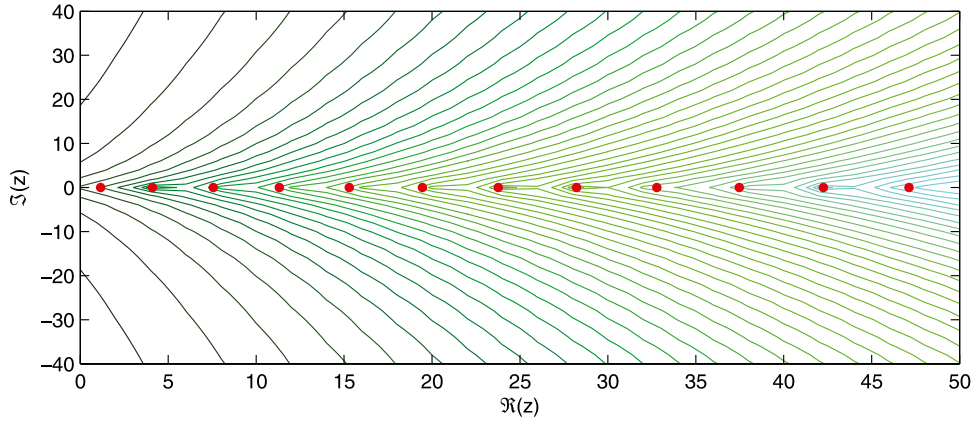

FIGURE 1
Spectrum (red dots) and pseudospectra (enclosed by the green contour lines) of the imaginary cubic oscillator. (Courtesy of Miloš Tater.)

where the limits are allowed to be infinite. The assumption (Equation 2) can be interpreted as a "global" version of the Davies' condition $\mathfrak{I}V' \neq 0$, see [6] and also [7].

To simplify the presentation, the potential V will be assumed to be smooth and imaginary-valued. Typical examples to keep in mind are as follows:

$$V_1(x) := i\arctan(x), \qquad V_2(x) := ix^m \quad \text{with} \quad m \text{ odd}, \\ V_3(x) := i\sinh(x), \tag{3}$$

or their imaginary shifts. In particular, V_2 with $m = 3$ is the celebrated imaginary cubic (or Bender's) oscillator (with purely real and discrete spectrum, see Figure 1), which was made popular in the context of the so-called $\mathcal{PT}$-symmetric quantum mechanics in [8].

The objective is to develop a systematic construction of pseudomodes ensuring that, for any diminishing $\varepsilon \to 0$, there is a complex number λ with large magnitude $|\lambda| \to \infty$ such that $\lambda \in \sigma_\varepsilon(H_V)$. The results are particularly striking whenever this set of pseudoeigenvalues lie outside (in fact, "very far" from) the ε-tubular neighbourhood of $\sigma(H)$. This is particularly the case of the imaginary cubic oscillator, for which the analysis below show that for an arbitrarily small ε there exists a pseudoeigenvalue λ with an arbitrarily large imaginary part, despite the fact that the spectrum is purely real (see Figure 1 for a numerical quantification of the pseudospectrum level lines). This property implies the lack of Riesz basis for the eigenfunctions, challenging in the spirit of [9] the physical relevance of the $L^2(\mathbb{R})$-realisation of the Bender's oscillator. The follow-up [4] summarised in this report can be considered as a methodical and more advanced study of not necessarily polynomial potentials.

The feature of the approach of [4] is that it does not rely on semiclassical methods developed in [6, 7, 10]. In fact, we are able to construct large-energy pseudomodes for potentials (like of exponential type, see V_3 of Equation 3) which cannot be reduced (by scaling) to a small Planck's constant included in the kinetic energy. On the contrary, the known claims in the semiclassical setting follow immediately from our approach.

2 Methods

Our strategy of the construction of pseudomodes is based on the Liouville–Green approximation, also known as the JWKB method in mathematical physics. The key idea is that, if V were constant, exact solutions of the differential equation associated with $H_V g = \lambda g$ would be the two non-integrable functions

$$g_\pm(x) := \exp\left(\pm i\int_0^x \sqrt{\lambda - V(t)}\,\mathrm{d}t\right).$$

The starting point of the approximation scheme is to use the same ansatz for variable V as well. More specifically, we choose $g_0 := g_-$ for it is exponentially decaying under the hypothesis (Equation 2), whenever $\mathfrak{I}\lambda$ is small with respect to the limits of $\mathfrak{I}V$ at $\pm\infty$. A direct computation yields

$$(H_V - \lambda)g_0 = r_0\, g_0 \qquad \text{with} \qquad r_0 := -\frac{i}{2}\frac{V'}{\sqrt{\lambda - V}}. \tag{4}$$

Recalling the simplifying hypothesis that $\mathfrak{R}V = 0$ and assuming in addition that $\mathfrak{I}\lambda = 0$ and $\mathfrak{R}\lambda > 0$ (typically large), one has the estimate

$$\|r_0\|_\infty \leq \frac{1}{\sqrt{\mathfrak{R}\lambda}^{1-\delta}}\left\|\frac{|V'|}{2|V|^{\delta/2}}\right\|_\infty \tag{5}$$

for every $\delta \in [0, 1)$. It follows that large real energies always lie in the pseudospectrum, namely, for every positive ε,

$$\left\{\lambda \in \mathbb{C}:\ \sqrt{\mathfrak{R}\lambda}^{\,1-\delta} > \frac{1}{\varepsilon}\left\|\frac{|V'|}{2|V|^{\delta/2}}\right\|_\infty\right\} \subset \sigma_\varepsilon(H_V).$$

Of course, this result is interesting only if the supremum norm is bounded. From examples (Equation 3), relevant potentials are thus V_1 and V_2 with $m = 1$, in which case we can take $\delta = 0$ and obtain thus a pseudomode satisfying the decay $\|(H_V - \lambda)g_0\| = O((\mathfrak{R}\lambda)^{-1/2})\,\|g_0\|$ as $\mathfrak{R}\lambda \to \infty$. The latter is particularly interesting because the spectrum of the imaginary Airy operator is empty, see, e.g., ([3, 11], Section VII.A) or more generally [12], where the last reference includes also an elementary proof of the optimal resolvent norm estimate for the Airy operator.

It is not difficult to modify the exponentially decaying pseudomode g_0 to a compactly supported pseudomode f_0, while still keeping the same decay $\|(H_V-\lambda)f_0\| = O((\Re\lambda)^{-1/2})\,\|f_0\|$ as $\Re\lambda\to\infty$. Indeed, let $\xi_1\colon \mathbb{R}\to[0,1]$ be a smooth function such that $\xi_1 = 1$ on $[-1,1]$ and $\xi_1 = 0$ outside $[-2,2]$. Given any positive number l, let us define the rescaled cut-off function $\xi_l(x) := \xi_1(x/l)$. Then $f_0 := \xi_l\, g_0$ is compactly supported and one has

$$(H_V-\lambda)f_0 = \xi_l\, H_V g_0 + \left(-\xi_l'' + 2i\sqrt{\lambda-V}\,\xi_l'\right)g_0.$$

Using that $\xi_l\to 1$ pointwise as $l\to\infty$, while one gains one l^{-1} by each derivative, it is possible to verify the desired decay by the λ-dependent choice $l := \Re\lambda$.

To cover a larger class of potentials, let us consider a modified ansatz $g_1 := g_0\exp(-\psi_0)$, where ψ_0 is a function to be chosen later. A direct computation yields

$$(H_V-\lambda)g_1 = \left(r_0 - 2i\sqrt{\lambda-V}\,\psi_0' + \psi_0'' - \psi_0'^2\right)g_1.$$

Now we choose ψ_0 to annihilate the error term r_0 from Equation 4, by solving the first-order linear differential equation $r_0 - 2i\sqrt{\lambda-V}\psi_0' = 0$, namely, $\psi_0 := \log\sqrt[4]{\lambda-V}$. Thus we arrive at the familiar expression

$$g_1(x) = \frac{1}{\sqrt[4]{\lambda-V(x)}}\,\exp\left(-i\int_0^x\sqrt{\lambda-V(t)}\,\mathrm{d}t\right).$$

Then

$$(H_V-\lambda)g_1 = r_1\, g_1 \qquad \text{with} \qquad r_1 := -\frac{5}{16}\,\frac{V'^2}{(\lambda-V)^2} - \frac{1}{4}\,\frac{V''}{\lambda-V},$$

where the new error term r_1 can be estimated as follows:

$$\|r_1\|_\infty \le \frac{1}{\sqrt{\Re\lambda}^{2(1-\delta)}}\left\|\frac{5\,|V'|^2}{16\,|V|^{1+\delta}} + \frac{|V''|}{4\,|V|^\delta}\right\|_\infty.$$

This result is an improvement upon (Equation 4) with (Equation 5) in two respects. First, if the supremum norm is bounded for $\delta = 0$, we get a pseudomode with an improved decay $\|(H_V-\lambda)g_1\| = O((\Re\lambda)^{-1})\,\|g_1\|$ as $\Re\lambda\to\infty$. This is the case of V_1 and V_2 with $m = 1$ from examples (Equation 3). Second, keeping the decay $O((\Re\lambda)^{-1/2})$ by the choice $\delta = 1/2$, we can now cover V_2 with $m = 3$ from examples (Equation 3).

The above scheme can be continued by employing the general ansatz in square-root powers of λ:

$$g_k = \exp\left(-\lambda^{1/2}\,\psi_{-1} + \lambda^{-0/2}\,\psi_0 + \lambda^{-1/2}\,\psi_1 + \cdots + \lambda^{-(k-1)/2}\,\psi_{k-1}\right), \quad (6)$$

where $\psi_{-1}(x) := i\lambda^{-1/2}\int_0^x\sqrt{\lambda-V(t)}\,\mathrm{d}t$ and ψ_{k-1} with $k\in\mathbb{N}$ is iteratively chosen in such a way to annihilate the previous error term r_{k-1}. By enlarging k, more derivatives of V are required. On the other hand, a better decay (in negative powers of $\Re\lambda\to\infty$) of the new error term is achieved and a larger class of potentials can be covered. For instance, all the examples (Equation 3) are already covered by the choice $k = 2$, namely, $\|(H_V-\lambda)g_2\| = O((\Re\lambda)^{-1/2})\,\|g_2\|$ as $\Re\lambda\to\infty$.

3 Results

To make the above procedure rigorous, it is important to ensure that g_0 in the expansion (Equation 6) is dominant, in order to guarantee that $g_k(x)$ have appropriate decay properties at $x = \pm\infty$. One of the main achievements of [4] is the formulation of the robust sufficient condition

$$\frac{|V^{(n)}(x)|}{|V(x)|} = O(|x|^{m}) \qquad \text{and} \qquad |x|^{4(1+\nu)} = O(|V(x)|) \quad (7)$$

to hold as $|x|\to\infty$ with some real number $\nu\le 0$ for every $n = 1,\dots,k+1$. Note that $\nu = -2$, -1 and 0 for the potentials V_1, V_2 and V_3 of Equation 3, respectively. In fact, it is possible to allow for $\nu > 0$ (corresponding to superexponentially growing potentials). Moreover, different behaviours at $x\to\pm\infty$ may be allowed. However, let us stick to Equation 7 to make the presentation here as simple as possible.

To get a compactly supported pseudomode, it turns out that the adequate λ-dependent cut-off function should be supported in the interval $[-l_-,l_+]$, where (denoting $\langle l\rangle := (1+l^2)^{1/2}$)

$$l_\pm := \begin{cases} \inf\left\{l\ge 0:\ \dfrac{|V(\pm l)|^2}{\langle l\rangle^{4(1+\nu)}} = \lambda\right\} & \text{if } V \text{ is unbounded at } \pm\infty, \\ \lambda^{1-\frac{\nu}{4}} & \text{if } V \text{ is bounded at } \pm\infty\,. \end{cases}$$

Recall that we assume $\Im\lambda = 0$ and note that $l_\pm\to\infty$ as $\lambda\to\infty$. In particular, $l_\pm = \lambda^{3/2}$, $\lambda^{1/(2m)}$ and $\log\lambda$ as $\lambda\to\infty$ for the potentials V_1, V_2 and V_3 of Equation 3, respectively.

Under the present simplifying hypotheses (in particular, $\Im\lambda = 0$, $\Re V = 0$ and $\nu\le 0$), the general result of Krejčiřík and Siegl [4] (Thm. 3.7) can be formulated as follows.

Theorem 1. Let $V\colon\mathbb{R}\to i\mathbb{R}$ be smooth satisfying Equations 2, 7 with given $k\in\mathbb{N}$. If

$$\lambda^{-(k+1)/2}\sup_{x\in(-l_-,l_+)}|V(x)|\,\langle x\rangle^{(k+1)\nu}\xrightarrow[\lambda\to+\infty]{}0, \quad (8)$$

then there exists $\{\psi_\lambda\}_\lambda\subset C_0^\infty(\mathbb{R})$ such that $\|\psi_\lambda\| = 1$ and

$$\lim_{\lambda\to+\infty}\|(H_V-\lambda)\psi_\lambda\| = 0. \quad (9)$$

The extra condition (Equation 8) with the choice $k = 0$ is clearly satisfied for the potential V_1 of Equation 3 (in fact, for any bounded potential satisfying Equations 2, 7). To satisfy Equation 8 for all the polynomial potentials V_2 of Equation 3, it is sufficient to take $k = 1$. Finally, Equation 8 is verified for the exponential potential V_3 of Equation 3 with $k = 2$.

In Krejčiřík and Siegl [4], the decay rate in Equation 9 is carefully quantified in terms of the left-hand side of Equation 8 and other quantities related to the behaviour of a general potential V at infinity.

4 Discussion

4.1 Generality

The JWKB-type scheme sketched in Section 2 is made rigorous in [4] for a fairly general class of potentials V, beyond the present simplifying hypotheses. In particular, the potential V is allowed to have a real part, however, its largeness must be suitably "small" with respect to its imaginary part. This is quantified by natural

modifications of Equations 2, 7. What is more, pseudoeigenvalues along general curves (beyond the present simplifying hypothesis $\Im\lambda = 0$) diverging in the complex plane are located. In particular, the rotated harmonic (or Davies') oscillator $V(x) = ix^2$ made popular in the pioneering work [13] or shifted harmonic oscillator $V(x) = (x+i)^2$ studied in [3, 14] are covered. At the same time, potentials decaying at infinity are included. Finally, possibly discontinuous potentials (like $V(x) = i\mathrm{sgn}(x)$) are comprised by a refined mollification argument.

4.2 Optimality

It turns out that the conditions on potentials identified in [4] as well as the regions in the complex plane where the pseudoeigenvalues are located are optimal. The latter can be checked directly for the rotated harmonic (or Davies') oscillator $V(x) = ix^2$ with help of the conjecture due to [15] solved by [16], More generally, the optimality of the pseudospectral regions follows by upper resolvent estimates performed in [17, 18].

4.3 Generalisations

The method of [4] is fairly robust and can be generalised to other models. So far, this has been done for the damped wave equation in [19], Dirac operators in [20] and biharmonic operators in [21].

Data availability statement

The original contributions presented in the study are included in the article/supplementary material, further inquiries can be directed to the corresponding author.

Author contributions

DK: Writing–review and editing, Writing–original draft, Visualization, Validation, Supervision, Software, Resources, Project administration, Methodology, Investigation, Funding acquisition, Formal Analysis, Data curation, Conceptualization. PS: Writing–review and editing, Writing–original draft, Visualization, Validation, Supervision, Software, Resources, Project administration, Methodology, Investigation, Funding acquisition, Formal Analysis, Data curation, Conceptualization.

Funding

The author(s) declare financial support was received for the research, authorship, and/or publication of this article. DK was supported by the EXPRO grant No. 20-17749X of the Czech Science Foundation.

Conflict of interest

The authors declare that the research was conducted in the absence of any commercial or financial relationships that could be construed as a potential conflict of interest.

Publisher's note

All claims expressed in this article are solely those of the authors and do not necessarily represent those of their affiliated organizations, or those of the publisher, the editors and the reviewers. Any product that may be evaluated in this article, or claim that may be made by its manufacturer, is not guaranteed or endorsed by the publisher.

References

1. Trefethen LN, Embree M. *Spectra and pseudospectra*. Princeton University Press (2005).

2. Davies EB. *Linear operators and their spectra*. Cambridge University Press (2007).

3. Krejčiřík D, Siegl P, Tater M, Viola J. Pseudospectra in non-Hermitian quantum mechanics. *J Math Phys* (2015) 56:103513. doi:10.1063/1.4934378

4. Krejčiřík D, Siegl P. Pseudomodes for Schrödinger operators with complex potentials. *J Funct Anal* (2019) 276:2856–900. doi:10.1016/j.jfa.2018.10.004

5. Edmunds DE, Evans WD. *Spectral theory and differential operators*. Oxford: Oxford University Press (1987).

6. Davies EB. Semi-classical states for non-self-adjoint Schrödinger operators. *Comm Math Phys* (1999) 200:35–41. doi:10.1007/s002200050521

7. Zworski M. A remark on a paper of E. B. Davies. *Proc Amer Math Soc* (2001) 129: 2955–7. doi:10.1090/s0002-9939-01-05909-3

8. Bender CM, Boettcher PN. Real spectra in non-Hermitian Hamiltonians having *PT* symmetry. *Phys Rev Lett* (1998) 80:5243–6. doi:10.1103/physrevlett.80.5243

9. Siegl P, Krejčiřík D. On the metric operator for the imaginary cubic oscillator. *Phys Rev D* (2012) 86:121702(R. doi:10.1103/physrevd.86.121702

10. Dencker N, Sjöstrand J, Zworski M. Pseudospectra of semiclassical (pseudo-) differential operators. *Comm Pure Appl Math* (2004) 57:384–415. doi:10.1002/cpa.20004

11. Helffer B. *Spectral theory and its applications*. New York: Cambridge University Press (2013).

12. Arnal A, Siegl P. Generalised airy operators preprint on arXiv:2208.14389 (2022).

13. Davies EB. Pseudo-spectra, the harmonic oscillator and complex resonances. *Proc R Soc Lond A* (1999) 455:585–99. doi:10.1098/rspa.1999.0325

14. Mityagin B, Siegl P, Viola J. Differential operators admitting various rates of spectral projection growth. *J Funct Anal* (2017) 272:3129–75. doi:10.1016/j.jfa.2016.12.007

15. Boulton L. The non-self-adjoint harmonic oscillator, compact semigroups and pseudospectra. *J Operator Theor* (2002) 47:413–29.

16. Pravda-Starov K. A complete study of the pseudo-spectrum for the rotated harmonic oscillator. *J Lond Math. Soc.* (2006) 73:745–61. doi:10.1112/s0024610706022952

17. Bordeaux Montrieux W. Estimation de résolvante et construction de quasimode près du bord du pseudospectre (2013). Preprint on arXiv:1301.3102

18. Arnal A, Siegl P. Resolvent estimates for one-dimensional Schrödinger operators with complex potentials. *J Funct Anal* (2023) 284:109856. doi:10.1016/j.jfa.2023.109856

19. Arifoski A, Siegl P. Pseudospectra of the damped wave equation with unbounded damping. *SIAM J Math Anal* (2020) 52:1343–62. doi:10.1137/18m1221400

20. Krejčiřík D, Nguyen Duc T. Pseudomodes for non-self-adjoint Dirac operators. *J Funct Anal* (2022) 282:109440. doi:10.1016/j.jfa.2022.109440

21. Nguyen Duc T. Pseudomodes for biharmonic operators with complex potentials. *SIAM J Math Anal* (2022) 55:6580–624. doi:10.1137/22m1470682

frontiers | Frontiers in Physics

TYPE Mini Review
PUBLISHED 23 October 2024
DOI 10.3389/fphy.2024.1460268

Check for updates

OPEN ACCESS

EDITED BY
Jose Luis Jaramillo,
Université de Bourgogne, France

REVIEWED BY
Brad Cownden,
University College Dublin, Ireland
Valentin Boyanov,
Associação do Instituto Superior Técnico de Investigação e Desenvolvimento (IST-ID), Portugal

*CORRESPONDENCE
Daniel Areán,
daniel.arean@uam.es

RECEIVED 05 July 2024
ACCEPTED 19 September 2024
PUBLISHED 23 October 2024

CITATION
Areán D, Garcia-Fariña D and Landsteiner K (2024) Pseudospectra of quasinormal modes and holography.
Front. Phys. 12:1460268.
doi: 10.3389/fphy.2024.1460268

COPYRIGHT
© 2024 Areán, Garcia-Fariña and Landsteiner. This is an open-access article distributed under the terms of the Creative Commons Attribution License (CC BY). The use, distribution or reproduction in other forums is permitted, provided the original author(s) and the copyright owner(s) are credited and that the original publication in this journal is cited, in accordance with accepted academic practice. No use, distribution or reproduction is permitted which does not comply with these terms.

Pseudospectra of quasinormal modes and holography

Daniel Areán[1,2]*, David Garcia-Fariña[1,2] and Karl Landsteiner[1]

[1]Instituto de Física Teórica UAM-CSIC, Madrid, Spain, [2]Departamento de Física Teórica, Universidad Autónoma de Madrid, Madrid, Spain

The holographic duality (also known as AdS/CFT correspondence or gauge/gravity duality) postulates that strongly coupled quantum field theories can be described in a dual way in asymptotically anti-de Sitter space. One of the cornerstones of this duality is the description of thermal states as black holes with asymptotically anti-de Sitter boundary conditions. This idea has led to valuable insights into fields such as transport theory and relativistic hydrodynamics. In this context, the quasinormal modes of such black holes play a decisive role, and therefore their stability properties are of utmost interest for the holographic duality. We review recent results using the method of pseudospectra.

KEYWORDS

quasinormal modes, gauge/gravity duality, black holes, anti-de Sitter space, pseudospectra

1 Introduction

1.1 Blitz review of holographic duality

Before discussing the role of quasinormal modes, we first need to understand the basics of the AdS/CFT correspondence. Gauge/gravity duality has its roots in Maldacena's conjecture that type IIB string theory on $AdS_5 \times S_5$ is dual to $\mathcal{N} = 4$ supersymmetric gauge theory [1, 2].[1] Let us quickly unpack this statement. $\mathcal{N} = 4$ supersymmetric gauge theory is a non-abelian, four-dimensional quantum field theory whose field content consists of six scalars, four Majorana fermions, and a gauge field. They all transform under the adjoint representation of the gauge group $SU(N)$. It features four supersymmetries, and this fixes all the couplings between the different fields. As it is a gauge theory, physical observables are gauge-invariant operators such as $\mathrm{tr}(F_{\mu\nu}F^{\mu\nu})$. The global symmetry group $SO(6)$ acts on the scalars and fermions (in the $SU(4)$ spin representation of $SO(6)$). In addition, the theory has conformal symmetry and 32 supercharges.

The dual theory is a theory of gravity (type IIB string theory) but exists in 10 dimensions. Five of these are a geometric realization of the internal $SO(6)$ symmetry as the isometry of the five-dimensional sphere S_5. Supersymmetry is generated by two ten-dimensional spinors of equal chirality, which also results in 32 supercharges. Conformal symmetry arises as the isometry group on AdS_5.

1 Both descriptions arise from the low energy limit of a stack of N D3-branes in string theory in flat 10-dimensional spacetime [2].

The field theory gauge coupling g_{YM} and rank of the gauge group N are related to the dual string theory string coupling g_s (the amplitude for a string to split in two) and to the ratio of the AdS_5 curvature scale $R = -20/L$ and string scale l_s in the following way:

$$g_{YM}^2 N \propto \frac{L^4}{l_s^4},$$
$$1/N \propto g_s.$$

Gauge/gravity duality is therefore a strong–weak coupling duality; for weak curvature, we have large L and therefore also large 't-Hooft coupling $g_{YM}^2 N$. In this regime of weak curvature, stringy effects are negligible, and we can approximate the string theory by type IIB supergravity. If we furthermore take the rank of the gauge group N to be very large, we can also neglect quantum loop effects and end up with classical supergravity. This is the form of the correspondence most useful for the applications to many body physics. Classical (super)gravity on $(d+1)$-dimensional anti-de Sitter space is the infinite coupling and infinite rank limit of a gauge theory in d dimensions.

This is now promoted to a principle that (quantum-)gravity in asymptotically $(d+1)$-dimensional anti-de Sitter space can be understood as a strong coupling version of a dual quantum field theory in d dimensions [3, 4]. For applications to quantum field theory, the most useful coordinate system is the so-called Poincaré patch.

$$ds^2 = \frac{r^2}{L^2}\left(-dt^2 + d\vec{x}^2\right) + \frac{L^2}{r^2}dr^2. \tag{1}$$

The space on which the dual quantum field theory exists is recovered by taking the limit $ds^2_{\mathrm{QFT}} = \lim_{r\to\infty} r^{-2} ds^2$.

Since the correspondence relates a $(d+1)$-dimensional theory to a d-dimensional theory, it is also called "holographic" duality. The radial coordinate has a physical interpretation as energy scale. The high-energy or UV limit in the field theory is identified with the $r \to \infty$ limit in the AdS geometry, whereas the low-energy IR limit is $r \to 0$.

On shell, the asymptotic behavior of the fields in AdS in a large r expansion is

$$\Phi(r,x) = r^{-\Delta_-}\left(\Phi_0(x) + O\left(r^{-2}\right)\right) + r^{-\Delta_+}\left(\Phi_1(x) + O\left(r^{-2}\right)\right). \tag{2}$$

The exponents $\Delta_\pm$ obey $\Delta_- < \Delta_+$ and depend on the nature of the field, e.g., for a scalar field of mass m, they are $\Delta_\pm = \frac{1}{2}\left(d \pm \sqrt{d^2 + 4m^2L^2}\right)$. We note that for the scalar field in asymptotically AdS, masses in the range $-d^2/4 < m^2 < 0$ are perfectly regular and do not imply any acausality or instability [5].

It turns out that the leading solution given by $\Phi_0(x)$ is non-normalizable and thus non-dynamical. It is interpreted as a boundary condition $\Phi_0(x) = J(x)$ on the AdS field $\Phi(r,x)$. The classical on-shell action becomes a functional of these boundary conditions $S_{\mathrm{cl}}[J]$. In the (super)gravity limit, the on-shell action is interpreted as the generating functional of (connected) Green's functions $Z_c[J] = S_{\mathrm{cl}}[J]$ in the dual field theory. The boundary condition J is now interpreted as a source for an operator $\mathcal{O}$ in the dual field theory whose correlation functions can be obtained from

$$\langle \mathcal{O}_1(x_1)\ldots\mathcal{O}_n(x_n)\rangle = \frac{\delta^n S_{\mathrm{cl}}}{\delta J_1(x_1)\ldots\delta J_n(x_n)}. \tag{3}$$

More specifically, the expectation value of the operator $\mathcal{O}$ is given by

$$\langle \mathcal{O}(x)\rangle \propto \Phi_1(x).$$

In this way, the leading and subleading terms in the asymptotic expansion Equation 2 have dual field theory interpretations. The mass range $-d^2/4 \le m^2 \le 0$ corresponds to renormalizable operators.[2]

Generically, the equation of motion for $\Phi(r,x)$ is a second-order partial differential equation. In order to solve it, one needs to supply additional boundary conditions. The metric shown in Equation 1 has a (degenerate) horizon at $r = 0$, and it was argued in [7] that for time-dependent solutions, retarded Green's functions of the dual quantum field theory

$$G_R(t,\vec{x}) = -i\Theta(t)\langle[\mathcal{O}(t,\vec{x}),\mathcal{O}(0,0)]\rangle, \tag{4}$$

are obtained by imposing *infalling* boundary conditions.

The infalling boundary condition is, of course, the main constituent for the existence of quasinormal modes. In anti-de Sitter space, it does, however, not lead to quasinormal modes because the horizon is degenerate. The corresponding (holographic) retarded Green's function does not have poles but rather a branch cut along the positive real axis [7]. This changes as soon as we consider a black hole with asymptotic AdS boundary conditions and planar horizon topology (AdS black brane). Its line element for $d = 4$ is

$$ds^2/L^2 = r^2\left(-f(r)dt^2 + d\vec{x}^2\right) + \frac{dr^2}{r^2 f(r)}, \tag{5}$$
$$f(r) = 1 - \frac{r_h^4}{r^4}.$$

This metric has a non-degenerate horizon at $r = r_h$. The Hawking temperature is $\pi T L^2 = r_h$. The holographic (or gauge/gravity) interpretation is that the dual field theory is now in a thermal state with the temperature given by the Hawking temperature [8, 9].

The field Φ is expanded in (boundary) plane waves as

$$\Phi(r,t,\vec{x}) = \int \frac{d\omega d^3k}{(2\pi)^4}\tilde{\Phi}_0\left(\omega,\vec{k}\right)e^{-i\omega t + i\vec{k}\vec{x}}F_{\omega,\vec{k}}(r).$$

For every fixed $\omega, \vec{k}$, the linearized equation of motion for the fluctuation boils down then to an ordinary second-order differential equation for $F_{\omega,\vec{k}}$. The point at infinity is a regular singular point with characteristic exponents $\Delta_\pm$. We impose infalling boundary conditions by demanding that $F_{\omega,\vec{k}} \sim e^{-i\omega(t+r_*)}$ on the horizon (we use a tortoise coordinate here $dr_* = dr/f(r)$ such that the horizon sits at $r_* \to -\infty$). The asymptotic expansion of $F_{\omega,\vec{k}}(r)$ is

$$F_{\omega,\vec{k}} = A\left(\omega,\vec{k}\right)r^{-\Delta_-}[1 + O(1/r)] + B\left(\omega,\vec{k}\right)r^{-\Delta_+}[1 + O(1/r)],$$

2 We note that this is the so-called standard quantization scheme and allows only for operators of dimensions larger than $d/2$. In order to describe operators of smaller dimensions, one needs to exchange the role of the source and operator ("alternative quantization"). For further details on that, see [6].

where $A(\omega,\vec{k})$ and $B(\omega,\vec{k})$ are the Fourier transforms of $\Phi_0(x)$ and $\Phi_1(x)$, respectively. The Fourier transform of the retarded two-point Green's function Equation 4 can now be calculated as

$$\tilde{G}_R\left(\omega,\vec{k}\right) = K\frac{B\left(\omega,\vec{k}\right)}{A\left(\omega,\vec{k}\right)},$$

where K is some normalization constant [7].

1.2 Holographic quasinormal modes

The definition of the holographic retarded Green's function depends on a subtlety. It is impossible to calculate a retarded (or advanced) Green's function from an action, as is indicated in Equation 3. In thermal field theory, one needs to use the Schwinger–Keldysh formalism in which the time coordinate exists on a (complex) contour [10]. It turns out that the Schwinger–Keldysh contour is naturally implemented on the maximally analytic extension of the AdS black brane metric. In that case, one has a second boundary on which the direction of the time-like Killing vector is reversed in comparison to the direction covered by the coordinate patch Equation 5. Strictly speaking, retarded holographic Green's functions can only be *defined* on this maximally analytically continued double-sided Kruskal-type manifold [11]. Infalling boundary conditions then correspond to the analytic continuation of the solution to the whole Kruskal manifold. For all practical purposes, the retarded Green's function can however be *computed* on the patch Equation 5 by the simple method. The quasinormal modes describe the return to the thermal equilibrium [12]. Their frequencies are the poles of the holographic Green's function in the complexified ω plane [13, 14].

Retarded two-point functions are the central objects in the linear response theory. The response in the operator $\mathcal{O}$ under a perturbation (source) $J(t,x)$ with Fourier transform $\tilde{J}(\omega,\vec{k})$ is

$$\begin{aligned}\langle\mathcal{O}(t,\vec{x})\rangle &= \int\frac{d\omega d^3k}{(2\pi)^4}e^{-i\omega t+i\vec{k}\vec{x}}G_R\left(\omega,\vec{k}\right)\tilde{J}\left(\omega,\vec{k}\right)\\ &= -i\Theta(t)\int\frac{d^3k}{(2\pi)^3}\sum_n R_n(k)\tilde{J}\left(\omega_n\left(\vec{k}\right),\vec{k}\right)e^{-i\omega_n t+i\vec{k}\vec{x}},\end{aligned}$$

where R_n is the residue of G_R at the pole ω_n[3]. As long as all the quasinormal frequencies lie in the lower half of the complex ω-plane, the response decays exponentially fast. A mode in the upper half indicates an instability, leading eventually to a phase transition.

A special role is played by linearized perturbations of gauge fields and the metric. In this case, the dual operator corresponds to a conserved current, and the quasinormal mode spectrum contains the so-called hydrodynamic modes [15], i.e., those fulfilling

$$\lim_{k\to 0}\omega_H\left(\vec{k}\right) = 0.$$

For a gauge field, one finds in this way a diffusive mode that obeys in the small $|\vec{k}|$ limit $\omega_{\text{diffusive}} = -iD\vec{k}^2$, where the diffusion constant $D = \frac{1}{2\pi T}$. The metric fluctuations contain a shear-channel with a similar diffusive law $\omega_{\text{shear}} = -i\frac{\eta}{\epsilon+p}\vec{k}^2$, where $\epsilon + p = sT$ are the energy density ϵ, pressure p, and entropy density s of the dual field theory. Famously, one finds $\frac{\eta}{s} = \frac{1}{4\pi}$ [16].

In some exceptional cases, exact solutions for the holographic Green's function can be found. If there are only three regular singular points of the differential equation, it can then be mapped to the hypergeometric differential equation. This happens for the case of a gauge field in the five-dimensional AdS black brane background at vanishing momentum $\vec{k} = 0$. The holographic retarded Green's function is [17]

$$G_R(\omega) = K\left[2i\omega + \omega^2\psi\left(\frac{(1-i)\omega}{4}\right) + \omega^2\psi\left(-\frac{(1+i)\omega}{4}\right)\right],$$

where $\psi(z)$ is the digamma function. The poles are at[4] $\omega_n = 2n\,(\pm 1 - i)$. More generally, the corresponding differential equation has more than three regular singular points and cannot be solved exactly. In these cases, one needs to resort to numerical approximations.

2 Pseudospectra of holographic quasinormal modes

The infalling boundary conditions on the horizon of the AdS black brane have the consequence that the differential operator is a non-Hermitian and non-normal operator. Its eigenvalues are complex numbers, precisely the quasinormal frequencies. It is a well-known fact that eigenvalues of non-normal operators suffer from spectral instability. This means that a small perturbation of the operator can change the value of the eigenvalues dramatically. In fact, it is this spectral instability that makes the prediction and calculation of quasinormal frequencies challenging. The method of pseudospectra has emerged as an ideal tool to assess the spectral instability of non-normal operators in a quantitative (and also qualitative) way [18].

The calculation of the pseudospectra of quasinormal modes was pioneered in [19] and further explored in [20–36] in various astrophysical and cosmological contexts. We will concentrate here on the simple case of pseudospectra for a gauge field in the AdS black brane [33]. Pseudospectra answer the question of how far a quasinormal frequency can be displaced by a given perturbation of size ϵ. This means, of course, that we need a way to measure the size of an operator that can be added as a perturbation. Consequently, we need to define an appropriate measure on a function space that contains the quasinormal modes. On physical grounds, it is generally suggested to use a suitable norm based on the energy functional. Only in certain coordinate systems the quasinormal modes have "nice" or regular behavior on the horizon. It turns out that in the coordinates shown in Equation 5, the energy functional is not well-defined. There are two strategies to deal with this problem. One is to use infalling Eddington–Finkelstein coordinates. These are often used in the literature on holographic

3 We assume here that there are no contributions from the integral along the large radius half circle in the lower complex ω half-plane.

4 We have rescaled the frequency such that the physical values are $\omega_{\text{phys}} = \pi T\omega$. We further note that the surface gravity is $\kappa = 2\pi T$.

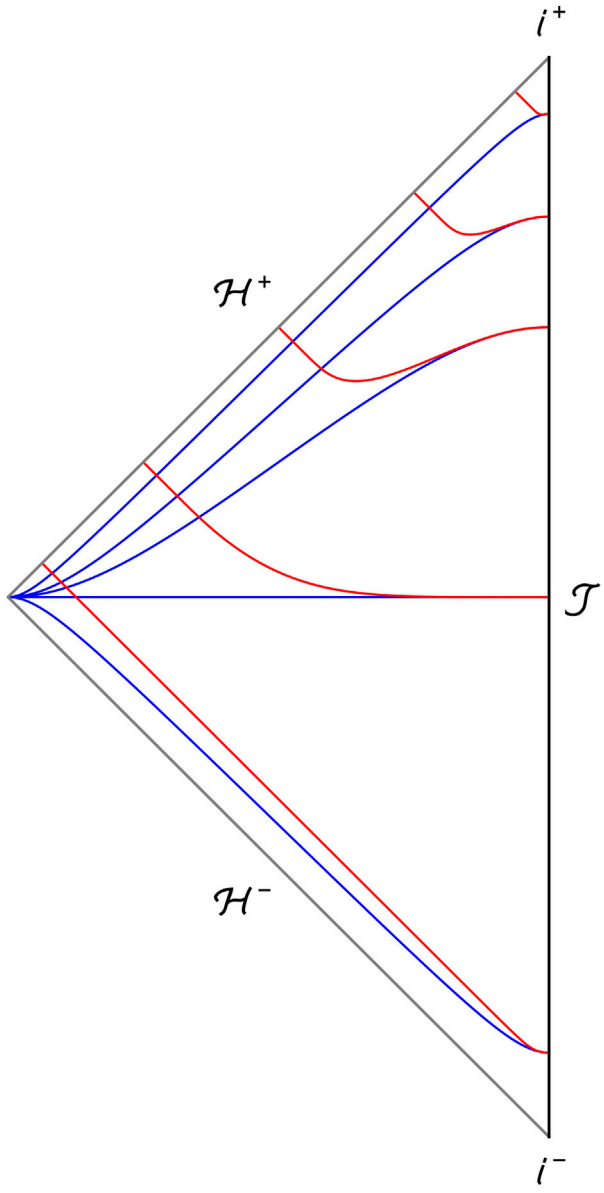

FIGURE 1
Penrose diagram of the exterior region of $SAdS_{4+1}$. The AdS boundary is denoted by $\mathcal{J}$, $\mathcal{H}^+$ ($\mathcal{H}^-$) represents the future (past) horizon, and i^+ (i^-) denotes the future (past) time-like infinity. The red lines correspond to constant τ hypersurfaces (Equation 6), and the blue lines represent constant t hypersurfaces (Equation 5).

quasinormal modes, and the energy functional is indeed well-defined. Another approach is to use the so-called regular coordinates that interpolate between the Schwarzschild-type coordinates near the boundary and infalling Eddington–Finkelstein coordinates near the horizon [37]. Figure 1 shows the Penrose diagram, which illustrates the geometrical nature of this slicing.

In both infalling Eddington–Finkelstein and regular coordinates, the infalling boundary condition is replaced by the condition of regularity at the horizon. There is, however, a difference between the coordinate systems concerning the resulting eigenvalue problem. In infalling Eddington–Finkelstein coordinates, one ends up with a generalized eigenvalue problem, whereas regular coordinates result in a standard eigenvalue problem. We chose the latter approach and briefly review the findings of [33].

A particular choice of regular coordinates for the black brane is

$$\tau = t - \left(1 - \frac{1}{r}\right) + \int \frac{dr}{f(r)}\left(\frac{1}{r}\right)^2, \qquad (6)$$
$$\rho = 1 - \frac{1}{r},$$

in which the line element takes the form

$$ds^2 = \frac{1}{(1-\rho)^2}\left(-f(\rho)d\tau^2 + (d\vec{x})^2 + 2(1 - f(\rho))d\tau d\rho + (2 - f(\rho))d\rho^2\right). \qquad (7)$$

Here, we have set the AdS curvature scale $L = 1$ and re-scaled coordinates such as to absorb the scale set by the horizon ($r_h = \pi T$). In these coordinates, the boundary is at $\rho = 1$ and the horizon at $\rho = 0$.

It is instructive to concentrate on a case in which we have actually exact analytic results about the spectrum of quasinormal frequencies, and therefore we only consider the (transverse) gauge field at zero momentum. This means that we consider a gauge field of the form $A_1(\rho, \tau, \vec{x}) = a(\rho)\exp(-i\omega\tau)$. The equation of motion for this gauge field ansatz in the metric Equation 7 is second order in ∂_τ. It can be reduced to a first-order system by introducing the auxiliary field α and the additional equation $\alpha = -i\omega a$. The energy functional takes the form:

$$E[a, \alpha] = \int_0^1 \frac{d\rho}{1-\rho}\left(f|\partial_\rho a|^2 + (2 - f)|\alpha|^2\right), \qquad (8)$$

where we have discarded an overall volume factor stemming from the integration over the x coordinates. Furthermore, we have taken into account that $a(\rho)$ and $\alpha(\rho)$ are Fourier modes and therefore complex valued. The equation of motion is given by

$$\omega\Psi = \mathcal{L}\Psi = i\begin{pmatrix} 0 & 1 \\ L_1 & L_2. \end{pmatrix}\Psi,$$
$$L_1 = \frac{1}{f-2}\left[-(1-\rho)\left(\frac{f}{1-\rho}\right)'\partial_\rho - f\partial_\rho^2\right],.$$
$$L_2 = \frac{1}{f-2}\left[(1-\rho)\left(\frac{f-1}{1-\rho}\right)' + 2(f-1)\partial_\rho\right],$$

where $\Psi = (a, \alpha)^T$.

Quasinormal modes can now be defined as the eigenvalues of the operator $\mathcal{L}$ with Dirichlet boundary conditions at $\rho = 1$ and regularity at the horizon $\rho = 0$. The energy can be promoted to an inner product

$$\langle \Psi_1, \Psi_2 \rangle = \int_0^1 \frac{d\rho}{1-\rho}\left[f\left(\partial_\rho a_2\right)^\star\left(\partial_\rho a_1\right) + (2 - f)\,\alpha_2^\star \alpha_1\right]. \qquad (9)$$

The operator $\mathcal{L}$ is self-adjoint up to a boundary term with respect to this inner product:

$$\mathcal{L}^\dagger = \mathcal{L} + \begin{pmatrix} 0 & 0 \\ 0 & -i\delta(\rho) \end{pmatrix},$$

which nicely reflects the fact that dissipation stems from the boundary condition at the horizon.

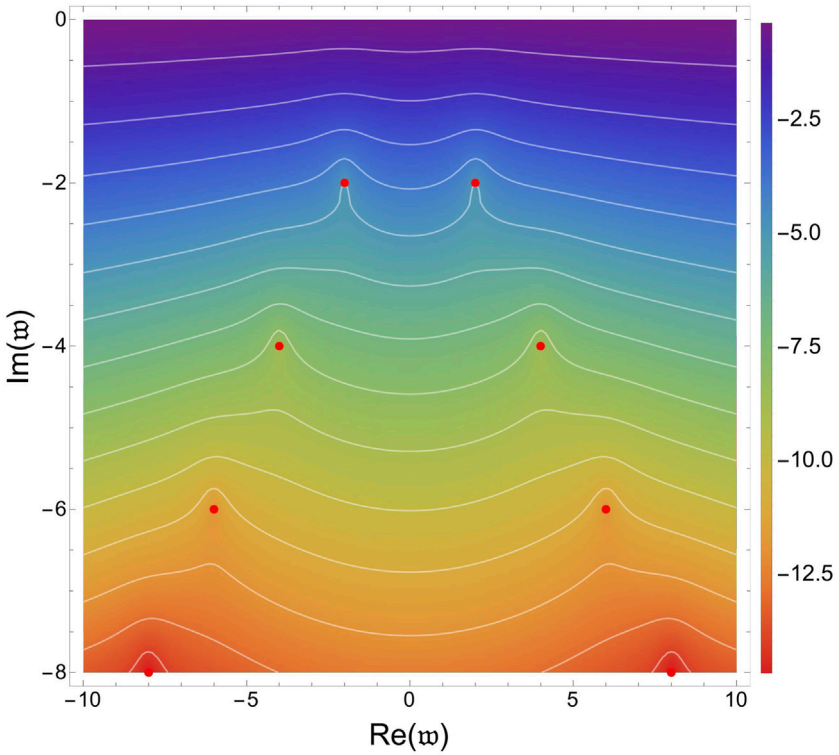

FIGURE 2
Pseudospectra of a vector field in the AdS black brane background. The color code indicates the values of $\log_{10}\epsilon$.

We note that the inner product Equation 9 induces a norm on the space of linear operators acting on Ψ. This operator norm can be used to define the ϵ-pseudospectrum of $\mathcal{L}$ as the set in the complex ω plane where

$$\sigma_\epsilon = \left\{\omega \in \mathbf{C}\colon \|(\mathcal{L}-\omega)^{-1}\| > \frac{1}{\epsilon}\right\}.$$

We refer to [38] for comprehensive information about the pseudospectrum. For our purpose, the most useful interpretation is that for any operator $\delta\mathcal{L}$ of operator norm $\|\delta\mathcal{L}\| < \epsilon$; the spectrum of $\mathcal{L} + \delta\mathcal{L}$ lies inside σ_ϵ.

It is convenient and informative to present the pseudospectra as a contour plot in which the contour lines correspond to different values of ϵ. In the case of a normal operator, these contour lines are concentric circles around the eigenvalues. In particular, for sufficiently small ϵ, the radius of the circle is also given by ϵ. This situation can be referred to as spectral stability. For non-normal operators, however, the contour lines are not necessarily circles. They can be much larger than circles of radius ϵ or even open lines in the complex ω plane. This indicates that small perturbations can displace the eigenvalues of the operator by large amounts.

Let us now consider the pseudospectrum shown in Figure 2. One can see that the contour lines are open. The colors indicate the ϵ values. Even tiny perturbations can completely destabilize the spectrum of quasinormal modes. It is important to note that this figure is obtained with a discretization of the differential operator $\mathcal{L}$ using pseudospectral methods at a grid size of $N = 120$ points for $\rho \in [0, 1]$. It turns out that the spectral instability gets stronger as the grid size increases. In fact, one can argue that the resolvent does not converge to a finite value for $N \to \infty$ [35]. The reason is that the energy norm cannot effectively exclude the modes which are outgoing from the horizon. These behave like $a \propto \rho^{i\omega/2}$ near the horizon. The energy norm, however, only demands integrability on the horizon. In fact, all functions which behave like the outgoing modes with $\Im(\omega) < 0$ have an integrable energy Equation 8. Furthermore, the domain on which the operator $\mathcal{L}$ is defined contains the outgoing modes with $\Im(\omega) < -1$. Therefore, in the continuum limit, all points with $\Im(\omega) < -1$ belong to the spectrum of the operator $\mathcal{L}$. For an in-depth mathematical discussion, see [37, 39]. We note that hydrodynamic modes for small enough momentum k obey $\Im(\omega) \geq -1$, and thus they lie in the convergent region of the pseudospectrum in the energy norm [34, 35].

3 Discussion

This finding on the spectral instability of quasinormal modes is somewhat puzzling. After all, we can construct the holographic Green's function exactly, and it does have a discrete set of poles in the complex ω plane. In contrast, the spectrum of $\mathcal{L}$ is continuous if it acts on functions with the finite energy norm.

We note that, as we have emphasized, the definition of the holographic Green's function implicitly relies on analytic continuation across the horizon. This analyticity requirement is much stronger than the requirement of the existence of the energy norm. A way to circumvent this has been suggested in [37] and consists in replacing the energy norm with a Sobolev norm. In

physicist terms, this corresponds to higher-order derivative terms in the norm. Higher-order derivative terms up to $|\partial_\rho^n a|^2$ amount to lowering the limit for integrability to $\mathfrak{I}(\omega) < 1 - 2n$. In order to recover the exact spectrum, one would, of course, have to take a limit with infinitely many derivatives. From the physics point of view, the significance of such higher-order derivative terms is not clear.

Another line of thought could be that one considers the underlying theory (being it a scalar field, a Maxwell field, or the metric itself) as an effective field theory valid down to a finite cutoff length scale Λ. Then, we would necessarily have some huge but finite value for N determined, e.g., by the criterion that the minimal distance between points of the discretization is larger than Λ. Alternatively, one could also impose the boundary conditions not directly at the horizon but slightly outside at a sort of "stretched" horizon [40].

Let us now emphasize the importance of the pseudospectra in the context of holography. From the gravitational side, pseudospectra probe how much the quasinormal frequencies change if the background is slightly modified in some way (e.g., by the change in the geometry and/or the background value of the fields). Consequently, in the dual quantum field theory, pseudospectra help us estimate how much the poles of the retarded Green's functions might change if the theory is slightly perturbed. In both cases, these perturbations should be understood as perturbations to the Lagrangian, leading to the change in the spectrum of excitations. Then, spectral instability suggests that holographic models might not be able to accurately capture the actual spectra of real physical systems such as quark–gluon plasma. However, valuable information, such as transient dynamics, can still be obtained by studying pseudospectra [24, 38].

We shall now point to additional results on quasinormal modes in anti-de Sitter space. The pseudospectrum in infalling Eddington–Finkelstein coordinates has been investigated in [34]. One of the main findings was that in certain cases, the pseudospectrum can significantly reach up into the upper half-plane, giving rise to possible transient behavior. The structural aspects of the pseudospectrum of quasinormal modes for AdS black holes have been pointed out and further investigated in [35]. In particular, the results in infalling Eddington–Finkelstein and regular coordinates have been contrasted. The dependence of pseudospectra on the choice of coordinates still needs further investigation. The properties of the pseudospectrum of black hole metrics have also been shown to give rise to transient behavior for which a sum of M quasinormal modes can be long lived of order $\log(M)$ in [41]. The stability of complex linear momenta ($\mathbb{C}$LMs) in anti-de Sitter space is studied in [42]. Remarkably, the pseudospectrum of $\mathbb{C}$LMs was observed to be convergent, allowing for quantitative results.

In this paper, we have reviewed the holographic perspective on the quasinormal modes and quasinormal frequencies of AdS black holes. In this context, the pseudospectrum analysis offers an invaluable tool for assessing the stability and investigating the existence of transient dynamics. Numerically computed pseudospectra do not converge in the energy norm because outgoing modes can still have finite energy. We believe that the lack of convergence is not a flaw of the construction but rather a fundamental feature that needs to be addressed using a physics-motivated regulator.

Author contributions

DA: writing–review and editing and writing–original draft. DGF: writing–review and editing and writing–original draft. KL: writing–review and editing and writing–original draft.

Funding

The author(s) declare that financial support was received for the research, authorship, and/or publication of this article. This work is supported through the grants CEX2020-001007-S and PID2021-123017NB-100, PID2021-127726NB-I00 funded by MCIN/AEI/10.13039/501100011033 and by ERDF "A way of making Europe." The work of DGF is supported by FPI grant PRE2022-101810.

Acknowledgments

The authors would like to thank V. Boyanov and especially J.L. Jaramillo for numerous insightful discussions on the properties of quasinormal modes and their pseudospectra.

Conflict of interest

The authors declare that the research was conducted in the absence of any commercial or financial relationships that could be construed as a potential conflict of interest.

Publisher's note

All claims expressed in this article are solely those of the authors and do not necessarily represent those of their affiliated organizations, or those of the publisher, the editors, and the reviewers. Any product that may be evaluated in this article, or claim that may be made by its manufacturer, is not guaranteed or endorsed by the publisher.

References

1. Maldacena JM. The Large N limit of superconformal field theories and supergravity. *Adv Theor Math Phys* (1998) 2:231–52. doi:10.4310/ATMP.1998.v2.n2.a1

2. Aharony O, Gubser SS, Maldacena JM, Ooguri H, Oz Y. Large N field theories, string theory and gravity. *Phys Rept* (2000) 323:183–386. doi:10.1016/S0370-1573(99)00083-6

3. Zaanen J, Sun YW, Liu Y, Schalm K. *Holographic duality in condensed matter physics*. Cambridge, United Kingdom: Cambridge Univ Press (2015). doi:10.1017/CBO9781139942492

4. Ammon M, Erdmenger J. *Gauge/gravity duality: foundations and applications*. Cambridge: Cambridge University Press (2015). doi:10.1017/CBO9780511846373

5. Breitenlohner P, Freedman DZ. Stability in gauged extended supergravity. *Ann Phys* (1982) 144:249–81. doi:10.1016/0003-4916(82)90116-6

6. Klebanov IR, Witten E. AdS/CFT correspondence and symmetry breaking. *Nucl Phys B* (1999) 556:89–114. doi:10.1016/S0550-3213(99)00387-9

7. Son DT, Starinets AO. Minkowski space correlators in AdS/CFT correspondence: recipe and applications. *JHEP* (2002) 09:042. doi:10.1088/1126-6708/2002/09/042

8. Gubser SS, Klebanov IR, Peet AW. Entropy and temperature of black 3-branes. *Phys Rev D* (1996) 54:3915–9. doi:10.1103/PhysRevD.54.3915

9. Witten E. Anti-de Sitter space, thermal phase transition, and confinement in gauge theories. *Adv Theor Math Phys* (1998) 2:505–32. doi:10.4310/ATMP.1998.v2.n3.a3

10. Bellac ML. Thermal field theory. In: *Cambridge monographs on mathematical physics*. Cambridge University Press (2011). doi:10.1017/CBO9780511721700

11. Herzog CP, Son DT. Schwinger-Keldysh propagators from AdS/CFT correspondence. *JHEP* (2003) 03:046. doi:10.1088/1126-6708/2003/03/046

12. Horowitz GT, Hubeny VE. Quasinormal modes of AdS black holes and the approach to thermal equilibrium. *Phys Rev D* (2000) 62:024027. doi:10.1103/PhysRevD.62.024027

13. Birmingham D, Sachs I, Solodukhin SN. Conformal field theory interpretation of black hole quasinormal modes. *Phys Rev Lett* (2002) 88:151301. doi:10.1103/PhysRevLett.88.151301

14. Kovtun PK, Starinets AO. Quasinormal modes and holography. *Phys Rev D* (2005) 72:086009. doi:10.1103/PhysRevD.72.086009

15. Policastro G, Son DT, Starinets AO. From AdS/CFT correspondence to hydrodynamics. *JHEP* (2002) 09:043. doi:10.1088/1126-6708/2002/09/043

16. Kovtun P, Son DT, Starinets AO. Viscosity in strongly interacting quantum field theories from black hole physics. *Phys Rev Lett* (2005) 94:111601. doi:10.1103/PhysRevLett.94.111601

17. Myers RC, Starinets AO, Thomson RM. Holographic spectral functions and diffusion constants for fundamental matter. *JHEP* (2007) 11:091. doi:10.1088/1126-6708/2007/11/091

18. Trefethen LN. *Spectral methods in MATLAB*. Philadelphia, United States: SIAM (2000).

19. Jaramillo JL, Panosso Macedo R, Al Sheikh L. Pseudospectrum and black hole quasinormal mode instability. *Phys Rev X* (2021) 11:031003. doi:10.1103/PhysRevX.11.031003

20. Destounis K, Macedo RP, Berti E, Cardoso V, Jaramillo JL. Pseudospectrum of Reissner-Nordström black holes: quasinormal mode instability and universality. *Phys Rev D* (2021) 104:084091. doi:10.1103/PhysRevD.104.084091

21. Cheung MHY, Destounis K, Macedo RP, Berti E, Cardoso V. Destabilizing the fundamental mode of black holes: the elephant and the flea. *Phys Rev Lett.* (2022) 128:111103. doi:10.1103/PhysRevLett.128.111103

22. Gasperin E, Jaramillo JL. Energy scales and black hole pseudospectra: the structural role of the scalar product. *Class Quant Grav* (2022) 39:115010. doi:10.1088/1361-6382/ac5054

23. Jaramillo JL, Panosso Macedo R, Sheikh LA. Gravitational wave signatures of black hole quasinormal mode instability. *Phys Rev Lett* (2022) 128:211102. doi:10.1103/PhysRevLett.128.211102

24. Jaramillo JL. Pseudospectrum and binary black hole merger transients. *Class Quant Grav* (2022) 39:217002. doi:10.1088/1361-6382/ac8ddc

25. Berti E, Cardoso V, Cheung MHY, Di Filippo F, Duque F, Martens P, et al. Stability of the fundamental quasinormal mode in time-domain observations against small perturbations. *Phys Rev D* (2022) 106:084011. doi:10.1103/PhysRevD.106.084011

26. Konoplya RA, Zhidenko A. *First few overtones probe the event horizon geometry* (2022).

27. Al Sheikh L. *Scattering resonances and Pseudospectrum: stability and completeness aspects in optical and gravitational systems*: Bourgogne. Université de Bourgogne Franche-Comté (2022). Theses.

28. Destounis K, Duque F. *Black-hole spectroscopy: quasinormal modes, ringdown stability and the pseudospectrum* (2023).

29. Boyanov V, Destounis K, Panosso Macedo R, Cardoso V, Jaramillo JL. Pseudospectrum of horizonless compact objects: a bootstrap instability mechanism. *Phys Rev D* (2023) 107:064012. doi:10.1103/PhysRevD.107.064012

30. Cao LM, Chen JN, Wu LB, Xie L, Zhou YS. *The pseudospectrum and spectrum (in) stability of quantum corrected black hole* (2024).

31. Sarkar S, Rahman M, Chakraborty S. Perturbing the perturbed: stability of quasinormal modes in presence of a positive cosmological constant. *Phys Rev D* (2023) 108:104002. doi:10.1103/PhysRevD.108.104002

32. Destounis K, Boyanov V, Panosso Macedo R. Pseudospectrum of de Sitter black holes. *Phys Rev D* (2024) 109:044023. doi:10.1103/PhysRevD.109.044023

33. Areán D, Fariña DG, Landsteiner K. Pseudospectra of holographic quasinormal modes. *JHEP* (2023) 12:187. doi:10.1007/JHEP12(2023)187

34. Cownden B, Pantelidou C, Zilhão M. The pseudospectra of black holes in AdS. *JHEP* (2024) 05:202. doi:10.1007/JHEP05(2024)202

35. Boyanov V, Cardoso V, Destounis K, Jaramillo JL, Panosso Macedo R. Structural aspects of the anti–de Sitter black hole pseudospectrum. *Phys Rev D* (2024) 109:064068. doi:10.1103/PhysRevD.109.064068

36. Courty A, Destounis K, Pani P. Spectral instability of quasinormal modes and strong cosmic censorship. *Phys Rev D* (2023) 108:104027. doi:10.1103/PhysRevD.108.104027

37. Warnick CM. On quasinormal modes of asymptotically anti-de Sitter black holes. *Commun Math Phys.* (2015) 333:959–1035. doi:10.1007/s00220-014-2171-1

38. Trefethen LN, Embree M. *Spectra and pseudospectra: the behavior of nonnormal matrices and operators*. Princeton University Press (2005).

39. Warnick C *(In)stability of de Sitter Quasinormal Mode spectra* (2024).

40. Price RH, Thorne KS. Membrane viewpoint on black holes: properties and evolution of the stretched horizon. *Phys Rev D* (1986) 33:915–41. doi:10.1103/PhysRevD.33.915

41. Carballo J, Withers B. *Transient dynamics of quasinormal mode sums* (2024).

42. Garcia-Fariña D, Landsteiner K, Romeu PG, Saura-Bastida P. *Pseudospectra of complex momentum modes* (2024).

frontiers | Frontiers in Applied Mathematics and Statistics

TYPE Mini Review
PUBLISHED 02 December 2024
DOI 10.3389/fams.2024.1508973

Check for updates

OPEN ACCESS

EDITED BY
Jose Luis Jaramillo,
Université de Bourgogne, France

REVIEWED BY
Wenfeng Chen,
SUNY Polytechnic Institute, United States

*CORRESPONDENCE
Martin Vogel
✉ vogel@math.unistra.fr

RECEIVED 10 October 2024
ACCEPTED 11 November 2024
PUBLISHED 02 December 2024

CITATION
Vogel M (2024) Pseudospectra and eigenvalue asymptotics for disordered non-selfadjoint operators in the semiclassical limit.
Front. Appl. Math. Stat. 10:1508973.
doi: 10.3389/fams.2024.1508973

COPYRIGHT
© 2024 Vogel. This is an open-access article distributed under the terms of the Creative Commons Attribution License (CC BY). The use, distribution or reproduction in other forums is permitted, provided the original author(s) and the copyright owner(s) are credited and that the original publication in this journal is cited, in accordance with accepted academic practice. No use, distribution or reproduction is permitted which does not comply with these terms.

Pseudospectra and eigenvalue asymptotics for disordered non-selfadjoint operators in the semiclassical limit

Martin Vogel*

Institut de Recherche Mathématique Avancée - UMR 7501, Université de Strasbourg et CNRS, Strasbourg, France

The purpose of this note is to review certain recent results concerning the pseudospectra and the eigenvalues asymptotics of non-selfadjoint semiclassical pseudo-differential operators subject to small random perturbations.

KEYWORDS

semiclassical analysis, non-selfadjoint operators, random matrix, spectral theory, partial differential equation (PDE)

1 Introduction

The spectral theory of non-selfadjoint operators acting on a Hilbert space is an established and highly developed subject. Non-selfadjoint operators are prevalent naturally in a wide range of modern problems. For instance, in the field of quantum mechanics, the study of scattering systems naturally leads to the notion of quantum resonances. These can be described as the complex values of the meromorphic. The continuation of the scattering matrix or of the cut-off resolvent of the Hamiltonian to the non-physical sheet of the complex plane. Alternatively, through a complex deformation of the initial Hamiltonian, these resonances can be characterized as the genuine complex valued eigenvalues of a non-selfadjoint operator [1, 3, 60]. We recommend the reader to reference [18] for an in-depth discussion of the mathematics of scattering poles. Another aspect of quantum mechanics is the examination of a *small* system that is linked to a *larger* environment. The effective dynamics of the small systems are governed by a non-selfadjoint operator: the Lindbladian [39].

A major obstacle to the spectral analysis of non-selfadjoint operators is the possible strong *spectral instability* of their spectrum with respect to small perturbations. This phenomenon, sometimes referred to as the *pseudospectral effect*, was initially considered to be a drawback, as it could lead to the origin of immense numerical errors, see Embree and Trefethen [19] and the references therein. However, a recent line of research has also demonstrated that the pseudospectral effect can provide novel insights into the spectral distribution of non-selfadjoint operators that are subjected to small generic perturbations.

2 Spectral instability of non-selfadjoint operators

We commence by recalling the definition of the *pseudospectrum* of a linear operator, a crucial concept that which quantifies its spectral instability. This notion appears to have originated in the second half of the 20^{th} century in various contexts, see reference [65] for a historic overview. It quickly became an important notion in numerical analysis, as it allows us to quantify how much eigenvalues can *spread out* under the influence of small perturbations, see references [64, 65] and the book [19]. We follow here the latter reference.

Let $\mathcal{H}$ be a complex Hilbert space (assumed separable for simplicity) with norm $\|\cdot\|$ and scalar product $(\cdot|\cdot)$. Let $P:\mathcal{H}\to\mathcal{H}$ be a closed densely defined linear operator, with resolvent set $\rho(P)$ and spectrum $\mathrm{Spec}(P)=\mathbb{C}\backslash\rho(P)$.

Definition 1. For any $\varepsilon>0$, we define the ε-pseudospectrum of P by

$$\mathrm{Spec}_\varepsilon(P):=\mathrm{Spec}(P)\cup\{z\in\rho(P);\ \|(P-z)^{-1}\|>\varepsilon^{-1}\}. \quad (1)$$

We note that some authors define the ε-pseudospectrum with a $\geqslant$ rather than a $>$. We, however, follow here reference [19]. It is noteworthy that with this choice of non-strict inequality results in the $\mathrm{Spec}_\varepsilon(P)$ being an open set in $\mathbb{C}$.

For P selfadjoint (or even normal), the spectral theorem implies that

$$\mathrm{Spec}_\varepsilon(P)\subset\mathrm{Spec}(P)+D(0,\varepsilon), \quad (2)$$

where $D(0,\varepsilon)\subset\mathbb{C}$ denotes the open disk with radius ε centered at 0. For P non-selfadjoint, the pseudospectrum of P can be much larger, as illustrated by the following example.

Example 1. For $N\gg 1$, consider the Jordan block matrix

$$P_N=\begin{pmatrix}0&1&0&\dots&0\\0&0&1&\ddots&\vdots\\\vdots&\ddots&\ddots&\ddots&0\\\vdots&\dots&\ddots&\ddots&1\\0&\dots&\dots&\dots&0\end{pmatrix}:\mathbb{C}^N\to\mathbb{C}^N. \quad (3)$$

The spectrum of P_N is given by $\{0\}$. Consider the vector $e_+=(1,z,\dots,z^{N-1})$, $|z|\leqslant r<1$. Then,

$$\|(P_N-z)e_+\|=|z|^N=\mathcal{O}\left(\mathrm{e}^{-N|\log r|}\right)\|e_+\|.$$

So, Theorem 2 shows that for any $\varepsilon>0$ and any $r\in]0,1[$ we have that for $N>1$ sufficiently large

$$D(0,r)\subset\mathrm{Spec}_\varepsilon(P_N).$$

An immediate consequence of Equation 1 is the property that pseudospectra are nested. More precisely,

$$\mathrm{Spec}_{\varepsilon_2}(P)\subset\mathrm{Spec}_{\varepsilon_1}(P),\quad \varepsilon_1>\varepsilon_2>0. \quad (4)$$

The set (Equation 1) describes a region of spectral instability of the operator P, since any point in the ε-pseudospectrum of P lies within the spectrum of a certain ε-perturbation of P [19].

Theorem 1. Let $\varepsilon>0$. Then

$$\mathrm{Spec}_\varepsilon(P)=\bigcup_{\substack{Q\in\mathcal{B}(\mathcal{H})\\\|Q\|<1}}\mathrm{Spec}(P+\varepsilon Q). \quad (5)$$

Proof. See reference [19, p. 31].

A third, equivalent definition of the ε-pseudospectrum of P is provided by the existence of approximate solutions to the eigenvalue problem $(P-z)u=0$.

Theorem 2. Let $\varepsilon>0$ and $z\in\mathbb{C}$. Then the following statements are equivalent:

1. $z\in\mathrm{Spec}_\varepsilon(P)$;
2. $z\in\mathrm{Spec}(P)$ or there exists a $u_z\in\mathcal{D}(P)$ such that $\|(P-z)u_z\|<\varepsilon\|u_z\|$, where $\mathcal{D}(P)$ denotes the domain of P.

Proof. See reference [19, p. 31].

Such a state u_z is referred to as an ε-quasimode, or simply a *quasimode* of $P-z$.

3 Spectral instability of semiclassical pseudo-differential operators

Although the notion of ε-pseudospectrum defined in Definition 1 is valid in the context of semiclassical pseudo-differential operators, we present here a somewhat different, but still related notion, which is more suited to the semiclassical setting. Here, the term "semiclassical" implies that our operators are dependent on a parameter $h\in]0,1]$ (often referred to as "Planck's parameter"), and that our focus we will be on the asymptotic (*semiclassical*) regime $h\searrow 0$. This small parameter will provide us with a natural threshold for defining the pseudospectrum, and thereby measuring the spectral instability. The following discussion is based on the studies of Davies [13] and Dencker et al. [16].

Let $d\geqslant 1$ and $h\in]0,1]$. An *order function* $m\in\mathcal{C}^\infty(\mathbb{R}^{2d};[1,\infty[)$, is a function satisfying the following growth condition:

$$\exists C_0\geqslant 1,\ \exists N_0>0:\quad m(\rho)\leqslant C_0\langle\rho-\mu\rangle^{N_0}m(\mu),\quad \forall\rho,\mu\in\mathbb{R}^{2d}, \quad (6)$$

where $\langle\rho-\mu\rangle:=\sqrt{1+|\rho-\mu|^2}$ denotes the "Japanese brackets." We will also sometimes write $(x,\xi)=\rho\in\mathbb{R}^{2d}$, so that $\xi\in\mathbb{R}^d$. To such an order function m, we may associate a semiclassical symbol class [17, 71]. We assert that a smooth function $p\in\mathcal{C}^\infty(\mathbb{R}^{2d}_\rho,]0,1]_h)$ belongs to the symbol class $S(m)$ if for any multiindex $\alpha\in\mathbb{N}^{2d}$ when there exists a constant $C_\alpha>0$ such that

$$|\partial^\alpha_\rho p(\rho;h)|\leqslant C_\alpha m(\rho),\quad \forall\rho\in\mathbb{R}^{2d},\ \forall h\in]0,1]. \quad (7)$$

We recommend the reader for further reading on semiclassical analysis to [17, 41, 71].

Let the symbol $p\in S(m)$, $m\geqslant 1$, be a "classical" symbol, which satisfies an asymptotic expansion in the limit $h\to 0$:

$$p(\rho;h)\sim p_0(\rho)+hp_1(\rho)+\dots\quad \text{in } S(m), \quad (8)$$

where each $p_j\in S(m)$ is independent of h. We assume that there exists a $z_0\in\mathbb{C}$ and a $C_0>0$ such that

$$|p_0(\rho)-z_0|\geqslant m(\rho)/C_0,\quad \rho\in T^*\mathbb{R}^d. \quad (9)$$

Here, $T^*\mathbb{R}^d\simeq\mathbb{R}^{2d}$ denotes the cotangent space of $\mathbb{R}^d$. In this case, we call p_0 the (semiclassical) principal symbol of p. We then define two subsets of $\mathbb{C}$ associated with p_0:

$$\Sigma:=\Sigma(p_0):=\overline{p_0(T^*\mathbb{R}^d)},$$
$$\Sigma_\infty:=\{z\in\Sigma;\ \exists(\rho_j)_{j\geqslant 1}\text{ s.t. }|\rho_j|\to\infty,\ p_0(\rho_j)\to z\}. \quad (10)$$

Here, the $\overline{p_0(T^*\mathbb{R}^d)}$ denotes the closure of the set $p_0(T^*\mathbb{R}^d)$, and we will use this notation in the sequel. The set Σ is the *classical spectrum*, and Σ_∞ can be called the *classical spectrum at infinity* of the h-Weyl quantization of p was defined by

$$\begin{aligned} P_h u(x) &\coloneqq p^w(x, hD_x)u(x) \\ &= \frac{1}{(2\pi h)^d} \iint e^{\frac{i}{h}(x-y)\cdot\xi} p\left(\frac{x+y}{2}, \xi; h\right) u(y)dyd\xi, \\ &\quad u \in S(\mathbb{R}^d), \end{aligned} \tag{11}$$

seen as an oscillatory integral in ξ. The operator P_h maps $S \to S$, and by duality $S' \to S'$, continuously.

3.1 Semiclassical pseudospectrum

Similar to Dencker et al. [16], we define for a symbol $p \in S(m)$ as in Equation 8 the sets

$$\Lambda_\pm(p) \coloneqq \left\{p(\rho);\ \pm\frac{1}{2i}\{\overline{p}, p\}(\rho) < 0\right\} \subset \Sigma \subset \mathbb{C}, \tag{12}$$

where $\{\cdot,\cdot\}$ denotes the Poisson bracket. It should be noted that the condition $\frac{1}{2i}\{\overline{p}, p\} \neq 0$ is the classical analog of the $[P_h^*, P_h] \neq 0$. As in Dencker et al. [16], we call the set

$$\Lambda(p) : = \overline{\Lambda_- \cup \Lambda_+} \tag{13}$$

the *semiclassical pseudospectrum*.

Theorem 3 ([16]). Suppose that $n \geqslant 2$, $C_b^\infty(T^*\mathbb{R}^d) \ni p \sim p_0 + hp_1 + \ldots$, and $p_0^{-1}(z)$ is compact for a dense set of values $z \in \mathbb{C}$. If $P_h = p^w(x, hD_x)$, then

$$\Lambda(p_0)\backslash\Sigma_\infty \subset \overline{\Lambda_+(p_0)}$$

and for every $z \in \Lambda_+(p_0)$ and every $\rho_0 \in T^*\mathbb{R}^d$ with

$$p_0(\rho_0) = z, \quad \frac{1}{2i}\{\overline{p}_0, p_0\}(\rho_0) < 0,$$

there exists $0 \neq e_+ \in L^2(\mathbb{R}^d)$ such that

$$\|(P_h - z)e_+\| = \mathcal{O}(h^\infty)\|e_+\|, \quad \mathrm{WF}_h(e_+)^1 = \{\rho_0\}. \tag{14}$$

If, in addition, p has a bounded holomorphic continuation to to $\{\rho \in \mathbb{C}^{2d},\ |\mathrm{Im}\,\rho| \leqslant 1/C\}$, then Equation 14 holds with the h^∞ replaced by $\exp(-1/(Ch))$.

If $n = 1$, then the same conclusion holds, provided that in addition to the general assumptions, each component of $\mathbb{C}\backslash\Sigma_\infty$ has a nonempty intersection with $\complement\Lambda(p)$.[2]

This result can be extended to unbounded symbols $p \in S(T^*\mathbb{R}^d, m)$, as shown in Equation 8, and the corresponding operators P_h with principal symbol p_0, by applying Theorem 3 to $\widetilde{P}_h = (P_h - z_0)^{-1}(P_h - z)$, with principal symbol $\widetilde{p}_0 \in C_b^\infty(T^*\mathbb{R}^d)$ and z_0 as in Equation 9 and $z_0 \neq z$. Indeed, note that $z \in \Sigma(p_0)$ if and only if $0 \in \Sigma(\widetilde{p}_0)$, and that $\rho \in p_0^{-1}(z)$ with $\pm\{\mathrm{Re}\,p_0, \mathrm{Im}\,p_0\}(\rho) < 0$ is equivalent to $\rho \in \widetilde{p}_0^{-1}(0)$ with $\pm\{\mathrm{Re}\,\widetilde{p}_0, \mathrm{Im}\,\widetilde{p}_0\}(\rho) < 0$. Furthermore, a quasimode u as in Theorem 3 for $\widetilde{P}_h$ then provides, after a possible truncation, a quasimode for $P_h - z$ in the same sense.

By replacing P_h with its formal adjoint, P_h^*, and thus p with $\overline{p}$, Theorem 3 yields that for every $z \in \Lambda_-(p)$ and every $\rho_0 \in T^*\mathbb{R}^d$ with

$$p_0(\rho_0) = z, \quad \frac{1}{2i}\{\overline{p}_0, p_0\}(\rho_0) > 0,$$

there exists $0 \neq e_- \in L^2(\mathbb{R}^d)$ such that

$$\|(P_h - z)^* e_-\| = \mathcal{O}(h^\infty)\|e_-\|, \quad \mathrm{WF}_h(e_-) = \{\rho_0\}.$$

The additional statements of Theorem 3 regarding symbols that permit a holomorphic extension to a complex neighborhood of $\mathbb{R}^{2d}$, and the case where $n = 1$ hold as well.

Example 2. The case study to be considered is the case of the non-selfadjoint Harmonic oscillator

$$P_h = (hD_x)^2 + ix^2$$

is seen as an unbounded operator $L^2(\mathbb{R}) \to L^2(\mathbb{R})$. The principal symbol for P_h is given by $p(x,\xi) = \xi^2 + ix^2 \in S(T^*\mathbb{R}, m)$, with a weight function $m(x,\xi) = 1+\xi^2+x^2$. We equip P_h with the domain $H(m) := (P_h + 1)^{-1}L^2(\mathbb{R})$, where the operator on the right is the pseudo-differential inverse of P_h+1. This choice of domain renders P_h a closed and densely defined operator. Using, for instance, the method of complex scaling, it can be observed that the spectrum of P_h is determined by

$$\mathrm{Spec}(P_h) = \{e^{i\pi/4}(2n+1)h;\ n \in \mathbb{N}\}. \tag{15}$$

Furthermore, Σ is the closed first quadrant in the complex plane, whereas $\Sigma_\infty = \emptyset$. For $\rho = (x,\xi) \in T^*\mathbb{R}$, we find that

$$\frac{1}{2i}\{\overline{p}, p\}(x,\xi) = 2\xi \cdot x. \tag{16}$$

Thus, for every $z \in \overset{\circ}{\Sigma}$[3] there exist points

$$\begin{aligned} \rho_+^j(z) &= (-1)^j(-\sqrt{|\mathrm{Re}\,z|}, \sqrt{|\mathrm{Im}\,z|}), \\ \rho_-^j(z) &= (-1)^j(-\sqrt{|\mathrm{Re}\,z|}, -\sqrt{|\mathrm{Im}\,z|}|), \quad j = 1, 2, \end{aligned}$$

such that

$$\pm\frac{1}{2i}\{\overline{p}, p\}(\rho_\pm^j(z)) < 0, \quad j = 1, 2.$$

---

1 This implies that the semiclassical wavefront set of e_+ is defined by ρ_0. In other words, the state e_+ is concentrated in position and frequency near the point ρ_0. See, for instance, Zworski [71] for a definition. For $u = (u(h))_{h\in(0,1)}$ a bounded family in $L^2(\mathbb{R}^d)$, its semiclassical wavefront set $\mathrm{WF}_h(u)$ denotes the phase space region where u is h-microlocalized:

$$\mathrm{WF}_h(u) \overset{\mathrm{def}}{=} \complement\Big\{(x,\xi) \in T^*\mathbb{R}^d;\ \exists a \in C_c^\infty(T^*\mathbb{R}^d),\ a(x,\xi) = 1, \\ \|a^w(x, hD_x)u(h)\|_{L^2} = \mathcal{O}(h^\infty),\Big\}$$

where a^w denotes the Weyl quantization of a, and $\complement U$ denotes the complement of a given set U.

2 $\complement\Lambda(p)$ denotes the complement of the set $\Lambda(p)$.

3 $\overset{\circ}{\Sigma}$ denotes the interior of the set Σ.

Using the WKB method, it is possible to construct quasimodes of the form $e_+^j(x;h) = a_+^j(x;h)e^{i\phi_+^j(x)/h}$ with $a_+^j(x;h) \in C_c^\infty(\mathbb{R})$ admitting an asymptotic expansion $a_+^j(x;h) \sim a_{+,0}^j(x)+ha_{+,1}^j(x)+\ldots$ with $\mathrm{WF}_h(e_+^j) = \{\rho_+^j(z)\}$ and

$$\|(P_h - z)e_+^j\| = \mathcal{O}(e^{-1/Ch}), \tag{17}$$

see Davies [13, 14] for an explicit computation, and Dencker et al. [16] for a more general construction.

In fact, the works of Davies [13, 14] provide an explicit WKB construction for a quasimode u for one-dimensional non-selfadjoint Schrödinger operators $P_h - z = (hD_x)^2 + V(x) - z$ on $L^2(\mathbb{R})$ with $V \in C^\infty(\mathbb{R})$ complex-valued and $z = V(a) + \eta^2$, for some $a \in \mathbb{R}$, $\eta > 0$. Furthermore, one assumes that $\mathrm{Im}\, V'(a) \neq 0$. These studies served as the foundation for the quasimode construction of non-selfadjoint (pseudo-)differential operators. Zworski [69] compared Davies' quasimode construction under the condition on the gradient of $\mathrm{Im}\, V$ to a quasimode construction under a non-vanishing condition of the Poisson bracket $\frac{1}{2i}\{\overline{p}, p\}$. Furthermore, Zworski [69] established the link to the famous commutator condition of Hörmander [32, 33]. A full generalization of the quasimode construction under a non-vanishing condition of the poisson bracket, see Theorem 3, was then achieved by Dencker et al. [16]. Finally, Pravda-Starov [46–48] improved these results by modifying a quasimode construction by Moyer and Hörmander, see reference [34, Lemma 26.4.14], for adjoints of operators that do not satisfy the Nirenberg-Tréves condition (Ψ) for local solvability.

For a quasimode construction for non-selfadjoint boundary value problems, we recommend the reader refer to the study of Galkowski [20].

It is noteworthy, that Equation 14 (or Equation 17 in the aforementioned example) implies that if the resolvent $(P_h - z)^{-1}$ exists then its norm is larger than any power of h when $h \to 0$, or even larger than $e^{1/Ch}$ in the analytical case. Each family $(e_+^j(z,h))$ is an h^∞-quasimode of $P_h - z$, or for short a quasimode of $P_h - z$.

From the quasimode Equation 14, it is easy to observe an operator Q of unity norm and a parameter $\delta = \mathcal{O}(h^\infty)$, such that the perturbed operator $P_h + \delta Q$ has an eigenvalue at z. For instance, if we call the error $r_+ = (P_h - z)e_+$, we may take the rank 1 operator $\delta Q = -r_+ \otimes (e_+)^*$. According to Theorem 3, it can be observed that the interior of the set $\Lambda(p)$, situated away from the set Σ_∞, is a zone of strong spectral instability for P_h. For this reason, we may refer to the semiclassical pseudospectrum $\Lambda(p)$ also as the (h^∞-) pseudospectrum of P_h. Finally, we recommend the reader also to the refer studies of Pravda-Starov [46–48] for further refinement of the notion of semiclassical pseudospectrum.

3.2 Outside the semiclassical pseudospectrum

When

$$z \in \mathbb{C}\backslash\Sigma(p),$$

then by condition (Equation 9), we have $(p_0(\rho) - z) \geqslant m(\rho)/C$ for some sufficiently large $C > 0$ and so we know that the inverse $(P_h - z)^{-1}$ is a pseudo-differential operator with principal symbol $(p_0 - z)^{-1} \in S(1/m) \subset S(1)$. Hence, $(P_h - z)^{-1}$ maps $L^2 \to L^2$ and

$$\|(P_h - z)^{-1}\| = \mathcal{O}(1) \tag{18}$$

uniformly in $h > 0$. Therefore, from the semiclassical point of view, we may consider $\mathbb{C}\backslash\Sigma$ as a *zone of spectral stability*.

3.3 At the boundary of the semiclassical pseudospectrum

At the boundary of the semiclassical pseudospectrum, a transition occurs between the zone of strong spectral instability and stability. Indeed, at the boundary we find an improvement over the resolvent bounds, assuming some additional non-degeneracy:

Splitting a symbol $p \in C_b^\infty(T^*\mathbb{R}^d)$ into real and imaginary part, $p = p_1 + ip_2$, we consider the iterated Poisson bracket

$$p_I := \{p_{i_1}, \{p_{i_2}, \{\ldots, \{p_{i_{k-1}}, p_{i_k}\}\}\ldots\}\}$$

where $I \in \{1,2\}^k$, and $|I| = k$ is called the *order* of the Poisson bracket. The *order* of p at $\rho \in T^*\mathbb{R}^d$ is given by

$$k(\rho) := \max\{j \in \mathbb{N};\, p_I(\rho) = 0,\ 1 < |I| \leqslant j\}.$$

The *order* of $z_0 \in \Sigma\backslash\Sigma_\infty$ is the maximum of $k(\rho)$ for $\rho \in p^{-1}(z_0)$.

Theorem 4. See Dencker et al. [16, 56] Assume that $C_b^\infty(T^*\mathbb{R}^d) \ni p \sim p_0 + hp_1 + \ldots$. Let $P_h = p^w(x, hD_x)$ and let $z_0 \in \partial\Sigma(p_0)\backslash\Sigma_\infty(p_0)$. Assume that $dp_0 \neq 0$ at every point in $p_0^{-1}(z_0)$, and that z_0 has a finite order $k \geqslant 1$ for p. Then, k is equal and $h > 0$ is small enough for

$$\|(P_h - z)^{-1}\| \leqslant Ch^{-\frac{k}{k+1}}.$$

In particular, there exists a $c_0 > 0$, such that $h > 0$ is small enough for

$$\{z \in \mathbb{C};\, |z - z_0| \leqslant c_0 h^{\frac{k}{k+1}}\} \cap \mathrm{Spec}(P_h) = \emptyset.$$

This result was proven in dimension 1 by Zworski [70], and in certain cases by Boulton [8]. Further refinements have been obtained from Sjöstrand [56]. Similar to the discussion after Theorem 3, we can extend Theorem 4 to unbounded symbols $p \in S(T^*\mathbb{R}^d, m)$ and their corresponding quantizations.

Example 3. Recall the non-selfadjoint Harmonic oscillator $P_h = (hD_x)^2 + ix^2$ from Example 2. Here $\partial\Sigma = \mathbb{R}_+ \cup i\mathbb{R}_+$, so we see by Equation 16 that for $0 \neq z_0 \in \Sigma$

$$\frac{1}{2i}\{\overline{p}, p\}(\rho) = \{\mathrm{Re}\, p, \mathrm{Im}\, p\}(\rho) = 0, \quad \rho \in p^{-1}(z_0).$$

However,

$$\text{either } \{\mathrm{Re}\, p, \{\mathrm{Re}\, p, \mathrm{Im}\, p\}\}(\rho) = 4\xi^2 \neq 0,$$
$$\text{or } \{\mathrm{Im}\, p, \{\mathrm{Re}\, p, \mathrm{Im}\, p\}\}(\rho) = -4x^2 \neq 0,$$

indicating that z_0 is of order 2 for $p = \xi^2 + ix^2$, and Theorem 4 reveals that

$$\|(P_h - z_0)^{-1}\| \leqslant Ch^{-\frac{2}{3}}.$$

In order for a the ε-pseudospectrum of P_h to reach the boundary of Σ, we require $\varepsilon > h^{2/3}/C$.

3.4 Pseudospectra and random matrices

In this section, we present a brief discussion on pseudospectra for large $N \times N$ random matrices. One may interpret the $1/N$, where $N \gg 1$, as an analog to the semiclassical parameter. By recalling the example of the non-selfadjoint harmonic oscillator, as illustrated in Example 2, we see that pseudospectra can be very large in general. However, in a generic setting, they are typically much smaller.

Let $M \in \mathbb{C}^{N\times N}$ be a complex $N \times N$ matrix and let $s_1(M) \geqslant \ldots \geqslant s_N(M) \geqslant 0$ denotes its singular values, which are the eigenvalues of $\sqrt{M^*M}$ ordered in a decreasing manner and counting multiplicities. It should be noted that if $M - z$ is bijective for some $z \in \mathbb{C}$, then

$$\|(M - z)^{-1}\| = s_N(M - z)^{-1}.$$

In view of Equation 1, the ε-pseudospectrum of M is then characterized by the condition that $z \in \mathrm{Spec}_\varepsilon(M)$

$$z \in \mathrm{Spec}_\varepsilon(M) \quad \Longleftrightarrow \quad s_N(M - z) < \varepsilon.$$

A classical result from Sankar et al. [51, Lemma 3.2] (stated there for real Gaussian random matrices) indicates that with a high probability, the smallest singular value of a deformed random matrix is not too small.

Theorem 5 ([51]). There exists a constant $C > 0$ such that the following holds true. Let $N \geqslant 2$, let X_0 be an arbitrary complex $N \times N$ matrix, and let Q be an $N \times N$ complex Gaussian random matrix, whose entries are all independent copies of a complex Gaussian random variable $q \sim \mathcal{N}_{\mathbb{C}}(0, 1)$. Subsequently, for any $\delta > 0$

$$\mathbf{P}\left(s_N(X_0 + \delta Q) < \delta t\right) \leqslant CNt^2.$$

Proof. For real matrices the proof can be found in Sankar et al. [51, Lemma 3.2], see also reference [63, Theorem 2.2]. For complex matrices a proof is presented for instance in Vogel [66, Appendix A].

Theorem 5 states us that any fixed $z \in \mathbb{C}$ is not included in the ε-pseudospectrum of $X + \delta Q$ with a probability $\geqslant 1 - CN\varepsilon^2\delta^{-2}$. This result suggests that the pseudospectrum of random matrices is typically *not too large*. Theorem 5 has received many extensions. For instance Rudelson and Vershynin [50] consider the case of random matrices with iid (independent and identically distributed) sub-Gaussian entries. Tao and Vu [62] consider iid entries with a nonzero variance. Cook [12] considers the case of random matrices whose of entries have an inhomogeneous variance profile under appropriate assumptions. We conclude this section by noting the following, quantitative outcome obtained by Tao and Vu.

Theorem 6 ([63]). Let q be a random variable with a mean zero and a bounded second moment, and let $\gamma \geqslant 1/2$, $A \geqslant 0$ be constants. Then, there exists a constant $C > 0$, depending on q, γ, and A such that the following holds true. Let Q be the random matrix of size N, whose entries are independent and identically distributed copies of q, and let X_0 be a deterministic matrix satisfying $\|X_0\| \leqslant N^\gamma$. Then,

$$\mathbf{P}\left(s_n(X_0 + Q) \leqslant n^{-\gamma(2A+2)+1/2}\right) \leqslant C\left(n^{-A+o(1)} + \mathbf{P}(\|Q\| \geqslant n^\gamma)\right). \tag{19}$$

Example 4. Consider the case where q is a random variable satisfying the moment conditions

$$\mathbb{E}[q] = 0, \quad \mathbb{E}[|q|^2] = 1, \quad \mathbb{E}[|q|^4] < +\infty. \tag{20}$$

Form [37] reveals that Equation 20 implies that $\mathbb{E}[\|Q\|] \leqslant CN^{1/2}$, which, using Markov's inequality, yields that for any $\varepsilon > 0$

$$\mathbf{P}\left[\|Q\| \geqslant CN^{1/2+\varepsilon}\right] \leqslant C^{-1}N^{-1/2-\varepsilon}\mathbb{E}[\|Q\|] \leqslant N^{-\varepsilon}. \tag{21}$$

In this case (Equation 19) becomes

$$\mathbf{P}\left(s_n(X_0 + Q) \leqslant n^{-(\varepsilon+1/2)(2A+2)+1/2}\right) \leqslant C\left(n^{-A+o(1)} + N^{-\varepsilon}\right). \tag{22}$$

4 Eigenvalue asymptotics for non-selfadjoint (random) operators

Consider the operator $P_h = p^w(x, hD_x)$ depicted in Equations 8, 11, which is viewed as an unbounded operator $L^2(\mathbb{R}^d) \to L^2(\mathbb{R}^d)$. We equip P_h with the domain $H(m) := (P_h - z_0)^{-1}L^2(\mathbb{R}^d)$. It should be noted that $(P_h - z_0)^{-1}$ exists for $h > 0$ that is sufficiently small by the elipticity condition (Equation 9). We will denote by $\|u\|_m := \|(P_h - z_0)u\|$ the associated norm on $H(m)$. Although this norm depends on the selection of the symbol $p_0 - z_0$, it is equivalent to the norm defined by any operator with an elliptic principal symbol $q \in S(m)$, so that the space $H(m)$ solely depends on the order function m. Since $H(m)$ contains the Schwartz functions $\S(\mathbb{R}^d)$, it is dense in $L^2(\mathbb{R}^d)$.

Let us verify that P_h equipped with domain $H(m)$ is closed. Let $(P_h - z_0)u_j \to v$ and $u_j \to u$ in L^2. Since $(P_h - z_0) : H(m) \to L^2$ is bijective, it follows that $u_j \to (P_h - z_0)^{-1}v$ in $H(m)$ and also in L^2. So $u = (P_h - z_0)^{-1}v$. In summary, P_h equipped with the domain $H(m)$ is a densely defined closed linear operator.

Recall Equation 10, and let

$$\Omega \Subset \mathbb{C}\backslash\Sigma_\infty \tag{23}$$

be open, relatively compact, not entirely contained in Σ and so that $\overline{\Omega} \subset \mathbb{C}\backslash\Sigma_\infty$. Using the ellipticity assumption (Equation 9), it was proven in reference [25, Section 3] that

- $\mathrm{Spec}(P_h) \cap \Omega$ is discrete for $h > 0$ small enough,
- For all $\varepsilon > 0$ there exists an $h(\varepsilon) > 0$ such that

$$\mathrm{Spec}(P_h) \cap \Omega \subset \Sigma + D(0, \varepsilon), \quad 0 < h \leqslant h(\varepsilon),$$

where $D(0, \varepsilon)$ denotes the disc in $\mathbb{C}$ of radius ε and centered at 0.

4.1 The selfadjoint setting

If P_h above is selfadjoint, which implies in particular that p is real-valued, we have the classical Weyl asymptotics. We follow here Dimassi and Sjöstrand [17] for a brief review.

Theorem 7. Let Ω be as in Equation 23. For every h-independent interval $I \subset \Omega \cap \mathbb{R}$ with $\mathrm{Vol}_{\mathbb{R}^{2d}}(\partial I) = 0$,

$$\#(\mathrm{Spec}(P_h) \cap I) = \frac{1}{(2\pi h)^d} \left(\int_{p_0^{-1}(I)} dx d\xi + o(1) \right), \quad h \to 0. \quad (24)$$

This result is, in increasing generality, attributed to Chazarin [10], Helffer and Robert [26, 27], Petkov and Robert [45] and Ivrii [35]. See also Dimassi and Sjöstrand [17] for an overview. We highlight two special cases: when $I = [a, b]$, $a < b$, and a, b are not critical points of p_0, then the error term becomes $\mathcal{O}(h)$, see Chazarin [10], Helffer-Robert [26], and Ivrii [35]. When additionally the unions of periodic H_{p_0} trajectories[4] in the energy shell $p_0^{-1}(a)$ and $p_0^{-1}(b)$ are of the Liouville measure 0, then the error term is of the form

$$h \left(\int_{p_0=a} p_1(\rho) L_a(d\rho) - \int_{p_0=b} p_1(\rho) L_b(d\rho) \right) + o(h), \quad (25)$$

where L_λ denotes the Liouville measure on $p_0^{-1}(\lambda)$. See Petkov and Robert [45] and Ivrii [35] and Dimassi and Sjöstrand [17] for details. Let us also highlight that similar results obtained from Theorem 7 are also valid for compact smooth manifolds, see, for instance, Grigis and Sjöstrand [21, Chapter 12] and the references therein.

The corresponding results in the setting of self-adjoint partial differential operators in the high energy limit go back to the seminal study of Weyl [68] and have a long and very rich history. These are, however, beyond the scope of this review.

Example 5. The guiding example to keep in mind is the self-adjoint Harmonic oscillator

$$P_h = (hD_x)^2 + x^2 : L^2(\mathbb{R}) \to L^2(\mathbb{R})$$

seen as an unbounded operator. The principal symbol of P_h is represented by $p(x, \xi) = \xi^2 + x^2 \in S(T^*\mathbb{R}, m)$, and the weight function $m(x, \xi) = 1 + \xi^2 + x^2$. P_h is represented by the domain $H(m) := (P_h + 1)^{-1} L^2(\mathbb{R})$, where the operator on the right is the pseudo-differential inverse of $P_h + 1$. This choice of domain makes P_h a densely defined closed operator. It is widely acknowledged (see, for instance, reference [71, Theorem 6.2]) that the spectrum of P_h is determined by

$$\mathrm{Spec}(P_h) = \{(2n + 1)h; n \in \mathbb{N}\}.$$

Counting the points $(2n + 1)h$ contained in an interval $[a, b]$, $0 \leqslant a < b < \infty$, gives

$$\#(\mathrm{Spec}(P_h) \cap [a, b]) = \frac{b - a}{2h} + \mathcal{O}(1).$$

Since $\mathrm{Vol}_{\mathbb{R}^2}(\{a \leqslant \xi^2 + x^2 \leqslant b\}) = \pi(b - a)$, we confirm Theorem 7 for the Harmonic oscillator.

4 H_{p_0} denotes the Hamilton vector field induced by p_0.

4.2 The non-self-adjoint setting

The natural counterpart of Theorem 7 for non-self-adjoint operators would be eigenvalue asymptotics in a complex domain $\Omega \Subset \mathbb{C}$ as in Equation 23. Recall the non-self-adjoint Harmonic oscillator P_h from Example 2 with principal symbol $p(x, \xi) = \xi^2 + ix^2$. In this case, $\Sigma = \{z \in \mathbb{C}; \mathrm{Re}\, z, \mathrm{Im}\, z \geqslant 0\}$ and $\Sigma_\infty = \emptyset$. Any $\emptyset \neq \Omega \Subset \Sigma$ away from the line $e^{i\pi/4}\mathbb{R}_+$, indicates the view of Equation 15 that

$$\#(\mathrm{Spec}(P_h) \cap \Omega) = 0.$$

On the other hand,

$$\frac{1}{2\pi h} \int_{p^{-1}(\Omega)} dx d\xi > 0.$$

This example suggests that a direct generalization of Theorem 7 to non-self-adjoint operators with a complex valued principal symbol cannot hold.

Let us comment on two settings where a form of Weyl asymptotics is known to hold: Upon assuming analyticity, one may recover a sort of Weyl asymptotics. More precisely, as shown in the studies of Melin and Sjöstrand [43], Sjöstrand [53], Hitrik and Sjöstrand [28–30], Hitrik et al. [31], and Rouby [49], the discrete spectrum of certain analytic non-self-adjoint pseudo-differential operators is confined to curves in Σ. Moreover, one can recover eigenvalue asymptotics using Bohr-Sommerfeld quantization conditions.

The second setting occurs when the non-self-adjointness of the operator P_h arises not from the principal symbol p_0 (assumed to be real-valued), but from the subprincipal symbol p_1. For instance, when studying the damped wave equation on a compact Riemannian manifold X, one is led to study the eigenvalues of the corresponding stationary operator

$$P_h(z) = -h^2\Delta + 2ih\sqrt{a(x)}\sqrt{z}, \quad a \in C^\infty(X; \mathbb{R}).$$

Here, Δ denotes the Laplace-Beltrami operator on X, and we call $z \in \mathbb{C}$ an eigenvalue of $P_h(z)$ if there exists a corresponding L^2 function u is present in the kernel of $P_h(z) - z$. In fact, such a u is smooth by elliptic regularity. Using Fredholm theory, one can show that these eigenvalues form a discrete set in $\mathbb{C}$.

The principal part of $P_h = P_h(z)$ is given by $-h^2\Delta$, and thus is self-adjoint. The principal symbol is $p_0(x, \xi) = |\xi|_x^2$ (the norm here is with respect to the Riemannian metric on X). However, the subprincipal part is complex valued and non-self-adjoint.

Lebeau [38] has established that there exists $a_\pm \in \mathbb{R}$, wherein for every $\varepsilon > 0$ there exist a finite number of eigenvalues such that

$$\frac{\mathrm{Im}\, z}{h} \notin [a_- - \varepsilon, a_+ + \varepsilon].$$

Remark 1. In fact Lebeau provided precise expressions for $a_\pm$ in terms of the infimum and the supremum over the co-sphere bundle S^*X of the long time average of the damping function a evolved via the geodesic flow. Further refinements have been obtained by Sjöstrand [52], and when X is negatively curved by Anantharaman [2] and Jin [36].

Additionally, Markus and Matsaev [40] and Sjöstrand [52] have demonstrated the following analog of the Weyl law. For $0 < E_1 < E_2 < \infty$ and for $C > 0$ sufficiently large

$$\#\big(\mathrm{Spec}(P_h) \cap ([E_1, E_2] + i[-Ch, Ch])\big) = \frac{1}{(2\pi h)^d}\left(\iint_{p_0^{-1}([E_1,E_2])} dxd\xi + \mathcal{O}(h)\right). \tag{26}$$

Finer results have been obtained by Anantharaman [2] and Jin [36] when X is negatively curved.

4.3 Probabilistic Weyl asymptotics

In a series of studies by Hager [23–25] and Sjöstrand [54, 55], the authors proved a Weyl law, with overwhelming probability, for the eigenvalues in a compact set $\Omega \Subset \mathbb{C}$ as in Equation 23 for randomly perturbed operators

$$P^\delta = P_h + \delta Q_\omega, \quad 0 < \delta = \delta(h) \ll 1, \tag{27}$$

where P_h is as per in Section 3, and the random perturbation Q_ω is one of the following two types.

4.3.1 Random matrix

Let $N(h) \to \infty$ sufficiently fast as $h \to 0$. Let $q_{j,k}$, $0 \leqslant j,k < N(h)$ be independent copies of a complex Gaussian random variable $\alpha \sim \mathcal{N}_{\mathbb{C}}(0,1)$. We consider the random matrix

$$Q_\omega = \sum_{0\leqslant j,k<N(h)} q_{j,k}\, e_j \otimes e_k^*, \tag{28}$$

where $\{e_j\}_{j\in\mathbb{N}} \subset L^2(\mathbb{R}^d)$ is an orthonormal basis and $e_j \otimes e_k^* u = (u|e_k)e_j$ for $u \in L^2(\mathbb{R})$. The condition on $N(h)$ is determined by the requirement that the microsupport of the vectors in the orthonormal system $\{e_j\}_{j<N(h)}$, "covers" the compact set $p_0^{-1}(\Omega) \subset T^*\mathbb{R}^d$, where p_0 is the principal symbol of P_h. For instance, we could consider the first $N(h)$ eigenfunctions (ordered according to increasing eigenvalues) of the Harmonic oscillator $P_h = -h^2\Delta + x^2$ on $\mathbb{R}^d$. The number $N(h)$ is then determined by the condition that the semiclassical wavefront sets of e_j, $j \geqslant N(h)$, are disjoint from $p_0^{-1}(\Omega)$. Alternatively, as in Hager and Sjöstrand [25], one may also take $N(h) = \infty$; however, then one must conjugate Q_ω by suitable elliptic Hilbert–Schmidt operators. We recommend the reader to Hager and Sjöstrand [25] for further information.

4.3.2 Random potential

We take $N(h)$ and an orthonormal family $(e_k)_{k\in\mathbb{N}}$ as above. Let v be real or complex random vector in $\mathbb{R}^{N(h)}$ or $\mathbb{C}^{N(h)}$, respectively, with joint probability law

$$v_*(d\mathbf{P}) = Z_h^{-1}\, \mathbf{1}_{B(0,R)}(v)\, \mathrm{e}^{\phi(v)} L(dv), \tag{29}$$

where $Z_h > 0$ is a normalization constant, $B(0,R)$ is either the real ball $\Subset \mathbb{R}^{N(h)}$ or the complex ball $\Subset \mathbb{C}^{N(h)}$ of radius $R = R(h) \gg 1$, and centered at 0, $L(dv)$ denotes the Lebesgue measure on either $\mathbb{R}^{N(h)}$ or $\mathbb{C}^{N(h)}$ and $\phi \in C^1$ with

$$\|\nabla_v \phi\| = \mathcal{O}(h^{-\kappa_4}) \tag{30}$$

uniformly, for an arbitrary but fixed value of $\kappa_4 \geqslant 0$. In Hager [24] the case of non-compactly supported probability law was considered. More precisely, the entries of the random vector v were supposed to be independent and identically distributed (iid) complex Gaussian random variables $\sim \mathcal{N}_{\mathbb{C}}(0,1)$. In Sjöstrand [54, 55], the law Equation 29 was considered. For the sake of simplicity, we will not elaborate here the precise conditions on the e_k, $R(h)$, and $N(h)$, in this case, but refer the reader to Sjöstrand [54, 55]. However, one example of a random vector v with law (Equation 30) is a truncated complex or real Gaussian random variables with expectation 0, and uniformly bounded covariances. In fact, the methods in Sjöstrand [54, 55] can be extended to non-compactly supported probability distributions, provided sufficient decay conditions at infinity are assumed. For instance, iid complex Gaussian random variables, as in the one dimensional case [24], are permissable. Finally, we conclude that the methods in Sjöstrand [54, 55] can probably also be modified to allow for the case of more general independent and identically distributed random variables. We define the random function as

$$V_\omega = \sum_{0\leqslant j<N(h)} v_j\, e_j. \tag{31}$$

We call this perturbation a "random potential," even though V_ω is complex valued. When we consider this type of perturbation, we will make the additional symmetry assumption:

$$p(x,\xi;h) = p(x,-\xi;h). \tag{32}$$

Let $\Omega \Subset \mathbb{C}$ be an open simply connected set as in Equation 23. For $z \in \Omega$ and $0 \leqslant t \ll 1$ we set

$$V_z(t) = \mathrm{Vol}\{\rho \in T^*\mathbb{R}^d;\, |p_0(\rho) - z|^2 \leqslant t\}. \tag{33}$$

Let $\Gamma \Subset \Omega$ be open with $\mathcal{C}^2$ boundary and make the following non-flatness assumption

$$\exists \kappa \in]0,1], \text{ such that } V_z(t) = \mathcal{O}(t^\kappa), \text{ uniformly for } z \in \mathrm{neigh}(\partial\Gamma),\ 0 \leqslant t \ll 1. \tag{34}$$

The above mentioned works have yielded the following result.

Theorem 8 (Probabilistic Weyl's law). Let Ω be as in Equation 23. Let $\Gamma \Subset \Omega$ be open with $\mathcal{C}^2$ boundary. Let P_h^δ be a randomly perturbed operators as in Equation 27 with $\mathrm{e}^{-1/Ch} \ll \delta \leqslant h^\theta$ with $\theta > 0$ sufficiently large. Then, in the limit $h \to 0$,

$$\#\big(\mathrm{Spec}(P_h^\delta) \cap \Gamma\big) = \frac{1}{(2\pi h)^d}\left(\iint_{p_0^{-1}(\Gamma)} dxd\xi + o(1)\right) \text{ with probability } \geqslant 1 - Ch^\eta, \tag{35}$$

for some fixed $\eta > 0$.

The studies [23–25, 54, 55] also provide an explicit control over θ, the error term in Weyl's law, and the error term in the probability estimate. Theorem 8 is remarkable because such Weyl laws are typically a feature of self-adjoint operator, whereas in the non-selfadjoint case they generally fail. Indeed, as laid out in Section 4.2, the discrete spectrum of the (unperturbed) non-selfadjoint operator P_h is usually localized to curves in the pseudospectrum

Σ, see Melin and Sjöstrand [43], Hitrik and Sjöstrand [28–31], and Rouby [49]. In contrast, Theorem 8 shows that a "generic" perturbation of size $\mathcal{O}(h^\infty)$ is sufficient for the spectrum to "fill out" Σ.

To illustrate this phenomenon, recall the non-selfadjoint harmonic oscillator $P_h = -h^2\partial_x^2 + ix^2$ on $\mathbb{R}$ from Example 2. Its spectrum is given by $\{e^{i\pi/4}(2n+1)h; n \in \mathbb{N}\}$ [14] on the line $e^{i\pi/4}\mathbb{R}_+ \subset \mathbb{C}$. The Theorem 8 shows that a "generic" perturbation of arbitrarily small size is sufficient to produce spectrum roughly equidistributed in any fixed compact set in its classical spectrum Σ, which is in this case the upper right quadrant of $\mathbb{C}$.

As observed in Christiansen and Zworski [11], the real analytic p condition (Equation 34) consistently holds for some $\kappa > 0$. Similarly, when p is truly analytical and such that $\Sigma \subset \mathbb{C}$ has non-empty interior, then

$$\forall z \in \partial\Omega : dp\restriction_{p^{-1}(z)} \neq 0 \quad \Longrightarrow \quad \text{(4.12) holds with } \kappa > 1/2. \tag{36}$$

For smooth p, we have that when for every $z \in \partial\Omega$

$$dp, d\overline{p} \text{ are linearly independent at every point of } p^{-1}(z), \text{ then (4.12) holds with } \kappa = 1. \tag{37}$$

Observe that dp and $d\overline{p}$ are linearly independent at ρ when $\{p,\overline{p}\}(\rho) \neq 0$, where $\{a,b\} = \partial_\xi a\cdot\partial_x b - \partial_x a\cdot\partial_\xi b$ denotes the Poisson bracket. Moreover, in dimension $d = 1$, the condition $\{p,\overline{p}\} \neq 0$ on $p^{-1}(z)$ is equivalent to dp, with $d\overline{p}$ being linearly independent at every point of $p^{-1}(z)$. However, in dimensions $d > 1$, this cannot in hold general, as the integral of $\{p,\overline{p}\}$ with respect to the Liouville measure on $p^{-1}(z)$ vanishes on every compact connected component of $p^{-1}(z)$, see reference [42, Lemma 8.1]. Furthermore, condition (Equation 37) cannot hold when $z \in \partial\Sigma$. However, some iterated Poisson brackets may not have zero there. For example, it has been observed in [25, Example 12.1] that if

$$\forall \rho \in p^{-1}(\partial\Omega) : \{p,\overline{p}\}(\rho) \neq 0 \text{ or } \{p,\{p,\overline{p}\}\}(\rho) \neq 0, \text{ then (4.12) holds with } \kappa = \frac{3}{4}. \tag{38}$$

4.3.3 Related results

Theorem 8 has also been extended to the case of elliptic semiclassical differential operators on compact manifolds by Sjöstrand [55], to the Toeplitz quantization of the torus by Christiansen and Zworski [11] and Vogel [66], and to general Berezin-Toeplitz quantizations on compact Kähler manifolds by Oltman [44] in the context of complex Gaussian noise. A further extension of Theorem 8 has been achieved by Becker, Oltman and the author in Becker et al. [6]. There we prove a probabilistic Weyl law for the non-selfadjoint off-diagonal operators of the Bistritzer-MacDonald Hamiltonian [7] for twisted bilayer graphene, see also Cancés et al. [9] and Watson et al. [67], subject to random tunneling potentials. This probabilistic Weyl has an interesting physical consequence as it demonstrates the instability of the so-called *magic angels* for this model of twisted bilayer graphene. Similar results have been achieved in random matrix theory. The case of Toeplitz matrices is represented by symbols on $\mathbb{T}^2$ of the form $\sum_{n\in\mathbb{Z}} a_n e^{in\xi}$, $(x,\xi) \in \mathbb{T}^2$, has been conducted in a series of recent studies by Śniady [61], Davies and Hager [15], Guionnet et al. [22], Basak et al. [4, 5], Sjöstrand and the author of this text [57–59]. Such symbols amount to the case of symbols which are constant in the x variable. In these studies the non-selfadjointness of the problem, however, does not come from the symbol itself, but from the boundary conditions destroying it. The periodicity of the symbol in x is achieved by allowing for a discontinuity. Nevertheless, these studies demonstrate that by adding a small random matrix, the limit of the empirical eigenvalues counting measure μ_N of the perturbed operator converges in probability (or even almost surely in some cases) to $p_*(d\rho)$.

Author contributions

MV: Writing – original draft, Writing – review & editing.

Funding

The author(s) declare financial support was received for the research, authorship, and/or publication of this article. I am partly supported by the ANR Grant ADYCT ANR-20-CE40-0017.

Conflict of interest

The author declares that the research was conducted in the absence of any commercial or financial relationships that could be construed as a potential conflict of interest.

Publisher's note

All claims expressed in this article are solely those of the authors and do not necessarily represent those of their affiliated organizations, or those of the publisher, the editors and the reviewers. Any product that may be evaluated in this article, or claim that may be made by its manufacturer, is not guaranteed or endorsed by the publisher.

References

1. Aguilar J, Combes J-M. A class of analytic perturbations for one-body schrödinger Hamiltonians. *Commun Math Phys.* (1971) 22:269–79. doi: 10.1007/BF01877510

2. Anantharaman N. Spectral deviations for the damped wave equation. *Geom Funct Anal.* (2010) 20:3. doi: 10.1007/s00039-010-0071-x

3. Balslev E, Combes J-M. Spectral properties of many-body Schrödinger operators with dilation analytic interactions. *Comm Math Phys*. (1971) 22:280–94. doi: 10.1007/BF01877511

4. Basak A, Paquette E, Zeitouni O. Regularization of non-normal matrices by Gaussian noise - the banded Toeplitz and twisted Toeplitz cases. *Forum of Mathematics, Sigma*. (2019) 7:e3. doi: 10.1017/fms.2018.29

5. Basak A, Paquette E, Zeitouni O. Spectrum of random perturbations of Toeplitz matrices with finite symbols. *Trans Amer Math Soc*. (2020) 373:4999–5023. doi: 10.1090/tran/8040

6. Becker S, Oltman I, Vogel M. Absence of small magic angles for disordered tunneling potentials in twisted bilayer graphene. *arXiv preprint arXiv:2402*.12799. (2024).

7. Bistritzer R, MacDonald A. Moiré bands in twisted double-layer graphene. *PNAS*. (2011) 108:12233–7. doi: 10.1073/pnas.1108174108

8. Boulton L. Non-self-adjoint harmonic oscillator, compact semigroups and pseudospectra. *J Operator Theory*. (2002) 47:413–29.

9. Cancès E, Garrigue L, Gontier D. A simple derivation of moiré-scale continuous models for twisted bilayer graphene. *Phys Rev B*. (2023) 107:155403. doi: 10.1103/PhysRevB.107.155403

10. Chazarain J. Spectre d'un hamiltonien quantique et mécanique classique. *Comm PDE*. (1980) 5:595–644. doi: 10.1080/0360530800882148

11. Christiansen TJ, Zworski M. Probabilistic Weyl laws for quantized tori. *Comm Math Phys*. (2010) 299:305–34. doi: 10.1007/s00220-010-1047-2

12. Cook N. Lower bounds for the smallest singular value of structured random matrices. *Ann Probab*. (2018) 46:3442–500. doi: 10.1214/17-AOP1251

13. Davies EB. Pseudo–spectra, the harmonic oscillator and complex resonances. *Proc Royal Soc London A*. (1999) 455:585–99. doi: 10.1098/rspa.1999.0325

14. Davies EB. Semi-classical states for non-self-adjoint Schrödinger operators. *Comm Math Phys*. (1999) 200:35–41. doi: 10.1007/s002200050521

15. Davies EB, Hager M. Perturbations of Jordan matrices. *J Approx Theory*. (2009) 156:82–94. doi: 10.1016/j.jat.2008.04.021

16. Dencker N, Sjöstrand J, Zworski M. Pseudospectra of semiclassical (pseudo-) differential operators. *Commun Pure Appl Mathem*. (2004) 57:384–415. doi: 10.1002/cpa.20004

17. Dimassi M, Sjöstrand J. *Spectral Asymptotics in the Semi-Classical Limit*. London Mathematical Society Lecture Note Series 268, Cambridge: Cambridge University Press (1999).

18. Dyatlov S, Zworski M. *Mathematical Theory of Scattering Resonances*. London: American Mathematical Society (2019).

19. Embree M, Trefethen LN. *Spectra and Pseudospectra: The Behavior of Nonnormal Matrices and Operators*. Princeton: Princeton University Press (2005). doi: 10.1515/9780691213101

20. Galkowski J. Pseudospectra of semiclassical boundary value problems. *J Inst Math Jussieu*. (2014) 2:405–49. doi: 10.1017/S1474748014000061

21. Grigis A, Sjöstrand J. *Microlocal Analysis for Differential Operators, London Mathematical Society Lecture Note Series 196*. Cambridge: Cambridge University Press (1994).

22. Guionnet A, Wood PM, Zeitouni O. Convergence of the spectral measure of non-normal matrices. Proc *AMS*. (2014) 142:667–79. doi: 10.1090/S0002-9939-2013-11761-2

23. Hager M. Instabilité Spectrale Semiclassique d'Opérateurs Non-Autoadjoints II. *Ann Henri Poincare*. (2006) 7:1035–64. doi: 10.1007/s00023-006-0275-7

24. Hager M. Instabilité spectrale semiclassique pour des opérateurs non-autoadjoints I: un modèle. *Ann faculté des Sci Toulouse Sé*. (2006) 6:243–80. doi: 10.5802/afst.1121

25. Hager M, Sjöstrand J. Eigenvalue asymptotics for randomly perturbed non-selfadjoint operators. *Mathem Ann*. (2008) 342:177–243. doi: 10.1007/s00208-008-0230-7

26. Helffer B, Robert D. Comportement semi-classique du spectre des hamiltoniens quantiques elliptiques. *Ann Inst Fourier, Grenoble*. (1981) 31:169–223. doi: 10.5802/aif.844

27. Helffer B, Robert D. Calcul fonctionnel par la transformation de mellin et opérateurs admissibles. *J Funct Anal*. (1983) 53:246–68. doi: 10.1016/0022-1236(83)90034-4

28. Hitrik M, Sjöstrand J. Non-selfadjoint perturbations of selfadjoint operators in 2 dimensions I. *Ann Henri Poincaré*. (2004) 5:1–73. doi: 10.1007/s00023-004-0160-1

29. Hitrik M, Sjöstrand J. Non-selfadjoint perturbations of selfadjoint operators in 2 dimensions II. Vanishing averages. *Comm Partial Differ Equat*. (2005) 30:1065–1106. doi: 10.1081/PDE-200064447

30. Hitrik M, Sjöstrand J. Non-selfadjoint perturbations of selfadjoint operators in 2 dimensions III a. One branching point. *Canadian J Math*. (2008) 60:572–657. doi: 10.4153/CJM-2008-028-3

31. Hitrik M, Sjöstrand J, Vũ Ngọc S. Diophantine tori and spectral asymptotics for non-selfadjoint operators. *Amer J Math*. (2007) 129:105–82. doi: 10.1353/ajm.2007.0001

32. Hörmander L. Differential Equations without Solutions. *Math Annalen*. (1960) 140:169–173. doi: 10.1007/BF01361142

33. Hörmander L. Differential operators of principal type. *Math Annalen*. (1960) 140:124–146. doi: 10.1007/BF01360085

34. Hörmander L. *The Analysis of Linear Partial Differential Operators IV, Grundlehren der mathematischen Wissenschaften, vol*. 275. Cham: Springer-Verlag (1985).

35. Ivrii V. *Microlocal Analysis and Precise Spectral Asymptotics*. New York: Springer (1998). doi: 10.1007/978-3-662-12496-3

36. Jin L. Damped wave equations on compact hyperbolic surfaces. *Comm Math Phys*. (2020) 373:771–94. doi: 10.1007/s00220-019-03650-x

37. R. Latala. Some estimates of norms of random matrices. *Proc Amer Math Soc*. (2005) 133:1273–82. doi: 10.1090/S0002-9939-04-07800-1

38. Lebeau G. *Équation des ondes amorties, Algebraic and Geometric Methods in Mathematical Physics (Kaciveli, 1993)*. Dordrecht: Kluwer Academy Publication (1996). doi: 10.1007/978-94-017-0693-3_4

39. Lindblad G. On the generators of quantum dynamical semigroups. *Commun Math Phys*. (1976) 48:119–30. doi: 10.1007/BF01608499

40. Markus AS, Matsaev VI. Comparison theorems for spectra of linear operators and spectral asymptotics Trudy Moskov. *Mat Obshch*. (1982) 45:133–81.

41. Martinez A. *An Introduction to Semiclassical and Microlocal Analysis*. Cham: Springer (2002). doi: 10.1007/978-1-4757-4495-8

42. Melin A, Sjöstrand J. Determinants of pseudodifferential operators and complex deformations of phase space. *Methods Appl Anal*. (2002) 9:177–237. doi: 10.4310/MAA.2002.v9.n2.a1

43. Melin A, Sjöstrand J. Bohr-Sommerfeld quantization condition for non-selfadjoint operators in dimension 2. *Astérisque*. (2003) 284:181–244.

44. Oltman I. A probabilistic Weyl-law for Berezin-Toeplitz operators. *J Spectral Theory*. (2023) 13:727–54. doi: 10.4171/jst/459

45. Petkov V, Robert D. Asymptotique semi-classique du spectre d'hamiltoniens quantiques et trajectoires classiques périodiques. *Comm in PDE*. (1985) 10:365–90. doi: 10.1080/03605308508820382

46. Pravda-Starov K. A general result about the pseudo-spectrum of Schrödinger operators. *Proc R Soc London Ser A Math Phys Eng Sci*. (2004) 460:471–7. doi: 10.1098/rspa.2003.1194

47. Pravda-Starov K. *Étude du pseudo-spectre d'opérateurs non auto-adjoints*. Ph.D. thesis (2006).

48. Pravda-Starov K. Pseudo-spectrum for a class of semi-classical operators. *Bull Soc Math France*. (2008) 136:329–372. doi: 10.24033/bsmf.2559

49. Rouby O. Bohr-Sommerfeld quantization conditions for non-selfadjoint perturbations of selfadjoint operators in dimension one. *Int Math Res Not IMRN*. (2018) 7:2156–207. doi: 10.1093/imrn/rnw309

50. Rudelson M, Vershynin R. The least singular value of a randomsquare matrix is $O(n^{-1/2})$. *C R Math Acad Sci Paris*. (2008) 346:893–6. doi: 10.1016/j.crma.2008.07.009

51. Sankar A, Spielmann DA, Teng SH. Smoothed analysis of the condition numbers and growth factors of matrices. *SIAM J, Matrix Anal Appl*. (2006) 28:446–76. doi: 10.1137/S0895479803436202

52. Sjöstrand J. *Asymptotic Distribution of Eigenfrequencies for Damped Wave Equations. Publ RIMS, Kyoto Univ*. (2000) 36:573–611. doi: 10.2977/prims/1195142811

53. Sjöstrand J. Perturbations of selfadjoint operators with periodic classical flow. In: *Wave Phenomena and Asymptotic Analysis*. RIMS Kokyuroku (2003). p. 1315.

54. Sjöstrand J. Eigenvalue distribution for non-self-adjoint operators with small multiplicative random perturbations. *Ann Fac Sci Toulouse*. (2009) 18:739–795. doi: 10.5802/afst.1223

55. Sjöstrand J. Eigenvalue distribution for non-self-adjoint operators on compact manifolds with small multiplicative random perturbations. *Ann Fac Toulouse*. (2010) 19:277–301. doi: 10.5802/afst.1244

56. Sjöstrand J. Resolvent estimates for non-selfadjoint operators via semigroups. In: *Around the Research of Vladimir Maz'ya III, International Mathematical Series 13*. New York: Springer (2010). p. 359–384. doi: 10.1007/978-1-4419-1345-6_13

57. Sjöstrand J, Vogel M. Large bi-diagonal matrices and random perturbations. *J Spectral Theory*. (2016) 6:977–1020. doi: 10.4171/jst/150

58. Sjöstrand J, Vogel M. General Toeplitz matrices subject to Gaussian perturbations. *Ann Henri Poincaré*. (2021) 22:49–81. doi: 10.1007/s00023-020-00970-w

59. Sjöstrand J, Vogel M. Toeplitz band matrices with small random perturbations. *Indagationes Mathem*. (2021) 32:275–322. doi: 10.1016/j.indag.2020.09.001

60. Sjöstrand J, Zworski M. Complex scaling and the distribution of scattering poles. *J Am Mathem Soc*. (1991) 43:4. doi: 10.2307/2939287

61. Śniady P. Random regularization of brown spectral measure. *J Functional Anal*. (2002) 193:291–313. doi: 10.1006/jfan.2001.3935

62. Tao T, Vu V. Random matrices: the circular law. *Commun Contemp Math*. (2008) 10:261–307. doi: 10.1142/S0219199708002788

63. Tao T, Vu V. Smooth analysis of the condition number and the least singular value. *Math Comp*. (2010) 79:2333–52. doi: 10.1090/S0025-5718-2010-02396-8

64. Trefethen LN. Pseudospectra of matrices. *Numer Anal*. (1992) 91:234–66.

65. Trefethen LN. Pseudospectra of linear operators. *SIAM Rev*. (1997) 39:383–406. doi: 10.1137/S0036144595295284

66. Vogel M. Almost sure Weyl law for quantized tori. *Comm Math Phys 378*. (2020) 2:1539–85. doi: 10.1007/s00220-020-03797-y

67. Watson AB, Kong T, MacDonald AH, Luskin M. Bistritzer-macdonald dynamics in twisted bilayer graphene. *J Math Phys*. (2023) 64:031502. doi: 10.1063/5.0115771

68. Weyl H. Das asymptotische verteilungsgesetz der eigenwerte linearer partieller differentialgleichungen (mit einer anwendung auf die theorie der hohlraumstrahlung). *Math Ann*. (1912) 71:441–79. doi: 10.1007/BF01456804

69. Zworski M. A remark on a paper of E.B. Davies. *Proc AMS*. (2001) 129:2955–2957. doi: 10.1090/S0002-9939-01-05909-3

70. Zworski M. *Pseudospectra of semi-classical operators*. Unpublished Leture, King's College (2001).

71. Zworski M. *Semiclassical Analysis, Graduate Studies in Mathematics 138*. New York: American Mathematical Society (2012). doi: 10.1090/gsm/138

frontiers | Frontiers in Applied Mathematics and Statistics

TYPE Perspective
PUBLISHED 07 January 2025
DOI 10.3389/fams.2024.1512865

Check for updates

OPEN ACCESS

EDITED BY
Jose Luis Jaramillo,
Université de Bourgogne, France

REVIEWED BY
Delio Mugnolo,
University of Hagen, Germany
Gustav Conradie,
University of Cambridge, United Kingdom

*CORRESPONDENCE
Catherine Drysdale
✉ c.n.d.drysdale@bham.ac.uk

RECEIVED 17 October 2024
ACCEPTED 30 November 2024
PUBLISHED 07 January 2025

CITATION
Drysdale C and Johnson S (2025) The connection between non-normality and trophic coherence in directed graphs. *Front. Appl. Math. Stat.* 10:1512865. doi: 10.3389/fams.2024.1512865

COPYRIGHT
© 2025 Drysdale and Johnson. This is an open-access article distributed under the terms of the Creative Commons Attribution License (CC BY). The use, distribution or reproduction in other forums is permitted, provided the original author(s) and the copyright owner(s) are credited and that the original publication in this journal is cited, in accordance with accepted academic practice. No use, distribution or reproduction is permitted which does not comply with these terms.

The connection between non-normality and trophic coherence in directed graphs

Catherine Drysdale[1]* and Samuel Johnson[2]

[1]Centre for Systems Modelling and Quantitative Biomedicine, University of Birmingham, Edgbaston, United Kingdom, [2]School of Mathematics, University of Birmingham, Edgbaston, United Kingdom

Trophic coherence and non-normality are both ways of describing the overall directionality of directed graphs or networks. Trophic coherence can be regarded as a measure of how neatly a graph can be divided into distinct layers, whereas non-normality is a measure of how unlike a matrix is with its transpose. We explore the relationship between trophic coherence and non-normality by first considering the connections that exist in literature and calculating the trophic coherence and non-normality for some toy networks. We then explore how persistence of an epidemic in an SIS model depends on coherence and how this relates to the non-normality. A similar effect on dynamics governed by a linear operator suggests that it may be useful to extend the concept of trophic coherence to matrices, which do not necessarily represent graphs.

KEYWORDS

directed graphs, trophic coherence, non-normality, pseudospectra, trophic levels, epidemic modeling

1 Introduction

In this perspective article, we aimed to explore the relationship between trophic coherence and non-normality, which are both qualities used to describe directed graphs. Non-normality refers to the overall asymmetry of an adjacency matrix. Trophic coherence is defined as how neatly the network can be divided into distinct layers, but it can also be interpreted as a tendency of edges to align with a global direction. These two notions come together in directed graphs. A directed graph can be represented with an $N \times N$ adjacency matrix A. If the graph is unweighted then A is binary: $A_{ij} = 1$ if there is an edge from node v_i to node v_j, else $A_{ij} = 0$. When there is an edge from v_i to v_j, we will say that v_i "sees" v_j. A weighted directed graph can be represented with a matrix whose entries are real numbers. For our purposes here, we will always assume that A is non-negative. Each node has an in-degree and an out-degree: $k_i^{in} = \sum_j A_{ji}$ and $k_i^{out} = \sum_j A_{ij}$. These are sometimes referred to as "strengths" if the directed graph is weighted.

Definition 1.1. *(Non-normality.) Given a real matrix A and its transpose A^T, we say that the matrix A is normal if $AA^T - A^TA = 0$. It is non-normal otherwise.*

Definition 1.2. *(Trophic Coherence) A directed graph is said to be maximally coherent if it is possible to assign to each node a natural number such that nodes assigned to n only see others assigned to $n + 1$. The greater the deviation from such a configuration, the more incoherent the graph.*

The need to understand non-normal matrices and operators arises in the fields of fluid dynamics [1–4], PT-symmetry [5–12], and mathematical biology [13] among other disciplines. In particular, non-normal systems are often characterized by eigenvalues that are sensitive to perturbation. It is for this non-normality is considered an asset in information transfer and communication as it can amplify small environmental changes [14, 15]. Additionally, non-normal linear operators are difficult to capture numerically as small discrepancies arising from machine precision can manifest as large perturbations in the eigenvalues. This has given rise to the study of pseudospectra; the ϵ-pseudospectrum of a matrix A is defined as the set $\{z \in \mathbb{C} : ||(A - zI)^{-1}|| < \epsilon^{-1}\}$). The definition of pseudospectra corresponds to a measure of sensitivity to perturbations of size ϵ; an equivalent definition of pseudospectra is the set $\{z \in Sp(A + B) : ||B|| \leq \epsilon\}$ [16]. Despite this being one of the most useful tools for understanding how eigenvalues respond to perturbation, it is not necessarily the best way of understanding the sensitivity of directed graphs to operators such as changing the weights of edges or edge deletion. This is equivalent to putting a structure on the matrix B, which thus breaks the correspondence between the "perturbation view of pseudospectra" and the "transient phenomena" view of pseudospectra. The latter is particularly relevant when the adjacency matrix represents a discrete dynamical system.

Ecologists define the "trophic level" of a species as the average level of its prey, plus one [17]. Trophic coherence was first proposed as a solution to May's paradox: the fact that large ecosystems are stable [18]. If the trophic difference of each edge in a graph is the difference between the trophic levels of the in- and out-neighbors, then the broader the distribution of differences (i.e., the larger the standard deviation of this distribution), the more incoherent the network. It was found that ecosystem models based on sufficiently coherent graphs became more stable, rather than less so, with increasing size. It was subsequently shown, by means of graph ensembles and numerical simulations, that trophic coherence could be related to several aspects of directed networks more generally, including the spectral radius and distribution of cycles [19]; motif profiles [20]; non-normality and strong connectivity [21, 22]; pseudospectra [23]; and various dynamical processes [24–26]. However, relying on the ecological definition of trophic levels restricted the application of trophic coherence to networks with at least one node with in-degree zero. Hence, a new measure of trophic levels was proposed that can be applied to any directed graph [27]. This is the method we use here.

In this article, we wish to emphasize the connection between trophic coherence and non-normality and to suggest that this may be relevant not only for directed graphs but for other systems described by matrices. In the first section, "Measuring Trophic Coherence and Non-normality," we take a deeper look into literature and present results that connect the two ideas. We also calculate the non-normality and trophic coherence of some toy networks in order to help the reader build an intuition. In the second section, we study an SIS model and a simple linear dynamics, both of which are affected by the coherence of an underlying matrix. We see how non-normality, strong connectivity, and the spectral radius also change with the trophic coherence. We then conclude by discussing potential further avenues of research to establish stronger bonds between these topics.

2 Measuring trophic coherence and non-normality

Definition 2.1. *The vector of trophic levels* $\mathbf{h}$ *of a directed graph with adjacency matrix* A *is the solution to the equation*

$$\Lambda \mathbf{h} = \mathbf{v}, \tag{1}$$

where

$$\Lambda = diag(\mathbf{u}) - A - A^T, \tag{2}$$

and the vectors of total degree and degree imbalance are, respectively, $\mathbf{u} = \mathbf{k}^{\mathbf{in}} + \mathbf{k}^{\mathbf{out}}$ *and* $\mathbf{v} = \mathbf{k}^{\mathbf{in}} - \mathbf{k}^{\mathbf{out}}$ *[27]. As the solution to Equation 1 is defined only up to an additive constant, the convention that* $min(h_i) = 0$ *is used (i.e., all the elements of* $\mathbf{h}$ *are positive except for the smallest value which is set to zero.)*

While Equation 1 always has a solution, which is unique given the convention stated at the end of the definition, we should note that one cannot obtain this solution by inverting Λ, as this matrix is always singular. One must therefore use some other method to find the solution, such as LU decomposition, the Moore-Penrose pseudo-inverse or an iterative method.

We can measure the trophic coherence of a directed graph with the *incoherence parameter* F, given by:

Definition 2.2. *The trophic incoherence of a directed graph with adjacency matrix* A *and trophic levels* $\mathbf{h}$ *given by Equation 1 is as follows:*

$$F = \frac{\sum_{ij} A_{ij}(h_j - h_i - 1)^2}{\sum_{ij} A_{ij}}. \tag{3}$$

The incoherence F would coincide with the square of the parameter q proposed by Johnson et al. [18] if trophic levels were calculated as in ecology ($F = q^2$) [18]. Using the trophic levels given by Equation 1, F is bounded between zero and one: $F = 0$ implies a perfectly coherent directed graph in which vertices fit into integer trophic levels; and $F = 1$ corresponds to maximum incoherence, which occurs if and only if the directed graph is balanced ($\mathbf{v} = \mathbf{0}$) [27].

Definitions 2.1 and 2.2 were originally derived by first writing down (Equation 3) for generic levels, and then finding the solution $\mathbf{h}$ that minimized F—which leads to Equation 1. In other words, the trophic levels, under this definition, are those which minimize the trophic incoherence.

The average trophic difference is $z = 1 - F$, so one interpretation of trophic coherence is as the "directedness" of the graph, and z can be referred to as the trophic coherence [27]. Another interpretation is given by SpringRank [28], which likens each edge to a spring with natural length $l = 1$. F is then the energy, which is minimized at the solution $\mathbf{h}$. However, another interpretation of the same equation is Helmholtz-Hodge

decomposition, whereby a vector field can be decomposed into a gradient part and a zero divergence part [29]. When applied to graphs, F is then its "circularity." The fact the same equation has appeared independently at least three times testifies to its wide applicability [27]. We note also that if the "-1" in Equation 3 were replaced with a constant "$-a$," this would simply multiply the trophic levels by a: $\mathbf{h}' = a\mathbf{h}$. Hence, $a = 1$ is a natural choice that does not reduce generality.

Λ is twice the Laplacian of the undirected version of the graph $(A + A^T)/2$, which can be considered an undirected graph as all edges now have an opposite edge of the same weight. In particular, an interpretation is that $\Lambda\mathbf{h} = \mathbf{v}$ is the corresponding inhomogenous equation to the homogenous equation $(L(A) + L(A^T))\mathbf{x} = 0$. The multiplicity of the eigenvalue 0 corresponds to the number of connected components in the undirected case, hence can be seen as when we "force" $(L(A) + L(A^T))\mathbf{x} = 0$, by unbalancing the in and out degrees on each node.

Whereas the trophic coherence can be captured by a single number, it is not so easy to have a single number which captures non-normality. Various measures have been proposed to quantify the non-normality of matrices, the most obvious being $||AA^T - A^TA||$ for some suitable norm (here and in the paper we use the Frobenius norm). Another method is Henrici's deviation from normality: $Hen(A) = \sqrt{||A||_F^2 - \sum_{i=1}^n |\lambda_i|^2}$, where $||\cdot||_F$ is the Frobenius norm and $\{\lambda_i\}$ are the eigenvalues of A. This can be normalized by dividing through by the $||A||_F^2$ giving the parameter

$$d_F = \sqrt{1-\nu}, \qquad \text{where} \qquad \nu = \frac{\sum_{i=1}^n |\lambda_i|^2}{||A||_F^2} \tag{4}$$

is known as the "normality" [27]. Note that a directed graph with normal adjacency matrix A would have $\sum_{j=1}^N |\lambda_j|^2 = ||A||_F^2$ and hence $\nu = 1$ ($d_F = 0$), but a "very non-normal" network would have $|\lambda_j| = 0$ for all j and in this case $\nu = 0$ ($d_F = 1$). However, we stress that the idea of "very non-normal" is also subjective with respect to which measure. The norm $||AA^T - A^TA||$ can be considered more sensitive to structural features such as skewness or asymmetry, whereas Henrici's measure aggregates deviations related to eigenvalue magnitudes, potentially smoothing out localized anomalies. In particular, for matrices close to being symmetric, but not normal, the two measures might diverge significantly. The measure $||AA^T - A^TA||$ could show a large deviation, while Henrici's measure may remain small if the eigenvalues are unaffected.

In Table 1, we compute the trophic coherence and non-normality measures for two graphs (the loop on five vertices and the so-called vortex graph on five vertices). We consider these measures for both the adjacency matrix and the non-symmetric Laplacian $L(A)$. We also add an edge to the cycle and delete an edge. We see that trophic coherence increases (trophic incoherence F decreases) in both settings. In addition, we can relate back to our previous discussion regarding pseudospectra. where deletion and addition of an edge can be considered a norm of the same size; hence, a more nuanced approach is needed. In addition, we have that the two measures of non-normality behave differently as the Henrici norm perceives the graph with edge deletion as more non-normal regarding the adjacency matrix and the Laplacian, whereas the converse is true for the other measure. Further analysis is needed to establish if there is a physical meaning to this in certain scenarios, i.e., the graph represents a dynamical system. Although, in both cases, the orientation of each edge can be reversed resulting in the same graph, the fact that flow is not conserved on the "loop under edge addition" may make this graph more asymmetric. Further study must be done in this direction to establish this.

Asllani et al. [30] have recently studied the effects of non-normality in directed graphs, where it was shown that d_F correlates strongly with a measure of structural asymmetry. Furthermore, the structures of graphs with different degree distributions were calculated. The approach of the Henrici norm has also been used recently in work looking at non-normality in the context of trophic coherence [21, 27].

It is possible to estimate the expected value of various magnitudes given that a network has a specified trophic coherence, by means of graph ensembles [19, 21, 27]. The "coherence ensemble" is the set of all possible directed graphs with a given degree sequence and trophic coherence. Thus, the expected value of the spectral radius is as follows:

$$\overline{\rho} = e^{\tau}, \qquad \text{where} \qquad \tau = \ln\alpha + \frac{L_B}{2(L-L_B)} - \frac{1-F}{2F}, \tag{5}$$

and the bar denotes expectation [19]. L is the number of edges, L_B is the number of edges connected to the source or sink nodes (those with no incoming or outgoing edges), and the "branching factor" is $\alpha = \langle k^{in}k^{out}\rangle/\langle k\rangle$ where the brackets are averages over vertices. τ is referred to as the "loop exponent." Because τ is positive for $F \simeq 1$ but becomes negative when $F \simeq 0$, directed graphs fall into one of two regimes, referred to as "loopful" ($\tau > 0$) and "loopless" ($\tau < 0$) [19]. In the former the number of circuits of length l increases exponentially with l, whereas in the latter they decay exponentially. This can have a crucial bearing on many other topological and dynamical features of complex systems, as we illustrate below with the example of an SIS model: an epidemic perdures indefinitely when $\tau > 0$ but quickly goes extinct when $\tau < 0$.

This approach has been used to show that the expected non-normality is bounded, $\overline{d_F} \geq \sqrt{1 - e^{2\tau}/\langle k\rangle}$ [21], and approximated by $\overline{d_F} \simeq \sqrt{1 - \exp(1 - 1/F)}$ [27]. Hence, trophically coherent graphs ($F \to 0$ or $\tau \to -\infty$) are non-normal ($d_F \to 1$). The fact that the expected value of the non-normality is bounded below by the expected spectral radius [21] is natural when considering the transient wave-packet phenomena that can happen with non-normal matrices [16].

3 Spreading processes with graphs and operators

It is known that the trophic coherence of directed graphs can exert an important influence on the dynamics of various complex systems [21]. Similarly, in dynamical systems governed by linear operators, the non-normality thereof will fundamentally affect system behavior [16]. We go on to show, using two simple examples of spreading processes, that there are close similarities between these two kinds of phenomena. First we look at the SIS model on coherent directed graphs and then we compare this to the action of a non-normal linear operator. These examples also show that

TABLE 1 Comparison of various properties for different types of networks (vortex graph on five vertices, loop on five vertices, loop under edge addition, loop under edge deletion).

Property	Vortex graph on five vertices V_5	Loop on five vertices P_5	Loop under edge deletion (chain)	Loop under edge addition
	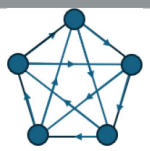	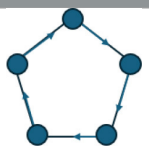	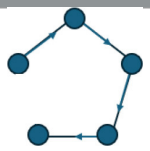	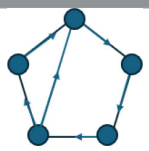
Adjacency Matrix	$\begin{pmatrix} 0&1&1&0&0\\ 0&0&1&1&0\\ 0&0&0&1&1\\ 1&0&0&0&1\\ 1&1&0&0&0 \end{pmatrix}$	$\begin{pmatrix} 0&1&0&0&0\\ 0&0&1&0&0\\ 0&0&0&1&0\\ 0&0&0&0&1\\ 1&0&0&0&0 \end{pmatrix}$	$\begin{pmatrix} 0&1&0&0&0\\ 0&0&1&0&0\\ 0&0&0&1&0\\ 0&0&0&0&1\\ 0&0&0&0&0 \end{pmatrix}$	$\begin{pmatrix} 0&1&0&0&0\\ 0&0&1&0&0\\ 0&0&0&1&0\\ 0&0&0&0&1\\ 1&1&0&0&0 \end{pmatrix}$
Laplacian ($L = D^{out} - A$)	$\begin{pmatrix} 2&-1&-1&0&0\\ 0&2&-1&-1&0\\ 0&0&2&-1&-1\\ -1&0&0&2&-1\\ -1&-1&0&0&2 \end{pmatrix}$	$\begin{pmatrix} 1&-1&0&0&0\\ 0&1&-1&0&0\\ 0&0&1&-1&0\\ 0&0&0&1&-1\\ -1&0&0&0&1 \end{pmatrix}$	$\begin{pmatrix} 1&-1&0&0&0\\ 0&1&-1&0&0\\ 0&0&1&-1&0\\ 0&0&0&1&-1\\ 0&0&0&0&0 \end{pmatrix}$	$\begin{pmatrix} 1&-1&0&0&0\\ 0&1&-1&0&0\\ 0&0&1&-1&0\\ 0&0&0&1&-1\\ -1&-1&0&0&2 \end{pmatrix}$
Trophic incoherence (F)	1	1	0	0.91
Trophic levels	(0,0,0,0,0)	(0,0,0,0,0)	(0,1,2,3,4)	(0,0.18, 0.27, 0.36, 0.54)
Adjacency non-normality $\|\|A^TA - AA^T\|\|$	0	0	1.41	2.44
Laplacian non-normality $\|\|L^TL - LL^T\|\|$	0	0	2	4
Adjacency non-normality (Henrici)	0	0	1	0.37
Laplacian non-normality (Henrici)	0	0	0.71	0.38

the methods which have been proposed to generate directed graphs with tunable trophic coherence might also be useful for studying other matrices numerically [24, 31].

The SIS (susceptible-infectious-susceptible) model is perhaps the simplest which can be used to study the spread through a population of an infectious disease—typically one which confers little or no immunity [32]. We will use this paradigm to demonstrate the influence of trophic coherence or non-normality on even the simplest of dynamical processes.

Consider an unweighted, directed network given by the $N \times N$ adjacency matrix A. To each node i is associated with a dynamical variable $s_i(t)$ which can take, at each discrete time t, either the value 0 or 1, representing susceptible or infectious states, respectively. Let $g_i(t) = \sum_j A_{ji} s_j(t)$. The system then evolves according to:

$$s_i(t+1) = 1 \qquad \text{if } s_i(t) = 0 \text{ and } g_i(t) > 0, \text{or} \tag{6}$$

$$s_i(t+1) = 0 \qquad \text{otherwise,} \tag{7}$$

with all nodes updated in parallel. In other words, a susceptible node becomes infectious for one time step if at least one of its in-neighbors is infectious.

Will an epidemic die out naturally or go on indefinitely? We study this by beginning with all nodes being susceptible except for %5 which are chosen at random to be made infectious. We generate networks using the generalized preferential preying model [24]. This model has a parameter, T, which allows one to set the trophic coherence of the network: $T = 0$ produces maximally coherent structures, and incoherence increases with positive T.

Not that in this scheme the only randomness is in the generation of the network and the choice of initial conditions; the dynamics thereafter are deterministic. Figure 1 top left shows the stationary proportion of nodes which remain infectious indefinitely against T. At low values of T the epidemic dies out, but for higher values, there is a continuous transition to a regime in which a significant proportion of the nodes remain infectious. This can be understood by considering that the epidemic requires a strongly connected component of nodes to sustain itself, which only exists in sufficiently incoherent networks [22]. Or, more formally, it is known that the critical rate of infection required for an epidemic to survive is lower bounded by the inverse of the spectral radius of the adjacency matrix [33], which depends on trophic coherence [19].

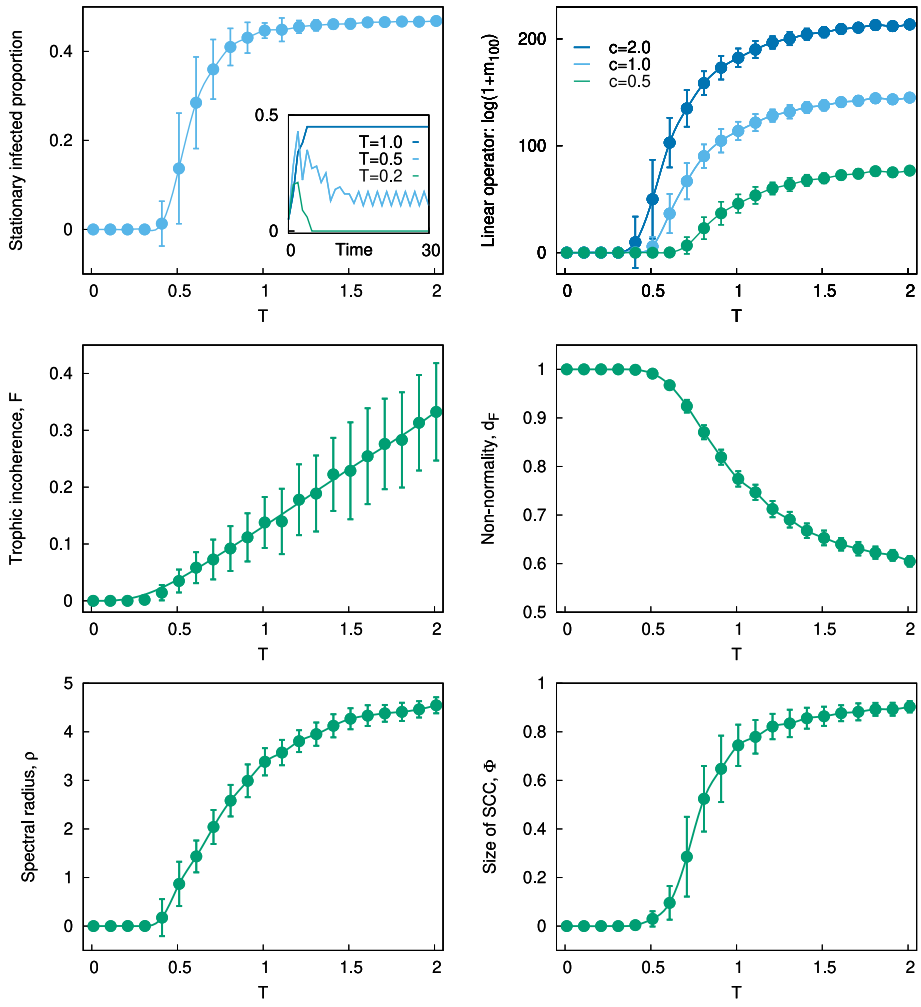

FIGURE 1
Top left: Stationary proportion of infected nodes against parameter T for networks generated with the generalized preferential preying model [24]. Number of nodes and edges: $N = 100$ and $L = 500$. Averages over 100 networks; error bars are standard deviations. Stationary values computed as the average from $t = 90$ to $t = 100$. Inset: Time series of the proportion of infected nodes for three networks, generated with $T = 1$, 0.5, and 0.2. **Top right:** Mean activity $m(t)$ at $t = 100$ according to Equations 8, 9, where A is the adjacency matrix of the networks used in the top left panel. Initially, all elements have $x(0) = 0$, except for a randomly chosen 5% which are set to $x(0) = 1$. The extent of activity is measured as $\ln[1 + m(100)]$, for $c = 0.5$, 1, and 2. **Middle left:** Trophic incoherence F against T for the same directed graphs as in the panels above. **Middle right:** Non-normality d_F against T for the same directed graphs. **Bottom left:** Spectral radius ρ against T for the same directed graphs. **Bottom right:** Size of the strongly connected component Φ against T for the same directed graphs.

As we have seen, non-normality also varies with trophic coherence. Hence, in the inset we see a "bump" in the time series for lower values of T (which produces small F and high d_F), which corresponds to transient phenomena. In a future study, we will consider the average difference between the pseudospectral abscissa and the spectral radius at early times to establish transient phenomena [16]. In our SIS model computations, we see that as trophic coherence increases, the size of the strongly-connected component increases. Unlike in undirected graphs, the multiplicity of the $\lambda = 0$ eigenvalue of the Laplacian $L(A)$ does not equal the number of components, but rather the number of reaches [34] (a reach is the maximal unilaterally connected set). Whereas dynamical processes such as these have been related to the existence and size of strongly connected components, we have yet to investigate the effect of different reach structures.

Consider now the following dynamical system with N elements. Every element i is characterized by a continuous dynamical variable $x_i(t)$ at discrete time t. The system evolves according to

$$\mathbf{x}(t+1) = cA\mathbf{x}(t), \tag{8}$$

where c is a constant parameter and A is a non-negative, $N \times N$ real matrix. We might consider A as a linear operator or as a directed graph on which the process is taking place. In particular, we can take A to be infinite dimensional in which case we could be giving a graphical interpretation to such linear operators. We begin with a small number of randomly chosen agents in state $x(0) = 1$ and all others $x(0) = 0$, and track the average value of the activity,

$$m(t) = \frac{1}{N}\sum_{i=1}^{N} x_i(t). \tag{9}$$

This will either decay to zero or diverge according to the spectral radius of A and the parameter c, as shown in Figure 1 top right. However, for significantly non-normal networks (low T) there may be transient behavior that eventually dies out, as in the SIS case on a trophically coherent graph. This might correspond to an epidemic, rumor or other spreading process, which reaches most of the system but goes on to disappear, whereas in the more normal or incoherent case, even a process that only reaches some of the system might continue to fuel itself indefinitely thanks to feedback.

Figure 1 middle left, middle right shows how the trophic incoherence F and the non-normality d_F also vary in this network model with the parameter T. A comparison with Figure 1 top left reveals that some nodes begin to sustain the epidemic once $F > 0$ or $d_F < 1$; and a similar effect is evident in the linear operator case (Figure 1 top right). Figure 1 bottom left, bottom right shows how the two topological features we can relate to both the SIS dynamic and the linear operator – namely, the spectral radius ρ and the size of the strongly connected component Φ— undergo a similar transition with increasing T as the stationary proportion of infected nodes or the logarithm of $m(t)$. Just as degree heterogeneity can drastically reduce the size of epidemic waves [35], trophic coherence can affect their extinction. Moreover, whereas trophic coherence has to date been thought of only as a property of directed graphs, this example suggests that it can be studied in the case of operators and square matrices more broadly.

4 Discussion

In this article, we have discussed the relationship between trophic coherence and non-normality. We have mentioned some existing connections in the literature and studied some small graphs for illustration. We have also presented numerical experiments in the form of an SIS model and a linear dynamics, which show how trophic coherence and non-normality are related and have significant effects on dynamical systems governed by matrices.

There are many relationships still to be discovered, particularly regarding the connection between non-normality and trophic coherence in matrices in general. Also of interest is the relationship with strongly connected components, and how edge deletion and edge addition may be considered in a way that is amenable to the calculation of pseudospectra. In future work, we aim to explore which kind of edge perturbations can create the largest change in non-normality, trophic coherence, or even other measures such as algebraic connectivity (which is non-trivial to compute in a directed graph and is so far yet to profit from the advances in the computations of non-self-adjoint problems). By studying how such edge perturbations change the non-normality, trophic coherence, and algebraic connectivity, we may improve our understanding of how such magnitudes are related and their effects on dynamical systems. This is the subject of upcoming study.

Data availability statement

The original contributions presented in the study are included in the article/supplementary material, further inquiries can be directed to the corresponding author.

Author contributions

CD: Conceptualization, Data curation, Formal analysis, Investigation, Methodology, Project administration, Validation, Visualization, Writing – original draft, Writing – review & editing. SJ: Conceptualization, Data curation, Formal analysis, Investigation, Methodology, Validation, Writing – original draft, Writing – review & editing.

Funding

The author(s) declare financial support was received for the research, authorship, and/or publication of this article. This work was funded by a Seedcorn grant from the N-CODE Network and the Centre for Systems Modelling and Quantitative Biomedicine, University of Birmingham.

Acknowledgments

The authors would like to thank Vagabond in Birmingham and Black Sheep Coffee for providing wine and Lion's mane lattes, respectively.

Conflict of interest

The authors declare that the research was conducted in the absence of any commercial or financial relationships that could be construed as a potential conflict of interest.

Publisher's note

All claims expressed in this article are solely those of the authors and do not necessarily represent those of their affiliated organizations, or those of the publisher, the editors and the reviewers. Any product that may be evaluated in this article, or claim that may be made by its manufacturer, is not guaranteed or endorsed by the publisher.

References

1. Cossu C, Chomaz JM. Global measures of local convective instabilities. *Phys Rev Lett*. (1997) 78:4387. doi: 10.1103/PhysRevLett.78.4387

2. Chomaz JM. Global instabilities in spatially developing flows: non-normality and nonlinearity. *Annu Rev Fluid Mech*. (2005) 37:357–92. doi: 10.1146/annurev.fluid.37.061903.175810

3. Sujith R, Juniper M, Schmid P. Non-normality and nonlinearity in thermoacoustic instabilities. *Int J Spray Combust Dyn*. (2016) 8:119–46. doi: 10.1177/1756827716651571

4. Schmid PJ, Henningson DS, Jankowski D. Stability and transition in shear flows. Applied mathematical sciences, vol 142. *Appl Mech Rev*. (2002) 55:B57–9. doi: 10.1115/1.1470687

5. Bender CM, Brody DC, Jones HF. Complex extension of quantum mechanics. *Phys Rev Lett*. (2002) 89:270401. doi: 10.1103/PhysRevLett.89.270401

6. Bender CM. Making sense of non-Hermitian Hamiltonians. *Rep Prog Phys*. (2007) 70:947–1018. doi: 10.1088/0034-4885/70/6/R03

7. Bender CM, Boettcher S. Real spectra in non-Hermitian Hamiltonians having PT symmetry. *Phys Rev Lett*. (1998) 80:5243–6. doi: 10.1103/PhysRevLett.80.5243

8. Bender CM, Brody DC, Jones HF. Must a Hamiltonian be Hermitian? *Am J Phys*. (2003) 71:1095–102. doi: 10.1119/1.1574043

9. Bender CM, Meisinger PN, Wang Q. Calculation of the hidden symmetry operator in PT-symmetric quantum mechanics. *J Phys A Math Gen*. (2003) 36:1973–83. doi: 10.1088/0305-4470/36/7/312

10. Mostafazadeh A. Metric operator in pseudo-Hermitian quantum mechanics and the imaginary cubic potential. *J Phys A Math Gen*. (2006) 39:10171–88. doi: 10.1088/0305-4470/39/32/S18

11. Siegl P, Krejčiřík D. On the metric operator for the imaginary cubic oscillator. *Phys Rev D*. (2012) 86:121702. doi: 10.1103/PhysRevD.86.121702

12. Davies EB. Wild spectral behaviour of anharmonic oscillators. *Bull Lond Math Soc*. (2000) 32:432–8. doi: 10.1112/S0024609300007050

13. Drysdale C, Colbrook MJ. A novel use of pseudospectra in mathematical biology: understanding HPA axis sensitivity. *arXiv preprint arXiv:240800845*. (2024).

14. Baggio G, Zampieri S. Non-normality improves information transmission performance of network systems. *IEEE Trans Control Netw Syst*. (2021) 8:1846–58. doi: 10.1109/TCNS.2021.3088795

15. Baggio G, Rutten V, Hennequin G, Zampieri S. Efficient communication over complex dynamical networks: the role of matrix non-normality. *Sci Adv*. (2020) 6:eaba2282. doi: 10.1126/sciadv.aba2282

16. Trefethen LN, Embree M. *Spectra and Pseudospectra: The Behavior of Nonnormal Matrices and Operators*. Princeton: Princeton University Press. (2005). doi: 10.1515/9780691213101

17. Levine S. Several measures of trophic structure applicable to complex food webs. *J Theor Biol*. (1980) 83:195–207. doi: 10.1016/0022-5193(80)90288-X

18. Johnson S, Domínguez-García V, Donetti L, Muñoz MA. Trophic coherence determines food-web stability. *Proc Natl Acad Sci*. (2014) 111:17923–8. doi: 10.1073/pnas.1409077111

19. Johnson S, Jones NS. Looplessness in networks is linked to trophic coherence. *Proc Natl Acad Sci USA*. (2017) 114:5618–23. doi: 10.1073/pnas.1613786114

20. Klaise J, Johnson S. The origin of motif families in food webs. *Sci Rep*. (2017) 7:16197. doi: 10.1038/s41598-017-15496-1

21. Johnson S. Digraphs are different: Why directionality matters in complex systems. *J Phys*. (2020) 1:015003. doi: 10.1088/2632-072X/ab8e2f

22. Rodgers N, Tiňo P, Johnson S. Strong connectivity in real directed networks. *Proc Natl Acad Sci*. (2023) 120:e2215752120. doi: 10.1073/pnas.2215752120

23. Rodgers N, Tiňo P, Johnson S. Influence and influenceability: global directionality in directed complex networks. *R Soc Open Sci*. (2023) 10:221380. doi: 10.1098/rsos.221380

24. Klaise J, Johnson S. From neurons to epidemics: How trophic coherence affects spreading processes. *Chaos*. (2016) 26:065310. doi: 10.1063/1.4953160

25. Pilgrim C, Guo W, Johnson S. Organisational social influence on directed hierarchical graphs, from tyranny to anarchy. *Sci Rep*. (2020) 10:1–13. doi: 10.1038/s41598-020-61196-8

26. Rodgers N, Tiňo P, Johnson S. Network hierarchy and pattern recovery in directed sparse Hopfield networks. *Phys Rev E*. (2022) 105:064304. doi: 10.1103/PhysRevE.105.064304

27. MacKay RS, Johnson S, Sansom B. How directed is a directed network? *R Soc Open Sci*. (2020) 7:201138. doi: 10.1098/rsos.201138

28. De Bacco C, Larremore DB, Moore C. A physical model for efficient ranking in networks. *Sci Adv*. (2018) 4:eaar8260. doi: 10.1126/sciadv.aar8260

29. Kichikawa Y, Iyetomi H, Iino T, Inoue H. Community structure based on circular flow in a large-scale transaction network. *Appl Netw Sci*. (2019) 4:1–23. doi: 10.1007/s41109-019-0202-8

30. Asllani M, Lambiotte R, Carletti T. Structure and dynamical behavior of non-normal networks. *Sci Adv*. (2018) 4:eaau9403. doi: 10.1126/sciadv.aau9403

31. Rodgers N, Tiňo P, Johnson S. Fitness-based growth of directed networks with hierarchy. *J Phys*. (2024) 5:035013. doi: 10.1088/2632-072X/ad744e

32. Hethcote HW. Three basic epidemiological models. In: *Applied Mathematical Ecology*. Springer (1989). p. 119–144. doi: 10.1007/978-3-642-61317-3_5

33. Van Mieghem P, Van de Bovenkamp R. Non-Markovian infection spread dramatically alters the susceptible-infected-susceptible epidemic threshold in networks. *Phys Rev Lett*. (2013) 110:108701. doi: 10.1103/PhysRevLett.110.108701

34. Veerman J, Lyons R, A. primer on Laplacian dynamics in directed graphs. *Nonlinear Phenom Compl Syst*. (2020) 23:196–206. doi: 10.33581/1561-4085-2020-23-2-196-206

35. Johnson S. Epidemic modelling requires knowledge of the social network. *J Phys*. (2024) 5:01LT01. doi: 10.1088/2632-072X/ad19e0

frontiers | Frontiers in Physics

TYPE Brief Research Report
PUBLISHED 07 January 2025
DOI 10.3389/fphy.2024.1511757

Check for updates

OPEN ACCESS

EDITED BY
Piotr Bizon,
Jagiellonian University, Poland

REVIEWED BY
Izzet Sakalli,
Eastern Mediterranean University, Türkiye
José Luis Díaz,
Universidad a Distancia de Madrid, Spain

*CORRESPONDENCE
Valentin Boyanov,
valentinboyanov@tecnico.ulisboa.pt

RECEIVED 15 October 2024
ACCEPTED 10 December 2024
PUBLISHED 07 January 2025

CITATION
Boyanov V (2025) On destabilising quasi-normal modes with a radially concentrated perturbation.
Front. Phys. 12:1511757.
doi: 10.3389/fphy.2024.1511757

COPYRIGHT
© 2025 Boyanov. This is an open-access article distributed under the terms of the Creative Commons Attribution License (CC BY). The use, distribution or reproduction in other forums is permitted, provided the original author(s) and the copyright owner(s) are credited and that the original publication in this journal is cited, in accordance with accepted academic practice. No use, distribution or reproduction is permitted which does not comply with these terms.

On destabilising quasi-normal modes with a radially concentrated perturbation

Valentin Boyanov*

CENTRA, Departamento de Física, Instituto Superior Técnico – IST, Universidade de Lisboa – UL, Lisboa, Portugal

In this work we explore some aspects of the spectral instability of back hole quasi-normal modes, using a specific model as an example. The model is that of a small bump perturbation to the effective potential of linear axial gravitational waves on a Schwarzschild background, and our focus is on three different aspects of the instability: identifying and distinguishing between the two different types of instabilities studied previously in the literature, quantifying the size of the perturbations applied to the system and testing the validity of the pseudospectral numerical method in providing a convergent result for this measure, and finally, relating the size and other features of the perturbation to the degree of destabilisation of the spectrum.

KEYWORDS

black hole, quasinormal modes, pseudospectrum, energy norm, spectral stability

1 Introduction

The quasi-normal modes (QNMs) of black holes (BHs) have been shown to suffer from a spectral instability, which shifts these characteristic frequencies by disproportionately large distances in the complex plane when the system is subjected to seemingly small environmental perturbations. This has been shown through calculations of the QNM spectrum after a variety of generic perturbations are added to the system [1–16], and quantitatively explored through the full pseudospectrum of the linear perturbation problem [1, 3, 8–13, 17, 18], generally in a physically motivated norm [19]. On the other hand, a seemingly qualitatively different instability has been observed when the perturbation involved is specifically the addition of a single small "bump" to the effective potential of the propagating waves at different distances from the black hole horizon, intended to mimic some radially concentrated distribution of matter [20–22], or, more generally, the addition of a second length scale in the problem [22, 23]. The former of these approaches stands out through its consistent attempt to precisely quantify the magnitude of the perturbations applied to the system, and thus the amount by which the QNM migration exceeds the threshold of stability. The latter approach, on the other hand, has found a rich phenomenology which includes the appearance of new branches of QNMs which can contain modes with a longer lifetime than the BH fundamental mode, akin to the "shape resonances" discussed in, e.g., [24, 25].

However, in spite of the varied nature of these results, the endeavour to obtain a complete physical picture of this instability has not yet come to fruition. On the one hand, not all results have been put in the context of the quantitative scheme devised in [1] involving the energy norm. On the other hand, this scheme itself may not be the most adequate for precise quantitative conclusions. As discussed already in [1], two perturbations of the same energy norm can have vastly different destabilisation effects depending on their high-wave-number

content (i.e., on the magnitude of derivatives in r of the perturbation function). Additionally, as shown in [13] for one particular model, some of the numerically computed quantities involved in pseudospectrum calculations may not be well behaved in the continuum limit.

The present work is intended as a short review of the subject, particularly highlighting some of the above mentioned issues, using a specific example to further clarify them and progress towards their resolution. The example system chosen is that of axial gravitational perturbations on a Schwarzschild BH, with a gaussian bump added to the effective potential of their governing wave equation, akin to the one used in [20].

Section 2 provides a brief overview of the QNM instability and the tools used to capture and quantify it. Section 3 uses the gaussian bump setup for: 3.1 providing a simple example of the instability, 3.2 bringing the results of the analysis in [20] to the context of the energy norm, quantifying the "smallness" of the bumps added to the potential, as well as discussing the emergence of new mode branches due to a qualitative change in the phase space of the evolution operator [24, 25] (see in particular footnote nine of [26] and footnote 13 of [19]), 3.3 exploring the dependence of the degree of destabilisation on the "high-wave-number" content [1], or sharpness, of the added bump, as well as presenting an analysis regarding the numerical convergence of the results. Finally, Section 4 presents a summary of the conclusions which can be drawn from this analysis and used as guidance for future work in this field.

2 Linear perturbations and norm

The background spacetime we will work with is the Schwarzschild geometry,

$$ds^2 = -f(r)\,dt^2 + \frac{1}{f(r)}dr^2 + r^2 d\Omega^2,$$

where the redshift function reads $f(r) = 1 - 2M/r$, and $d\Omega^2$ is the line element of the unit sphere. The maximal extension of this spacetime has a bifurcate Killing horizon at $r = 2M$, though for QNMs the important part is the outgoing horizon which in the future is equivalent to the event horizon of a dynamically formed (non-evaporating) black hole.

The dynamics of linear perturbations around this background is given by a wave equation,

$$-\partial_t^2\phi + \partial_{r^*}^2\phi - V(r)\,\phi = 0,$$

where r^* is the tortoise coordinate, $dr^* = dr/f(r)$, and the potential V depends on the nature of the perturbation and on its angular multipole number ℓ. In the example below we will analyse the case of axial gravitational perturbations,

$$V = \frac{f}{r^2}\left[\ell(\ell+1) - \frac{6M}{r}\right].$$

Quasi-normal modes are a discrete set of analytic solutions to (2) which behave as ingoing waves,

$$\phi \sim e^{i\omega(t+r^*)}$$

at the horizon, and as outgoing waves,

$$\phi \sim e^{i\omega(t-r^*)}$$

at infinity. These conditions can be imposed geometrically in the wave equation by expressing it in a hyperboloidal coordinate system [27, 28], with the transformation $\{t, r^*\} \to \{\tau, \chi\}$ given by

$$\frac{t}{2M} = \tau - h(\chi),$$
$$\frac{r^*}{2M} = g(\chi),$$

where $h(\chi) \sim g(\chi)$ when approaching the horizon, and $h(\chi) \sim -g(\chi)$ when approaching infinity. A standard choice is the so-called minimal gauge [29], which for the Schwarzschild case is given by

$$h(\chi) = \log(1-\chi) - \frac{1}{\chi} - \log\chi,$$
$$g(\chi) = \log(1-\chi) + \frac{1}{\chi} + \log\chi.$$

The compactified radial coordinate $\chi = 2M/r$ spans the range $\chi \in (0, 1)$ between (future null) infinity and the (future) horizon. The QNM boundary conditions now amount to simply requiring regularity of the solutions at the boundaries.

Following ref. [1], we perform this coordinate transformation along with an order reduction in time through the introduction of the auxiliary variable $\psi = \partial_\tau\phi$, recasting the problem in the form

$$iL \quad u = \partial_\tau u,$$

where

$$u = \begin{pmatrix}\phi\\ \psi\end{pmatrix}, \qquad L = \frac{1}{i}\begin{pmatrix}0 & \mathbb{I}\\ L_1 & L_2\end{pmatrix},$$

with

$$L_1 = \frac{p}{w}\partial_\chi^2 + \frac{p'}{w}\partial_\chi - \frac{q}{w},$$
$$L_2 = 2\frac{\gamma}{w}\partial_\chi + \frac{\gamma'}{w},$$

and we have defined the functions

$$w = \frac{|g'|}{g'^2 - h'^2}, \quad p = \frac{1}{|g'|}, \quad \gamma = \frac{h'}{|g'|}, \quad q = |g'|V,$$

a prime denoting differentiation with respect to χ. The QNM frequency spectrum can be defined [30, 31] as the eigenvalues of the evolution operator L, or equivalently as the poles of the resolvent operator

$$R_L(\lambda) = (L - \lambda\mathbb{I})^{-1}.$$

Since L is non-self-adjoint (due to the dissipative boundaries of the problem), solutions to the wave equation cannot be expressed simply as convergent series of the eigenvalues, i.e., of QNMs. Additionally, and crucially, the QNM frequencies can be unstable to "small" perturbations of the system. Perturbations can come in many shapes and sizes, and the effect they can have on the spectrum is just as varied. The instability originally studied in ref. [1] consists in the displacement of modes in the complex plane by distances much

larger than the size (energy norm) of the perturbations would allow for a spectrally stable operator.

However, one interesting conclusion in ref. [1] is the apparent stability of the fundamental mode, and the absence of any displaced overtones which would have a slower decay rate (smaller imaginary part) than this fundamental one after a perturbation. In contrast to this result, ref. [20] found that perturbing the effective potential with a seemingly very small bump placed sufficiently far from the horizon can easily destabilise the fundamental mode, leaving a mode with a much smaller imaginary part as the new fundamental one. The apparent contradiction between these conclusions is mainly due to a qualitative difference in the type of perturbations and instability considered. We will now present a summary of some aspects of these two analyses, and highlight the differences between them. Then, in the following section, we will proceed to analyse an example, originally treated in ref. [20], which turns out to lead to a combination of both destabilising effects.

2.1 Mode displacement and pseudospectrum

The case of QNM instability analysed in [1] and related works is one in which (at least part of) the already existing BH QNM spectrum is displaced by a disproportionately large amount due to a small perturbation to the operator L. The smallness of this perturbation is defined quantitatively through the energy norm [19], which has a natural physical interpretation. The overall instability to *any* perturbation of L is captured by the pseudospectrum in this norm, which is defined as

$$\sigma^{\epsilon}(L) = \{\lambda \in \mathbb{C} : \|R_L(\lambda)\|_E > 1/\epsilon\},$$

where $\|\cdot\|_E$ indicates the energy norm of the operator, defined from the product

$$\begin{aligned}\langle u_1, u_2\rangle_E &= \left\langle \begin{pmatrix}\phi_1\\ \psi_1\end{pmatrix}, \begin{pmatrix}\phi_2\\ \psi_2\end{pmatrix} \right\rangle_E \\ &= \frac{1}{2}\int_0^1 \left(w(\chi)\,\bar{\psi}_1\psi_2 + p(\chi)\,\partial_\chi\bar{\phi}_1\partial_\chi\phi_2 + q(\chi)\,\bar{\phi}_1\phi_2 \right) d\chi,\end{aligned}$$

An equivalent definition is the one which directly relates the level sets of the pseudospectrum to the space of possible new eigenvalue positions after a perturbation,

$$\sigma^{\epsilon}(L) = \{\lambda \in \mathbb{C}, \exists \delta L, \|\delta L\| < \epsilon : \lambda \in \sigma(L + \delta L)\}. \tag{1}$$

Note that this second definition involves any perturbation to L which has a small energy norm, including ones which can potentially be related to a physical modification of the environment of the black hole, but also ones which completely change the nature of the operator (e.g., changing the structure of the derivatives). That said, it was shown in [1] that the instability is in fact triggered by *physical* perturbations, encoded in the addition of a perturbation function δV to the effective potential, without disturbing the structure of the differential part of the operator. Additionally, it was shown that the degree to which the spectrum is destabilised depends strongly on the "high wave-number" content of the perturbation, that is, the sharpness of the variation of δV in r.

While the particular choices for the perturbations δV used in ref. [1] may not correspond to the addition of classically reasonable matter content to the system [22], they are a proof of principle which shows that whatever the perturbation may be, as long as it has a large enough gradient in r, it will trigger the instability. Ref. [10] in fact explicitly shows the relation between the magnitude of the derivatives of δV and the rate of displacement of the QNMs in a specific example, further solidifying this result.

The above-mentioned stability of the fundamental mode was also one of the key results, which can directly be related to the fact that gravitational wave observations of compact object collisions which result in a black hole as an end state appear to contain a part which matches well with a fundamental-mode-dominated ringdown [32].

2.2 Emergence of new long-lived modes

The second type of "instability" is due to the emergence of new mode branches. It is important to understand that the characteristics of the spectrum depend strongly on the shape of the potential V. For the axial gravitational case, the potential has a single barrier with a peak close to the photon sphere, from which it decreases to zero exponentially (in r^*) towards the horizon and polynomially towards infinity. The corresponding "barrier top" modes are not very long-lived (in terms of the characteristic scale of the problem). However, seemingly small perturbations can lead to a qualitative change in the shape of the potential, such as the addition of a well which goes below the asymptotic values, or of a second barrier (or bump). The former can lead to the presence of bound states, while the latter to slowly decaying "shape resonances" [25].

Some examples of such qualitative modifications to the potential in the context of QNMs are the double barrier model in [33], or some of the models explored in [22], such as the addition of a perturbatively small mass parameter. As the new families of modes that these modifications introduce can have a slower decay than the fundamental "barrier top" QNM, the new fundamental mode and first overtones can be said to have been displaced disproportionately to the size of the perturbation, even if the original modes (which are no longer the fundamental and first overtones) happen to still be present in the new spectrum with only a slight displacement. In other words, what can occur is that the label of "fundamental" and of the overtone numbers may jump to modes in the new branch (according to the usual assignment of these labels), rather than the old modes being displaced. This can also happen by changing the parameters of a problem such that QNMs in two different branches which are already present can switch roles as the fundamental mode, such as in the overtaking of the fundamental oscillatory mode by a de Sitter mode discussed in [12].

It is important to note that this by itself is distinct from the usual definition of (perturbative) spectral instability discussed above, in which already existing modes are displaced by large distances in the complex plane. It is also interesting that for a spectrally unstable system such as the case of QNMs, adding, say, a bump to the effective potential, can lead to a combination of both of the above effects: the emergence of new long-lived modes, as well as the large displacement of (some of) the already existing modes. This is precisely the case in the example below, for which the perturbed

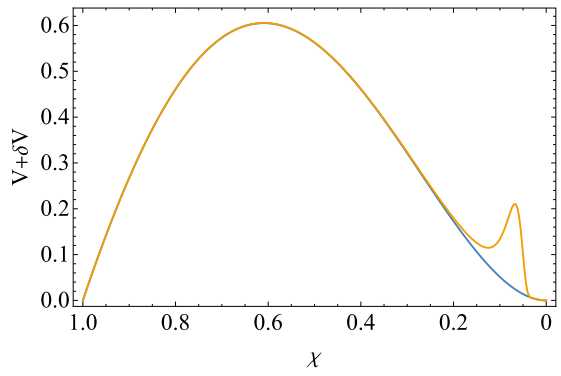

FIGURE 1
Potential for the $\ell = 2$ axial gravitational perturbation on Schwarzschild, with an added Gaussian bump at $r_b = 30M$. The horizontal axis is the compactified radial coordinate χ, and for illustrative purposes an amplitude $a = 0.2$ has been used, which is 40 times larger than the one used for computation.

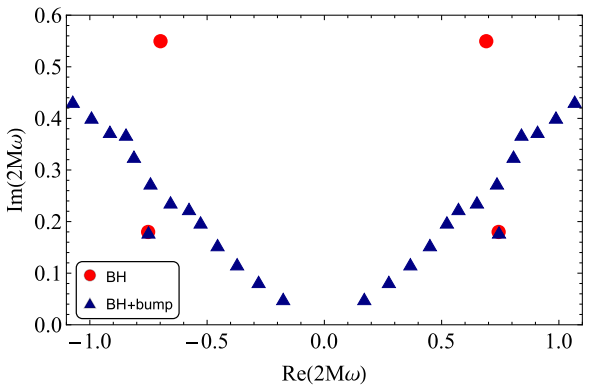

FIGURE 2
QNMs of an axial gravitational $\ell = 2$ perturbation of Schwarzschild, with and without a gaussian perturbation. The units are set to $2M = 1$. The gaussian bump has parameters $a = 0.005$, $r_b = 25$, $s = 4$, and the spectrum is calculated with $N = 400$ grid points. The unperturbed BH fundamental mode is located at $\pm 0.74734 + 0.17792i$, the mode which seemingly overlaps with it after the perturbation is at $\pm 0.74729 + 0.17780i$, and the new fundamental mode is at $\pm 0.17287 + 0.048828i$. The non-convergent "branch-cut" modes have been removed from the plot (see [1]).

potential goes from having a single barrier to a double barrier, the latter being akin to the case dubbed a "well on an island" in ref. [25].

3 Potential with a bump

This section presents an analysis of the above-mentioned perturbation δV in the form of a gaussian bump (see Figure 1),

$$\delta V = f(r)\, a \exp\left(-\frac{(r-r_b)^2}{2s^2}\right),$$

where a, r_b and s are positive constants, and the multiplication by $f(r)$ is to ensure that the total potential $V + \delta V$ still has the appropriate tendency to zero when the horizon is approached. Ref. [20] analysed in detail the position of the new long-lived fundamental mode in the presence of such a perturbation. Here we will rather focus on some qualitative features of the modified spectrum as a function of the free parameters in δV, as well as on quantifying the magnitude of this perturbation using the energy norm. We will use the computational tools employed in ref. [1], namely, a Chebyshev-Lobatto grid in χ and a pseudospectral approximation to the differential operator L and to the integration operator involved in the energy product.

3.1 Fundamental mode (in)stability

Let us begin with a particularly illustrative example of a perturbation of this type, which will be the centre-point of this analysis. We set the units to the characteristic scale of the problem by taking $2M = 1$, and we set a (seemingly) small amplitude for the bump $a = 0.005$, a position for the peak at $r_b = 25$ and a width $s = 4$. The spectrum of axial $\ell = 2$ modes with this perturbation is shown in Figure 2. We see that there is indeed a new branch of modes, some of which decay more slowly than the unperturbed BH fundamental mode. In this sense, the distance between the old and new fundamental mode does indeed seem quite large compared to the size of the perturbation, as discussed in ref. [20]. However, it is also clear form Figure 2 that the spectrum after the perturbation contains a mode which coincides with the unperturbed fundamental one (in fact it is only $\sim 10^{-3}$ away), implying that this mode was actually stable under the perturbation.

This is therefore a case in which it is the qualitative change in the shape of the potential has lead to the appearance of new long-lived modes, while *part of* the old spectrum has remained stable, in this case only the BH fundamental mode. From the first overtone onwards, the BH spectrum is in fact destabilised, much like it is in some of the cases studied in ref. [1].

The behaviour of the new fundamental mode depends strongly on the parameters of the gaussian bump a, r_b and s, and while a detailed analysis of this dependence is not within the scope of this work (see [20, 22] for a quantitative analysis of part of the parameter space), we will make some general remarks regarding the behaviour we have observed from a few spectra.

- Increasing the amplitude a tends to decrease the imaginary part of the fundamental mode, as the modes trapped between the two peaks (the bump and the light-ring peak) need to tunnel out of a larger barrier to decay. Conversely, if a is made smaller, the imaginary part increases. At around $a = 10^{-5}$ the longest-lived of these new modes is no longer the fundamental one, as its imaginary part is larger than that of the BH mode.
- Increasing the radial position of the bump r_b decreases the imaginary part of the new modes, as well as destabilising the old BH spectrum more strongly. We will make some remarks regarding the reason for this in the next section.
- Increasing the width of the bump s also makes the mode longer-lived, since this increases the tunnelling (Agmon) distance [25]. On the other hand, a larger s (at a fixed energy norm) makes the old BH spectrum more stable, since then the perturbation has a lesser "high-wavenumber" content, as discussed in [1].

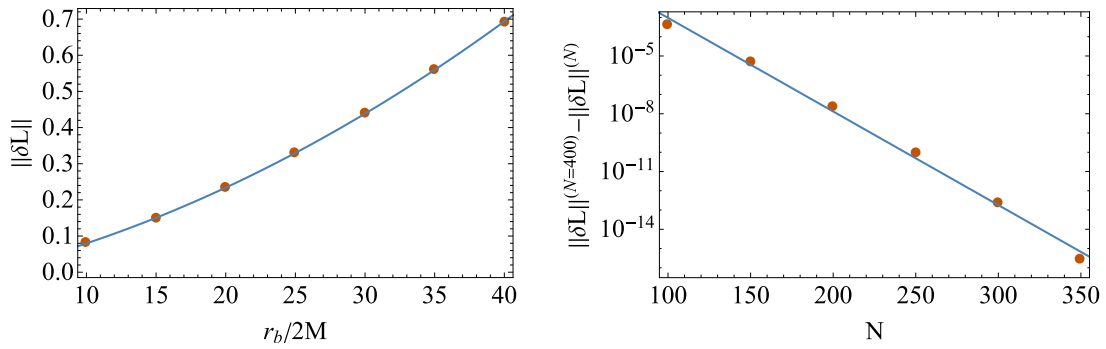

FIGURE 3
Left: energy norm of δL as function of r_b, for $s = 4$ and $a = 0.005$, in units $2M = 1$. The quadratic fit is $-0.024 + 0.0079 r_b + 0.00025 r_b^2$ (the variance is ~10^{-6}, though at smaller radii this relation can be expected to start breaking down, since the norm must be positive). Right: energy norm of δL calculated with N points, dubbed $\|\delta L\|^{(N)}$, subtracted from a reference value $\|\delta L\|^{(400)}$, for the same case with $r_b = 25$. The vertical axis is log scaled to showcase the exponential convergence (the slight discrepancy from the linear fit is due to the finite N reference value).

It is also worth noting that while we identify these longer-lived modes as a new branch due to the qualitative change in the potential and the stability of the BH fundamental mode, from the numerical results alone it is not clear where exactly this new branch becomes entwined with the perturbed BH overtones. To identify which modes go to infinity and which to BH overtones in the zero perturbation limit, a more detailed study which traces the migration of individual overtones would be required.

3.2 Flea or elephant?

The perturbation operator being added to L can be written as

$$\delta L = \begin{pmatrix} 0 & 0 \\ \frac{\delta q}{w}\mathbb{I} & 0 \end{pmatrix},$$

where $\delta q = |g'|\delta V$. In order to give a physical measure of the size of this perturbation, the energy norm of δL can be computed. Contrary to what might be expected from the small a parameter, the energy norm of the example case used for Figure 2 is actually quite significant: in units of the horizon scale, it is approximately 0.33, on the very high end of what can reasonably be considered a "perturbation". The reason for this apparent discrepancy between the intended smallness in the choice of a and the large energetic contribution of this perturbation lies in the simple fact that the energy measure comes from an integral related to the full three dimensional space of constant time slices [19], rather than just the one dimension of the wave problem (although in the end it simplifies to the latter). It therefore encodes the fact that a perturbation at a large radius would require a thick shell of this same radius, the size and matter content of which would scale with r^2. This is indeed the scaling we can observe in the left plot of Figure 3, where the energy norm is calculated as a function of r_b (with all other parameters remaining the same), and fitted to a parabola.

Therefore, the increased destabilisation of the BH QNMs (effectively, the lowering of the mode branches seen in Figure 2) for a larger r_b which was commented above can be related to precisely this increase of the energy norm. The dependence of this energy on the parameters a and s is just as predictable: an increase in both these parameters leads to a proportional (linear) increase in the energy norm.

3.3 Size vs. instability

This example has shown the importance of quantifying the size of perturbations added to the problem, since, for instance, the increase of the energy contained in perturbations at larger radii is something that could easily have been overlooked otherwise. However, using the energy norm in particular, while having many advantages [19], may not be the most adequate choice in some respects. One particular issue, raised in [13], is the fact that the energy norm of the resolvent operator, used to calculate the pseudospectrum, is not well behaved in a large part of the complex plane, which includes the vicinity of most (if not all) QNMs. Numerically, this norm tends to a divergence in the limit of infinite grid point number N in most of the upper half of the complex plane. Since the issue in that case stems from the presence of additional eigenmodes of a lower regularity class [30], and not simply from a numerical problem, it is likely to be a generic property of other setups as well.

One may then ask whether this issue extends to calculating the energy norm of other operators as well, particularly that of δL, since the pseudospectrum can equivalently be defined from its norm (albeit for a very large set of perturbations). Fortunately, it appears that the norm of this operator actually does have a good convergent behaviour. The second plot in Figure 3 shows a convergence test in a representative example. The result is clear: the convergence is in fact exponential. Such convergence was previously observed for other quantities computed with this discretisation scheme, such as the spectrum itself (see fig. 8 of [1]), but had thus far not been tested for energy norms of operators, except for the case of the non-convergent resolvent norm in [13].

The convergence of $\|\delta L\|$ in fact confirms that the issue with the resolvent norm studied in [13] goes beyond the particular numerical implementation. It also gives an appealing potential alternative

approach to calculating the pseudospectrum by exploring a sufficiently large space of perturbation operators and applying Equation 1; [9, 34]. However, there would be two issues with such an approach. First, it would be computationally very expensive to attempt to span a "full" space of perturbation operators δL. This would not be a critical impediment, at least for a small numerical resolution N. However, the second and most crucial issue is the fact that the result would differ depending on the resolution, as a higher N could capture perturbations with a higher wave-number content, which would destabilise the spectrum ever more strongly. It is not clear that the limit of operators δL with the same energy norm but with ever higher gradients in r (which would need a correspondingly higher N to be resolved) would lead to a convergent definition of the pseudospectrum, or if this issue would turn out to be equivalent to the non-convergence observed in the resolvent approach.

Testing whether this claim is true, while absolutely crucial, goes beyond the scope of the present work. If it were indeed proven true, then a consistent definition of a QNM pseudospectrum would require a modification of the scheme summarised above. One example of such a modification would be the use of norms with higher order spatial derivatives, as introduced in [30], and applied to the pseudospectral calculation in [13] (see also [35]). However, a reasonable physical interpretation of such norms and their associated stability analyses would need to be devised.

4 Discussion

The spectral instability of BH QNMs is by now a well established result in the field of black hole spectroscopy. As we have seen here, QNMs are susceptible to (al least) two different types of instability: either the direct migration of the already existing QNMs by a large distance in the complex plane ("perturbative" instability), or the appearance of new branches of modes to which the new label of fundamental or overtone number are assigned, and which are far away from their unperturbed counterparts ("branch" instability).

One important aspect in analysing both perturbative and branch instabilities is quantifying the size of the perturbations introduced into system. A physically reasonable measure of this size is given by the energy norm [19], which comes from an inner product space associated to the energy of the linear field. As we have seen in the above examples, a seemingly small perturbation to the effective potential can in fact have a large energy norm, and have a correspondingly large destabilising effect on the spectrum.

Keeping track of this norm is therefore crucial. Indeed, in the example of a gaussian bump studied in the present work, there is a clear correlation between the energy norm of δL and the distance between the old and new fundamental modes. However, there are two issues with establishing a direct one-to-one relation between this norm and the expected degree of destabilisation of the spectrum. First, the fact remains that (some of) the original BH modes can in fact remain stable in spite of the appearance of the new branches of longer-lived modes. Second, the degree to which these original modes are actually destabilised does not depend only on the energy norm, but also on the high-wave-number content of the perturbation involved, as observed in [1]. For the gaussian bump perturbation used here, decreasing the width of the bump decreases its associated energy norm, but the resulting sharper variation in r can in fact lead to an increase in the instability of the original spectrum. Exploring this issue in detail is particularly difficult because of the numerics involved, since a sharper bump requires a higher resolution to be captured, making the degree to which a bump of any given energy norm can destabilise the spectrum hard to establish.

This difficulty can in fact be seen as a potential issue with providing a convergent result for the pseudospectrum in the energy norm, since if there were such a result, a bound on the possible migration of modes could be easily placed through Equation 1. However, obtaining such a convergent pseudospectrum has been an elusive task, as discussed in [13]. Finding a solution to this issue would likely require changing parts of the above-described prescription to this calculation, as is currently being explored by the present author and collaborators [35].

Regarding the observability of these instabilities in gravitational wave signals, the results of Refs. [2, 36] suggest that while environmental perturbations are detectable in time-domain evolution, their effect on ringdown signals is not as disproportionately large as it is on the QNM spectrum itself. However, a systematic study of the effect of different types of perturbations, particularly involving the branch instability analysed here, is lacking.

Overall, the study of the QNM spectral instability has led to a myriad of different results in many different spacetime setups, but there are just as many open questions left to be addressed in the coming years.

Data availability statement

The raw data supporting the conclusions of this article will be made available by the authors, without undue reservation.

Author contributions

VB: Writing–original draft, Writing–review and editing.

Funding

The author(s) declare that financial support was received for the research, authorship, and/or publication of this article. Financial support was provided by the European Union's H2020 ERC Advanced Grant "Black holes: gravitational engines of discovery" grant agreement no. Gravitas–101052587, and by the Spanish Government through the Grants No. PID2020-118159GB-C43, PID2020-118159GB-C44, PID2023-149018NB-C43 and PID2023-149018NB-C44 (funded by MCIN/AEI/10.13039/501100011033).

Acknowledgments

The author would like to thank Jose Luis Jaramillo for a detailed discussion and feedback on this manuscript, as well as Vitor Cardoso, Kyriakos Destounis and Rodrigo Panosso Macedo for our many group discussions on this topic.

Conflict of interest

The author declares that the research was conducted in the absence of any commercial or financial relationships that could be construed as a potential conflict of interest.

Generative AI statement

The authors declare that no Generative AI was used in the creation of this manuscript.

Publisher's note

All claims expressed in this article are solely those of the authors and do not necessarily represent those of their affiliated organizations, or those of the publisher, the editors and the reviewers. Any product that may be evaluated in this article, or claim that may be made by its manufacturer, is not guaranteed or endorsed by the publisher.

References

1. Jaramillo JL, Panosso Macedo R, Al Sheikh L. Pseudospectrum and black hole quasinormal mode instability. *Phys Rev X* (2021) 11(3):031003. doi:10.1103/physrevx.11.031003

2. Jaramillo JL, Panosso Macedo R, Sheikh LA. Gravitational wave signatures of black hole quasinormal mode instability. *Phys Rev Lett* (2022) 128(21):211102. doi:10.1103/physrevlett.128.211102

3. Sheikh LA. *Scattering resonances and Pseudospectrum: stability and completeness aspects in optical and gravitational systems*. France: Institut de Mathématiques de Bourgogne [Dijon] (2022) PhD thesis.

4. Nollert H-P. About the significance of quasinormal modes of black holes. *Phys Rev D* (1996) 53:4397–402. doi:10.1103/physrevd.53.4397

5. Nollert H-P, Price RH. Quantifying excitations of quasinormal mode systems. *J Math Phys* (1999) 40:980–1010. doi:10.1063/1.532698

6. Daghigh RG, Green MD, Morey JC. Significance of black hole quasinormal modes: a closer look. *Phys Rev D* (2020) 101(10):104009. doi:10.1103/physrevd.101.104009

7. Qian W-L, Lin K, Shao C-Y, Wang B, Yue R-H. Asymptotical quasinormal mode spectrum for piecewise approximate effective potential. *Phys Rev D* (2021) 103(2):024019. doi:10.1103/physrevd.103.024019

8. Boyanov V, Destounis K, Panosso Macedo R, Cardoso V, Jaramillo JL. Pseudospectrum of horizonless compact objects: a bootstrap instability mechanism. *Phys Rev D* (2023) 107(6):064012. doi:10.1103/physrevd.107.064012

9. Areán D, Fariña DG, Landsteiner K. Pseudospectra of holographic quasinormal modes. *JHEP* (2023) 12:187. doi:10.1007/jhep12(2023)187

10. Warnick C, "(In)stability of de Sitter Quasinormal Mode spectra," 7 (2024).

11. Sarkar S, Rahman M, Chakraborty S. Perturbing the perturbed: stability of quasinormal modes in presence of a positive cosmological constant. *Phys Rev D* (2023) 108(10):104002. doi:10.1103/physrevd.108.104002

12. Destounis K, Boyanov V, Panosso Macedo R. Pseudospectrum of de Sitter black holes. *Phys Rev D* (2024) 109(4):044023. doi:10.1103/physrevd.109.044023

13. Boyanov V, Cardoso V, Destounis K, Jaramillo JL, Panosso Macedo R. Structural aspects of the anti–de Sitter black hole pseudospectrum. *Phys Rev D* (2024) 109(6):064068. doi:10.1103/physrevd.109.064068

14. Ianniccari A, Iovino AJ, Kehagias A, Pani P, Perna G, Perrone D, et al. Deciphering the instability of the black hole ringdown quasinormal spectrum. *Phys Rev Lett* (2024) 133(21):211401. doi:10.1103/physrevlett.133.211401

15. Gogoi DJ, Bora J, Studnička F, Hassanabadi H, "Optical properties, quasinormal modes and greybody factors of deformed AdS-schwarzschild black holes," (2024) 11.

16. Skvortsova M, "Quantum corrected black holes: testing the correspondence between grey-body factors and quasinormal modes," (2024) 11.

17. Destounis K, Macedo RP, Berti E, Cardoso V, Jaramillo JL. Pseudospectrum of Reissner-Nordstr"om black holes: quasinormal mode instability and universality. *Phys Rev D* (2021) 104(8):084091. doi:10.1103/physrevd.104.084091

18. Chen J-N, Wu L-B, Guo Z-K, "The pseudospectrum and transient of Kaluza-Klein black holes in Einstein-Gauss-Bonnet gravity," (2024) 7.

19. Gasperin E, Jaramillo JL. Energy scales and black hole pseudospectra: the structural role of the scalar product. *Class Quant Grav* (2022) 39(11):115010. doi:10.1088/1361-6382/ac5054

20. Cheung MH-Y, Destounis K, Macedo RP, Berti E, Cardoso V. Destabilizing the fundamental mode of black holes: the elephant and the flea. *Phys Rev Lett* (2022) 128(11):111103. doi:10.1103/physrevlett.128.111103

21. Berti E, Cardoso V, Cheung MH-Y, Di Filippo F, Duque F, Martens P, et al. Stability of the fundamental quasinormal mode in time-domain observations against small perturbations. *Phys Rev D* (2022) 106(8):084011. doi:10.1103/physrevd.106.084011

22. Cardoso V, Kastha S, Panosso Macedo R. Physical significance of the black hole quasinormal mode spectra instability. *Phys Rev D* (2024) 110(2):024016. doi:10.1103/physrevd.110.024016

23. Qian W-L, Li G-R, Daghigh RG, Randow S, Yue R-H, "On universality of instability in the fundamental mode," (2024) 9.

24. Zworski M. Mathematical study of scattering resonances. *Bull Math Sci* (2017) 7:1–85. doi:10.1007/s13373-017-0099-4

25. Bindel D, Zworski M. Theory and computation of resonances in 1D scattering (2006) Available from: https://www.cs.cornell.edu/bindel/cims/resonant1d/ (access September 10, 2024).

26. Jaramillo JL. Pseudospectrum and binary black hole merger transients. *Class Quant Grav* (2022) 39(21):217002. doi:10.1088/1361-6382/ac8ddc

27. Zenginoglu A. A Geometric framework for black hole perturbations. *Phys Rev D* (2011) 83:127502. doi:10.1103/physrevd.83.127502

28. Panosso Macedo R, Zenginoglu A, "Hyperboloidal approach to quasinormal modes," 9 (2024).

29. Panosso Macedo R. Hyperboloidal approach for static spherically symmetric spacetimes: a didactical introductionand applications in black-hole physics. *Phil Trans Roy Soc Lond* (2024) 382(2267):20230046. doi:10.1098/rsta.2023.0046

30. Warnick CM. On quasinormal modes of asymptotically anti-de Sitter black holes. *Commun Math Phys* (2015) 333(2):959–1035. doi:10.1007/s00220-014-2171-1

31. Ansorg M, Panosso Macedo R. Spectral decomposition of black-hole perturbations on hyperboloidal slices. *Phys Rev D* (2016) 93(12):124016. doi:10.1103/physrevd.93.124016

32. Abbott BP, Abbott R, Abbott T, Abernathy M, Acernese F, Ackley K, et al. Observation of gravitational waves from a binary black hole merger. *Phys Rev Lett* (2016) 116(6):061102. doi:10.1103/physrevlett.116.061102

33. Barausse E, Cardoso V, Pani P. Can environmental effects spoil precision gravitational-wave astrophysics? *Phys Rev D* (2014) 89(10):104059. doi:10.1103/physrevd.89.104059

34. Trefethen L, Embree M, Spectra and pseudospectra: the behavior of nonnormal matrices and operators. (2005).

35. Besson J, Boyanov V, Jaramillo J, "Black hole quasi-normal modes as eigenvalues: definition and stability problem," (2024).

36. Spieksma TFM, Cardoso V, Carullo G, Della Rocca M, Duque F Black hole spectroscopy in environments: detectability prospects, (2024) 9.

frontiers | Frontiers in Physics

TYPE Mini Review
PUBLISHED 17 January 2025
DOI 10.3389/fphy.2024.1497601

Check for updates

OPEN ACCESS

EDITED BY
Piotr Bizon,
Jagiellonian University, Poland

REVIEWED BY
Edgar Gasperin,
University of Lisbon, Portugal
Claude Warnick,
University of Cambridge, United Kingdom

*CORRESPONDENCE
Rodrigo Panosso Macedo,
rodrigo.macedo@nbi.ku.dk
Anıl Zenginoğlu,
anil@umd.edu

RECEIVED 17 September 2024
ACCEPTED 12 December 2024
PUBLISHED 17 January 2025

CITATION
Panosso Macedo R and Zenginoğlu A (2025) Hyperboloidal approach to quasinormal modes.
Front. Phys. 12:1497601.
doi: 10.3389/fphy.2024.1497601

COPYRIGHT
© 2025 Panosso Macedo and Zenginoğlu. This is an open-access article distributed under the terms of the Creative Commons Attribution License (CC BY). The use, distribution or reproduction in other forums is permitted, provided the original author(s) and the copyright owner(s) are credited and that the original publication in this journal is cited, in accordance with accepted academic practice. No use, distribution or reproduction is permitted which does not comply with these terms.

Hyperboloidal approach to quasinormal modes

Rodrigo Panosso Macedo[1]* and Anıl Zenginoğlu[2]*

[1]Niels Bohr International Academy, Niels Bohr Institute, Copenhagen, Denmark, [2]Institute for Physical Science and Technology, University of Maryland, College Park, MD, United States

Oscillations of black hole spacetimes exhibit divergent behavior near the bifurcation sphere and spatial infinity. In contrast, these oscillations remain regular when evaluated near the event horizon and null infinity. The hyperboloidal approach provides a natural framework to bridge these regions smoothly, resulting in a geometric regularization of time-harmonic oscillations, known as quasinormal modes (QNMs). This review traces the development of the hyperboloidal approach to QNMs in asymptotically flat spacetimes, emphasizing both the physical motivation and recent advancements in the field. By providing a geometric perspective, the hyperboloidal approach offers an elegant framework for understanding black hole oscillations, with implications for improving numerical simulations, stability analysis, and the interpretation of gravitational wave signals.

KEYWORDS

hyperboloidal, frequency domain, quasinormal modes, black holes, non-selfadjoint operators

1 Introduction

When a black hole (BH) spacetime is perturbed, gravitational waves (GW) carry the energy of the perturbation towards the BH horizon and to infinity. These perturbations show oscillations that decay exponentially at characteristic frequencies and are called quasinormal modes (QNM) [1–4]. Studying these QNMs is central to the black hole spectroscopy program [5–7], which aims to measure the oscillation frequencies from GW detections and thereby probe the BH geometry and its surrounding environment [1, 3, 4, 8]. The dominant quadrupole QNMs have already been measured in gravitational wave signals [9–11], while the detection of higher modes remains under debate [12–25].

Mathematically, the QNM problem is often formulated as an eigenvalue problem, where QNM frequencies appear as the eigenvalues of a second-order differential operator. However, in their traditional representation, the corresponding QNM eigenfunctions grow exponentially near the black hole and at spatial infinity, which does not seem physically acceptable for small perturbations of a background spacetime [26]. Reformulating the problem using hyperboloidal surfaces—regular spacelike surfaces that extend smoothly from the black hole event horizon to null infinity—reveals that QNMs are globally regular

[27, 28]. This geometric regularization[1] of time-harmonic black hole perturbations has found many recent applications, which we review in this paper.

2 The traditional approach to QNMs

The Schwarzschild solution, the simplest black-hole (BH) solution to Einstein's equations, is given by

$$ds^2 = -f(r)\,dt^2 + \frac{1}{f(r)}dr^2 + r^2 d\bar{\omega}^2, \quad \text{with} \quad f(r) = 1 - \frac{2M}{r},$$

where $d\bar{\omega}^2 = d\theta^2 + \sin^2\theta d\phi^2$ is the metric on the unit sphere, and M the black-hole's mass. Perturbations of this solution are described by the Regge-Wheeler-Zerilli type wave equation:

$$\left(-\partial_t^2 + \partial_{r_*}^2 - V(r_*)\right) u(t, r_*) = 0, \tag{1}$$

where $r_* \in (-\infty, \infty)$ is the tortoise coordinate and $V(r_*)$ is the effective potential that behaves as $V \sim f(r)$ near the black-hole horizon and as $V \sim 1/r^2$ toward spatial infinity.

Solutions to (Equation 1) evolve through a transient phase, followed by a ringdown characterized by exponentially damped vibrations (QNMs) [34], and eventually a polynomial, non-oscillatory decay known as the tail [35, 36].

To analyze the QNM phase, one typically considers time-harmonic solutions

$$u(t, r_*) = e^{-i\omega t} R(r_*), \tag{2}$$

that reduce the wave equation to a Helmholtz equation,

$$\left(\frac{d^2}{dr_*^2} + \omega^2 - V(r_*)\right) R(r_*) = 0. \tag{3}$$

Sommerfeld recognized in 1912 that the Helmholtz equation, in stark contrast to the elliptic case, does not admit unique solutions even when we require that the solution vanishes at infinity [37, 38]. To ensure uniqueness, an outgoing radiation condition must be imposed. In the BH context, a Sommerfeld condition applies also near the BH. We therefore impose

$$\lim_{r_* \to \pm\infty} \left(\frac{d}{dr_*} \mp i\omega\right) R(r_*) = 0 \quad \Leftrightarrow \quad R(r_*) \sim e^{\pm i\omega r_*} \text{ as } r_* \to \pm\infty. \tag{4}$$

It turns out, however, that the boundary conditions (Equation 4) are not sufficient [2, 39] and a more precise notion of purely outgoing solution is needed to uniquely define the QNMs [40]. The formal definition of QNMs followed a different route than the intuitive notion of QNMs as the eigenvalues of a given differential operator.

The time-harmonic Ansatz (Equation 2), closely related to a Fourier transformation, provides a general formalism oblivious to the specific form of initial data causing the perturbation. To define QNMs formally, one considers an initial value problem. Then, a Laplace transformation [2, 39, 41, 42] leads to a inhomogeneous spatial differential equation, with a source term accounting for the initial data. One must then ensure that the spacetime solution $u(t, r_*)$ remains bounded as $t \to \infty$ [43]. In the Laplace formalism, the solution $u(t, r_*)$ results from the convolution of the Green's functions with the source term carrying information from the initial data. The inverse Laplace transformation requires an integration along a frequency values $\omega_I > 0$, and there is only one possible choice of homogenous solutions $R_\pm(r_*; \omega)$ to construct the correct Green's function: they must satisfy the boundary conditions (Equation 4) at both ends $r_* \to \pm\infty$. Once the Green's functions are fixed in the complex half-plane $\omega_I > 0$, one analytically extends them into the region $\omega_I < 0$. The QNMs are then uniquely defined as the poles of Green's functions, or equivalently in the one-dimensional case, the roots of the Wronskian.

The Laplace approach uniquely defines QNMs via Green's functions, bypassing the notions of eigenvalues and eigenfunctions. Such definition via this Green's functions is also understood under the Lax-Phillips approach [44, 45]. However, this definition still allows QNM functions to blow up asymptotically, creating a puzzle: while black hole stability demands that linearized perturbations decay over time, the associated time-harmonic perturbations remain singular in the asymptotic regions.

The resolution lies in the global structure of spacetime. The QNM behavior at asymptotic boundaries results from the singular properties of the coordinates used in Equation 3. In Schwarzschild coordinates, as $r_* \to \pm\infty$, the limits correspond to spatial infinity i^0 and the bifurcation sphere B. These loci connect to future and past null infinity at i^0 and white and black hole horizon at B, and the blow-up of QNM eigenfunctions is a coordinate effect due to the accumulation of infinitely many time surfaces thereon.

When QNMs are represented on regular, hyperboloidal time slices, they do not exhibit this unbounded growth[1] [27, 28, 33], as we discuss in the next section.

3 The hyperboloidal approach to QNMs

The singularity of Schwarzschild time slices at the bifurcation sphere is well-known today, but understanding its causal structure took over four decades [46–49]. Given this singularity, it is not surprising that QNMs blow up near the black hole, but they also blow up near spatial infinity. Thus, switching to regular coordinates at the bifurcation sphere does not resolve the issue.

Part of the historical confusion about BHs was that it takes infinite Schwarzschild time for radiation to fall into a BH. The same statement is true concerning spatial infinity: it takes infinite Schwarzschild time for outgoing radiation to reach spatial infinity. Because this is "reasonable" from a physical point of view, it has been widely accepted that QNMs have a singular representation at both asymptotic regions.

The first suggestion that outgoing perturbations are regular in the frequency domain toward null infinity was made by Friedman and Schutz in a 1975 paper on the stability of relativistic stars [50]. Friedman and Schutz recognize the problem with standard time

1 Note that we focus here on the geometric developments around the hyperboloidal framework in asymptotically flat spacetimes. The analytic aspects of QNM regularity beyond the mere coordinate singularity of standard time slices were clarified in a series of papers [29–33], discussed in Section 3.3.

slices where outgoing modes behave asymptotically like $r^k e^{i\omega(t-r)}$ implying that stable modes with $\omega_I < 0$ grow exponentially as $r \to \infty$. To make the representation finite, they recommend to use null hypersurfaces. In a footnote, they comment that the representation is regular also "if one uses a spacelike hypersurface that is only asymptotically null."

Schmidt picked up this idea in a 1993-essay for the Gravity Research Foundation on relativistic stellar oscillations [26] arguing that QNMs on hyperboloids "are represented by proper eigenvalues and eigenfunctions." However, the presentation includes no details beyond the 1975 paper.

To understand why it took almost 20 years from Schmidt's essay [26] to the construction of a regular geometric framework to describe QNMs in asymptotically flat spacetimes[1] [27, 28, 33], we provide a short historical review of hyperboloidal coordinates.

3.1 A brief history of hyperboloidal coordinates

The central role of spacetime hyperbolas in relativity was recognized already by Minkowski in 1908 [51]. The Milne model from 1933 [52] or Dirac's point-form of quantum field theory from 1949 are hyperboloidal [53]. In the 1970s, hyperboloidal studies were performed for the analysis of wave equations [54–56] and quantum field theory [57–60]. However, these early studies use a time-dependent formulation in which time freezes at null infinity.

The first hyperboloidal coordinates foliating null infinity are implicit in Penrose's work on the global causal structure of spacetimes via conformal compactification [61, 62]. Indeed, one can obtain a hyperboloidal surface from any textbook discussing the Penrose diagram simply by looking at the level sets of Penrose time [63]. In the context of numerical relativity, it was recognized that hyperboloidal time functions that asymptotically approach the retarded time should be beneficial for the computation of gravitational waves [64, 65]. Explicit hyperboloidal coordinates in black-hole spacetimes were constructed in the context of the analysis of constant mean curvature foliations [66]. A remarkable but largely ignored paper by Gowdy in 1981 includes many key elements of the hyperboloidal approach used today in black-hole perturbation theory [67], including the height function approach to preserve time-translation symmetry, compactification fixing null infinity (scri-fixing), hyperboloidal solutions to the wave equation, and the structure of time-harmonic solutions relevant for the frequency domain. These ideas were not picked up by the community at the time.

The first systematic study of the hyperboloidal initial value problem for Einstein equations was initiated by Friedrich in 1983 [68]. Friedrich devised a reformulation of the Einstein equations with respect to a conformally rescaled metric that is regular across null infinity. The conformal field equations are well-suited for the analysis of the asymptotic behavior of Einstein's equations and have led to seminal results such as the nonlinear, semi-global stability of de Sitter-type and Minkowski-type spacetimes [69, 70]. The developments around conformal field equations and attempts to use them numerically are reviewed in [71, 72].

Twenty years after Gowdy's paper, Moncrief presented the hyperboloidal compactification of Minkowski spacetime using time-shifted hyperboloids in an unpublished talk [73] leading to the first numerical studies using hyperboloidal foliations in Minkowski spacetime [74–77]. Around this time, various suggestions for hyperboloidal coordinates and numerical simulations in black-hole spacetimes were made [78–83].

The construction widely used today in black-hole perturbation theory is based on scri-fixing coordinates with time-shifted hyperboloids presented in 2008 [84]. The idea is to combine the height function technique that preserves the time-symmetry of the underlying spacetime with an explicit radial compactification whose singular Jacobian at infinity is proportional to a prescribed conformal factor. In the following years, this method was used primarily in the time domain for solving wave-propagation problems [85–97].

The translation of the hyperboloidal method to the frequency domain was presented in [27], where it was demonstrated that hyperboloidal time functions regularize the QNM eigenfunctions in the asymptotic domains. Warnick used a related idea in [31] for AdS spacetimes in which spatial slices are naturally hyperbolic (see also [29, 30]). The first detailed analysis of QNMs in asymptotically flat black-hole spacetimes using the hyperboloidal approach was presented in [28]. We summarize the basic ideas of the hyperboloidal approach below.

3.2 A geometric framework

The construction of globally regular coordinates consists of a time transformation respecting the time symmetry of the background, a suitable spatial compactification, and conformal rescaling [84]. We first introduce the time function τ via [67, 82, 84].

$$\tau = t + h(r). \tag{5}$$

The time transformation implies an exponential scaling in frequency domain [27]. Writing the time-harmonic ansatz in Equation 2 with respect to the new time coordinate in Equation 5, we get

$$u(t, r_*) = e^{-i\omega t} R(r_*) = e^{-i\omega\tau} e^{i\omega h} R(r_*) = e^{-i\omega\tau} \bar{R}(r_*).$$

The rescaled radial function $\bar{R}(r_*) = e^{i\omega h} R(r_*)$ is regular both near the event horizon and toward null infinity. To see this in an explicit example, consider the height function for the so-called minimal gauge [98–100]

$$h_{\mathrm{MG}}(r) = -r + 2M \log\left|\frac{r}{2M} - 1\right| - 4M \log\left(\frac{r}{2M}\right) = -r_* - 4M \log\left(\frac{r}{2M}\right).$$

The minimal gauge height function has the following asymptotic behavior

$$h_{\mathrm{MG}} \sim -r_* \text{ for } r \to \infty, \qquad h_{\mathrm{MG}} \sim +r_* \text{ for } r \to 2M.$$

The height function regularizes the QNM eigenfunctions in the asymptotic domains. The regularity of the QNM eigenfunctions is directly related to the regularity of the minimal gauge at the

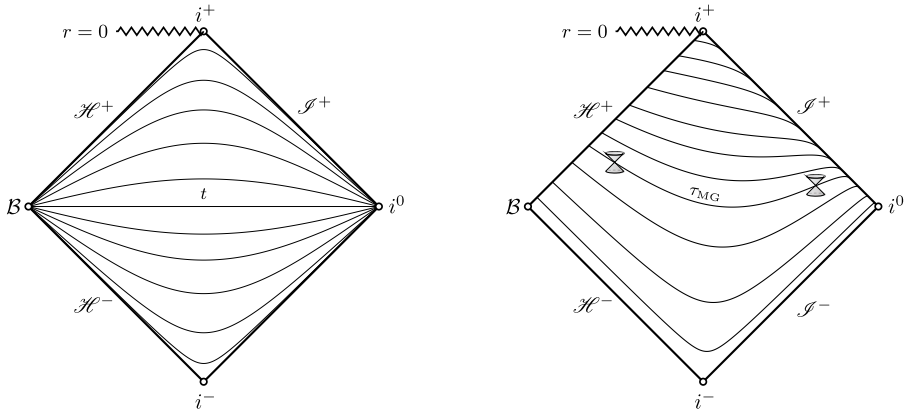

FIGURE 1
Penrose diagrams of the exterior domain in Schwarzschild spacetime contrasts the level sets of the standard Schwarzschild time (left panel) and the hyperboloidal minimal gauge (right panel). Schwarzschild time slices intersect at the bifurcation sphere, B, and spatial infinity, i^0. Minimal gauge slices provide a smooth foliation of the future event horizon, $\mathcal{H}^+$, and future null infinity, $\mathscr{I}^+$.

asymptotic boundaries near the horizon and near infinity (see Figure 1). The minimal gauge is unique in its simplicity and appears in different setups as a natural construction [101, 102]. Surprisingly, the minimal gauge was implicitly used by Leaver in his papers on QNMs in BH spacetime [103, 104]. Related hyperboloidal regularization procedures have been suggested over the years by various authors without an explicit recognition of the geometric background of their construction [105–111].

In [27], it was shown that the time translation must be combined with a suitable rescaling to arrive at a regular representation of QNMs. The rescaling takes into account the asymptotic fall-off behavior of the QNM eigenfunctions toward the BH and toward infinity. The resulting equations have short-range potentials suitable for compactification of the exterior black region from the radial coordinate $r \in [r_h, \infty)$ — or equivalently, $r_* \in (-\infty, +\infty)$ — into a compact domain $\sigma \in [\sigma_h, \sigma_{\mathscr{I}^+}]$. This rescaling is related to the conformal compactification of black-hole spacetimes.

The external boundary conditions (Equation 4) are automatically satisfied in terms of a radially compact hyperboloidal coordinates (τ, σ)[27, 100], when the underlying function $\overline{R}(\sigma)$ is regular at the black-hole horizon (σ_h) and future null infinity $(\sigma_{\mathscr{I}^+})$. Thus, we no longer need to impose boundary conditions to the wave equation by hand. The boundary condition is replaced by a regularity condition on the underlying solution $\overline{R}(\sigma)$ in the entire domain $\sigma \in [\sigma_h, \sigma_{\mathscr{I}^+}]$. In practical terms, one derives the regularity condition at the boundary directly from the hyperboloidal differential equation. When formulating the frequency-domain problem in coordinates (τ, σ), the resulting differential equation equivalent to Helmoltz Equation 3 assumes a generic form [28, 99, 100].

$$\left(\alpha_2(\sigma)\frac{d^2}{d\sigma^2} + \alpha_1(\sigma)\frac{d}{d\sigma} + \alpha_0(\sigma)\right)\overline{R}(\sigma) = 0, \tag{6}$$

with coefficients α_2, α_1 and α_0 depending on the particular choice for the hyperboloidal height function. The most important property of the above equation is that it is a singular ordinary differential equation, i. e., its principal part behaves as $\alpha_2 \sim (\sigma - \sigma_{\mathscr{I}^+})^2(\sigma - \sigma_h)$ and therefore $\alpha_2(\sigma_h) = \alpha_2(\sigma_{\mathscr{I}^+}) = 0$. Hence, at the boundaries, Equation 6 provides us directly with the relation between the field and its first σ-derivatives serving as boundary data ensuring a bounded solution. From the spacetime perspective, and the resulting wave equation, the same condition $\alpha_2(\sigma_h) = \alpha_2(\sigma_{\mathscr{I}^+}) = 0$ ensures that, at the boundaries, the light cones point outwards the numerical domain, or equivalently, that the characteristic speeds of incoming modes vanish [27, 100].

The finite behaviour of the function $\overline{R}(\sigma)$ is one of the most important aspects in the hyperboloidal approach. As we discuss below, this feature allows us to unveil new properties of the QNM eigenfunctions, develop novel numerical algorithms and attack new problems relevant to black-hole physics and gravitational wave astronomy.

3.3 From geometry to analysis

The hyperboloidal framework regularizes solutions to the Helmholtz problem Equation 3. In fact, any bounded solution satisfying the singular ordinary differential Equation 6 automatically fulfills the Sommerfeld conditions (Equation 4). One would naively think that bounded solutions exist only at the QNMs frequencies. However, we saw in Section 2 that the conditions (Equation 4) are necessary, but not sufficient to specify the QNM problem uniquely. In the traditional formulation, the QNM eigenfunctions grow asymptotically. The complex plane spanned by the frequency ω might contain regions with solution satisfying (Equation 4), but contaminated by unwanted solutions that decrease at the boundaries. Removing the asymptotic blow-up allows us to peek directly into these unphysical solutions, which exist in the entire half-plane $\mathrm{Im}(\omega) < 0$ [28, 31].

The left panel of Figure 2 shows two solutions to Equation 6 which are bounded in the entire exterior BH domain, from $\sigma = 0$ representing future null infinity and $\sigma = 1$ the BH horizon: the solution in blue is obtained at a given QNM frequency $\omega_{\rm QNM}$, whereas the solution in red corresponds to a given frequency in the half-plane $\mathrm{Im}(\omega) < 0$, but with $\omega \neq \omega_{\rm QNM}$. These solutions

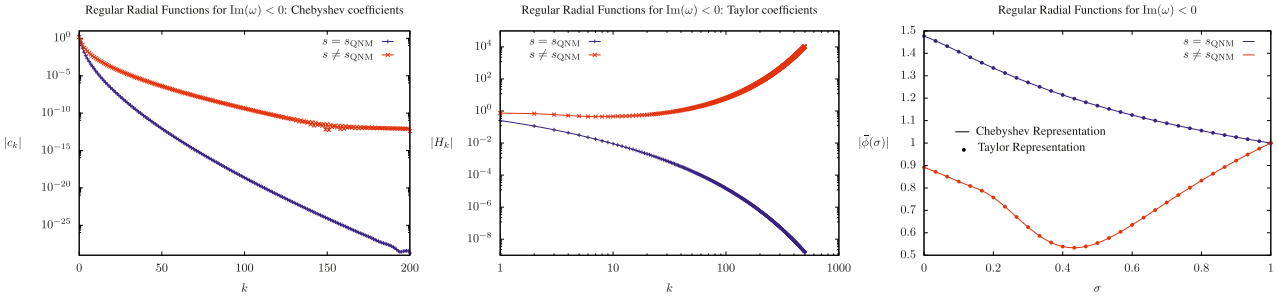

FIGURE 2
Solutions to hyperboloidal radial equation (left panel). Bounded solutions exist in the entire half-plane for $\mathrm{Im}(\omega) < 0$, regardless whether ω is a QNM or not. The continuous lines were obtained with a spectral method code based on a Chebyshev representation of the solution. Independently, the dots result from a Taylor representation of the solution as power series around the horizon (Leaver's strategy). The QNM eigenfunctions are characterised by the solutions with a higher degree of regularity, heuristically verified via the faster decay of the corresponding Chebyshev coefficients $|c_k|$ (middle panel) or the asymptotic decay of the Taylor coefficients $|a_k|$.

are obtained with two different numerical approaches: the solid line results from solving the ODE with a Chebyshev collocation point spectral method [112], whereas the dotted points arise when using Leaver's Taylor expansion, which corresponds to a frequency domain hyperboloidal formulation in the minimal gauge [28, 99, 113]. Both strategies yield the same results. At first glance, there is nothing special in the behavior of the solutions that allows us to distinguish a QNM from a non-QNM eigenfunction. Indeed, it is even possible to specify a hyperboloidal initial data such that the corresponding time evolution has an arbitrary exponentially damped oscillation [28].

What distinguishes a QNM from a non-QNM solution is their regularity class. By studying the convergence rate of their discrete numerical representation, one can infer that these functions belong to different regularity classes. The middle panel of Figure 2 shows the Chebyshev coefficients from the Chebyshev collocation point spectral method. These coefficients decay exponentially for C^Ω analytic functions or algebraically for C^k singular functions. We observe an intermediary decay, suggesting the regularity class of these functions is between C^k and C^Ω. The Chebyshev coefficients for QNM eigenfunctions decay faster than for non-QNM eigenfunctions, indicating QNM eigenfunctions belong to a better regularity class. A similar conclusion arises from the Taylor expansion coefficients (right panel 2). For QNM eigenfunctions, $|a_k|$ decays asymptotically. For non-QNM functions, $|a_k|$ grows asymptotically. Even though the series does not converge absolutely, it converges conditionally due to oscillations in $\mathrm{Im}(a_k)$ (left panel of Figure 2). These conclusions are formalized by interpreting QNM as a formal eigenvalue problem of the generator of time translations for a null foliation, acting on an appropriate Hilbert space [29–33, 114–116], where QNM eigenfunctions belong to the Gevrey-2 regularity class.

4 Applications

The QNM problem plays a fundamental role in the era of gravitational wave astronomy. The BH spectroscopy program faces three main challenges: (i) the measurability of the QNMs frequencies, limited by the GW detection signal-to-noise ratios; (ii) the relevance of nonlinear effects to the ringdown dynamics; and (iii) the QNMs spectral instability. As discussed in the previous sections, hyperboloidal formalism provides crucial theoretical tools to tackle different aspects of these challenges.

4.1 QNM excitation factors and tail decay

Even though challenge (i) mainly concerns the GW detection's signal-to-noise ratio, it heavily relies on accurate predictions for the expected QNM excitations [117]. The excitation of each QNM depends on the particular initial perturbation triggering the dynamics. This perturbation also excites the late-time power-law tail decay. Determining these excitation factors has always been challenging due to the blow-up of the underlying modes at the bifurcation sphere and spatial infinity [118]. A common approach to avoid the infinities at the bifurcation sphere when calculating integrals along the physical coordinate $r_* \in (-\infty, \infty)$ is to deform the integration path into the complex plane [119–121].

The hyperboloidal formalism offers an alternative strategy to determine such excitation factors due to the globally regular behavior of the QNM eigenfunctions. The direct identification of Leaver's continued fraction strategy with spacetime solutions defined on hyperboloidal hypersurfaces allows the further development of the Leaver method to calculate QNMs (and tail decay) excitation factors for problems formulated on hyperboloidal slices [28, 99]. While Leaver's method relies on a Taylor expansion around the horizon for the underlying hyperboloidal functions, the strategy can be adapted to directly solve a linear partial differential equation having the QNM excitation amplitude as an unknown parameter in the equation [122], or alternatively via the so-called Keldysh scheme [123]. The hyperboloidal formalism is also essential for recent advances in the understanding of the role played by the tail decay in BH spectroscopy [124–126].

4.2 Quadratic QNMs

Since GR is a nonlinear theory, challenge (ii) emphasizes that BH spectroscopy must also account for second-order, quadratic perturbations [21, 127–136]. The quadratic coupling of first-order solutions dictates the dynamics at second order in perturbation theory [137–139]. When formulated in the standard t slices, the blow-up of QNM eigenfunctions at the bifurcation sphere and spatial infinity imposes severe restrictions for second-order studies, both at theoretical and numerical levels. The hyperboloidal framework for black-hole perturbations beyond the linear order becomes indispensable for regular evolutions [23, 132, 140], as well as for studies in the frequency domain [134, 141].

4.3 QNM instability and the pseudospectrum

Apart from his groundbreaking work in QNM [34], Vishveshwara also highlighted that the QNM spectra is very sensitive to small modifications in the black-hole potential [142, 143]. At the same time, the QNM spectra destabilisation was also observed by Nollter and Price [144, 145], but the phenomenon's impact in the BH spectroscopy programme has been largely overlooked over the past decades. Only recently has the challenge (iii) gained a greater attention [112, 146–155].

Small modifications in oscillatory frequencies for wave equations result in minor spectral responses only if the wave operators are self-adjoint. However, the flow of GWs into the BH and out into the wave zone places BH perturbation theory within the framework of non-self-adjoint operators. The successful application of non-self-adjoint operator theory to gravitational systems was only made possible by the hyperboloidal approach to black-hole perturbations [112] (see also Ref. [156] for an alternative approach akin to "complex scaling"). In this approach, one can use the mathematical formalism of pseudospectra [157] to study the QNM spectral instability [112] and perform a non-modal analysis [151] that a traditional mode analysis might overlook. Since the breakthrough offered by the hyperboloidal framework, the analysis of QNM pseudospectra has been performed in several different contexts, from astrophysically relevant scenarios to applications in the gauge-gravity duality [158–167].

5 Discussion

The hyperboloidal approach to QNMs offers a geometric regularization of black-hole perturbations. By connecting the regular oscillations near BHs with those observed far away, this method bypasses the problematic divergences inherent in the traditional approach at the bifurcation sphere and spatial infinity.

With hindsight, the hyperboloidal approach relies on a simple coordinate transformation that resolves the asymptotic singularity of the standard time [84]. It is astonishing that it took decades for relativists to adopt regular coordinates to describe black-hole perturbations. We suspect that part of the confusion arose from the asymptotic behavior of time functions. It is not widely appreciated that the standard time coordinate in flat spacetime is singular at infinity with respect to the causal structure. Large-scale wave phenomena demand coordinates tailored to wave propagation—characteristic or hyperboloidal. This approach is critical not only for gravitational waves but also for addressing general wave propagation problems.

In recent years, the hyperboloidal approach has led to significant breakthroughs in the study of black-hole perturbations. As discussed, the regularity of the QNM eigenfunctions in the frequency domain enables a direct identification of the QNM excitation factors and tail decay 4.1, facilitates the efficient computation of second-order perturbations 4.2, and supports the analysis of the QNM pseudospectrum 4.3. Moreover, recent work has demonstrated that the hyperboloidal method can be extended to non-relativistic operators [168], further broadening its scope and applicability.

From a numerical perspective, finding the optimal choices among the many ways to construct hyperboloidal coordinates, particularly for high-precision and large-scale simulations, remains a challenge. Exploring gauge conditions and optimizing numerical algorithms to leverage advanced computational resources will be essential for practical applications, going beyond linear perturbations and including the numerical solution of the full Einstein equations along hyperboloidal surfaces [169, 170].

Much of the current work has focused on asymptotically flat, vacuum spacetimes. The formalism for black hole perturbation theory is fully developed for spherically symmetric spacetimes, but the same concepts are also valid for the Kerr solution [102, 113]. The hyperboloidal approach is versatile and extendable to more general settings, including those with different asymptotic structures, and nonvaccum spacetimes. Developing these extensions will be crucial for applying this framework to a broader range of physical scenarios.

Author contributions

RP: Writing–original draft, Writing–review and editing. AZ: Writing–original draft, Writing–review and editing.

Funding

The author(s) declare that financial support was received for the research, authorship, and/or publication of this article. RPM acknowledges support from the Villum Investigator program supported by the VILLUM Foundation (grant no. VIL37766) and the DNRF Chair program (grant no. DNRF162) by the Danish National Research Foundation and the European Union's Horizon 2020 research and innovation programme under the Marie Sklodowska-Curie grant agreement No 101131233. AZ is supported by the National Science Foundation under Grant No. 2309084.

Conflict of interest

The authors declare that the research was conducted in the absence of any commercial or financial relationships that could be construed as a potential conflict of interest.

Publisher's note

All claims expressed in this article are solely those of the authors and do not necessarily represent those of their affiliated organizations, or those of the publisher, the editors and the reviewers. Any product that may be evaluated in this article, or claim that may be made by its manufacturer, is not guaranteed or endorsed by the publisher.

References

1. Kokkotas KD, Schmidt BG. Quasi-normal modes of stars and black holes. *Living Rev Relativity* (1999) 2:2–72. doi:10.12942/lrr-1999-2

2. Nollert HP. Quasinormal modes: the characteristic 'sound' of black holes and neutron stars. *Classical Quan Gravity* (1999) 16:R159–216. doi:10.1088/0264-9381/16/12/201

3. Berti E, Cardoso V, Starinets AO. Quasinormal modes of black holes and black branes. *Classical Quan Gravity* (2009) 26:163001. doi:10.1088/0264-9381/26/16/163001

4. Konoplya RA, Zhidenko A. Quasinormal modes of black holes: from astrophysics to string theory. *Rev Mod Phys* (2011) 83:793–836. doi:10.1103/RevModPhys.83.793

5. Dreyer O, Kelly BJ, Krishnan B, Finn LS, Garrison D, Lopez-Aleman R. Black hole spectroscopy: testing general relativity through gravitational wave observations. *Class Quant Grav* (2004) 21:787–803. doi:10.1088/0264-9381/21/4/003

6. Berti E, Cardoso V, Will CM. Gravitational-wave spectroscopy of massive black holes with the space interferometer LISA. *Phys Rev D* (2006) 73:064030. doi:10.1103/PhysRevD.73.064030

7. Berti E, Sesana A, Barausse E, Cardoso V, Belczynski K. Spectroscopy of Kerr black holes with Earth- and space-based interferometers. *Phys Rev Lett* (2016) 117:101102. doi:10.1103/PhysRevLett.117.101102

8. Franchini N, Völkel SH. Testing general relativity with black hole quasi-normal modes. *arXiv:2305.01696* (2023). doi:10.1007/978-981-97-2871-8_9

9. Abbott BP, Abbott R, Abbott T, Abernathy M, Acernese F, Ackley K, et al. Observation of gravitational waves from a binary black hole merger. *Phys Rev Lett* (2016) 116:061102. doi:10.1103/PhysRevLett.116.061102

10. Abbott R, Abbott T, Abraham S, Acernese F, Ackley K, Adams A, et al. Tests of general relativity with binary black holes from the second LIGO-Virgo gravitational-wave transient catalog. *Phys Rev D* (2021) 103:122002. doi:10.1103/PhysRevD.103.122002

11. The LIGO Scientific Collaboration, the Virgo Collaboration, the KAGRA Collaboration, Abbott R, Abe H, Acernese F, et al. Tests of general relativity with GWTC-3 (2021) arXiv:2112.06861.

12. Isi M, Giesler M, Farr WM, Scheel MA, Teukolsky SA. Testing the no-hair theorem with GW150914. *Phys Rev Lett* (2019) 123:111102. doi:10.1103/PhysRevLett.123.111102

13. Capano CD, Nitz AH. Binary black hole spectroscopy: a no-hair test of GW190814 and GW190412. *Phys Rev D* (2020) 102:124070. doi:10.1103/PhysRevD.102.124070

14. Capano CD, Cabero M, Westerweck J, Abedi J, Kastha S, Nitz AH, et al. Multimode quasinormal spectrum from a perturbed black hole. *Phys Rev Lett* (2023) 131:221402. doi:10.1103/PhysRevLett.131.221402

15. Cotesta R, Carullo G, Berti E, Cardoso V. Analysis of ringdown overtones in GW150914. *Phys Rev Lett* (2022) 129:111102. doi:10.1103/PhysRevLett.129.111102

16. Capano CD, Abedi J, Kastha S, Nitz AH, Westerweck J, Wang YF, et al. Estimating false alarm rates of sub-dominant quasi-normal modes in GW190521 class. *Quantum Grav* (2024) 41:245009. doi:10.1088/1361-6382/ad84ae

17. Forteza XJ, Bhagwat S, Kumar S, Pani P. Novel ringdown amplitude-phase consistency test. *Phys Rev Lett* (2023) 130:021001. doi:10.1103/PhysRevLett.130.021001

18. Finch E, Moore CJ. Searching for a ringdown overtone in GW150914. *Phys Rev D* (2022) 106:043005. doi:10.1103/PhysRevD.106.043005

19. Abedi J, Capano CD, Kastha S, Nitz AH, Wang YF, Westerweck J, et al. Spectroscopy for asymmetric binary black hole mergers. *Phys Rev D* (2023) 108:104009. doi:10.1103/PhysRevD.108.104009

20. Carullo G, Cotesta R, Berti E, Cardoso V, Carullo et al. Reply:. *Phys Rev Lett* (2023) 131:169002. doi:10.1103/PhysRevLett.131.169002

21. Baibhav V, Cheung MHY, Berti E, Cardoso V, Carullo G, Cotesta R, et al. Agnostic black hole spectroscopy: quasinormal mode content of numerical relativity waveforms and limits of validity of linear perturbation theory. *Phys Rev D* (2023) 108:104020. doi:10.1103/PhysRevD.108.104020

22. Nee PJ, Völkel SH, Pfeiffer HP. Role of black hole quasinormal mode overtones for ringdown analysis. *Phys Rev D* (2023) 108:044032. doi:10.1103/PhysRevD.108.044032

23. Zhu H, Ripley JL, Cárdenas-Avendaño A, Pretorius F. Challenges in quasinormal mode extraction: perspectives from numerical solutions to the Teukolsky equation. *Phys Rev D* (2024) 109:044010. doi:10.1103/PhysRevD.109.044010

24. Siegel H, Isi M, Farr WM. Ringdown of GW190521: hints of multiple quasinormal modes with a precessional interpretation. *Phys Rev D* (2023) 108:064008. doi:10.1103/PhysRevD.108.064008

25. Gennari V, Carullo G, Del Pozzo W. Searching for ringdown higher modes with a numerical relativity-informed post-merger model. *Eur Phys J C* (2024) 84:233. doi:10.1140/epjc/s10052-024-12550-x

26. Schmidt BG. *On relativistic stellar oscillations*. Massachusetts, United States: Gravity Research Foundation essay (1993).

27. Zenginoğlu A. A geometric framework for black hole perturbations. *Phys Rev D* (2011) 83:127502. doi:10.1103/PhysRevD.83.127502

28. Ansorg M, Macedo RP. Spectral decomposition of black-hole perturbations on hyperboloidal slices. *Phys Rev D* (2016) 93:124016. doi:10.1103/PhysRevD.93.124016

29. Horowitz GT, Hubeny VE. Quasinormal modes of ads black holes and the approach to thermal equilibrium. *Phys Rev D* (2000) 62:024027. doi:10.1103/physrevd.62.024027

30. Vasy A. Microlocal analysis of asymptotically hyperbolic and kerr-de sitter spaces (with an appendix by semyon dyatlov). *Inventiones mathematicae* (2013) 194:381–513. doi:10.1007/s00222-012-0446-8

31. Warnick CM. On quasinormal modes of asymptotically anti-de Sitter black holes. *Commun Math Phys* (2015) 333:959–1035. doi:10.1007/s00220-014-2171-1

32. Gajic D, Warnick C. A model problem for quasinormal ringdown of asymptotically flat or extremal black holes. *J Math Phys* (2020) 61:102501. doi:10.1063/5.0024699

33. Gajic D, Warnick CM. Quasinormal modes on Kerr spacetimes. *arXiv preprint gr-qc:2407* (2024):04098. Available at: https://arxiv.org/abs/2407.04098.

34. Vishveshwara CV. Scattering of gravitational radiation by a schwarzschild black-hole. *Nature* (1970) 227:936–8. doi:10.1038/227936a0

35. Price RH. Nonspherical perturbations of relativistic gravitational collapse. i. scalar and gravitational perturbations. *Phys Rev D* (1972) 5:2419–38. doi:10.1103/PhysRevD.5.2419

36. Gundlach C, Price RH, Pullin J. Late-time behavior of stellar collapse and explosions. i. linearized perturbations. *Phys Rev D* (1994) 49:883–9. doi:10.1103/PhysRevD.49.883

37. Sommerfeld A. Die greensche funktion der schwingungsgleichung. *J.-Ber Deutsch Math.-Verein* (1912) 21:309–53. Available at: https://eudml.org/doc/145344.

38. Schot SH. Eighty years of Sommerfeld's radiation condition. *Historia Mathematica* (1992) 19:385–401. doi:10.1016/0315-0860(92)90004-U

39. Nollert HP, Schmidt BG. Quasinormal modes of schwarzschild black holes: defined and calculated via laplace transformation. *Phys Rev D* (1992) 45:2617–27. doi:10.1103/PhysRevD.45.2617

40. Bachelot A, Motet-Bachelot A. Les résonances d'un trou noir de schwarzschild. *Ann de l'IHP Physique théorique* (1993) 59:3–68. Available at: http://www.numdam.org/item/AIHPA_1993__59_1_3_0/.

41. Leaver EW. Spectral decomposition of the perturbation response of the schwarzschild geometry. *Phys Rev D* (1986) 34:384–408. doi:10.1103/PhysRevD.34.384

42. Sun Y, Price RH. Excitation of quasinormal ringing of a schwarzschild black hole. *Phys Rev D* (1988) 38:1040–52. doi:10.1103/PhysRevD.38.1040

43. Kay BS, Wald RM. Linear stability of Schwarzschild under perturbations which are non-vanishing on the bifurcation 2-sphere. *Class Quan Gravity* (1987) 4:893–8. doi:10.1088/0264-9381/4/4/022

44. Zworski M. Mathematical study of scattering resonances. *Bull Math Sci* (2017) 7:1–85. doi:10.1007/s13373-017-0099-4

45. Dyatlov S, Zworski M. Mathematical theory of scattering resonances. American Mathematical Society (2019) Graduate Studies in Mathematics.

46. Israel W. *Dark stars: the evolution of an idea*. Cambridge, United Kingdom: Three hundred years of gravitation (1987) p. 199–276.

47. Senovilla JMM, Garfinkle D. The 1965 Penrose singularity theorem. *Classical Quan Gravity* (2015) 32:124008. doi:10.1088/0264-9381/32/12/124008

48. Nielsen N. On the origin of the Gullstrand–Painlevé coordinates. *The Eur Phys J H* (2022) 47:6. doi:10.1140/epjh/s13129-022-00038-9

49. Landsman K. Penrose's 1965 singularity theorem: from geodesic incompleteness to cosmic censorship. *Gen Relativity Gravitation* (2022) 54:115. doi:10.1007/s10714-022-02973-w

50. Friedman JL, Schutz BF. On the stability of relativistic systems. *The Astrophysical J* (1975) 200:204–20. doi:10.1086/153778

51. Minkowski H. *Raum und Zeit (Jahresbericht der Deutschen Mathematiker-Vereinigung)* (1908) p. 75–88.

52. Milne EA. Relativity, gravitation, and world-structure. *Philosophy* (1936) 11. Available at: https://archive.org/details/dli.ernet.7948/page/n3/mode/2up.

53. Dirac PA. Forms of relativistic dynamics. *Rev Mod Phys* (1949) 21:392–9. doi:10.1103/revmodphys.21.392

54. Chen YW, Lewy H. Solutions of the n-dimensional wave equation in the exterior of the characteristic cones (I). *Indiana Univ Mathematics J* (1970) 20:33–55. doi:10.1512/iumj.1971.20.20003

55. Chen YW, Lewy H. On the hyperboloidal means and the wave equation. *Indiana Univ Mathematics J* (1971) 21:437–47. Available at: https://www.jstor.org/stable/24890372.

56. Strichartz RS. Harmonic analysis on hyperboloids. *J Funct Anal* (1973) 12:341–83. doi:10.1016/0022-1236(73)90001-3

57. Fubini S, Hanson AJ, Jackiw R. New approach to field theory. *Phys Rev D* (1973) 7:1732–60. doi:10.1103/physrevd.7.1732

58. DiSessa A. Quantization on hyperboloids and full space-time field expansion. *J Math Phys* (1974) 15:1892–900. doi:10.1063/1.1666554

59. Sommerfield CM. Quantization on spacetime hyperboloids. *Ann Phys* (1974) 84:285–302. doi:10.1016/0003-4916(74)90304-2

60. Hostler L. Coulomb-like quantization of the electromagnetic field on spacelike hyperboloids. *J Math Phys* (1978) 19:2094–9. doi:10.1063/1.523565

61. Penrose R. Zero rest-mass fields including gravitation: asymptotic behaviour. *Proc R Soc Lond Ser A. Math Phys Sci* (1965) 284:159–203. doi:10.1098/rspa.1965.0058

62. Penrose R. Asymptotic properties of fields and space-times. *Phys Rev Lett* (1963) 10:66–8. doi:10.1103/PhysRevLett.10.66

63. Zenginoğlu A. Hyperbolic times in Minkowski space. *Am J Phys* (2024) 92:965–74. doi:10.1119/5.0214271

64. Smarr L, York JW. Kinematical conditions in the construction of spacetime. *Phys Rev D* (1978) 17:2529–51. doi:10.1103/PhysRevD.17.2529

65. Eardley DM, Smarr L. Time functions in numerical relativity: marginally bound dust collapse. *Phys Rev D* (1979) 19:2239–59. doi:10.1103/PhysRevD.19.2239

66. Brill DR, Cavallo JM, Isenberg JA. *K* -surfaces in the Schwarzschild space-time and the construction of lattice cosmologies. *J Math Phys* (1980) 21:2789–96. doi:10.1063/1.524400

67. Gowdy RH. The wave equation in asymptotically retarded time coordinates: waves as simple, regular functions on a compact manifold. *J Math Phys* (1981) 22:675–8. doi:10.1063/1.524975

68. Friedrich H. Cauchy problems for the conformal vacuum field equations in general relativity. *Commun Math Phys* (1983) 91:445–72. doi:10.1007/bf01206015

69. Friedrich H. Existence and structure of past asymptotically simple solutions of einstein's field equations with positive cosmological constant. *J Geometry Phys* (1986) 3:101–17. doi:10.1016/0393-0440(86)90004-5

70. Friedrich H. On the existence of n-geodesically complete or future complete solutions of einstein's field equations with smooth asymptotic structure. *Commun Math Phys* (1986) 107:587–609. doi:10.1007/bf01205488

71. Frauendiener J. Conformal infinity. *Living Rev Relativity* (2004) 7:1. doi:10.12942/lrr-2004-1

72. Kroon JAV. *Conformal methods in general relativity*. Cambridge: Cambridge University Press (2016).

73. Moncrief V. Conformally regular ADM evolution equations (2000) Available from: Http://online.itp.ucsb.edu/online/numrel00/moncrief (Accessed December 27, 2024).

74. Husa S. Numerical relativity with the conformal field equations. In: *Current trends in relativistic astrophysics: theoretical, numerical, observational*. Springer (2003) p. 159–92.

75. Fodor G, Racz I. What does a strongly excited 't Hooft-Polyakov magnetic monopole do? *Phys Rev Lett* (2004) 92:151801. doi:10.1103/physrevlett.92.151801

76. Fodor G, Racz I. Numerical investigation of highly excited magnetic monopoles in su (2) yang-mills-higgs theory. *Phys Rev D—Particles, Fields, Gravitation, Cosmology* (2008) 77:025019. doi:10.1103/physrevd.77.025019

77. Bizoń P, Zenginoğlu A. Universality of global dynamics for the cubic wave equation. *Nonlinearity* (2009) 22:2473–85. doi:10.1088/0951-7715/22/10/009

78. Gentle AP, Holz DE, Kheyfets A, Laguna P, Miller WA, Shoemaker DM. Constant crunch coordinates for black hole simulations. *Phys Rev D* (2001) 63:064024. doi:10.1103/PhysRevD.63.064024

79. Gowdy RH. The compactification of initial data on constant mean curvature time slices in spherically symmetric spacetimes. *arXiv:gr-qc/0107016* (2001). Available at: https://arxiv.org/abs/gr-qc/0107016.

80. Schmidt BG. Data for the numerical calculation of the kruskal space-time. In: R Beig, BG Englert, U Frisch, P Hänggi, K Hepp, W Hillebrandt, et al. editors. *The conformal structure of space-time*, 604. Berlin, Heidelberg: Springer Berlin Heidelberg (2002) p. 283–95. doi:10.1007/3-540-45818-2_14

81. Pareja MJ, Frauendiener J. Constant scalar curvature hypersurfaces in extended Schwarzschild space-time. *Phys Rev D* (2006) 74:044026. doi:10.1103/PhysRevD.74.044026

82. Calabrese G, Gundlach C, Hilditch D. Asymptotically null slices in numerical relativity: mathematical analysis and spherical wave equation tests. *Classical Quan Gravity* (2006) 23:4829–45. doi:10.1088/0264-9381/23/15/004

83. Misner CW, van Meter JR, Fiske DR. Excising das All: Evolving Maxwell waves beyond scri. *Phys Rev D—Particles, Fields, Gravitation, Cosmology* (2006) 74:064003. doi:10.1103/physrevd.74.064003

84. Zenginoğlu A. Hyperboloidal foliations and scri-fixing. *Classical Quan Gravity* (2008) 25:145002. doi:10.1088/0264-9381/25/14/145002

85. Zenginoğlu A. A hyperboloidal study of tail decay rates for scalar and Yang–Mills fields. *Classical Quan gravity* (2008) 25:175013. doi:10.1088/0264-9381/25/17/175013

86. Zenginoğlu A, Nunez D, Husa S. Gravitational perturbations of schwarzschild spacetime at null infinity and the hyperboloidal initial value problem. *Classical Quan Gravity* (2009) 26:035009. doi:10.1088/0264-9381/26/3/035009

87. Zenginoğlu A, Tiglio M. Spacelike matching to null infinity. *Phys Rev D* (2009) 80:024044. doi:10.1103/PhysRevD.80.024044

88. Zenginoğlu A. Asymptotics of Schwarzschild black hole perturbations. *Classical Quan Gravity* (2010) 27:045015. doi:10.1088/0264-9381/27/4/045015

89. Zenginoğlu A, Kidder LE. Hyperboloidal evolution of test fields in three spatial dimensions. *Phys Rev D* (2010) 81:124010. doi:10.1103/physrevd.81.124010

90. Bizoń P, Rostworowski A, Zenginoğlu A. Saddle-point dynamics of a Yang–Mills field on the exterior Schwarzschild spacetime. *Classical Quan Gravity* (2010) 27:175003. doi:10.1088/0264-9381/27/17/175003

91. Lora-Clavijo F, Cruz-Osorio A, Guzmán F. Evolution of a massless test scalar field on boson star space-times. *Phys Rev D* (2010) 82:023005. doi:10.1103/physrevd.82.023005

92. Jasiulek M. Hyperboloidal slices for the wave equation of kerr–schild metrics and numerical applications. *Classical Quan gravity* (2011) 29:015008. doi:10.1088/0264-9381/29/1/015008

93. Racz I, Tóth GZ. Numerical investigation of the late-time Kerr tails. *Classical Quan Gravity* (2011) 28:195003. doi:10.1088/0264-9381/28/19/195003

94. Vega I, Wardell B, Diener P. Effective source approach to self-force calculations. *Classical Quan Gravity* (2011) 28:134010. doi:10.1088/0264-9381/28/13/134010

95. Bernuzzi S, Nagar A, Zenginoğlu A. Binary black hole coalescence in the extreme-mass-ratio limit: testing and improving the effective-one-body multipolar waveform. *Phys Rev D* (2011) 83:064010. doi:10.1103/PhysRevD.83.064010

96. Bernuzzi S, Nagar A, Zenginoğlu A. Binary black hole coalescence in the large-mass-ratio limit: the hyperboloidal layer method and waveforms at null infinity. *Phys Rev D* (2011) 84:084026. doi:10.1103/PhysRevD.84.084026

97. Zenginoğlu A, Khanna G. Null infinity waveforms from extreme-mass-ratio inspirals in kerr spacetime. *Phys Rev X* (2011) 1:021017. doi:10.1103/physrevx.1.021017

98. Schinkel D, Ansorg M, Macedo RP. Initial data for perturbed Kerr black holes on hyperboloidal slices. *Classical Quan Gravity* (2014) 31:165001. doi:10.1088/0264-9381/31/16/165001

99. Panosso Macedo R, Jaramillo JL, Ansorg M. Hyperboloidal slicing approach to quasi-normal mode expansions: the Reissner-Nordström case. *Phys Rev D* (2018) 98:124005. doi:10.1103/PhysRevD.98.124005

100. Panosso Macedo R. Hyperboloidal approach for static spherically symmetric spacetimes: a didactical introduction and applications in black-hole physics. *Phil Trans Roy Soc Lond A* (2024) 382:20230046. doi:10.1098/rsta.2023.0046

101. Aimer JWA. Quasinormal modes of black holes (2023). New Zealand: University of Canterbury Christchurch. Doctoral dissertation. doi:10.26021/14994

102. Ripley JL. Computing the quasinormal modes and eigenfunctions for the Teukolsky equation using horizon penetrating, hyperboloidally compactified coordinates. *Class Quant Grav* (2022) 39:145009. doi:10.1088/1361-6382/ac776d

103. Leaver EW. An analytic representation for the quasi-normal modes of kerr black holes. *Proc R Soc Lond A. Math Phys Sci* (1985) 402:285–98. doi:10.1098/rspa.1985.0119

104. Leaver EW. Quasinormal modes of Reissner-Nordström black holes. *prd* (1990) 41:2986–97. doi:10.1103/PhysRevD.41.2986

105. Dolan SR, Ottewill AC. On an expansion method for black hole quasinormal modes and Regge Poles. *Classical Quan Gravity* (2009) 26:225003. doi:10.1088/0264-9381/26/22/225003

106. Dolan SR. Quasinormal mode spectrum of a Kerr black hole in the eikonal limit. *Phys Rev D* (2010) 82:104003. doi:10.1103/PhysRevD.82.104003

107. Jansen A. Overdamped modes in Schwarzschild-de Sitter and a Mathematica package for the numerical computation of quasinormal modes. *The Eur Phys J Plus* (2017) 132:546. doi:10.1140/epjp/i2017-11825-9

108. Langlois D, Noui K, Roussille H. Black hole perturbations in modified gravity. *Phys Rev D* (2021) 104:124044. doi:10.1103/PhysRevD.104.124044

109. Langlois D, Noui K, Roussille H. Asymptotics of linear differential systems and application to quasinormal modes of nonrotating black holes. *Phys Rev D* (2021) 104:124043. doi:10.1103/PhysRevD.104.124043

110. Chung AKW, Wagle P, Yunes N. Spectral method for the gravitational perturbations of black holes: schwarzschild background case. *Phys Rev D* (2023) 107:124032. doi:10.1103/PhysRevD.107.124032

111. Chung AKW, Wagle P, Yunes N. Spectral method for metric perturbations of black holes: kerr background case in general relativity (2023) doi:10.48550/arXiv.2312.08435

112. Jaramillo JL, Panosso Macedo R, Al Sheikh L. Pseudospectrum and black hole quasinormal mode instability. *Phys Rev X* (2021) 11:031003. doi:10.1103/PhysRevX.11.031003

113. Panosso Macedo R. Hyperboloidal framework for the Kerr spacetime. *Class Quant Grav* (2020) 37:065019. doi:10.1088/1361-6382/ab6e3e

114. Gajic D, Warnick C. Quasinormal modes in extremal reissner–nordström spacetimes. *Commun Math Phys* (2021) 385:1395–498. doi:10.1007/s00220-021-04137-4

115. Bizoń P, Chmaj T, Mach P. A toy model of hyperboloidal approach to quasinormal modes. *Acta Physica Pol B* (2020) 51:1007. doi:10.5506/APhysPolB.51.1007

116. Warnick C. (In)completeness of quasinormal modes. *Acta Physica Pol B Proc Suppl* (2022) 15:1. doi:10.5506/APhysPolBSupp.15.1-A13

117. Carullo G. Ringdown amplitudes of nonspinning eccentric binaries. *arXiv preprint gr-qc:2406* (2024) 19442. doi:10.1088/1475-7516/2024/10/061

118. Berti E, Cardoso V. Quasinormal ringing of Kerr black holes: the excitation factors. *Phys Rev D* (2006) 74:104020. doi:10.1103/PhysRevD.74.104020

119. Zimmerman A, Yang H, Mark Z, Chen Y, Lehner L. Quasinormal modes beyond kerr. *Astrophys Space Sci Proc* (2015) 40:217–23. doi:10.1007/978-3-319-10488-1_19

120. Green SR, Hollands S, Sberna L, Toomani V, Zimmerman P. Conserved currents for a Kerr black hole and orthogonality of quasinormal modes. *Phys Rev D* (2023) 107:064030. doi:10.1103/PhysRevD.107.064030

121. London LT. A radial scalar product for Kerr quasinormal modes. *ArXiv: 2312.17678* (2023). Available at: https://arxiv.org/abs/2312.17678.

122. Ammon M, Grieninger S, Jimenez-Alba A, Macedo RP, Melgar L. Holographic quenches and anomalous transport. *JHEP* (2016) 09:131. doi:10.1007/JHEP09(2016)131

123. Besson J, Jaramillo JL. Quasi-normal mode expansions of black hole perturbations: a hyperboloidal Keldysh's approach. *arXiv preprint gr-qc:2412* (2024):02793. Available at: https://arxiv.org/abs/2412.02793.

124. Zenginoğlu A, Khanna G, Burko LM. Intermediate behavior of Kerr tails. *Gen Rel Grav* (2014) 46:1672. doi:10.1007/s10714-014-1672-8

125. Cardoso V, Carullo G, De Amicis M, Duque F, Katagiri T, Pereniguez D, et al. Hushing black holes: tails in dynamical spacetimes. *Phys Rev D* (2024) 109:L121502. doi:10.1103/PhysRevD.109.L121502

126. De Amicis M, Albanesi S, Carullo G. Inspiral-inherited ringdown tails. *arXiv preprint gr-qc:2406* (2024) 17018. Available at: https://arxiv.org/abs/2406.17018.

127. London L, Shoemaker D, Healy J. Modeling ringdown: beyond the fundamental quasinormal modes. *Phys Rev D* (2014) 90:124032. Erratum: Phys.Rev.D 94, 069902 (2016). doi:10.1103/PhysRevD.90.124032

128. Cheung MHY, Baibhav V, Berti E, Cardoso V, Carullo G, Cotesta R, et al. Nonlinear effects in black hole ringdown. *Phys Rev Lett* (2023) 130:081401. doi:10.1103/PhysRevLett.130.081401

129. Mitman K, Lagos M, Stein LC, Ma S, Hui L, Chen Y, et al. Nonlinearities in black hole ringdowns. *Phys Rev Lett* (2023) 130:081402. doi:10.1103/PhysRevLett.130.081402

130. Zlochower Y, Gomez R, Husa S, Lehner L, Winicour J. Mode coupling in the nonlinear response of black holes. *Phys Rev D* (2003) 68:084014. doi:10.1103/PhysRevD.68.084014

131. Sberna L, Bosch P, East WE, Green SR, Lehner L. Nonlinear effects in the black hole ringdown: absorption-induced mode excitation. *Phys Rev D* (2022) 105:064046. doi:10.1103/PhysRevD.105.064046

132. Redondo-Yuste J, Carullo G, Ripley JL, Berti E, Cardoso V. Spin dependence of black hole ringdown nonlinearities. *Phys Rev D* (2024) 109:L101503. doi:10.1103/PhysRevD.109.L101503

133. Cheung MHY, Berti E, Baibhav V, Cotesta R. Extracting linear and nonlinear quasinormal modes from black hole merger simulations. *arXiv preprint gr-qc:2310.04489* (2023). Available at: https://arxiv.org/abs/2310.04489.

134. Ma S, Yang H. Excitation of quadratic quasinormal modes for Kerr black holes. *Phys Rev D* (2024) 109:104070. doi:10.1103/PhysRevD.109.104070

135. Zhu H, Ripley JL, Pretorius F, Ma S, Mitman K, Owen R, et al. Nonlinear effects in black hole ringdown from scattering experiments: spin and initial data dependence of quadratic mode coupling. *Phys Rev D* (2024) 109:104050. doi:10.1103/PhysRevD.109.104050

136. Bucciotti B, Juliano L, Kuntz A, Trincherini E. Quadratic quasi-normal modes of a schwarzschild black hole. *arXiv preprint gr-qc:2405* (2024):06012. doi:10.1007/JHEP09(2024)119

137. Brizuela D, Martin-Garcia JM, Tiglio M. Complete gauge-invariant formalism for arbitrary second-order perturbations of a Schwarzschild black hole. *Phys Rev D* (2009) 80:024021. doi:10.1103/PhysRevD.80.024021

138. Loutrel N, Ripley JL, Giorgi E, Pretorius F. Second-order perturbations of Kerr black holes: formalism and reconstruction of the first-order metric. *Phys Rev D* (2021) 103:104017. doi:10.1103/PhysRevD.103.104017

139. Spiers A, Pound A, Moxon J. Second-order Teukolsky formalism in Kerr spacetime: formulation and nonlinear source. *Phys Rev D* (2023) 108:064002. doi:10.1103/PhysRevD.108.064002

140. May T, Ma S, Ripley JL, East WE. Nonlinear effect of absorption on the ringdown of a spinning black hole. *arXiv preprint gr-qc:2405* (2024):18303. doi:10.1103/PhysRevD.110.084034

141. Bourg P, Panosso Macedo R, Spiers A, Leather B, Bonga B, Pound A. Quadratic quasi-normal mode dependence on linear mode parity. *In preparation* (2024). Available at: https://arxiv.org/abs/2405.10270.

142. Vishveshwara CV. On the black hole trail.: a personal journey. *Curr Sci* (1996) 71:824–30.

143. Aguirregabiria JM, Vishveshwara CV. Scattering by black holes: a Simulated potential approach. *Phys Lett A* (1996) 210:251–4. doi:10.1016/0375-9601(95)00937-X

144. Nollert HP. About the significance of quasinormal modes of black holes. *Phys Rev D* (1996) 53:4397–402. doi:10.1103/PhysRevD.53.4397

145. Nollert HP, Price RH. Quantifying excitations of quasinormal mode systems. *J Math Phys* (1999) 40:980–1010. doi:10.1063/1.532698

146. Jaramillo JL, Panosso Macedo R, Sheikh LA. Gravitational wave signatures of black hole quasinormal mode instability. *Phys Rev Lett* (2022) 128:211102. doi:10.1103/PhysRevLett.128.211102

147. Gasperin E, Jaramillo JL. Energy scales and black hole pseudospectra: the structural role of the scalar product. *Class Quant Grav* (2022) 39:115010. doi:10.1088/1361-6382/ac5054

148. Cheung MHY, Destounis K, Macedo RP, Berti E, Cardoso V. Destabilizing the fundamental mode of black holes: the elephant and the flea. *Phys Rev Lett* (2022) 128:111103. doi:10.1103/PhysRevLett.128.111103

149. Al Sheikh L. Scattering resonances and Pseudospectrum: stability and completeness aspects in optical and gravitational systems. Besançon, France: Université Bourgogne Franche-Comté (2022). Theses.

150. Berti E, Cardoso V, Cheung MHY, Di Filippo F, Duque F, Martens P, et al. Stability of the fundamental quasinormal mode in time-domain observations against small perturbations. *Phys Rev D* (2022) 106:084011. doi:10.1103/PhysRevD.106.084011

151. Jaramillo JL. Pseudospectrum and binary black hole merger transients. *Class Quant Grav* (2022) 39:217002. doi:10.1088/1361-6382/ac8ddc

152. Cardoso V, Kastha S, Panosso Macedo R. Physical significance of the black hole quasinormal mode spectra instability. *Phys Rev D* (2024) 110:024016. doi:10.1103/PhysRevD.110.024016

153. Hirano S, Kimura M, Yamaguchi M, Zhang J. Parametrized black hole quasinormal ringdown formalism for higher overtones. *Phys Rev D* (2024) 110:024015. doi:10.1103/PhysRevD.110.024015

154. Warnick C. (In)stability of de Sitter quasinormal mode spectra. *Front Appl Mathematics Stat* (2024) 10:1472401. doi:10.3389/fams.2024.1472401

155. Boyanov V. On destabilising quasi-normal modes with a radially concentrated perturbation. *arXiv preprint gr-qc:2410* (2024) 11547. Available at: https://arxiv.org/abs/2410.11547.

156. Galkowski J, Zworski M. Outgoing solutions via gevrey-2 properties. *arXiv preprint math.AP:2004* (2020) 07868. doi:10.1007/s40818-021-00094-2

157. Trefethen L, Embree M. *Spectra and pseudospectra: the behavior of nonnormal matrices and operators*. Princeton University Press (2005).

158. Destounis K, Macedo RP, Berti E, Cardoso V, Jaramillo JL. Pseudospectrum of Reissner-Nordström black holes: quasinormal mode instability and universality. *Phys Rev D* (2021) 104:084091. doi:10.1103/PhysRevD.104.084091

159. Boyanov V, Destounis K, Panosso Macedo R, Cardoso V, Jaramillo JL. Pseudospectrum of horizonless compact objects: a bootstrap instability mechanism. *Phys Rev D* (2023) 107:064012. doi:10.1103/PhysRevD.107.064012

160. Areán D, Fariña DG, Landsteiner K. Pseudospectra of holographic quasinormal modes. *JHEP* (2023) 12:187. doi:10.1007/JHEP12(2023)187

161. Sarkar S, Rahman M, Chakraborty S. Perturbing the perturbed: stability of quasinormal modes in presence of a positive cosmological constant. *Phys Rev D* (2023) 108:104002. doi:10.1103/PhysRevD.108.104002

162. Destounis K, Boyanov V, Panosso Macedo R. Pseudospectrum of de Sitter black holes. *Phys Rev D* (2024) 109:044023. doi:10.1103/PhysRevD.109.044023

163. Boyanov V, Cardoso V, Destounis K, Jaramillo JL, Panosso Macedo R. Structural aspects of the anti–de Sitter black hole pseudospectrum. *Phys Rev D* (2024) 109:064068. doi:10.1103/PhysRevD.109.064068

164. Cownden B, Pantelidou C, Zilhão M. The pseudospectra of black holes in AdS. *JHEP* (2024) 05:202. doi:10.1007/JHEP05(2024)202

165. Chen JN, Wu LB, Guo ZK. The pseudospectrum and transient of Kaluza-Klein black holes in Einstein-Gauss-Bonnet gravity (2024).

166. Carballo J, Withers B. Transient dynamics of quasinormal mode sums. *arXiv preprint hep-th:2406* (2024):06685. doi:10.1007/JHEP10(2024)084

167. Garcia-Fariña D, Landsteiner K, Romeu PG, Saura-Bastida P. Pseudospectra of complex momentum modes. *arXiv preprint hep-th:2407* (2024):06104. Available at: https://arxiv.org/abs/2407.06104.

168. Burgess C, König F. Hyperboloidal method for quasinormal modes of non-relativistic operators. *Front Phys* (2024) 12:1457543. doi:10.3389/fphy.2024.1457543

169. Peterson C, Gautam S, Vañó-Viñuales A, Hilditch D. Spherical evolution of the generalized harmonic gauge formulation of general relativity on compactified hyperboloidal slices. *arXiv preprint gr-qc:2409* (2024):02994. Available at: https://arxiv.org/abs/2409.02994.

170. Vañó-Viñuales A, Valente T. Height-function-based 4d reference metrics for hyperboloidal evolution. *arXiv preprint gr-qc:2408* (2024):08952. doi:10.1007/s10714-024-03323-8

frontiers | Frontiers in Physics

TYPE Brief Research Report
PUBLISHED 17 February 2025
DOI 10.3389/fphy.2024.1517192

Check for updates

OPEN ACCESS

EDITED BY
Jose Luis Jaramillo,
Université de Bourgogne, France

REVIEWED BY
Guangqing Feng,
Henan Polytechnic University, China
Philipp OJ Scherer,
Technical University of Munich, Germany

*CORRESPONDENCE
Fernando Abalos,
j.abalos@uib.es

RECEIVED 25 October 2024
ACCEPTED 30 December 2024
PUBLISHED 17 February 2025

CITATION
Abalos F, Reula O and Hilditch D (2025) Hyperbolic extensions of constrained PDEs. *Front. Phys.* 12:1517192. doi: 10.3389/fphy.2024.1517192

COPYRIGHT
© 2025 Abalos, Reula and Hilditch. This is an open-access article distributed under the terms of the Creative Commons Attribution License (CC BY). The use, distribution or reproduction in other forums is permitted, provided the original author(s) and the copyright owner(s) are credited and that the original publication in this journal is cited, in accordance with accepted academic practice. No use, distribution or reproduction is permitted which does not comply with these terms.

Hyperbolic extensions of constrained PDEs

Fernando Abalos [1]*, Oscar Reula [2] and David Hilditch [3]

[1]Departament de Física and Institute of Applied Computing & Community Code (IAC3), Universitat de les Illes Balears, Palma deMallorca, Spain, [2]Facultad de Matemática, Astronomía y Física, Universidad Nacional de Córdoba and IFEG-CONICET, Ciudad Universitaria, Córdoba, Argentina, [3]CENTRA, Departamento de Física, Instituto Superior Técnico IST, Universidade de Lisboa UL, Lisboa, Portugal

Systems of partial differential equations (PDEs) comprising a combination of constraints and evolution equations are ubiquitous in physics. For both theoretical and practical reasons, such as numerical integration, it is desirable to have a systematic understanding of the well-posedness of the Cauchy problem for these systems. In this article, we first review the use of hyperbolic reductions, where the evolution equations are singled out for consideration. We then examine in greater detail the extensions, namely, systems in which constraints are evolved as auxiliary variables alongside the original variables, resulting in evolution systems with no constraints. Assuming a particular structure of the original system, we provide sufficient conditions for the strong hyperbolicity of an extension. Finally, this theory is applied to the examples of electromagnetism and a toy model of magnetohydrodynamics.

KEYWORDS

well-posed initial value problem, constraint equations, evolution equations, extensions, singular value decomposition (SVD), Kronecker decomposition, electromagnetism, magnetohydrodynamics

1 Introduction

In this work, we continue [1–4] the study of first-order systems of equations in which there are more equations than unknowns, but with a structure that permits, in principle, splitting suitable linear combinations of them into "evolution" and "constraint" equations. We restrict to the case of consistent systems, in which the number of equations is equal to the number of constraints plus the number of independent variables, and furthermore to the special case in which the number of independent variables matches the number of evolution equations. The latter means that we do not consider systems with gauge freedom remaining, which would imply the existence of variables with unspecified equations of motion. In this case, one can attempt a solution by carefully restricting the initial data and then directly solving the evolution equations. For an introductory review, see Hilditch [5]. One must then check that the constraint equations are satisfied in the time development. For this, integrability identities among the whole system of equations must be satisfied. These conditions will be assumed and spelled out in detail below. This "free evolution approach" requires us to establish the well-posedness of the Cauchy problem Gustafsson et al. [6]; Kreiss and Ortiz [7] (for a review of well-posedness applied to general relativity, see Sarbach and Tiglio [8]). We restrict ourselves to the concepts arising from the theory of strongly hyperbolic systems, in which well-posedness is determined by algebraic properties of the principal symbol of the equation system. For first-order systems, the principal symbol is simply the set of matrices multiplying the derivatives of the variables. The algebraic properties leading to well-posedness have

several equivalent characterizations summarized in the Kreiss matrix theorem Kreiss [9]. To assert well-posedness for the systems under consideration, we need to find a suitable square system, that is, a system where the number of variables equals the number of equations. This can be achieved by taking a subset of the equation system, called a *reduction*, resulting in a pure evolution system. The use of reductions is customary, but another possibility, which is often employed in numerical schemes, consists of making an *extension*, that is, extending the system by adding more variables. These extensions are commonly referred to as *divergence cleaning* [10]; Munz et al. [11, 12], from their use in magnetohydrodynamics, or as λ [13] or *Z-systems* [14] from their use in general relativity.

A paradigmatic example is given by the Maxwell equations,

$$\nabla_a F^{ab} = J^b, \qquad \varepsilon^{dabc}\nabla_a F_{bc} = 0, \qquad \nabla_a J^a = 0,$$

where the unknowns are the components of the Faraday tensor F_{ab}, an anti-symmetric tensor (so there are a total of six independent variables). J^a, the current vector, is a given vector fixed in space-time, which has vanishing divergence. This is necessary due to the integrability identity $\nabla_b(\nabla_a F^{ab}) = 0$. We work here in four-dimensional space-time (M, g_{ab}) with the Levi–Civita derivative ∇_a associated with g_{ab}. There are thus a total of $8 = 4 + 4$ equations for F^{ab}, so six of them should be evolution equations, and the remaining two should be constraints. Introducing a time-like covector n_a, one finds that contraction with that vector on both equations gives constraint, that is, equations which have derivatives only in directions perpendicular to n_a; while projection on the space perpendicular to n_a gives equations that have derivatives along n^a for each of the independent components of F^{ab}. Thus, in the terminology introduced above, a reduction is obtained by taking only these projections as the evolution equations. The integrability identity and divergence property of J^a together imply that constraints are satisfied in the time development if they are at an initial surface.

On the other hand, an extension is given by adding two auxiliary constraint variables (Z_1, Z_2), one for each Maxwell constraint, and making a choice for their equations of motion. To accomplish this in a covariant fashion, we need to define two tensor fields (g_1, g_2). The proposed extended system is

$$\nabla_a F^{ab} + g_1^{ba}\nabla_a Z_1 = J^b, \qquad \varepsilon^{dabc}\nabla_a F_{bc} + g_2^{ba}\nabla_a Z_2 = 0, \qquad \nabla_a J^a = 0, \tag{1}$$

It turns out that if the symmetric parts of (g_1, g_2) are Lorentzian metrics whose cones have non-zero intersections among each other and with the cone of g, then the extended system is well-posed. (We use the mathematical notion of a cone; when needed, we use the term light cone to refer to their boundaries). The equations that were constraints are now evolution equations for (Z_1, Z_2), and the others acquire spatial derivatives of these fields. As mentioned above, such extensions have been employed with enormous success in numerical relativity [15–20] and computational astrophysics, with works introducing this approach for magnetohydrodynamics [11, 12]; Dedner et al. [10] is particularly influential. Here, we investigate the space of possible extensions that lead to well-posed Cauchy problems and how to construct them in a natural, covariant fashion.

The article is organized as follows. In Section 2, we define the type of systems to be considered, including the necessary conditions they must satisfy in order to have a well-posed Cauchy problem. In Section 3, we introduce the Kronecker decomposition of matrix pencils and explain its implications to the study of strongly hyperbolic systems. In Section 4, we formalize the framework for extensions. Given the considerable freedom in choosing them, we use the Kronecker decomposition as a guide for making these choices. In Section 5, we demonstrate how this framework applies to two concrete examples: Maxwell's electrodynamics and a toy model of magnetohydrodynamics (MHD). Finally, in Section 6, we conclude with discussions and provide comments on how this line of research is being further developed.

2 Preliminaries and notation

To fix notation, we specify the systems we consider, following the notation of Geroch [1]; Abalos and Reula [3]; Abalos [4]. We consider a manifold M of dimension n, and the following system of the quasi-linear first-order partial differential equations on the fields ϕ,

$$E^A := \mathfrak{N}_\alpha^{Aa}(x,\phi)\,\nabla_a\phi^\alpha - J^A(x,\phi) = 0, \tag{2}$$

where the indices A, a, α are abstract, grouping several tensorial indices into one and merely indicating where the contractions are. We use lower-case Latin indices to denote single vector indices, lower-case Greek indices to indicate variable fields, and upper-case Latin to label the equations space. The $|\cdot|$ function on indices indicates their total dimension.

We impose the following conditions on $\mathfrak{N}^{Aa}{}_\alpha(x,\phi)$:

Condition 1: the generalized Kreiss condition.

We assume that the matrix $\mathfrak{N}_\alpha^{Aa}(x,\phi)$ is smooth in all arguments and that there exists a hypersurface orthogonal covector n_a such that for all values of k_a, not proportional to n_a, the matrix pencil

$$\mathfrak{N}_\alpha^{Aa} l_a(\lambda) = \mathfrak{N}_\alpha^{Aa}(\lambda n_a + k_a),$$

has a kernel only for a finite set of real values $\{\lambda_i(k)\}$ of λ (the term matrix pencil refers here to the uni-parametric combination $\lambda\mathfrak{N} + \mathfrak{B}$, where $\mathfrak{N}$ and $\mathfrak{B}$ are matrices that do not depend on the parameter λ).

In addition, the corresponding singular values of $\mathfrak{N}_\alpha^{Aa} l_a(\lambda)$ approach zero in a linear way, that is, $\sigma(\lambda) \geq c_i|(\lambda - \lambda_i)|$, with $c_i > 0$ in a neighborhood of λ_i. We recall that the singular values are the square roots of the eigenvalues of $(\mathfrak{N}_\alpha^{Aa} l_a)^T(\mathfrak{N}_\beta^{Ab} l_b)$. Because this is an $|\alpha| \times |\alpha|$ matrix, there are $|\alpha|$ singular values (see Abalos [2] for more details and for a more general definition).

These conditions imply two things: *i*) the rank of $\mathfrak{N}_\alpha^{Aa}(x,\phi)\,n_a$ is maximal. Therefore, by defining any vector t^a transversal to the surface flat defined by n_a (i.e., $t^a n_a \neq 0$), we can obtain all field derivatives along t^a from their values and their derivatives at that surface. This means that we have enough evolution equations for each field ϕ^α. Observe that once we have a choice of n_a satisfying Condition 1, then there is an open set of covectors satisfying the same condition. Thus, we can always form hypersurfaces in a neighborhood of any point, leading to a local initial value problem; *ii*) In the case that the number of equations equals the number of variables, these conditions imply there is a well-posed Cauchy problem, in the usual sense for strongly hyperbolic systems, off of the mentioned surface. This is the classic Kreiss condition.

In case there are more equations than variables, we need to make sure that there are no more linearly independent equations having derivatives along the transversal vector t^a; otherwise, we would have an inconsistency because two equations could give different values for the same transversal derivative. To accomplish that, we impose:

Condition 2: the Geroch constraint condition.

If the number of equations is larger than the number of variables $|A| > |\alpha|$, then we assume there exists a set of matrices $C^{\Gamma a}_A$, which are labeled by upper-case Greek indices, with

$$C^{\Gamma(a}_A \mathfrak{N}^{|A|b)}{}_\alpha = 0,$$

and that $\mathrm{rank}(C^{\Gamma a}_A n_a) = |A| - |\alpha| = |\Gamma|$. This condition ensures that the rest of the equations do not have derivatives off of the surface defined by n_a, so that the system is consistent. Indeed, the following linear combination of equations, called constraints,

$$\psi^\Gamma := C^{\Gamma a}_A n_a \left(\mathfrak{N}^{Ab}_\alpha \nabla_b \phi^\alpha - J^A\right),$$

have only derivatives on the flat defined by n_a.

There is a further consistency condition that would guarantee that if the initial data are such that constraint quantities vanish at the initial surface, then they would also vanish along evolution [4]. We require the following:

Condition 3: integrability.

$$\nabla_d \left(C^{\Gamma d}_A E^A\right) = L^\Gamma_{1A}(x,\phi,\nabla\phi)\, E^A(x,\phi,\nabla\phi),$$

In other words, there is a particular on-shell identity among derivatives of our equation system. In most cases of physical interest, this identity is a consequence of gauge or diffeomorphism invariance.

3 Kronecker decomposition

When studying the well-posedness of the Cauchy problem, the relevant aspect is the behavior of the system in the limit of high frequencies. We can thus restrict our attention to a neighborhood of each point and work in the frequency domain, employing the Fourier–Laplace transform in space and time, respectively. Explicitly, we consider a time function t and a foliation given by its level surfaces. We define $n_a = (dt)_a$ and take a vector t^a transversal to the foliation and adjust it such that $t^a n_a = 1$. We choose covectors k_a such that $t^a k_a = 0$ and define $l_a = \lambda n_a + k_a$. We perform Fourier in k_a, and Laplace in λ. Thus, we replace space derivatives by ik_a and time derivatives by $i\lambda$. Furthermore, in what follows, once any particular k_a is chosen, we take a coordinate base so that $n_a = (dx^0)_a$, and $k_a = (dx^1)_a$, and so $l_a = (\lambda n_a + k_a) = (\lambda dx^0 + dx^1)_a$. Finally, in the high frequency limit, we obtain $\mathfrak{N}^{Aa}_\alpha l_a \tilde{\phi}^\alpha = 0$.

The Kronecker decomposition of a matrix pencil is a canonical transformation that generalizes the Jordan decomposition of a square matrix pencil. Considering the (square or non-square) pencil $\mathfrak{N}\lambda + \mathfrak{B}$, the Kronecker decomposition is achieved by multiplying this pencil by specific matrices W and Q, which are independent of λ (as in the square Jordan decomposition case). This transformation results in a new pencil $(W\mathfrak{N}Q)\lambda + (W\mathfrak{B}Q)$ that has a block structure with particular canonical blocks (see Gantmakher [21, 22], for a detailed description and Equation 3 for an example).

It turns out that the Kronecker decomposition can be used naturally in the analysis of systems with constraints or gauge freedom. With the first two conditions assumed above, the Kronecker decomposition of the pencil $\mathfrak{N}^{Aa}_\alpha l_a(\lambda)$ is given by

$$\mathfrak{N}^{Aa}_\alpha l_a = \begin{bmatrix}
\lambda-\lambda_1 & 0 & 0 & 0 & \dots & & 0 \\
0 & \dots & 0 & & & & 0 \\
0 & 0 & \lambda-\lambda_d & 0 & \dots & & 0 \\
0 & \dots & 0 & \lambda & 0 & \dots & 0 \\
0 & \dots & 0 & 1 & 0 & \dots & 0 \\
0 & \dots & 0 & 0 & \lambda & \dots & 0 \\
0 & \dots & 0 & 0 & 1 & \dots & 0 \\
0 & \dots & & \dots & & \dots & 0 \\
0 & \dots & & \dots & & \dots & 0 \\
0 & \dots & & \dots & & 0 & \lambda \\
0 & \dots & & \dots & & 0 & 1 \\
0 & 0 & 0 & \dots & 0 & 0 & 0 \\
\dots & \dots & \dots & \dots & \dots & \dots & \\
0 & 0 & 0 & \dots & 0 & 0 & 0
\end{bmatrix} \tag{3}$$

Ultimately, this represents a change of basis of both the variable and equation spaces, which depends on k_a but not on λ. The first block is a diagonal $d \times d$ block, this diagonal represents the true degrees of freedom of the entire system. It contains as many elements as the "zeros" of the singular value decomposition, counting their multiplicity. The 2×1 blocks, called L_1^T in the literature, are due to the constraints; there are a total of $r = |\alpha| - d$ blocks. Because each block occupies two rows, we see that the number of zero rows is $s = |A| - d - 2r$. The zero rows are present in many systems; they represent differential constraints among the constraints themselves. The numbers defined above also satisfy:

$$\begin{aligned}
d &:= \dim\left(\mathrm{right_ker}\left(C^{\Gamma a}_A n_a \mathfrak{N}^{Ai}_\alpha k_i\right)\right), \\
r &:= \mathrm{rank}\left(C^{\Gamma a}_A n_a \mathfrak{N}^{Ai}_\alpha k_i\right), \\
s &=: \dim\left(\mathrm{left_ker}\left(C^{\Gamma a}_A n_a \mathfrak{N}^{Ai}_\alpha k_i\right)\right).
\end{aligned}$$

With this decomposition at hand, it is easy to see how to choose among them linear combinations that give evolution equations for all ϕ^α. Observe that the equations (rows) with a λ are certain to contain derivatives transversal to the n_a flats. So, we must include them, but we can add any combination of the other rows to them. It turns out that, by simply adding to each of these rows the immediate row below, multiplied by any number π_i, $i = 1, \dots, r$, and discarding all the remaining rows, we obtain the evolution equations.

$$h^\beta_A \mathfrak{N}^{Aa}_\alpha l_a := \begin{bmatrix}
\lambda-\lambda_1 & 0 & 0 & & & & \\
0 & \dots & 0 & & & & \\
0 & 0 & \lambda-\lambda_d & & & & \\
& & & \lambda-\pi_1 & 0 & 0 & \\
& & & & \dots & & \\
& & & 0 & 0 & \lambda-\pi_r &
\end{bmatrix}.$$

Thus, we have constructed a map from the equation space to the variable space, which we refer to as a reduction and denote by h_A^β. Thus, $h_A^\beta \mathfrak{N}_\alpha^{Aa} l_a$ is a map from the variable space into itself consisting of a set of diagonal matrices satisfying the classic Kreiss conditions (see point *ii*. within Condition 1). Notice that we can choose the extra roots of λ (i.e., the $\{\pi_i\}$) as we please. They are the propagation speed of extra constraint modes. This simple observation is the principle behind the results in Reula [23]; Abalos [4].

Thus, there is a reduction (a linear combination of the equations) such that the Cauchy problem of the system is well-posed. Furthermore, Condition 3 asserts that if the initial data satisfy all equations (including the vanishing of the constraints), then all the equations are satisfied for all times as long as the solution exists. See Abalos [4] for details.

4 Extensions

A generic extension would imply the addition of an extra matrix, $\tilde{\mathfrak{N}}^{\Delta Aa}(x,\phi)$ (and extra variables Z_Γ), to obtain a square system

$$\mathfrak{N}_\alpha^{Aa}(x,\phi)\nabla_a\phi^\alpha + \tilde{\mathfrak{N}}^{\Gamma Aa}(x,\phi)\nabla_a Z_\Gamma - J^A(x,\phi) + B^A(x,\phi,Z) = 0. \quad (4)$$

Here, $B^A(x,\phi,Z)$ is a term we can also freely choose that does not include derivatives of ϕ or Z and that goes to 0 when Z goes to 0. In general, B^A represents damping terms [13]; [10]; [24], which are important in numerical applications. For simplicity in our discussion, however, we omit it.

Because we are interested in solving Equation 2 for ϕ, our extension proposal only makes sense if we can show that for suitable initial data (for (ϕ,Z)), the solution of Equation 4 has $Z=0$ throughout the development, thereby ensuring that ϕ is a solution of Equation 2.

As we explained before, if we assume Conditions 1, 2, and 3 and take any initial data for ϕ satisfying the constraints, we know that the initial value problem for Equation 2 is "well-posed" and has a unique solution ϕ_{sol}. (Here, by well-posed, we mean that the map from Cauchy data to solutions is continuous. To establish this, one finds a hyperbolic reduction from which we may assert that the reduced system is well-posed for arbitrary initial data. Then, one shows that if the initial data satisfy the constraints, then the solutions of the reduced system also satisfy them. Thus, they are solutions to the whole system, and we call the whole system well-posed). Therefore, if we choose $\tilde{\mathfrak{N}}^{\Gamma Aa}$ such that the extended system, Equation 4, is well-posed, then for any initial data, there will be a unique solution. If we choose as initial data $(\phi_{\text{sol}}|_{t=0}, Z|_{t=0}=0)$, then $(\phi_{\text{sol}}, Z=0)$ will be a solution, and by uniqueness is the solution. Therefore, we only need to show that system Equation 4 satisfies Kreiss's condition.

4.1 Strong hyperbolicity of the extensions

A particularly interesting set of extensions is obtained by noticing the symmetry between the Kronecker decomposition of $\mathfrak{N}_\alpha^{Aa} l_a(\lambda)$ and $(C_B^{\Delta a} l_a(\lambda))^T$. So, we start by computing it:

$$\left(C_A^{\Gamma b} l_b\right)^T = \begin{bmatrix} 0 & 0 & 0 & 0 & 0 & 0 \\ 0 & 0 & 0 & 0 & 0 & 0 \\ 0 & 0 & 0 & 0 & 0 & 0 \\ -1 & & & & & \\ \lambda & & & & & \\ & \cdots & & & & \\ & & -1 & & & \\ & & \lambda & & & \\ & & & \lambda-\rho_1 & & \\ & & & & \cdots & \\ & & & & & \lambda-\rho_s \end{bmatrix}$$

Recalling that the matrices $C_B^{\Delta a} l_a$ can be thought of as a basis, labeled by Δ, for the kernel of $\mathfrak{N}_\alpha^{Aa} l_a$, it is easy to understand its structure. Here, the rows with zeros are d in number. This is so because the diagonal part of $\mathfrak{N}_\alpha^{Aa} l_a$ cannot contribute to the kernel. We then have r blocks $\begin{bmatrix} -1 & \lambda \end{bmatrix}^T$, observing that they have a minus sign on them. This is because they are kernels for the corresponding L_1^T blocks of $\mathfrak{N}_\alpha^{Aa} l_a$. Finally, there is a block that is a kernel of the zero rows of $\mathfrak{N}_\alpha^{Aa} l_a$. This part is completely undetermined, so we have simply added a diagonal matrix.

To make more apparent the extension we proposed, we reorganize the rows of $\mathfrak{N}_\alpha^{Aa} l_a$ and $(C_A^{\Gamma b} l_b)^T$ such that

$$\mathfrak{N}_\alpha^{Aa} l_a = \begin{bmatrix} J & 0 \\ 0 & \lambda I_r \\ 0 & I_r \\ 0 & 0 \end{bmatrix}, \quad \left(C_A^{\Gamma b} l_b\right)^T = \begin{bmatrix} 0 & 0 \\ -I_r & 0 \\ \lambda I_r & 0 \\ 0 & J_c \end{bmatrix}. \quad (5)$$

Here, all the matrices are blocks matrices where $J = (\lambda-\lambda_1,\ldots,\lambda-\lambda_d)$ of size $d\times d$, $J_c = (\lambda-\rho_1,\ldots,\lambda-\rho_s)$ of size $s\times s$, and I_r is the identity matrix of size $r\times r$. The zero rows of $\mathfrak{N}_\alpha^{Aa} l_a$ are of size $s\times|\alpha|$, and the zero rows of $\left(C_A^{\Gamma b} l_b\right)^T$ are of $d\times|\Gamma|$.

From this reorganization, it is apparent that a natural choice of $\tilde{\mathfrak{N}}^{\Gamma Aa}$ is given by

$$\tilde{\mathfrak{N}}^{\Gamma Aa} = G^{AB} C_B^{\Gamma a},$$

where G^{AB} now must be chosen to render the system diagonalizable. This is, of course, not the most general extension but is a natural and fully covariant proposal for $\tilde{\mathfrak{N}}^{\Gamma Aa}$. The principal symbol of Equation 4 becomes then

$$M_D^{Aa} l_a = \begin{bmatrix} \mathfrak{N}_\alpha^{Aa} & G^{AB} C_B^{\Delta a} \end{bmatrix} l_a,$$

a $|A|\times|A|$ square matrix.

We now propose a particular expression for G^{AB}, namely,

$$G^{AB} = \begin{bmatrix} I_d & 0 & 0 & 0 \\ 0 & -D^2 & 0 & 0 \\ 0 & 0 & I_r & 0 \\ 0 & 0 & 0 & I_s \end{bmatrix}, \quad (6)$$

where $D = \text{diag}(\pi_1,\ldots,\pi_r)$ is of size $r\times r$, and I_s is the identity matrix of size $s\times s$.

Using expressions Equations 5, 6, we conclude

$$M_D^{Aa} l_a = \begin{bmatrix} J & 0 & 0 & 0 \\ 0 & \lambda I & D^2 & 0 \\ 0 & I & \lambda I & 0 \\ 0 & 0 & 0 & J_c \end{bmatrix},$$

It is easy to verify that this matrix is pencil-similar to the following diagonal matrix:

$$M_D^{Aa} l_a \sim \mathrm{diag}\left(\ldots, \lambda - \lambda_i, \ldots, \lambda + \pi_j, \lambda - \pi_j, \ldots, \lambda - \rho_k, \ldots\right)$$

and so it satisfies Kreiss's condition. The extra $2r$ eigenvalues $\{\pi_i, -\pi_i\}$, introduced by G^{AB}, come in pairs, which means that there are r new null cones as characteristic. We shall see this in the examples below, where Lorentzian metrics are used to realize these null cones.

5 Examples

In this section, we present two implementation examples of our proposal, showing that they produce well-posed systems while largely preserving the covariance of the original theories. In all cases, extra Lorentzian metrics are introduced to avoid light cone intersections.

5.1 Maxwell's equations

We start with the example given in the introduction Equation 1. For them, we have a space of variables F^{ab} (anti-symmetric tensors), which is $|\alpha| = 6$ dimensional in a four-dimensional space-time of metric g_{ab}. The space of equations is $|A| = 8$, namely, two space-time vectors. We have (see Geroch [1])

$$\mathfrak{N}_\alpha^{Aa} = \begin{pmatrix} \delta^a_{[c}\,\delta^q_{d]} \\ \varepsilon^{pa}{}_{bc} \end{pmatrix} \qquad C_A^{b\Gamma} = \begin{pmatrix} \delta^b{}_q \\ \delta^b{}_p \end{pmatrix} \qquad C_A^{b\Gamma} l_b = \begin{pmatrix} l_q \\ l_p \end{pmatrix}$$

Given a time-like n_a, we have

$$\mathfrak{N}_\alpha^{Aa} n_a = \begin{pmatrix} n_{[c}\,\delta^q_{d]} \\ \varepsilon^{pa}{}_{bc} n_a \end{pmatrix}.$$

So, it is the map $F_{ab} \to (E_a, B_a)$, which is of the maximal rank. This system satisfies Condition 1; see Abalos and Reula [3] for more details.

The tensor $C_A^{b\Gamma} l_b$ is also of maximal rank for any $l\!b$[1]. Since the dimension of the image is 2-dimensional, we have $|A| = |\alpha| + |\Gamma|$, and the system is consistent, satisfying Condition 2.

We also have

$$\nabla_b (C_A^{b\Gamma} \mathfrak{N}_\alpha^{Aa} \nabla_a \phi^\alpha) = \nabla_b \begin{pmatrix} \delta^a_{[c}\,\delta^b_{d]} \nabla_a F^{cd} \\ \varepsilon^{ba}{}_{cd} \nabla_a F^{cd} \end{pmatrix} = \begin{pmatrix} \nabla_b J^b \\ 0 \end{pmatrix} = 0$$

and so Condition 3 is also satisfied.

1 Here the target space is two copies of R^4, and the image is 1-dimensional on each one of them.

A suitable reduction is

$$h_{\beta B} = (g_{q[r}\, t_{s]}, -\frac{3}{2}\varepsilon_{pars}\, t^a).$$

This renders the evolution equations symmetric hyperbolic. As we saw above, a simple extension is obtained introducing two tensors (g_1^{pq}, g_2^{pq}) and defining

$$G^{AB} = \begin{pmatrix} g_1^{pq} & 0 \\ 0 & g_2^{pq} \end{pmatrix}$$

If we take their symmetric parts to be any two Lorentzian metrics, each one of them sharing a common time-like covector n_a with g_{ab}, but not touching their null cones (for brevity, we do not consider here such degenerate cases), then the system is strongly hyperbolic and so has a well-posed Cauchy problem. To check this, we compute the characteristics of the system and the corresponding eigenvectors and see when we get a complete set, that is, a total of eight eigenvectors.

The characteristic equations are

$$l_b \delta F^{ab} + g_1^{ab} l_b \delta Z_1 = 0$$

$$\varepsilon^{abcd} l_b \delta F_{cd} + g_2^{ab} l_b \delta Z_2 = 0,$$

where we need to solve these equations for λ with $l_a = \lambda n_a + k_a$ and n_a, k_a given and for the eigenvectors δF^{ab} and $\delta Z_{1,2}$. The solutions split into three cases: first, when l_a is null with respect to g^{ab} (physical case), then when it is null with respect to g_1^{ab} or g_2^{ab} (extended cases), as we explain below.

We already know four of the eigenvectors, namely, the physical ones arising from the original system. To recover these, we set $\delta Z_1 = \delta Z_2 = 0$ and search for the value of δF_{ab}. The second equation then implies that $\delta F_{cd} = 2l_{[c} A_{d]}$ for some vector A_d, while the first implies that $(l_a l^a) A^b - (l_a A^a) l^b = 0$ where indices are raised with the space-time metric. Because A_a cannot be proportional to l_a (otherwise δF_{cd} would vanish), both terms must vanish and so we conclude

$$g^{ab} l_a l_b = 0,$$

which admits two real solutions for λ. Hence, A^a is orthogonal to l_a, which leaves two options remaining for A^a for each of the two values of λ.

Now, we want to find the rest of the eigenvectors. For that, we first choose $\delta Z_1 = 1$, $\delta Z_2 = 0$. Contracting the first equation with l_b, and using the anti-symmetry of δF, we get a condition for l_a,

$$g_1^{ab} l_a l_b = 0, \tag{7}$$

which again admits two real values of λ. Repeating the argument above, the first equation becomes

$$(l_a l^a) A^b - (l_a A^a) l^b + g_1^{ab} l_b = 0 \tag{8}$$

Because the null cones of g^{ab} and g_1^{ab} are by assumption not touching, we have $g^{ab} l_a l_b \neq 0$. It follows that $A^a = -g_1^{ab} l_b / (l_c l^c)$ satisfies Equation 8 provided that Equation 7 holds. Observe furthermore that $A^a + \alpha l^a$ satisfies the same equations and results in the same Faraday tensor δF_{ab} for any α. Thus, Equation 7 gives two additional eigenvectors.

If we drop the assumption that the null cones of g^{ab} and g_1^{ab} are non-touching and assume that they touch at l_a, then to have a solution, we need that $g^{ab}l_b$ must be proportional to $g_1^{ab}l_b$.

The final case is similar to the second. We choose $\delta Z_1 = 0$, $\delta Z_2 = 1$ and obtain

$$g_2^{ab} l_a l_b = 0$$

and the same equations for the dual of δF_{ab}, so we need not discuss it separately.

In summary, we have obtained the eight eigenvectors we require to satisfy the Kreiss condition and conclude that the system is strongly hyperbolic.

5.2 Toy MHD

Here we look at the evolution of a magnetic field b^a driven by a given velocity field u^a in a space-time (M, g_{ab}). The system is

$$\nabla_a (b^{[a} u^{b]}) = 0 \tag{9}$$

Here, we take u^a to be time-like and of norm one, $u^a u^b g_{ab} = -1$. We also take $u^a b^b g_{ab} = 0$. This last is a gauge condition to make the solutions unique for the whole system because otherwise, if (u^a, b^a) is a solution, then $(u^a, b^a + \eta u^a)$ also is a solution, with η an arbitrary function.

We observe that there are four equations for three variables. Three of them are evolution equations for the three components of b^c. We shall see below that the other is a constraint. Thus, Condition 2 is also satisfied.

The principal part of system Equation 9 is

$$\mathfrak{N}_c^{ba} \nabla_a b^c = u^{[a} \nabla_a b^{b]} = \delta_c^{[a} u^{b]} \nabla_a b^c.$$

It is easy to check that Condition 1 is satisfied. The Geroch matrices are also easy to obtain as $C_b^d l_d := \delta_b^d l_d$. They form a basis of the left kernel of $\mathfrak{N}_c^{ba} l_a$ and, as we explained before, this means that when Equation 9 is contracted with $C_b^d u_d = u_b$, a constraint is generated; this is

$$\nabla_a b^a - b^a a_a = 0,$$

where $a^a \equiv u^b \nabla_b u^a$. We notice that this is the spatial divergence of b^a in disguise.

On the other hand, the following integrability condition $C_b^d \nabla_d \nabla_a (b^{[a} u^{b]}) = \nabla_b \nabla_a (b^{[a} u^{b]}) = 0$ holds trivially; thus, the system satisfies Condition 3.

The extended system consists of adding a term $g_1^{ba} \nabla_a Z$ to Equation 9, with g_1^{ba} as in the previous example and with the extra variable Z. Its principal part is $u^{[a} \nabla_a b^{b]} + g_1^{bc} C_c^d \nabla_d Z = 0$, with $C_b^a = \delta_b^a$. The characteristic equation is

$$\frac{1}{2}\left(u^a l_a \delta b^b - u^b l_a \delta b^a\right) + g_1^{bd} l_d \delta Z = 0 \tag{10}$$

where we need to solve this equation for $l_a = -\lambda u_a + k_a$ with k_a given, and for the eigenvectors δZ and δb^a (with $u_a \delta b^a = 0$).

Without loss of generality, we choose k^a such that $u^a k_a = 0$, and we rewrite the characteristic equations projecting on to u_a and perpendicular to it (with the projector $h_{ab} \equiv g_{ab} + u_a u_b$). We obtain

$$\begin{aligned} \frac{1}{2} k_a \delta b^a + u_a g_1^{ab} l_b \delta Z &= 0 \\ \frac{1}{2} \lambda \delta b^a + h_c^a g_1^{cb} l_b \delta Z &= 0 \end{aligned}$$

The physical solution comes from choosing $\lambda = 0$, and the eigenvectors $\delta Z = 0$ and δb^a orthogonal to k_a. Because δb^a has two possible directions, we obtain two eigenvectors.

The remaining eigenvectors come from choosing λ such that

$$l_a g_1^{ab} l_b = 0, \tag{11}$$

and $\delta Z = \frac{1}{2}\lambda$, $\delta b^a = h_c^a g_1^{cb} l_b$. This expression satisfies the second characteristic equation trivially, and it is easy to verify that the first one reduces to

$$\frac{1}{2} k_a \delta b^a + u_a g_1^{ab} l_b \delta Z = \frac{1}{2} l_a g_1^{ab} l_b = 0.$$

Because, as before, there are two solutions for λ from Equation 11, we obtain two more eigenvectors. In summary, we have obtained the four eigenvectors we require to satisfy the Kreiss condition and conclude that the extended system is strongly hyperbolic. Finally, we notice that Equation 11 can also be rederived from the integrability condition, i.e., by multiplying Equation 10 by $C_b^d l_d = l_b$.

6 Conclusion

Similar extensions to those proposed here were previously known, starting with the divergence cleaning used in magnetohydrodynamics and later generalized as λ-systems for generic symmetric hyperbolic systems. To implement them, it was necessary to break the covariance of the system in the usual sense of performing a $3+1$ decomposition. For symmetric hyperbolic systems, such extensions can be obtained in our framework by committing to a frame and a reduction and adding an extra term that annihilates the time component of the constraint basis. This results in an extended symmetric hyperbolic system.

In this article, we have presented an extension scheme for first-order PDEs. With appropriate adaptation, however, these results can be applied to systems of two or even more orders. We will show in future articles how to apply these ideas to gravity theories to extend the system and to fix the gauge, allowing us to reinterpret and generalize known results such as those of Bona et al. [25]; Hilditch and Richter [26]; Kovács and Reall [27].

Although the existence of a strongly hyperbolic extension is performed in Fourier space and results in a system of pseudodifferential equations, our examples show that in cases of physical interest, one may obtain differential extensions. These extensions furthermore retain covariance of the theory in the sense that, contrary to earlier λ-system extensions, at least in the principal part, they do not rely on a preferred time direction but instead the addition of other Lorentzian metric tensors. Further details and a complete proof will be provided in a longer version of this work.

In our analysis, we resorted to previous work to argue that the constraints, if initially satisfied, are satisfied at later times. This helped us conclude that Z_Γ remains zero throughout the evolution. There are, however, more elegant ways to show this when the constraints do not have any kernel from the left, that is, no set of zero rows in their Kronecker decomposition (see Equation 3).

In such cases, it can be shown that the Z_Γ fields satisfy a second-order evolution system that is decoupled from ϕ^α and has a well-posed initial value problem. Choosing these fields to vanish at the initial surface and the ϕ^α fields satisfy the original constraints of the system, all derivatives of Z_Γ vanish on the initial surface, in particular any transversal derivative, so the unique solution to the second-order system is 0, and the constraints are satisfied for all times. Unfortunately, the presence of zeros may prevent the second-order system from being well-posed, so more care is needed. This will be further considered in the aforementioned longer article.

Data availability statement

The original contributions presented in the study are included in the article/supplementary material, further inquiries can be directed to the corresponding author.

Author contributions

FA: conceptualization, formal analysis, investigation, methodology, project administration, validation, writing–original draft, and writing–review and editing. OR: conceptualization, formal analysis, methodology, validation, writing–original draft, and writing–review and editing. DH: investigation, validation, writing–review and editing, and formal analysis.

Funding

The author(s) declare that financial support was received for the research, authorship, and/or publication of this article. This work was supported by the Grant PID2022-138963NB-I00 funded by MCIN/AEI/10.13039/501100011033/FEDER, UE, by CONICET, SeCyT-UNC, and MinCyT-Argentina and by FCT Project No. UIDB/00099/2020.

Acknowledgments

We thank Carlos Palenzuela for several helpful discussions associated with the article. We also thank the "Programa de projectes de recerca amb investigadors convidats de prestigi reconegut" of the Universitat de les Illes Balears through which Oscar Reula visited the UIB, making it possible to finalize this article.

Conflict of interest

The authors declare that the research was conducted in the absence of any commercial or financial relationships that could be construed as a potential conflict of interest.

Generative AI statement

The author(s) declare that no Generative AI was used in the creation of this manuscript.

Publisher's note

All claims expressed in this article are solely those of the authors and do not necessarily represent those of their affiliated organizations, or those of the publisher, the editors and the reviewers. Any product that may be evaluated in this article, or claim that may be made by its manufacturer, is not guaranteed or endorsed by the publisher.

References

1. Geroch R. *Partial differential equations of physics*. Scotland: General Relativity, Aberdeen (1996). p. 19–60.

2. Abalos F. A necessary condition ensuring the strong hyperbolicity of first-order systems. *J Hyperbolic Differential Equations* (2019) 16:193–221. doi:10.1142/s0219891619500073

3. Abalos F, Reula O. On necessary and sufficient conditions for strong hyperbolicity in systems with constraints. *Class Quant Grav* (2020) 37:185012. doi:10.1088/1361-6382/ab954c

4. Abalos JF. On constraint preservation and strong hyperbolicity. *Classical Quan Gravity* (2022) 39:215004. doi:10.1088/1361-6382/ac88af

5. Hilditch D. An introduction to well-posedness and free-evolution. *Int J Mod Phys A* (2013) 28:1340015. doi:10.1142/S0217751X13400150

6. Gustafsson B, Kreiss H-O, Oliger J. *Time dependent problems and difference methods*, 24. John Wiley and Sons (1995). doi:10.1002/9781118548448

7. Kreiss H-O, Ortiz OE. *Introduction to numerical methods for time dependent differential equations*. John Wiley and Sons (2014).

8. Sarbach O, Tiglio M. Continuum and discrete initial-boundary value problems and einstein's field equations. *Living Rev relativity* (2012) 15:9. doi:10.12942/lrr-2012-9

9. Kreiss H-O. Über die stabilitätsdefinition für differenzengleichungen die partielle differentialgleichungen approximieren. *BIT Numer Mathematics* (1962) 2:153–81. doi:10.1007/BF01957330

10. Dedner A, Kemm F, Kröner D, Munz C-D, Schnitzer T, Wesenberg M. Hyperbolic divergence cleaning for the mhd equations. *J Comput Phys* (2002) 175:645–73. doi:10.1006/jcph.2001.6961

11. Munz C-D, Omnes P, Schneider R, SonnendrÃ¼cker E, VoÃŸ U. Divergence correction techniques for maxwell solvers based on a hyperbolic model. *J Comput Phys* (2000) 161:484–511. doi:10.1006/jcph.2000.6507

12. Munz C-D, Ommes P, Schneider R. A three-dimensional finite-volume solver for the maxwell equations with divergence cleaning on unstructured meshes. *Computer Phys Commun* (2000) 130:83–117. doi:10.1016/s0010-4655(00)00045-x

13. Brodbeck O, Frittelli S, Hübner P, Reula OA. Einstein's equations with asymptotically stable constraint propagation. *J Math Phys* (1999) 40:909–23. doi:10.1063/1.532694

14. Bona C, Ledvinka T, Palenzuela C, Zacek M. General covariant constraint free evolution system for numerical relativity. *arXiv* (2002). doi:10.48550/arXiv.gr-qc/0209082

15. Baumgarte TW, Shapiro SL. Numerical integration of Einstein's field equations. *Phys Rev D* (1998) 59:024007. doi:10.1103/PhysRevD.59.024007

16. Shibata M, Nakamura T. Evolution of three-dimensional gravitational waves: harmonic slicing case. *Phys Rev D* (1995) 52:5428–44. doi:10.1103/PhysRevD.52.5428

17. Nakamura T, Oohara K, Kojima Y. General relativistic collapse to black holes and gravitational waves from black holes. *Prog Theor Phys Suppl* (1987) 90:1–218. doi:10.1143/ptps.90.1

18. Pretorius F. Numerical relativity using a generalized harmonic decomposition. *Class Quant Grav* (2005) 22:425–51. doi:10.1088/0264-9381/22/2/014

19. Bernuzzi S, Hilditch D. Constraint violation in free evolution schemes: comparing the BSSNOK formulation with a conformal decomposition of the Z4 formulation. *Phys Rev D* (2010) 81:084003. doi:10.1103/PhysRevD.81.084003

20. Alic D, Bona-Casas C, Bona C, Rezzolla L, Palenzuela C. Conformal and covariant formulation of the z4 system with constraint-violation damping. *Phys Rev D* (2012) 85:064040. doi:10.1103/physrevd.85.064040

21. Gantmakher FR. *The theory of matrices*, 1. New York: Chelsea Publishing Company (1998).

22. Gantmakher FR. *The theory of matrices*, 2. Providence, RI: American Mathematical Soc. (1998). p. 131.

23. Reula OA. Strongly hyperbolic systems in general relativity. *J Hyperbolic Differential Equations* (2004) 1:251–69. doi:10.1142/s0219891604000111

24. Gundlach C, Calabrese G, Hinder I, Martín-García JM. Constraint damping in the z4 formulation and harmonic gauge. *Classical Quan Gravity* (2005) 22:3767–73. doi:10.1088/0264-9381/22/17/025

25. Bona C, Ledvinka T, Palenzuela-Luque C, Zacek M. Constraint-preserving boundary conditions in the Z4 numerical relativity formalism. *Class Quant Grav* (2005) 22:2615–33. doi:10.1088/0264-9381/22/13/007

26. Hilditch D, Richter R. Hyperbolicity of physical theories with application to general relativity. *Phys Rev D* (2016) 94:044028. doi:10.1103/PhysRevD.94.044028

27. Kovács AD, Reall HS. Well-posed formulation of lovelock and horndeski theories. *Phys Rev D* (2020) 101:124003. doi:10.1103/PhysRevD.101.124003

frontiers | Frontiers in Physics

TYPE Mini Review
PUBLISHED 25 July 2025
DOI 10.3389/fphy.2025.1638583

Check for updates

OPEN ACCESS

EDITED BY
Jose Luis Jaramillo,
Université de Bourgogne, France

REVIEWED BY
Valentin Boyanov,
Associação do Instituto Superior Técnico de Investigação e Desenvolvimento (IST-ID), Portugal

*CORRESPONDENCE
Christiana Pantelidou,
christiana.pantelidou@ucd.ie
Benjamin Withers,
b.s.withers@soton.ac.uk

RECEIVED 30 May 2025
ACCEPTED 09 July 2025
PUBLISHED 25 July 2025

CITATION
Besson J, Carballo J, Pantelidou C and Withers B (2025) Transients in black hole perturbation theory.
Front. Phys. 13:1638583.
doi: 10.3389/fphy.2025.1638583

COPYRIGHT
© 2025 Besson, Carballo, Pantelidou and Withers. This is an open-access article distributed under the terms of the Creative Commons Attribution License (CC BY). The use, distribution or reproduction in other forums is permitted, provided the original author(s) and the copyright owner(s) are credited and that the original publication in this journal is cited, in accordance with accepted academic practice. No use, distribution or reproduction is permitted which does not comply with these terms.

Transients in black hole perturbation theory

Jérémy Besson[1,2], Javier Carballo[3], Christiana Pantelidou[4]* and Benjamin Withers[3]*

[1]Institut de Mathématiques de Bourgogne (IMB), Centre National de la Recherche Scientifique (CNRS), Université de Bourgogne, Dijon, France, [2]Albert-Einstein-Institut, Max-Planck-Institut für Gravitationsphysik, Germany and Leibniz Universität Hannover, Hannover, Germany, [3]Mathematical Sciences and STAG Research Centre, University of Southampton, Southampton, United Kingdom, [4]School of Mathematics and Statistics, University College Dublin, Dublin, Ireland

Black hole quasinormal modes arise as eigenmodes of a non-normal Hamiltonian and consequently they do not obey orthogonality relations with respect to commonly used inner products, for example, the energy inner product. A direct consequence of this is the appearance of transient phenomena. This review summarises current developments on the topic, both in frequency- and time-domain. In particular, we discuss the appearance of i) transient plateaus: arbitrarily long-lived sums of quasinormal modes, corresponding to localised energy packets near the future horizon; ii) transient growth, with the latter either appearing in the vicinity of black hole phase transitions or in the context of higher-derivative Sobolev norms.

KEYWORDS

non-modal, quasinormal modes (QNMs), black holes, transients, pseudospectra, black hole spectroscopy, non-normal, ringdown

1 Introduction

An indispensable tool in the study and characterisation of the dynamics of black holes is their spectrum of quasinormal modes (QNMs) – for recent reviews see [1, 2]. QNMs are solutions to the wave equation arising when general relativity is considered perturbatively at linear order, and they determine how small perturbations evolve over time, capturing their 'ringdown' behaviour.[1] As such, QNMs have received a lot of attention in the literature. Within holography, they determine the near-equilibrium properties of strongly coupled quantum field theories, in particular some transport coefficients, such as viscosity, conductivity and diffusion constants [5, 6]. In astrophysics, the detection of QNMs in gravitational wave experiments would allow precise measurements of the mass and spin of black holes–through the so-called black hole spectroscopy programme [7] – as well as new tests of general relativity. Similarly, QNMs also serve as indicators of black hole instabilities: a single unstable mode signals exponentially growing perturbations leading to a new equilibrium configuration, which is particularly important in higher dimensions as well as in the holographic context. In addition, QNMs also play an instrumental role in semiclassical gravity, e.g., in the context of Hawking

1 Second order QNMs, usually referred to as QQNMs, have also been constructed recently [3, 4].

radiation [8], as well as in Mathematical Relativity, e.g., in understanding properties of Cauchy horizons [9].

The defining property of a black hole is its event horizon, through which energy dissipates. This dissipative nature of black holes has a direct imprint on the operator that gives rise to QNMs: the operator is non-normal. This absence of normality leads to the QNM eigenfunctions being neither orthogonal[2] nor complete, while the QNM frequencies are highly sensitive to small perturbations, resulting in spectral instability. These features substantially complicate the interpretation of QNMs and, in fact, in certain contexts question the validity of their use. Note that non-normality is a generic feature of dissipative systems and as such, has been observed and investigated in both (i) quantum mechanics, where the introduction of non-selfadjoint operators in PT-symmetric quantum mechanics entails that the associated spectrum is insufficient to draw full, quantum-mechanically relevant conclusions [14], and in (ii) fluid dynamics in relation to the transition between laminar and turbulent flows [15].

In essence, to-date, we have only explored the 'tip of the iceberg' in terms of non-normality in black hole physics, especially in dynamical settings, where the non-orthogonality of QNMs can give rise to short-term, transient phenomena. Here we review progress in this direction.

In order to set the stage, in what follows we foliate spacetime with *hyperboloidal slices*, Σ_τ – spacelike slices that pierce the future event horizon. These slices are labeled by time τ and are traversed by a radial coordinate z with the future event horizon reached at $z = 1$. For brevity we suppress dependence in the transverse directions. In the spacetimes we consider here, the equation of motion for a perturbation $\psi(\tau, z)$ (scalar, electromagnetic, or spin-2), will obey a first-order-reduced equation of motion,

$$i\partial_\tau u = \mathcal{H} u, \tag{1}$$

where $\mathcal{H}$ is a 2×2 matrix and a second-order differential operator in z and $u = (\psi, \partial_\tau \psi)^T$. For initial data $u(0, z)$, the time-dependent solution of the system is given formally as $u(\tau, z) = e^{-i\mathcal{H}\tau} u(0, z)$, in terms of the evolution operator $e^{-i\mathcal{H}\tau}$. Given a harmonic decomposition $u(\tau, z) \sim \chi(z) e^{-i\omega\tau}$, QNMs are defined as solutions to the eigenvalue problem

$$\omega_n \chi_n = \mathcal{H}\chi_n,$$

subject to ingoing behaviour at the future event horizon and appropriate boundary conditions at infinity. Then, the spectrum of the theory is given by $\sigma(\mathcal{H}) = \{\omega_n, n \geq 0\}$. We can define an energy associated to matter on a hyperboloidal slice by

$$E \equiv \int_{\Sigma_\tau} T^\mu_\tau n_\mu \, d\Sigma_\tau, \tag{2}$$

where $n = \frac{-1}{\sqrt{-g^{\tau\tau}}} d\tau$ is the unit, future-directed normal to Σ_τ. $T^{\mu\nu}$ is the matter stress-energy tensor, and is at least quadratic in the perturbation ψ. Note that $T^{\mu\nu}$ can contain contributions from other fields. Due to local conservation of the currents $T^{\mu\nu}$, the total energy E is conserved up to boundary terms. The energy of ψ on Σ_τ is then given by Equation 2 with $T_{\mu\nu} = T^\psi_{\mu\nu}$, from which the *energy inner product* $\langle \cdot, \cdot \rangle_E$ (see [16] for an extended discussion) is defined such that

$$E[u] = \langle u, u \rangle_E = \|u\|_E^2. \tag{3}$$

2 Insights from the pseudospectrum

One can extract various insights about the time domain problem from spectral features. In particular, a useful object is the pseudospectrum,

$$\sigma_\epsilon(\mathcal{H}) = \{\, \omega \in \mathbb{C} \,|\, \omega \in \sigma(\mathcal{H} + \delta\mathcal{H}), \|\delta\mathcal{H}\| \leq \epsilon \,\}, \tag{4}$$

which, along with many of the definitions in this section, can be found in [15]. In the black hole context, Equation 4 has received much attention as a way to assess the stability of QNM frequencies under environmental perturbations [17], building upon the seminal observations of [18, 19]. Heuristically, σ_ϵ at fixed ϵ provides the contours of a useful topographic map of the complex frequency plane. Peaks are infinitely high and correspond to the point spectrum, while the width of the peaks have something to say about the associated spectral stability properties and transient effects.

In particular, for our purposes, a significant protrusion of pseudospectral contour lines into the unstable-half ω-plane points towards transient phenomena (in our conventions this is the upper-half ω-plane). A lower bound on the peak growth of the evolution operator is given as follows,

$$\sup_{\tau \geq 0} \|e^{-i\mathcal{H}\tau}\| \geq \frac{\alpha_\epsilon(\mathcal{H})}{\epsilon}, \quad \forall \epsilon > 0,$$

where we have introduced the pseudospectral abscissa, $\alpha_\epsilon(\mathcal{H}) = \sup \Im\mathfrak{m}\, \sigma_\epsilon(\mathcal{H})$. The strongest lower bound is given by the Kreiss constant, $\mathcal{K}(\mathcal{H}) = \sup_{\epsilon>0} \alpha_\epsilon(\mathcal{H})/\epsilon$. Relatedly, an upper bound on growth follows from

$$\|e^{-i\mathcal{H}\tau}\| \leq e^{-i\mathfrak{w}(\mathcal{H})\tau}, \qquad \forall \tau \geq 0,$$

where we have introduced the numerical abscissa $\mathfrak{w}(\mathcal{H}) = \sup_{\epsilon>0} (\alpha_\epsilon(\mathcal{H}) - \epsilon)$.

In the black hole context, these quantities were first studied in [20] in the context of binary black hole mergers in the close-limit approximation.[3] Specifically, in the case of a Schwarzschild black hole in the energy norm (Equation 3) [20], computed the numerical abscissa to be $\mathfrak{w}(\mathcal{H}) = 0$, which implies $\mathcal{K}(\mathcal{H}) = 1$. This implies there is no growth of energy of a perturbation in the exterior of

2 With respect to standard choices of inner product. See [10–13] for the construction of QNM orthogonality relations in other products.

3 See also [21] for a related study of extreme compact objects, where a Kreiss constant consistent with $K(\mathcal{H}) = 1$ was obtained numerically by computing the ratio of the pseudospectral abscissa $\alpha_\epsilon(\mathcal{H})/\epsilon$ in the limit $\epsilon \to \infty$.

Schwarzschild spacetime, which is simply a consequence of energy conservation [22].[4]

Going further, one may ask if the pseudospectrum can be used to identify scenarios in which perturbations of black holes can grow. However, a critical issue arises when Equation 4 is considered more generally in the black hole context. This is most easily stated using the following equivalent definition of Equation 4, which utilises the norm of the resolvent,

$$\sigma_\epsilon(\mathcal{H}) = \{\omega \in \mathbb{C} \,|\, \|R_{\mathcal{H}}(\omega)\| = \|(\mathcal{H} - \omega I)^{-1}\| \geq 1/\epsilon\}.$$

when the resolvent operator is approximated as a matrix for the purposes of numerical evaluation it does not always converge with increasing resolution [24]. See [25, 26] for further discussions. However, it is proven in [27] for asymptotically AdS and dS black holes that the norm of the resolvent exists in a band structure in the complex ω plane provided one uses a particular class of higher-derivative norms. There, higher-derivative norms were introduced in order to impose a higher degree of regularity for the purposes of defining QNMs. This motivates the use of higher-derivative norms both in the evaluation of pseudospectra and for assessing transient phenomena, as in [26]. In [26] the following higher-derivative norms are defined[5]

$$\langle u_1, u_2\rangle_{H^p} = \sum_{j=0}^{p} \langle \partial_x^j u_1, \partial_x^j u_2\rangle_E, \tag{5}$$

referred to as the Sobolev H^p-inner product, where here (τ, x) refer to the Bizoń-Mach hyperboloidal coordinates [28] for the Pöschl-Teller model. Note $p = 0$ corresponds to the energy-norm.

The Kreiss constant was also discussed in [29], where it was extracted from the pseudospectrum of a truncated Hamiltonian, $\mathcal{H}_W$, where the functional space was restricted to a subspace W of the first M quasinormal modes [29]. found that $\mathcal{K}(\mathcal{H}_W) > 1$, for a system describing charged scalar perturbations in a Reissner-Nordström (RN) - AdS_4 black brane. This indicates that there exist perturbations that exhibit transient energy growth in the scalar field when all the modes are stable.

3 Time domain

In the last section, we presented quantities computed from the pseudospectrum (and its respective limits) that provide insights into the time evolution of linear perturbations. In particular, a non-zero numerical abscissa, $\mathfrak{w}(\mathcal{H}) > 0$, and thus $\mathcal{K}(\mathcal{H}) > 1$, immediately implies that there exist perturbations whose time evolution exhibit transient growth in the observable defined by the chosen norm $\|\cdot\|$. The pseudospectral analysis is however incomplete, since it does not capture important transient effects that arise even in the absence of growth [22], and should be complemented with a full time domain evolution of perturbations.

Consider a black hole coupled to a scalar field. A natural choice of observable is the energy of the scalar field ψ on hyperboloidal slices as given by the energy norm $\|\cdot\|_E$ (Equation 3). A key feature now is that energy dissipation through the horizon and to $\mathcal{I}^+$ renders a non-normal $\mathcal{H}$ in Equation 1 under $\langle\cdot,\cdot\rangle_E$, and thus its regular normalisable eigenfunctions (the QNMs) are not orthogonal under this product. Consequently, the energy of a perturbation formed from a sum of QNMs, $u(\tau, z) = \sum_{n=1}^{M} c_n e^{-i\omega_n \tau}\chi_n(z)$, is not just the sum of the energies of each individual QNM, but rather

$$E[u] = \sum_{n=1}^{M} |c_n|^2 e^{2\Im\mathrm{m}\,\omega_n \tau} E[\chi_n] + \text{cross} - \text{terms}. \tag{6}$$

there are cross-terms arising from the non-orthogonality of QNMs under Equation 3 that allow for non-trivial transient dynamics. Note that without the cross-terms, the slowest possible energy decay is set by the fundamental mode ω_0.

In this context, the first systematic time domain study of transients in black hole perturbations was introduced in [22] using the *energy growth curve*, $G(\tau) \equiv \|e^{-i\mathcal{H}\tau}\|_E^2$, and *optimal perturbations*–tools inherited from hydrodynamics [30–35]. Considering a subspace of solutions W to Equation 1 spanned by the first $M = \dim(W)$ QNMs, $\{\chi_n\}_{n=1}^{M}$ (ordered by decreasing $\Im\mathrm{m}\,\omega$), $G_W(\tau) \equiv \|e^{-i\mathcal{H}_W\tau}\|_E^2$ determines the maximum possible energy at a specific time τ, relative to the energy at a fiducial initial time $\tau = 0$, over all solutions in W. Optimal perturbations, $u_{\text{opt.}} \in W$, are then those that maximise the energy at a target time τ_* such that $E[u_{\text{opt.}}(\tau_*, z)] = G_W(\tau_*)$. Both the value of $G_W(\tau_*)$ and the set of coefficients $\vec{c}$ in the initial data expansion.

$$u_{\text{opt.}}(0, z) = \sum_{n=1}^{M} c_n \chi_n(z) \tag{7}$$

where QNMs are normalised $\langle\chi_n(z), \chi_n(z)\rangle_E = 1$, are obtained from the singular value decomposition of $e^{-iH_W\tau_*} - H_W$ is the representation of $\mathcal{H}_W$ in an orthonormal basis of functions for W, an $M \times M$ matrix encoding the information of the spectrum (see [22, 29] for more details). Finally, $u_{\text{opt.}}$ evolves simply according to the time evolution of each QNM in Equation 7, i.e.,

$$u_{\text{opt.}}(\tau, z) = \sum_{n=1}^{M} c_n e^{-i\omega_n \tau}\chi_n(z).$$

Using this methodology, the main result of [22] consisted in demonstrating the existence and constructing (both analytically and numerically) arbitrarily long-lived linear black hole perturbations in a variety of spacetimes, due to transient effects, despite a lack of energy growth. An example of such perturbations for $s = 2$, $l = 2$ (spin and angular momentum) Regge-Wheeler QNMs of the Schwazschild black hole is presented in Figure 1. The top panel shows G_W for different values of M indicating the absence of growth in the energy of perturbations, in accordance with the $\omega(\mathcal{H}) = 0$ and $\mathcal{K}(\mathcal{H}) = 1$ results discussed in section 2. Note that the total (quadratic in perturbations) energy of the system E can only stay constant or decay, and its only contribution is the energy of the gravitational perturbation. However, G_W exhibits an initial transient plateau with duration $\sim \log M$ that demonstrates the existence of optimal perturbations with lifetimes scaling as $\log M$, followed by

4 Note that [23] reports transient growth in the context of Kaluza-Klein black holes in Gauss-Bonnet gravity. However, the system studied in [23] is conservative up to boundary terms and (3.19) there can be written as a total derivative. As such, the reported result on transient growth is incorrect.

5 Note that this is different to the corresponding inner product used in [24].

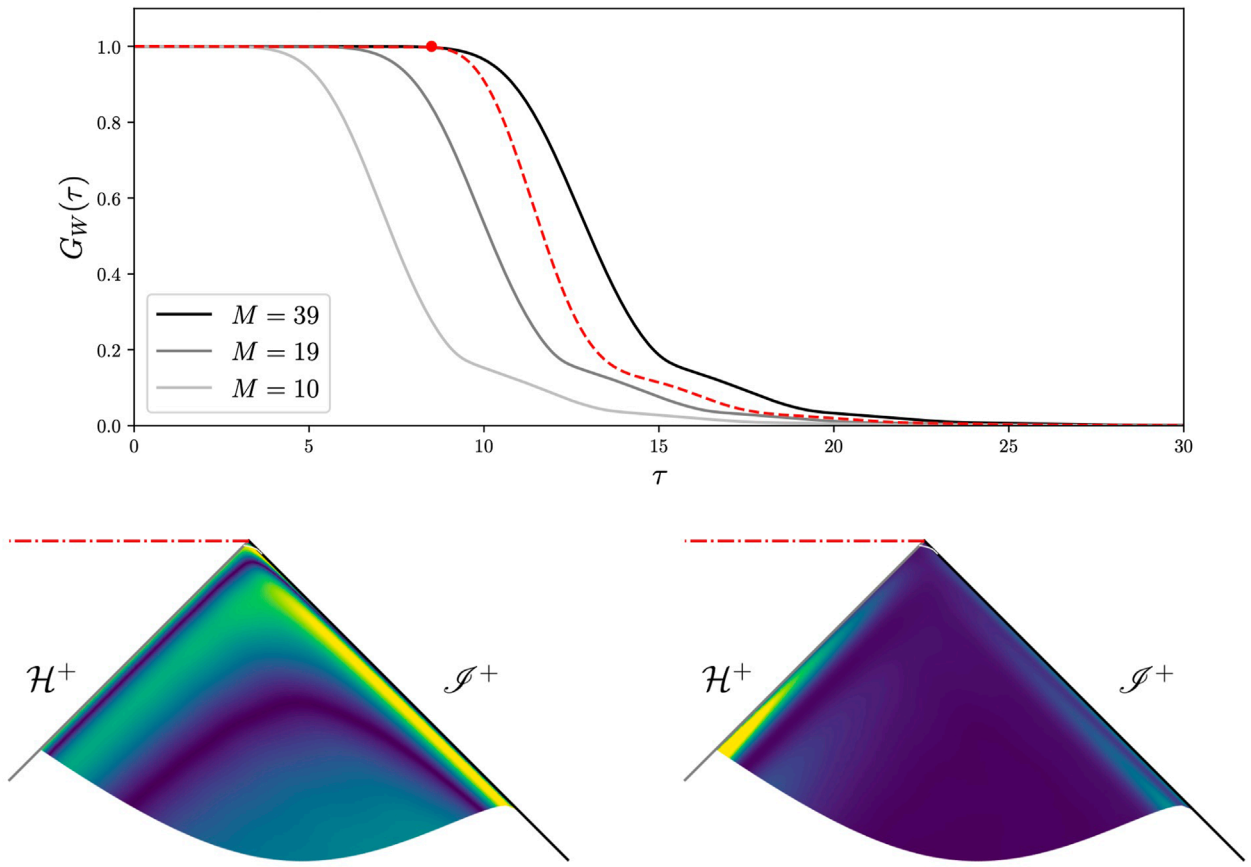

FIGURE 1
Energy growth curves and optimal perturbation for Schwarzschild $s = 2$, $l = 2$ Regge-Wheeler perturbations (figure taken from [22]). Top: G_W for various $M = \dim(W)$ (solid curves), and the energy of an optimal perturbation of $M = 39$ QNMs with $\tau_* = 8.5$ (red-dash). Bottom: Modulus (left) and energy density (right) of the optimal perturbation in the conformal diagram of Schwarzschild. The energy is initially localised at $\mathcal{H}^+$ and $\mathcal{I}^+$, and then propagates along them until it starts dispersing and decaying at $\tau \simeq \tau_*$ (indicated by the white slice near i^+). The dash-dotted red line represents the curvature singularity.

an exponential decay with the fundamental mode ω_0 decay rate. The energy of such a perturbation, $E[u_{\text{opt.}}(\tau, z)]$, is displayed in red-dash. In the bottom panels, $|u_{\text{opt.}}|$ (left) and its energy density (right) are plotted in the conformal diagram. From the energy density, it is clear that $u_{\text{opt.}}$ is physically realised as localised energy packets travelling along $\mathcal{H}^+$ and $\mathcal{I}^+$ that do not either fall into the black hole or escape to infinity, respectively, until $\tau \simeq \tau_*$. Mathematically, this is a direct consequence of the non-orthogonality of QNMs under the energy norm (Equation 3), ultimately due to non-normality of $\mathcal{H}_W$, which leads to the cross-terms in Equation 6 allowing for cancellations in the sum that keep the energy constant.

Building on [22, 29] established the first case of transient energy growth in linear black hole perturbations considering RN-AdS$_4$ black branes at chemical potential μ linearly perturbed by a complex scalar ψ with charge q. The key difference here is that the total energy of the system does not correspond to the energy of ψ alone. In particular, in the $q \to \infty$ limit suppressing backreaction to the metric, E receives contributions from both the scalar, ψ, and the gauge field, A,

$$E = E_\psi + E_F, \tag{8}$$

where $F = dA$, which are coupled to each other through q. Then, choosing $\|\cdot\|_{E_\psi}$ to construct optimal perturbations in the same fashion as before, E_ψ was shown to exhibit significant transient growth before asymptotic decay via a transient form of superradiance–borrowing from the energy bath E_F – in the modally stable regime.[6] This is shown in the left panel of Figure 2, which displays G_W and E_ψ for an optimal perturbation with $M = 10$ QNMs exhibiting transient growth. The first correction to the background gauge field energy, which appears at quadratic order in perturbations, $E_F^{(2)}$, takes negative values implying transfer of energy from A to ψ, while the total energy $E = E_\psi + E_F^{(2)}$ can only decrease due to losses to the horizon. Empirically, it was observed that the peak of the growth curve increases with M within the range of values considered. Note that this is not a special feature of the $q \to \infty$ limit, the finite q case is also examined in [29] with same qualitative results.

6 In AdS/CFT, this model is known as the holographic superconductor [36–38], and it is linearly unstable for $T < T_c$ (or equivalently $\mu > \mu_c$) corresponding to the superconducting phase.

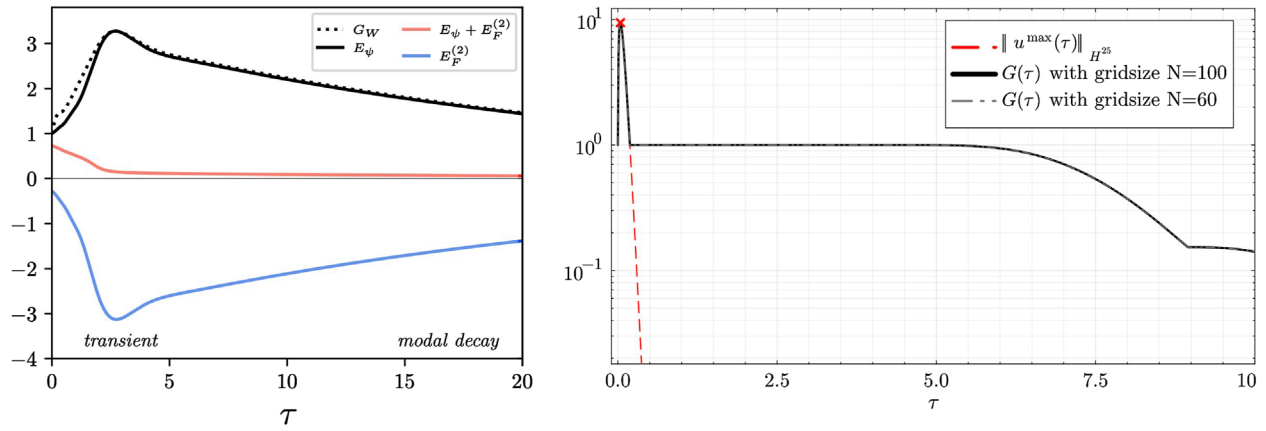

FIGURE 2
Left: optimal perturbation and energy growth curve $G_W(\tau)$ (black dash) for complex charged scalar QNMs of the RN-AdS$_4$ black brane with $M = 10$. E_ψ (solid black curve) is shown to transiently grow before modally decaying at asymptotic time. The additional energy is borrowed from the energy bath E_F via a transient form of superradiance, as can be seen from the first correction to E_F, $E_F^{(2)}$ (solid blue curve). The example shown corresponds to the probe limit $q \to \infty$ with $\mu q = 3.9$, spatial momentum $\vec{k} = 0$, with target time $\tau_* = 2.7$. Figure taken from [29]. Right: growth curve G and the norm of $u^{\max}(\tau, x)$ obtained by time-evolving the optimal perturbation $u_{\text{opt.}}(\tau_* = \tau_{\max}, x)$ in the Sobolev H^{25} norm. A transient growth is observed and yields a peak at $\tau_{\max} \approx \frac{1}{25} = 0.04$, before a modal oscillatory decay. The growth curve G is computed for two different resolutions $N = 60$ (dashed gray curve) and $N = 100$ (solid black curve), thus illustrating the convergence of the profile we observe on this panel. Figure taken from [26].

Transient behaviour has also been seen in Sobolev H^p norms Equation 5 in [26] in the Pöschl-Teller toy model, corresponding to the Klein-Gordon equation in the static patch of de Sitter spacetime. Following a similar approach to [22, 29], optimal perturbations $u_{\text{opt.}}(0, x)$ were obtained using a 'generalised' singular value decomposition of the finite rank approximant of the evolution operator $e^{-i\mathcal{H}\tau}$, but this time without relying on a subspace of solutions W. For a target time τ_*, these optimal perturbations maximise the Sobolev H^p inner product such that $\langle u_{\text{opt.}}(\tau_*, x), u_{\text{opt.}}(\tau_*, x) \rangle_{H^p} = G(\tau_*)$.

In the case of H^0 norm (corresponding to the energy norm), no transient growth is observed. Similar to [22], non-modal behaviour manifests itself as an initial transient plateau in G, followed by the expected modal decay, with a scalar field profile localised near the boundaries. However, unlike [22], the results are not convergent as the duration of the plateau scales as $\log N$ with the number of points N used in the numerical approximation, further motivating the use of H^p norms with $p > 0$.

In the case of H^p Sobolev norm with $p > 0$, transient growth is observed. Specifically, one obtains an initial 'peak', which is followed by modal decay according to the lowest-lying QNM at late times; the right panel of Figure 2 exemplifies this behaviour for $p = 25$, showing G and $\langle u_{\text{opt.}}(\tau_*, x), u_{\text{opt.}}(\tau_*, x) \rangle_{H^{25}}$ for $\tau_* = \tau_{\max}$ corresponding to the time of the peak. Note that $u_{\text{opt.}}(\tau_*, x)$ is an order-p polynomial. The profile of the optimal perturbation $u_{\text{opt.}}(\tau, x)$ is found to be numerically convergent and, importantly, it resides in the bulk of the geometry; this is different to the energy-norm case where the optimal perturbations was peaked near the boundaries. Applying the 'Keldysh' spectral decomposition scheme to $u_{\text{opt.}}(0, x)$ shows that most of the transient peak originates from the $(p+1)$-th pair of QNMs, ordered by decreasing $\Im\mathrm{m}\,\omega$; note that the decay rate of these modes is $\frac{1}{p}$.

As the order p of the H^p Sobolev norm is increased, the peak in the growth curve increase as $G(\tau_{\max}) = \max_{\tau \geq 0} G(\tau) \sim p$ and moves to shorter timescales, $\tau_{\max} \sim 1/p$. The scaling of $\tau_{\max}$ is a result of the decay rate of the QNM giving rise to the majority of the transient peak mentioned above.

Lastly, it is illuminating to understand the existence of H^p-transient growth in the context of energy conservation. Specifically, the H^p-norm satisfies

$$E[u] = \langle u, u \rangle_{H^p} - \sum_{j=1}^{p} \left\| \partial_x^j u \right\|_E^2, \tag{9}$$

where $E[u]$ is conserved up to boundary terms. In a way analogous to Equation 8, H^p-transient growth is permitted as a result of transfer of weight between the two terms in the right hand side of Equation 9.

Let us conclude this section with a comparison of the two methods discussed above: truncating the set of QNMs or using higher-derivative norms. Both approaches provide a way of regulating the UV and are equally easy to implement. The motivations for using them are different: in the former case the motivation was a physical truncation of the theory to low energy modes inspired by analogous constructions in hydrodynamics, while in the latter case the motivation was a consideration of regularity. The truncation method results in a finite dimensional Hilbert space which can be convenient to work with. The physical interpretation of the H^p-norm remains an open question.

4 Discussion

This short review summarises recent work on transient phenomena in black hole dynamics. The lack of normality of the evolution operator, emerging as a consequence of the dissipative nature of black hole spacetimes, results in the non-orthogonality of

QNMs. This, in turn, allows for linear perturbations to exhibit non-modal behaviour (either in the form of transient growth or lack of decay) before eventually conforming to modal decay.

The existence of transients can be inferred from frequency-domain computations involving the pseudospectrum: the protrusion of pseudospectral contour lines in the unstable half plane indicates an unstable perturbed spectrum, and hence non-modal behaviour. In order to observe transient growth, the protrusion needs to be larger than the size of the external perturbation ϵ, giving rise to a Kreiss constant $\mathcal{K} > 1$. This raises again the issue of the numerical convergence of the pseudospectrum as discussed in section 2, and motivates the exploration of the truncated-Hamiltonian pseudospectrum of [29].

Time-domain results exhibit striking qualitative similarities to the prototypical example of transient effects in the transition to turbulence in Navier-Stokes shear flows. Two particularly interesting questions that currently remain open relate to the non-linear evolution sourced by such initial data and the potential connection with the Aretakis instability.

Black hole QNMs have been a central focus of gravitational physics for over half a century, yet it remains striking that we still lack a full understanding of the consequences stemming from the absence of a spectral theorem in this context. This gap points to an exciting new direction in the field, suggesting that much remains to be uncovered. Particularly compelling questions include how much of the gravitational wave signal emanating from a binary merger can be attributed to linear transient dynamics, as well as the role of transients in strongly coupled systems, such as the quark-gluon plasma and high-temperature superconductors, via the AdS/CFT correspondence. Other arenas include analogue gravity systems, where fluid or optical setups mimic aspects of black hole spacetimes.

Author contributions

JB: Writing – review and editing, Writing – original draft. JC: Writing – review and editing, Writing – original draft. CP: Writing – original draft, Writing – review and editing. BW: Writing – review and editing, Writing – original draft.

Funding

The author(s) declare that financial support was received for the research and/or publication of this article. J.B. is supported by the project QuanTEdu-France 22-CMAS-0001. J.C. is supported by the Royal Society Research Grant RF\ERE \210267. C.P. is supported by a Royal Society – Research Ireland University Research Fellowship via grant URF\R1\211027. B.W. is supported by a Royal Society University Research Fellowship URF\R\231002 and in part by the STFC consolidated grant ST/T000775/1.

Acknowledgments

The authors would like to thank José Luis Jaramillo and Frans Pretorius for discussions.

Conflict of interest

The authors declare that the research was conducted in the absence of any commercial or financial relationships that could be construed as a potential conflict of interest.

Generative AI statement

The author(s) declare that no Generative AI was used in the creation of this manuscript.

Publisher's note

All claims expressed in this article are solely those of the authors and do not necessarily represent those of their affiliated organizations, or those of the publisher, the editors and the reviewers. Any product that may be evaluated in this article, or claim that may be made by its manufacturer, is not guaranteed or endorsed by the publisher.

References

1. Berti E, Cardoso V, Starinets AO. Quasinormal modes of black holes and black branes. *Class Quant Grav* (2009) 26:163001. doi:10.1088/0264-9381/26/16/163001

2. Konoplya RA, Zhidenko A. Quasinormal modes of black holes: from astrophysics to string theory. *Rev Mod Phys* (2011) 83:793–836. doi:10.1103/RevModPhys.83.793

3. Lagos M, Hui L. Generation and propagation of nonlinear quasinormal modes of a Schwarzschild black hole. *Phys Rev D* (2023) 107:044040. doi:10.1103/PhysRevD.107.044040

4. Pantelidou C, Withers B. Thermal three-point functions from holographic Schwinger-Keldysh contours. *JHEP* (2023) 04:050. doi:10.1007/JHEP04(2023)050

5. Policastro G, Son DT, Starinets AO. The Shear viscosity of strongly coupled N=4 supersymmetric Yang-Mills plasma. *Phys Rev Lett* (2001) 87:081601. doi:10.1103/PhysRevLett.87.081601

6. Kovtun PK, Starinets AO. Quasinormal modes and holography. *Phys Rev D* (2005) 72:086009. doi:10.1103/PhysRevD.72.086009

7. Baibhav V, Cheung MHY, Berti E, Cardoso V, Carullo G, Cotesta R, et al. Agnostic black hole spectroscopy: quasinormal mode content of numerical relativity waveforms and limits of validity of linear perturbation theory. *Phys Rev D* (2023) 108:104020. doi:10.1103/PhysRevD.108.104020

8. York JW, Jr. Dynamical origin of black hole radiance. *Phys Rev D* (1983) 28:2929–45. doi:10.1103/PhysRevD.28.2929

9. Hintz P, Vasy A. Analysis of linear waves near the Cauchy horizon of cosmological black holes. *J Math Phys* (2017) 58:081509. doi:10.1063/1.4996575

10. Jafferis DL, Lupsasca A, Lysov V, Ng GS, Strominger A. Quasinormal quantization in de Sitter spacetime. *JHEP* (2015) 1:004. doi:10.1007/JHEP01(2015)004

11. Green SR, Hollands S, Sberna L, Toomani V, Zimmerman P. Conserved currents for a Kerr black hole and orthogonality of quasinormal modes. *Phys Rev D* (2023) 107:064030. doi:10.1103/PhysRevD.107.064030

12. London LT. A radial scalar product for Kerr quasinormal modes. arXiv:2312.17678 (2023).

13. Arnaudo P, Carballo J, Withers B. QNM orthogonality relations for AdS black holes. arXiv:2505.04696 (2025).

14. Krejcirik D, Siegl P, Tater M, Viola J. Pseudospectra in non-Hermitian quantum mechanics. *J Math Phys* (2015) 56:103513. doi:10.1063/1.4934378

15. Trefethen L, Embree M. *Spectra and pseudospectra: the behavior of nonnormal matrices and operators*. Princeton University Press (2005).

16. Gasperin E, Jaramillo JL. Energy scales and black hole pseudospectra: the structural role of the scalar product. *Class Quant Grav* (2022) 39:115010. doi:10.1088/1361-6382/ac5054

17. Jaramillo JL, Panosso Macedo R, Al Sheikh L. Pseudospectrum and black hole quasinormal mode instability. *Phys Rev X* (2021) 11:031003. doi:10.1103/PhysRevX.11.031003

18. Nollert HP, Price RH. Quantifying excitations of quasinormal mode systems. *J Math Phys* (1999) 40:980–1010. doi:10.1063/1.532698

19. Nollert HP. About the significance of quasinormal modes of black holes. *Phys Rev D* (1996) 53:4397–402. doi:10.1103/PhysRevD.53.4397

20. Jaramillo JL. Pseudospectrum and binary black hole merger transients. *Class Quant Grav* (2022) 39:217002. doi:10.1088/1361-6382/ac8ddc

21. Boyanov V, Destounis K, Panosso Macedo R, Cardoso V, Jaramillo JL. Pseudospectrum of horizonless compact objects: a bootstrap instability mechanism. *Phys Rev D* (2023) 107:064012. doi:10.1103/PhysRevD.107.064012

22. Carballo J, Withers B. Transient dynamics of quasinormal mode sums. *JHEP* (2024) 10:084. doi:10.1007/JHEP10(2024)084

23. Chen JN, Wu LB, Guo ZK. The pseudospectrum and transient of Kaluza–Klein black holes in Einstein–Gauss–Bonnet gravity. *Class Quant Grav* (2024) 41:235015. doi:10.1088/1361-6382/ad89a1

24. Boyanov V, Cardoso V, Destounis K, Jaramillo JL, Macedo RP. Structural aspects of the anti–de sitter black hole pseudospectrum. *Phys Rev D* (2024) 109:064068. doi:10.1103/PhysRevD.109.064068

25. Warnick C. *Stability of de sitter quasinormal mode spectra* (2024) 19850. arXiv:2407.

26. Besson J, Jaramillo JL. Quasi-normal mode expansions of black hole perturbations: a hyperboloidal Keldysh's approach. *Gen Relativ Gravit* (2025) 57:110. doi:10.1007/s10714-025-03438-6

27. Warnick CM. On quasinormal modes of asymptotically anti-de Sitter black holes. *Commun Math Phys* (2015) 333:959–1035. doi:10.1007/s00220-014-2171-1

28. Bizoń P, Chmaj T, Mach P. A toy model of hyperboloidal approach to quasinormal modes. *Acta Phys Polon B* (2020) 51:1007. doi:10.5506/APhysPolB.51.1007

29. Carballo J, Pantelidou C, Withers B. Non-modal effects in black hole perturbation theory: transient Superradiance. arXiv:2503. 05871. (2025).

30. Reddy SC, Schmid PJ, Henningson DS. Pseudospectra of the orr-sommerfeld operator. *SIAM J Appl Mathematics* (1993) 53:15–47. doi:10.1137/0153002

31. Gustavsson LH. Energy growth of three-dimensional disturbances in plane Poiseuille flow. *J Fluid Mech* (1991) 224:241–60. doi:10.1017/S002211209100174X

32. Henningson DS, Lundbladh A, Johansson AV. A mechanism for bypass transition from localized disturbances in wall-bounded shear flows. *J Fluid Mech* (1993) 250:169–207. doi:10.1017/S0022112093001429

33. Butler KM, Farrell BF. Three-dimensional optimal perturbations in viscous shear flow. *Phys Fluids A: Fluid Dyn* (1992) 4:1637–50. doi:10.1063/1.858386

34. Reddy SC, Henningson DS. Energy growth in viscous channel flows. *J Fluid Mech* (1993) 252:209–38. doi:10.1017/S0022112093003738

35. Trefethen LN, Trefethen AE, Reddy SC, Driscoll TA. Hydrodynamic stability without eigenvalues. *Science* (1993) 261:578–84. doi:10.1126/science.261.5121.578

36. Gubser SS. Breaking an Abelian gauge symmetry near a black hole horizon. *Phys Rev D* (2008) 78, 065034. doi:10.1103/PhysRevD.78.065034

37. Hartnoll SA, Herzog CP, Horowitz GT. Building a holographic superconductor. *Phys Rev Lett* (2008) 101, 031601. doi:10.1103/PhysRevLett.101.031601

38. Hartnoll SA, Herzog CP, Horowitz GT. Holographic superconductors. *JHEP* (2008) 12, 015. doi:10.1088/1126-6708/2008/12/015

Frontiers in Physics

Investigates complex questions in physics to understand the nature of the physical world

Addresses the biggest questions in physics, from macro to micro, and from theoretical to experimental and applied physics.

Discover the latest Research Topics

See more →

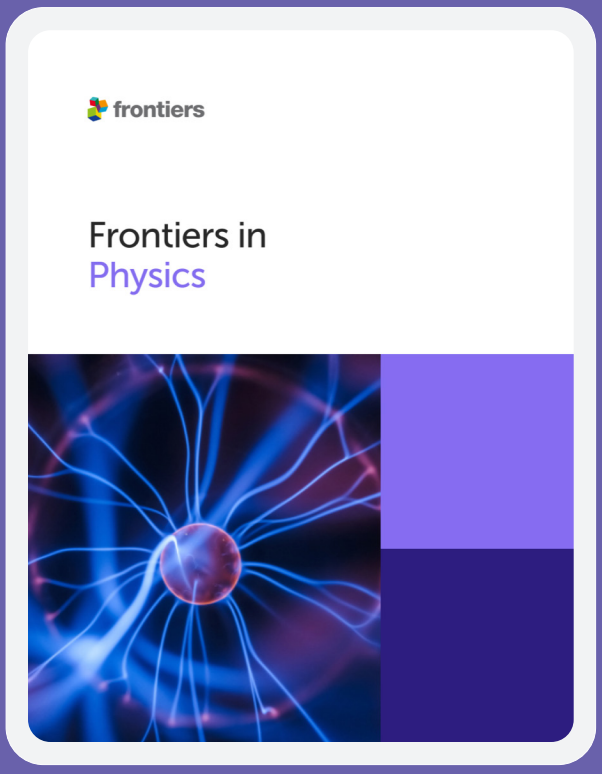

Frontiers

Avenue du Tribunal-Fédéral 34
1005 Lausanne, Switzerland
frontiersin.org

Contact us

+41 (0)21 510 17 00
frontiersin.org/about/contact